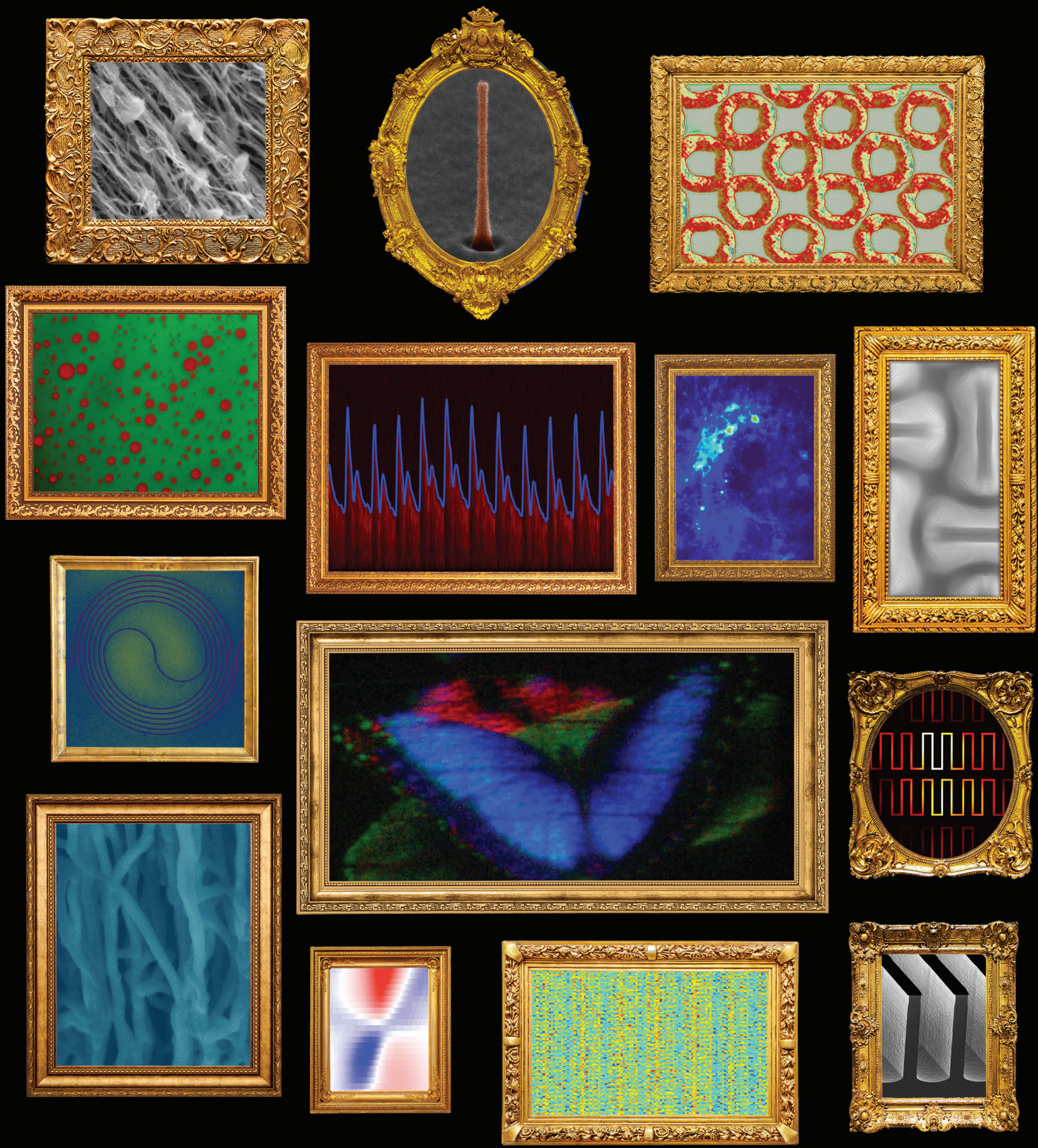

ANNUAL RESEARCH REPORT 2016

MICROSYSTEMS TECHNOLOGY LABORATORIES

MASSACHUSETTS INSTITUTE OF TECHNOLOGY

MTL Annual Research Report 2016

Director	Jesús A. del Alamo
Project Manager	Mara E. Karapetian
Production Assistant	Jami L. Hinds
Technical Editor	Elizabeth M. Fox
Proofreading	Robert J. Bicchieri
	Mary O'Neil

Front cover image credits

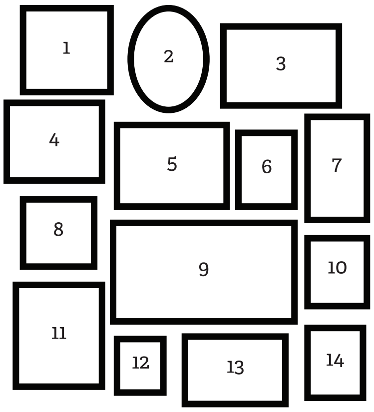

(1) "Optimizing Stability and Capacity for Lithium-Air Batteries," T. Batcho, D. Kwabi, D. Perego, R. Omampuliyur, Y. Shao-Horn, C. V. Thompson, p. 73. (2) "Source/Drain Asymmetry in InGaAs Vertical Nanowire MOSFETs," X. Zhao, C. Heidelberger, E. A. Fitzgerald, J. A. del Alamo, p. 49. (3) "Solar Water Splitting with Metallic-Semiconductor Photonic Crystals," X. H. Li, A. Elfaer, J. Chou, S. G. Kim, p. 72. (4) "Fabrication of Core-Shell Microparticles Using 3-D Printed Microfluidics," D. Olvera-Trejo, L. F. Velásquez-García, p. 95. (5) "A Wearable Transcranial Doppler Ultrasound Phased Array System," S. J. Pietrangelo, H.-S. Lee, C. G. Sodini, p. 9. (6) "Magnetic Nanoparticles for Wireless Manipulation of Neural Circuits," R. Chen, M. G. Christiansen, C. Loynachan, G. Romero, A. W. Senko, P. Anikeeva, p. 19. (7) "Germanium-on-Silicon Heteroepitaxy for High-Efficiency Photovoltaic Devices," B. R. Albert, L. C. Kimerling, J. Michel, p. 70. (8) "On-chip Mid-infrared Gas Detection Using Chalcogenide Glass Waveguide," Z. Han, P. Lin, V. Singh, L. C. Kimerling, J. Hu, K. Richardson, A. Agarwal, D. T. H. Tan, p. 139. (9) "Light Modulators for Holographic Video Displays," V. M. Bove, Jr., S. Jolly, N. Savidis, B. Datta, p. 136. (10) "Temporally and Spatially Resolved Photon-sensing in a Slow-wave Nanowire," Q. Zhao, D. Zhu, N. Calandri, F. Bellei, A. N. McCaughan, A. E. Dane, H. Wang, D. F. Santavicca, K. K. Berggren, p. 134. (11) "Liquid Spreading in Ceramic-Coated Carbon Nanotube Films and Patterned Microstructures," H. Zhao, A. J. Hart, p. 118. (12) "High-Responsivity Graphene-Boron Nitride Photodetector in a Silicon Photonic Integrated Circuit," R.-J. Shiue, Y. Gao, C. Peng, J. Goldstein, D. K. Efetov, D. R. Englund, p. 141. (13) "Variation Modeling in IC Technology," H. Chen, D. S. Boning, p. 101. (14) "Development of a Tabletop Deep Reactive-Ion Etching System for MEMS Development and Production," P. A. Gould, M. D. Hsing, K. K. Gleason, M. A. Schmidt, p. 85.

Back image cover credit

"Graphene-Based Thermopile for Thermal Imaging Applications," A. L. Hsu, P. K. Herring, N. M. Gabor, S. Ha, Y. C. Shin, Y. Song, M. Chin, M. Dubey, A. P. Chandrakasan, J. Kong, P. Jarillo-Herrero, and T. Palacios, Nano Letters, vol. 15, no. 11, pp. 7211-7216, 2015.

CONTENTS

Foreword

I am happy to bring to you the 2016 Annual Research Report of the Microsystems Technology Laboratories. It highlights the research and educational activities of faculty, staff, students, postdocs and visitors associated with MTL during MIT Fiscal Year 2016.

MTL's mission is to foster world-class research, education and innovation at the nanoscale. Nanoscale science and technology can help solve some of the world's greatest problems in areas of energy, communications, water, health, information and transportation, among others. In all these important areas of human concern, as showcased in this report, researchers at MIT are engineering new materials, structures, devices, circuits and systems using MTL's facilities and services in search of new solutions to persistent problems. MTL's activities encompass integrated circuits, systems, electronic and photonic devices, MEMS, bio-MEMS, molecular devices, nanotechnology, sensors and actuators, to name a few. MTL's research program is highly interdisciplinary. MTL's facilities are open to the entire MIT community and the outside world. Nearly 600 MIT students and postdocs from 21 different Departments, Laboratories or Centers carried out their research in MTL's facilities in the last fiscal year. In addition, researchers from several companies, as well as government research laboratories and domestic and international universities use MTL's facilities annually.

To accomplish its mission, MTL manages a set of experimental facilities in buildings 39 and 24 that host in excess of 150 fabrication and analytical tools. We strive to provide a flexible fabrication environment that is capable of long-flow integrated processes that yield complex devices while, at the same time, presenting low-barrier access to fast prototyping of structures and devices for users with very different levels of experience. Our fabrication capabilities include diffusion, lithography, deposition, etching, packaging and many others. Our lab can handle substrates from odd-shaped small pieces to 6-inch wafers. The range of materials continues to expand well beyond Si and Ge to include III-V compound semiconductors, nitride semiconductors, graphene and other 2D materials, polymers, glass, organics and many others.

MTL also manages an information technology infrastructure that supports state-of-the-art computer-aided design (CAD) tools for device, circuit and system design. Together with a set of relationships with major semiconductor manufacturers, MTL makes available to its community some of the most advanced commercial integrated circuit fabrication processes available in the world today.

MTL could not accomplish its mission without the vision, commitment and generosity of a number of companies that comprise the Microsystems Industrial Group (MIG). The MIG supports the operation of MTL's facilities, and it also advises the faculty on research directions, trends and industrial needs. The list of current MIG members can be found in the "Acknowledgments" section of this report.

In the fall of 2014, we celebrated the 30th anniversary of the creation of MTL. From an initial emphasis on semiconductors and electronics, over now 32 years of life, the technologies that underpin MTL's activities and their domains of application have greatly expanded. The 2016 Annual Report is the broadest in scope to date with abstracts describing research on nanoscale transistors, medical devices, microfluidics, organic lasers and perovskite photovoltaics, among many exciting research projects.

The research activities described in these pages would not be possible without the dedication and passion of the fabrication, IT and administrative staff of MTL. Day in and day out, they strive to support MTL users in the pursuit of their dreams. They do this in a professional and unassuming manner. Their names do not usually end up in the research papers, but that does not diminish the significance of their contributions. To them and to all of you who support in your own way the activities of MTL, a most sincere thank you!

Jesús A. del Alamo
Director, Microsystems Technology Laboratories
Donner Professor
Professor of Electrical Engineering
Department of Electrical Engineering and Computer Science
August 2016

Acknowledgments

MICROSYSTEMS INDUSTRIAL GROUP

Analog Devices
Applied Materials
Draper
Edwards Vacuum
Foxconn Electronics
HARTING
Hitachi High-Technologies
Intel
IBM
Lam Research Co.
NEC
Qualcomm
Samsung
STMicroelectronics
TSMC
Texas Instruments

MTL LEADERSHIP TEAM

Jesús A. del Alamo, Director
Sherene M. Aram, Administrative Officer
Duane S. Boning, Associate Director, Computation
Vicky Diadiuk, Associate Director, Facilities
Judy L. Hoyt, Associate Director
Jeffrey H. Lang, Associate Director
Evelyn N. Wang, Associate Director

MTL POLICY BOARD

Karl K. Berggren
Vladimir Bulović
Gang Chen
Karen K. Gleason
Lionel C. Kimerling
Michael F. Rubner
Charles G. Sodini
Timothy M. Swager

MTL TECHNICAL STAFF

Daniel A. Adams, Research Specialist
Bernard A. Alamariu, Research Engineer
Robert J. Bicchieri, Research Specialist
Kurt A. Broderick, Research Associate
Patricia Burkhart, EHS Coordinator
Michael J. Hobbs, Systems Administrator
Donal Jamieson, Research Specialist
Gongqin Li, Research Software Developer
Hanqing Li, Research Scientist
Eric Lim, Research Engineer
Thomas J. Lohman, Project Leader, Computation
William T. Maloney, Systems Manager
Paul J. McGrath, Research Specialist
Michael B. McIlrath, CAD Manager
Ryan O'Keefe, Technician C
Kristofor R. Payer, Research Specialist
Scott J. Poesse, Research Specialist and Technical Instructor
Gary Riggott, Research Associate
David M. Terry, Project Technician
Paul S. Tierney, Research Specialist
Timothy K. Turner, Technician A
Dennis J. Ward, Research Specialist
Paudely Zamora, Research Specialist

MTL ADMINISTRATIVE STAFF

Joseph Baylon, Administrative Assistant
Shereece P. Beckford, Administrative Assistant
Carolyn Collins, Administrative Assistant
Valerie J. DiNardo Administrative Assistant
Ramon Downes, Financial Officer
Margaret Flaherty, Administrative Assistant
Jami Hinds, Administrative Assistant
Debroah Hodges-Pabon, Personnel and Operations Administrator
Mara E. Karapetian, Manager of Media & Design
Elizabeth Kubicki, Administrative Assistant
Ludmila Leoparde, Financial Officer
Joanna MacIver, Administrative Assistant
Steven O'Hearn, Administrative Assistant
Mary O'Neil, Senior Administrative Assistant
Lindsay Shanahan, Administrative Assistant

PROCESS TECHNOLOGY COMMITTEE

Vicky Diadiuk, Chair
Akintunde I. Akinwande
Judy L. Hoyt
Jeffrey H. Lang
Wenjie Lu
Tomás Palacios
Jörg Scholvin
Rushabh Shah
Jay Sircar
Ahmad Zubair

MTL EQUIPMENT ACQUISITION COMMITTEE

Nicholas X. Fang, Chair
Vicky Diadiuk
Silvija Gradečak
Judy L. Hoyt
Pablo Jarillo-Herrero
Paulo C. Lozano
Tomás Palacios
Jörg Scholvin
Michael R. Watts

MTL SEMINAR SERIES COMMITTEE

Luis Velásquez-García, Chair
Valerie DiNardo
Silvija Gradečak
Jeffrey H. Lang
Evelyn N. Wang
Michael R. Watts

MARC2016 CONFERENCE ORGANIZERS

Steering Committee
Wenjie Lu, Steering Committee Co-Chair
Priyanka Raina, Steering Committee Co-Chair
Luca Daniel, Faculty Advisor
Jesús A. del Alamo, MTL Director
Daniel A. Adams, Meeting Organization & Logistics
Sherene M. Aram, Finance & Organization
Valerie J. DiNardo, Meeting Organization & Logistics
Debroah Hodges-Pabon, Meeting Organization & Logistics
Mara E. Karapetian, Publications & Proceedings
Ludmila Leoparde, Meeting Organization & Logistics
Nick Moscato, Proceedings
Paul J. McGrath, Meeting Organization & Logistics

Electronics & Quantum Devices Committee
Ujwal Radhakrishna, Chair
Marek Hempel
Redwan Noor Sajjad

Circuits & Systems Committee
Sirma Orguc, Chair
Arun Paidimarri
Mehul Tikekar

MEMS & NEMS Committee
Jörg Scholvin, Chair
Nachiket Desai

Medical Devices & Biotechnology Committee
Dan Wu, Chair
Phillip Nadeau
Sabino J. Pietrangelo

Photonics & Optoelectronics Committee
Giovanni Azzellino, Chair
Mengfei Wu
Melany Sponseller

Nanotechnology Committee
Luda Wang, Chair
Sam Nicaise
Michael Boutilier

Manufacturing & Materials Committee
Sameer Joglekar, Chair
Paul Rekemeyer
Sami Khan

Energy Committee
Piran Kidambi, Chair
Heena Mutha

Social Chairs
Evelina Polyzoeva, Co-Chair
Alex Guo, Co-Chair

Seminar Chair
Dina El-Damak

A/V & Sound Chair
Yufei Wu

Biological, Medical Devices, and Systems

MARIE: A MATLAB-Based Open Source MRI Electromagnetic Analysis Software

J. F. Villena, A. Polimeridis, J. E. C. Serralles, L. Wald, E. Adalsteinsson, J. White, L. Daniel.
Sponsorship: National Institutes of Health, Skoltech Initiative on Computational Mathematics

Our Magnetic Resonance Integral Equation suite (MARIE) is a numerical software platform for comprehensive frequency-domain fast electromagnetic (EM) analysis of MRI systems. The tool is based on a combination of surface and volume integral equation formulations. It exploits the characteristics of the different parts of an MRI system (coil array, shield, and realistic body model), and it applies sophisticated numerical methods to rapidly perform all the required EM simulations to characterize the MRI design: computing the un-tuned coil port parameters, obtaining the current distribution for the tuned coils, and obtaining the corresponding electromagnetic field distribution in the inhomogeneous body for each transmit channel.

The underlying engine of MARIE is based on integral equation methods applied to the different domains that exist in traditional MRI problems (for example, except in interventional cases, the coil and body occupy separate spaces). The natural domain decomposition of the problem allows us to apply and exploit the best modeling engine to each domain. The inhomogeneous human body model is discretized into voxels and modeled by volume integral equation (VIE) methods. The homogeneous conductors that form the coil design and shield are tessellated into surface triangles (that allow the modeling of complex and conformal geometries), and modeled by surface integral equation (SIE) methods. Both models are coupled by applying standard dyadic Green functions. Due to the nature of integral equation methods, there is no need to model or discretize the surrounding air or non-electromagnetic materials, although the solution fields can be computed anywhere outside the discretized domain by applying the same free-space Green functions. Also, no boundary condition needs to be defined (integral equations satisfy the radiation condition by construction), which simplifies the setting of the problem for the user: the inputs are the voxelized definition of the inhomogeneous body model, the tessellated geometry of the coil design (which the external ports defined), and the frequency of operation.

Once the models are generated, fast numerical methods are applied to solve the complete system. A set of nested iterative methods with the appropriate preconditioning is used to solve the effect of each port. Fast Fourier transform (FFT) techniques exploit the regularity of the voxelized grid and accelerate the matrix vector products. Depending on the different scenarios for analysis, some numerical models or tasks can be pre-computed to accelerate the solution, and many strategies are used to reduce either computational time or memory consumption.

The software runs on MATLAB and is able to solve a complex scattering problem in ~2-3 min. on a standard single GPU-accelerated windows desktop machine. On the same platform, it can perform a frequency sweep of a complex coil in ~3-5 min. per frequency point. Furthermore, it can solve the complete inhomogeneous body and coil system in ~5-10 min. per port, depending on the model resolution and error tolerance required. Intended to be a development platform, it includes a simple and intuitive graphic user interface (see Figure 1 for a snapshot) for standard analysis and a set of well-documented scripts to illustrate how to use the core numerical functions to perform more advanced analyses, to allow experienced users to create their own analysis by using or modifying the existing code. The input of the body is voxel-based and can be read from simple files that define position and tissue properties. The input of the coil design is based on standard triangular geometric descriptions, widely popular and with multiple open-source mesh generators available. The underlying numerical routines can be used to generate standard results, such as the B1+, B1-, and E maps presented in Figure 2, or to address other relevant problems, such as the generation of ultimate intrinsic SNR and SAR on realistic body models, fast coil design and optimization, and generation of patient-specific protocols, among others.

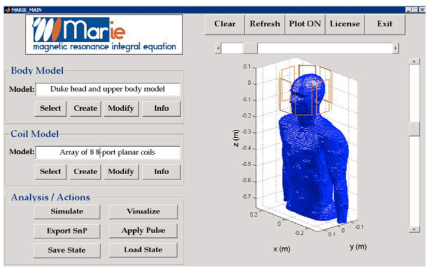

◀ Figure 1: Snapshot of MARIE's graphic user interface with body and coil models loaded, for which the simulation results are shown in Figure 2.

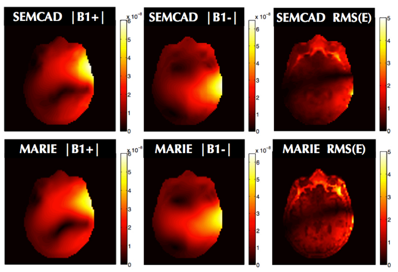

◀ Figure 2: Comparison of the (left) B1+, (center) B1-, and (right) RMS(E) maps for a body model. Top maps are with SEMCAD (SPEAG), bottom with MARIE.

FURTHER READING

- A. G. Polimeridis, J. F. Villena, L. Daniel, and J. K. White, "Stable FFT-JVIE Solvers for Fast Analysis of Highly Inhomogeneous Dielectric Objects," *Journal of Comp. Physics*, vol. 269, pp. 280-296, 2014.
- A. Hochman, J. F. Villena, A. G. Polimeridis, L. M. Silveira, J. K. White, and L. Daniel, "Reduced-order Models for Electromagnetic Scattering Problems," *IEEE Trans. on Antennas and Propagation*, vol. 62, no. 6, pp. 3150-3162, 2014.

Automated Modeling for Large-Scale Arterial Systems

Y.-C. Hsiao, Y. Vassilevski, S. Simakov, L. Daniel
Sponsorship: MIT-Skoltech

Diagnosing medical conditions based on non-invasive (or minimally invasive) measurements requires simultaneous modeling for both (1) local pathological arteries and (2) global arterial networks in order to correlate the available measurements with the actual pathologies. For instance, diagnosing atherosclerosis or an aneurysm requires detailed understanding of the pressure and flow inside the bifurcation segments. Such information is typically not measurable at pathological sites but may still be attainable if it can be inferred from other measurements. Therefore, it is crucial to develop accurate yet efficient global arterial models such that the correlations between the pathologies and the available measurements can be established. The final diagnosis can be obtained by solving an inverse problem for the pathological parameters, for instance, aneurysm internal diameter, arterial wall thickness, plague stiffness, etc.

For this strategy to be effective, the model for such a large-scale arterial network must be compact, computationally tractable, and field-solver-accurate. We have proposed an innovative technique to automatically generate nonlinear dynamic models using measurement data or simulations results from partial-differential-equation (PDE) solvers, as shown in Figure 1. The generated models are guaranteed numerically stable, both when simulated alone and when interconnected within a network. This stability enables the hierarchical modeling capability, generating models for local sub-networks, such as branches and bifurcations, and interconnecting them to form a global network. An example of such geometry decomposition is demonstrated in Figure 2. This approach allows full exploitation of artery geometries without compromise due to the shape complexity. In addition, because the entire modeling efforts are subdivided into local model generations, the corresponding finite-element problems for generating training data are at a tractable size. Therefore, the fluid dynamics PDEs, such as viscosity and turbulence, can be fully utilized to capture all types of nonlinearities without simplification.

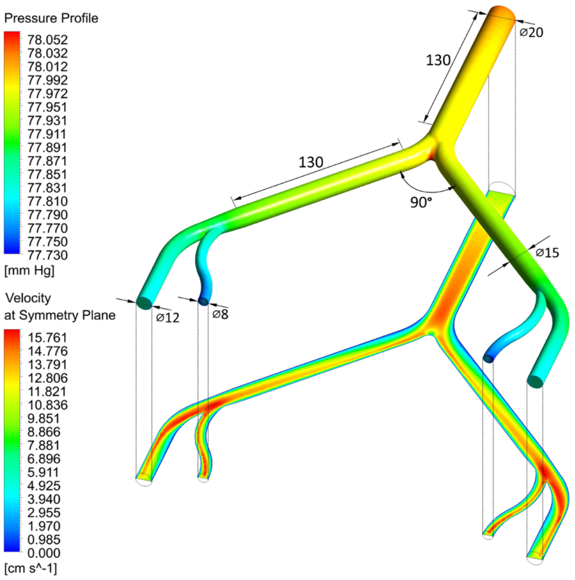

▲Figure 1: Pressure profile (upper) and velocity profile (lower) of the human abdominal aorta and iliac arteries.

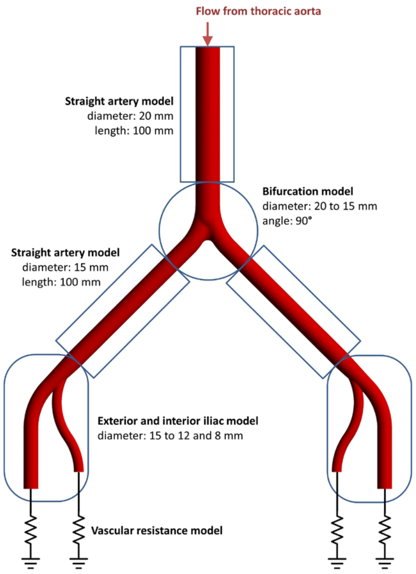

▲Figure 2: Arterial network decomposition into local models. Each model is automatically generated using our proposed algorithm. The simulation of the overall system is accurate, efficient, and guaranteed numerically stable.

FURTHER READING

- B. Bond, T. Moselhy, and L. Daniel, "System Identification Techniques for Modeling of the Human Arterial System," in *Proc. SIAM Conference on the Life Sciences*, pp. 12-15, 2010.
- Y.-C. Hsiao and L. Daniel, "Sparse Basis Pursuit on Automatic Nonlinear Circuit Modeling," presented at *IEEE International Conference on ASIC (ASICON)*, Shenzhen, China.

Three-Dimensional, Magnetic Resonance-Based Electrical Properties Mapping

J. E. C. Serrallés, A. G. Polimeridis, R. Lattanzi, D. K. Sodickson, J. K. White, L. Daniel
Sponsorship: NSF

Over the past few decades, magnetic resonance imaging (MRI) has proven to be a safe and versatile tool in medical practice and clinical research. Clinical MRI typically relies on magnetization, T_1-weighting, and T_2-weighting as its contrast mechanisms. The dependence on these mechanisms is disadvantageous because these quantities are not guaranteed to vary from tissue to tissue, potentially obscuring the true contrast of the tissues. Additionally, the use of magnetization discards valuable information that describes how the scatterer interacts with fields generated by a scanner. The aim of our research is instead to use this extraneous information to generate maps of relative permittivity and of conductivity, thereby significantly increasing contrast in MR images at the expense of computation time.

The task of inferring these material properties is referred to as inverse scattering, a subclass of what are called inverse problems. Inverse scattering problems typically suffer from slow convergence rates and require several full-wave electromagnetic simulations per iteration of the procedure. Our approach, called Global Maxwell Tomography, uses a volume integral equation suite, MARIE, which is custom-tailored for the typical MR setting and which results in runtimes that render inference process tractable. Our algorithm is capable of reconstructing the known electrical properties of objects, in simulation, with use of measured MR data on the horizon. The ability to infer electrical property maps rapidly from MR data would not only improve the reliability of MRI but would also pave the way for applications like automated tumor identification, patient-specific MR shimming, and real-time monitoring of heat deposition in tissue by MR coils, among others.

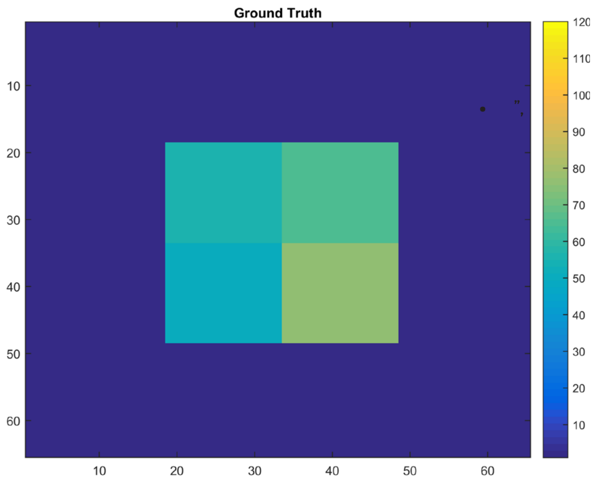

▲ Figure 1: Relative permittivity map of phantom with known electrical properties and geometry, along a central slice. This constitutes the ground truth to which the algorithm should converge.

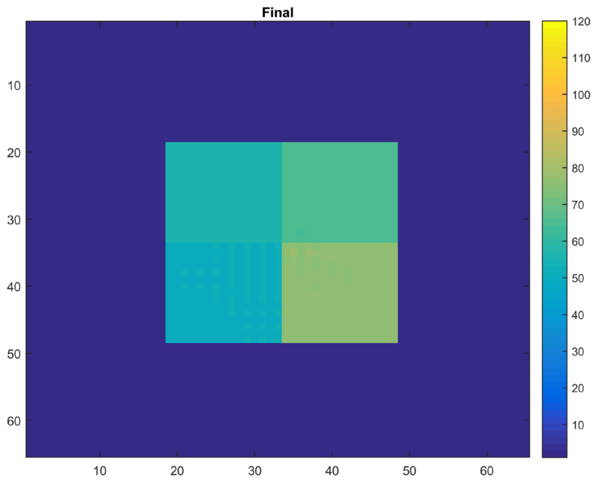

▲ Figure 2: Reconstructed relative permittivity map of the same phantom, when starting from a completely homogeneous initial guess. Reference fields are generated in simulation.

FURTHER READING

- J. E. C. Serrallés, A. G. Polimeridis, M. V. Vaidya, G. Haemer, J.K. White, D.K. Sodickson, L. Daniel, R. Lattanzi. "Global Maxwell Tomography: A Novel Technique for Electrical Properties Mapping without Symmetry Assumptions or Edge Artifacts," presented at *ISMRM 24th Annual Meeting*, Suntec City, Singapore, May 2016.
- J. E. C. Serrallés, L. Daniel, J.K. White, D.K. Sodickson, R. Lattanzi, and A.G. Polimeridis. "Global Maxwell Tomography: A Novel Technique for Electrical Properties Mapping based on MR Measurements and Volume Integral Equation Formulations," presented at *2016 IEEE International Symposium on AP-S–URSI National Radio Science Meeting*, Fajardo, Puerto Rico, June 2016.

A Portable Bioimpedance Spectroscopy Measurement System for Management of Congestive Heart Failure

M. K. Delano, C. G. Sodini
Sponsorship: MEDRC, Analog Devices, Inc.

An estimated five million people are currently diagnosed with congestive heart failure (CHF) in the United States, with over 400,000 new diagnoses annually. Almost one in two patients will be readmitted to the hospital within four to six months of discharge. Readmissions can occur when the patient becomes fluid-overloaded due to poor medication and/or diet compliance, among other reasons. Up to 50% of these early re-admissions may be prevented if symptoms are recognized early enough and medication and diet compliance improve.

CHF is frequently associated with significant fluid retention in the lungs and legs. Bioimpedance techniques can be used to estimate the fluid levels in a patient non-invasively. These measurements have been shown to be predictive of heart failure decompensation up to 14 days before an event occurs.

We have developed a portable bioimpedance system that can measure body impedance from 1 kHz to 1 MHz. The system uses the magnitude-ratio and phase-difference detection (MRPDD) method to calculate the magnitude and phase of the measured impedance (see Figure 1). The system is enclosed in aluminum box (see Figure 2) and can be used with four co-axial cables. Data from the device is transmitted over Bluetooth to an iOS device.

The device has been tested with RC networks and with two healthy participants at MIT's Clinical Research Center. The device will be tested in the hemodialysis unit at Massachusetts General Hospital in 2016.

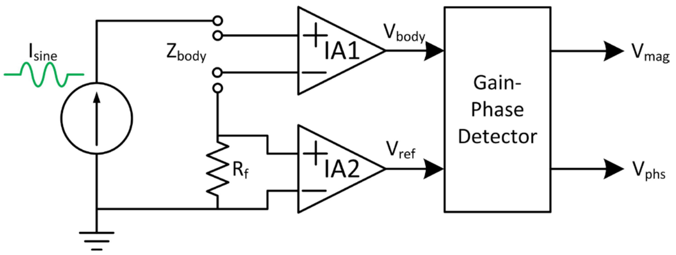

▲ Figure 1: A schematic overview of the MRPDD method. A fixed sinusoidal current is driven through the body and a sense resistor. The voltage is amplified and measured by a gain-phase detector chip (AD8302).

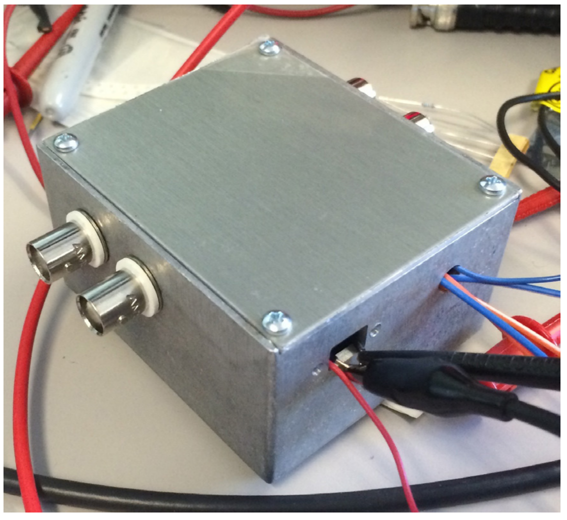

▲ Figure 2: The portable bioimpedance spectroscopy measurement system inside the enclosure.

FURTHER READING

- M. Delano and C. G. Sodini, "A Long Term Wearable Electrocardiogram Measurement System," *Body Sensor Networks Conference*, pp. 1-6, May 2013.
- E. Winokur, M. Delano, and C. G. Sodini, "A Wearable Cardiac Monitor for Long-Term Data Acquisition and Analysis," *IEEE Transactions on Biomedical Engineering*, vol. 60, pp. 189-92, Jan. 2013.
- D. He, E. S. Winokur, and C. G. Sodini, "An Ear-worn Vital Signs Monitor," *IEEE Transactions on Biomedical Engineering*, vol. 62, no. 11, pp. 2547-2552, November 2015.

Body-Coupled Communication and Implants

G. S. Anderson, C. G. Sodini
Sponsorship: Center for Integrated Circuits & Systems

Body-coupled communication (BCC) is achieved by creating a potential difference in one area of the body and sensing the resulting attenuated potential difference in another area of the body. To do this, the transmitter and receiver each have two electrodes that electrically connect to the body's conductive tissues beneath the epidermis. These connections can be formed either capacitively or galvanically. A capacitive link consists of the electrode forming one plate of a parallel plate capacitor while the conductive tissues form the other plate. A galvanic link is formed by directly putting the electrode or wire in the conductive tissue.

For an implant to communicate to a device outside the body using BCC, the channel utilizes both galvanic and capacitive links (capacitive for the device outside the body and galvanic for the implant). To test if this is possible a pork loin was used to simulate the conductive tissue of the body (see Figure 1). First, both the transmitter's and receiver's electrodes were connected to the pork loin using cardboard spacers between the pork loin and the electrodes, ensuring that both the transmitter and receiver would be capacitively coupled to the conductive tissue in the pork loin. Next, the transmitter's output was connected to two alligator clips that were inserted into the pork-loin while the receiver was connected capacitively as before. This configuration simulates an implanted transmitter that is galvanically coupled to the conductive tissue, communicating with a receiver that is capacitively coupled. The results, shown in Figure 2, validate the predictions of the body model detailed in the further reading below.

▲ Figure 1: A setup to test implants talking to devices outside the body using BCC.

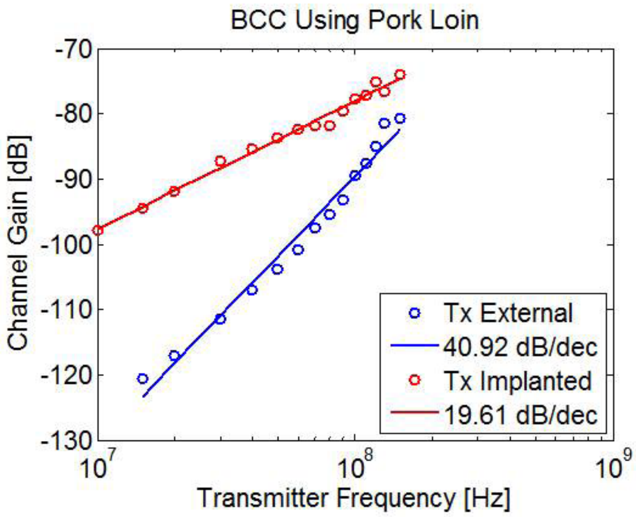

▲ Figure 2: BCC channel measurements.

FURTHER READING

- G. S. Anderson and C. G. Sodini, "Body Coupled Communication: The Channel and Implantable Sensors," *2013 IEEE International Conference on Body Sensor Networks (BSN)*, Cambridge, MA, pp. 1-5, 6-9 May 2013.
- T. G. Zimmerman, "Personal Area Networks (PAN): Near-field Intrabody Communication," *Master's thesis, Massachusetts Institute of Technology*, Cambridge, MA, 1995.
- A. Fazzi *et al*, "A 2.75mW Wideband Correlation-Based Transceiver for Body-Coupled Communication," *ISSCC Dig. Tech. Papers*, pp. 204-205, February 2009.

Miniaturized EEG System and Seizure Detector for Wearable and Subdermal Application

J. Yang, C. G. Sodini
Sponsorship: Center for Integrated Circuits and Systems

Electroencephalograms (EEGs) are used to diagnose and treat a wide range of neurological related topics by providing insight into a patient's brain activity. Their applications range from diagnosing epilepsy and sleep disorders to assisting doctors to administer anesthetic drugs and more.

Achieving long-term continuous EEG data in a wearable form has been a long-standing problem. In a conventional EEG, the patient must go to the hospital and be connected to bulky equipment. This is prohibitively expensive in the long run and prevents the patient from going about their daily lives, thereby reducing patient compliance in certain situations.

This work extends previous investigations on miniaturization of EEG by providing system-level improvements to expand the use-cases of the device. With optimized packaging of an EEG system-on-a chip (SoC) die, form-factors more suitable for implantation as well as wearable designs are realized. For the subdermal implanted design, an eight-channel EEG recorder with a seizure detector is implanted behind a patient's ear. Electrodes are threaded underneath the patient's scalp to the location of interest. EEG data is then sent wirelessly to a wearable external device that processes the data and provides power to the implant. This implantable system has the ability to continuously record EEG for more than 30 days with minimal maintenance.

For the wearable form factor, the miniaturized EEG SoC and wireless microprocessor are attached near the mastoid behind the patient's ear. Eight buffered electrodes are placed across the head at the location of interest. EEG data is collected and transmitted via BLE to a computer or smartphone for further processing.

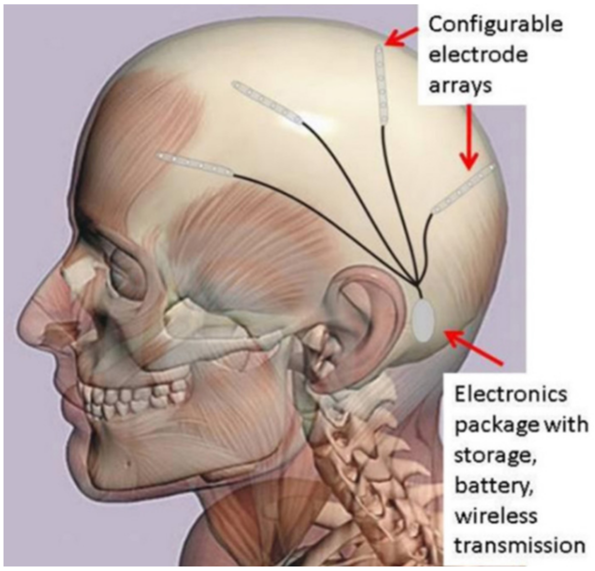

▲Figure 1: Implanted EEG system showing location of the SoC and electrodes.

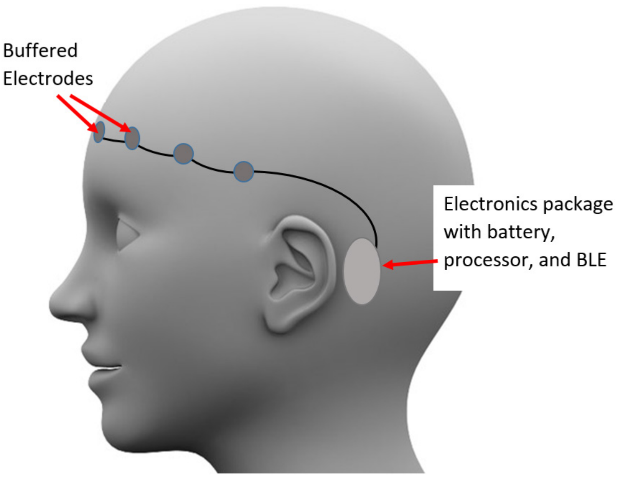

▲Figure 2: Wearable EEG system showing locations of electronics package and electrodes.

A Wearable Transcranial Doppler Ultrasound Phased Array System

S. J. Pietrangelo, H.-S. Lee, C. G. Sodini
Sponsorship: MEDRC, Maxim Integrated

The central objective of critical care for patients affected by traumatic brain injury (TBI), cerebrovascular accident (i.e., stroke), and other neurovascular pathologies is to monitor patient state and provide suitable medical intervention to mitigate secondary injury and aid in recovery. Transcranial Doppler (TCD) sonography is a specialized Doppler ultrasound technique that allows characterization of blood flow from the basal intracerebral vessels. While several non-invasive cerebrovascular diagnostic modalities exist, including positron emission tomography (PET), computed tomography (CT), and magnetic resonance angiography (MRA), the use of TCD sonography is highly compelling for certain diagnostic needs due to its safety in prolonged studies, high temporal resolution, modest capital equipment costs, and relative portability.

Despite a growing list of potential diagnostic applications, several constraints — notably operator-dependent measurement results, bulky instrumentation, and the need for manual vessel location — have generally confined the use of TCD ultrasound to highly specific clinical environments (e.g., neurocritical care units and vascular laboratories). This project seeks to develop a low-power miniaturized TCD ultrasound system for measuring blood flow velocity at the middle cerebral artery (MCA) in support of continuous cerebrovascular monitoring with limited operator interaction.

The TCD ultrasound system shown in Figure 1 employs multi-channel transceiver electronics and a two-dimensional transducer array to enable electronic steering of the ultrasound beam. The discrete prototype electronics measure 6.5" x 5.5" x 1" and are worn at the chest; the transducer array is affixed at the temporal region with an adjustable headframe. Electronic beam formation allows for algorithmic vessel location and tracking, thereby obviating the need for manual transducer alignment and operator expertise. Following automated vessel location, the system computes the flow velocity spectrogram and spectral envelope, as presented in Figure 2.

Although human validation is preliminary, this work demonstrates a compact, wearable, and algorithmically steered TCD system that largely resolves several key shortcomings of established TCD measurement techniques. The successful execution of our current objectives can profoundly alter the standard clinical approach to neurovascular evaluation, especially in applications where the role of non-invasive diagnostics has not yet been clearly established (e.g., extended monitoring, emergency assessment).

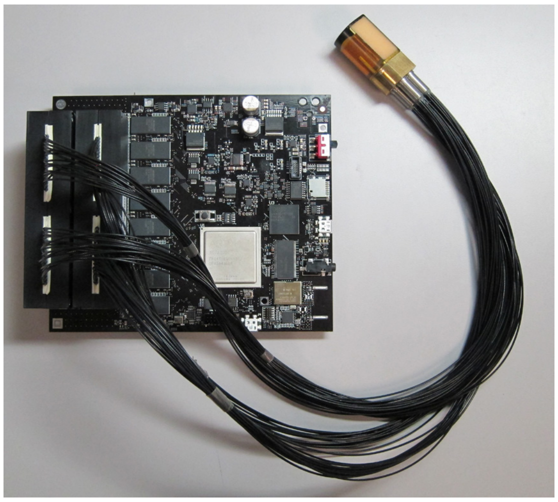

▲Figure 1: Discrete TCD phased array system connected to a custom two-dimensional transducer array.

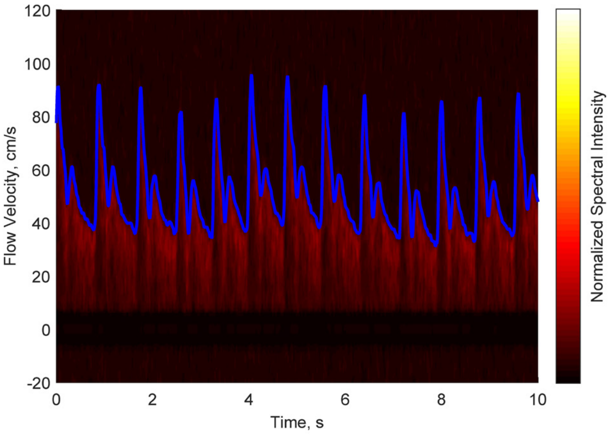

▲Figure 2: TCD spectrogram at algorithmically located Doppler power maxima.

FURTHER READING

- S. J. Pietrangelo, "An Electronically Steered, Wearable Transcranial Doppler Ultrasound System," Master's thesis, Massachusetts Institute of Technology, Cambridge, 2013.

Continuous and Non-Invasive Arterial Pressure Waveform Monitoring Using Ultrasound

J. Seo, H.-S. Lee, C. G. Sodini
Sponsorship: Samsung Electronics Fellowship, MEDRC - Phillips

An arterial blood pressure (ABP) waveform provides valuable information for understanding cardiovascular diseases. The ABP waveform is usually obtained through a pressure transducer connected to an arterial catheter. Although considered the gold standard, this method has the disadvantage of its invasive nature. Non-invasive methods based on vascular unloading, such as Finapres, are not suitable for prolonged or continuous monitoring due to their obstructive nature. Therefore, reliable non-invasive ABP waveform estimation has been desired for a long time by medical communities. In that sense, medical ultrasound is an attractive imaging modality because it is inexpensive, free of ionizing radiation, cuff-less, and suitable for portable system implementation.

The proposed ultrasonic ABP waveform monitoring is achieved by observing the pulsatile change of the cross-sectional area and identifying the elastic property of the arterial vessel, represented by the pulse wave velocity (PWV; the propagation speed of a pressure wave along an arterial tree) with a diastolic blood pressure measurement as a baseline. The PWV can be estimated by obtaining a flow-area plot and then measuring the slope of a linear part in the flow-area plot during a reflection-free period (e.g., the early systolic stage).

A prototype ultrasound device is designed to obtain both a blood flow waveform and a diameter waveform simultaneously to implement the proposed technique, shown in Figure 1. A clinical test was conducted on nine healthy human subjects to demonstrate the proof of concept of the proposed approach. Figure 2 presents a pressure waveform comparison between an ABP waveform obtained at a left middle finger and an estimated ABP waveform at the left common carotid artery from this method. Currently, the prototype is being re-designed to reduce the data acquisition time in a clinical setting and potentially to enable device operation without the guidance of a sonographer.

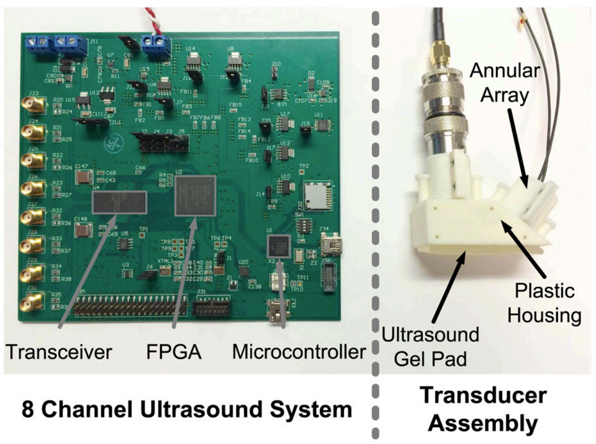

▲Figure 1: The prototype ultrasound system and transducer assembly. The system is capable of sufficient data rate to display blood flow and arterial pulsation simultaneously. Ultrasound gel pad is utilized to achieve acoustic coupling between the transducer surface and the skin.

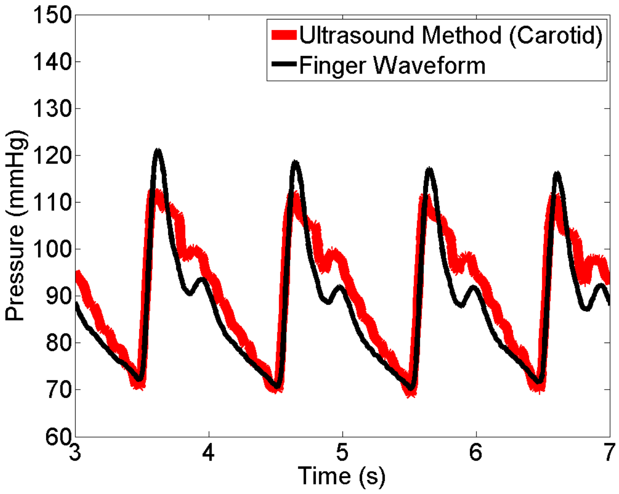

▲Figure 2: Comparison of the estimated carotid ABP waveform to the finger ABP waveform. The finger waveform shows a sharper systolic peak due to pulse pressure amplification at peripheral arterial sites.

FURTHER READING

- J. Seo, S. J. Pietrangelo, H.-S. Lee, and C. G. Sodini, "Carotid Arterial Blood Pressure Waveform Monitoring Using a Portable Ultrasound System," in *2015 37th Annual International Conference of the IEEE Engineering in Medicine and Biology Society (EMBC)*, pp. 5692-5695, 2015.
- J. Seo, S. J. Pietrangelo, H.-S. Lee, and C. G. Sodini, "Noninvasive Arterial Blood Pressure Waveform Monitoring Using Two-Element Ultrasound System," *IEEE Transactions on Ultrasonics, Ferroelectrics, and Frequency Control*, vol. 62, no. 4, pp. 776-784, 2015.

Improvement of a Capsule Endoscopic Ultrasound

D. Ibarra, J. H. Lee, B. W. Anthony
Sponsorship: Tecnológico de Monterrey, MIT

Wireless capsule endoscopy (WCE) has modernized the capacity for evaluation of the gastrointestinal (GI) tract. Even though WCE provides high-quality optical images of the GI tract, evaluation is restricted to the wall surface. This project studies design considerations for capsule endoscopic ultrasound (CEU) that combines the benefits of WCE and ultrasound imaging, enabling characterization of the deeper structures within the mucosal wall. The first part of the project has two goals: (1) to evaluate transducer designs and capsule materials appropriate for CEU and (2) to prove that the obtained ultra sound images have high-enough quality to work for us to design a wireless capsule. Mechanical scanning (MS) design is implemented using simulation and experimentation with a focused disc transducer and a motor. Measurements of 3-D printed phantoms were done using the TPX (4-methylpentene-1 based polyolefin) material for the capsule prototype. The MS-tethered capsule developed for imaging feasibility study shown in Figure 1(a) consists of a 10-MHz transducer and a micro stepper motor. Figure 1 (b) shows the first prototype with TPX material for the cover. A 3-D printed phantom was designed to evaluate image quality, and MS shows good performance in terms of image quality as well as system complexity. These findings support further development in the direction of a wireless capsule endoscopic ultrasound (WCEU) device with the goal of significantly expanding the diagnostic modalities for the GI tract.

Figure 2 (top) shows the 3-D printed phantom settled with a fishing line. Experimental results are shown in Figure 2 (bottom). Full circumferential coverage was done in a beaker of water with the capsule fitted in the 3-D printed phantom. The prototype acquires good B-mode images, the acoustic signal was stronger than expected due to the attenuation from the capsule wall. The further work is to test it in *in vivo* models to figure out the possibility of utilizing peristalsis such as acoustic coupling required for ultrasound imaging.

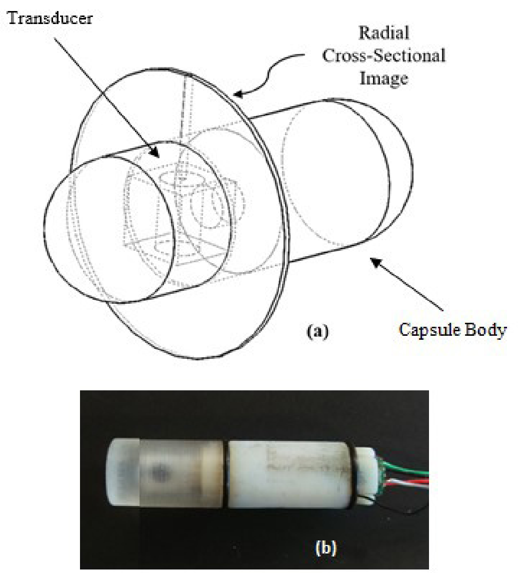

▲ Figure 1: The capsule design and the MS transducer rotated using a mechanical actuating element (a). The prototype of the capsule with cover of TPX material (b).

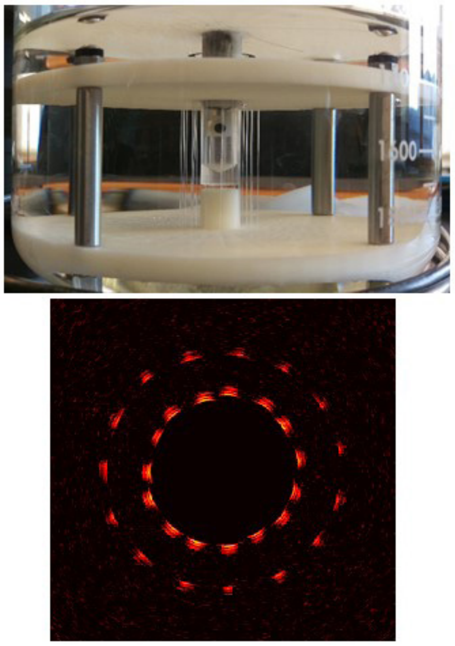

▲ Figure 2: The 3-D printed phantom settled with fishing line (top). The B-mode images of fishing line around 360° (bottom).

FURTHER READING

- J. H. Lee, G. Traverso, C. M. Schoellhammer, D. Blankschtein, R. Langer, K. E. Thomenius, D. S. Boning, and B. W. Anthony, "Towards Wireless Capsule Endoscopic Ultrasound (WCEU)," *2014 IEEE International Ultrasonics Symposium (IUS)*, pp. 734–737, 2014.
- L. B. Gerson, "Capsule Endoscopy and Deep Enteroscopy," *Gastrointest. Endosc.*, vol. 78, no. 3, pp. 439–443, September 2013.

Gastric Fluid-Activated Battery for Powering Ingestible Electronics

P. Nadeau, D. El-Damak, D. Glettig, S. Mo, C. Cleveland, L. Booth, R. Langer, A. P. Chandrakasan, G. Traverso
Sponsorship: Texas Instruments, Hong Kong Innovation and Technology Commission, ATIC-SRC Center of Excellence for Energy Efficient Electronics Systems, Alexander von Humboldt-Stiftung Foundation, National Institutes of Health

Ingestible electronics are revolutionizing the way we diagnose and treat diseases. Swallowable telemetry capsules are now used to take visual images of the gastrointestinal (GI) tract, record vital signs, and monitor temperature, pH, and medication compliance. In addition, techniques for longer-term gastric residency (up to 1 week) are extending the lifetime of ingestible devices and could provide a platform for longer term monitoring (Figure 1).

With the scaling of CMOS power consumption, primary cell batteries may not be the only option for powering these devices. Dissolving electrodes made from biocompatible materials could provide a safe and potentially lower cost solution for powering ingestible electronic sensors (Figure 2). In these electrochemical cells, the gastric fluid acts as the electrolyte and activates the battery on contact. The anode metal (either zinc or magnesium) dissolves into the acid while the inert cathode catalyzes the evolution of hydrogen gas, sending electrical power to the circuit.

The focus of this research includes the detailed un-tethered (wireless) characterization of the available amount of power from such an electrochemical cell as it traverses the GI tract, including such parameters as the electrode voltages and impedance levels. Due to food and fluid intake, the heterogeneous nature of the gastric pool, and varying position of the capsule within the stomach due to motion, the available amount of power is expected to have large variability. Understanding this variation can provide valuable input for system designers. As a first step we are gathering preliminary data on the *in vivo* performance of this cell in a large animal model. In addition to characterization, we seek to harness this energy to demonstrate fully self-powered measurements and wireless communication to an external base station receiver.

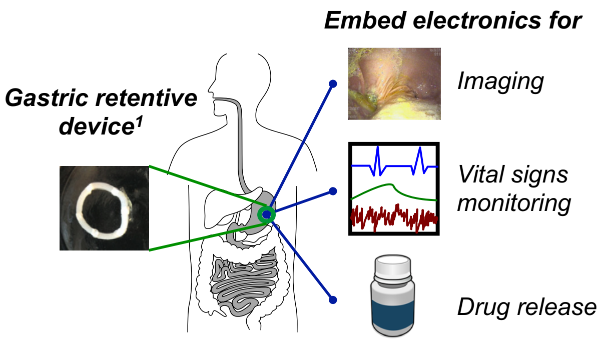

▲ Figure 1: Gastric retentive devices as a platform for health monitoring and treatment.

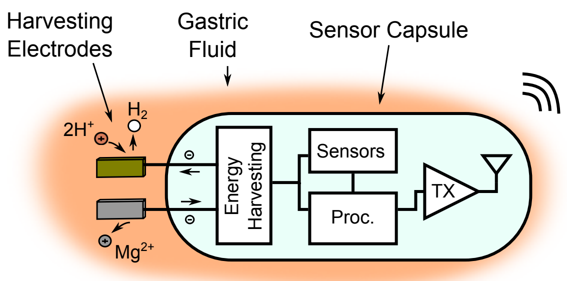

▲ Figure 2: Electronic device powered by harvesting from electrodes which are activated by gastric fluid.

FURTHER READING

- S. Zhang, A. M. Bellinger, D. L. Glettig, R. Barman, Y.-A. L. Lee, J. Zhu, C. Cleveland, V. A. Montgomery, L. Gu, L. D. Nash, D. J. Maitland, R. Langer, and G. Traverso, "A pH-Responsive Supramolecular Polymer Gel as an Enteric Elastomer for Use in Gastric Devices," *Nature Materials*, vol. 14, no. 10, pp. 1065–1071, July 2015.
- G. Traverso, G. Ciccarelli, S. Schwartz, T. Hughes, T. Boettcher, R. Barman, R. Langer, and A. Swiston, "Physiologic Status Monitoring via the Gastrointestinal Tract," *PLoS ONE*, vol. 10, no. 11, pp. e0141666, 2015.

High-Throughput Cell Sorting for Diagnostics using Microfluidics

M. Kim, K. Choi, H. Ryu, W. Ouyang, J. Han in collaboration with D. T. Hung, G. Alter, J. Lee, B. Levy
Sponsorship: NIH, Broad BN10, J-WAFS

Our group is collaborating on high-throughput cell and molecular sorting, often from challenging sample backgrounds such as blood or sputum, to enable advanced, functional assays and diagnostics. One of the common challenges in biomedical sciences is reliable sample preparation, and there are many situations where better sample preparation (which involves removal of backgrounds and concentration of target cells or molecules) can drastically enhance the sensitivity and specificity of the downstream assays.

As one of the main applications, we are focusing on bacterial sorting from blood to enable blood-borne pathogen diagnostics. Bacterial contamination and infection are a significant problem for public health, food industry, environmental biosafety, and many other areas. However, current techniques do not allow rapid and sensitive detection of bacteremia that are necessary for better clinical management. To address this problem, we developed a method to rapidly isolate bacteria from whole blood using inertial microfluidics and directly determine pathogen identity and antibiotic susceptibility with hybridization-based RNA detection. The Dean Flow Fractionation (DFF) cell-sorting technology described here and applied to bacterial isolation was previously developed by our group for direct isolation of circulating tumor cells (CTCs) from whole blood. Unlike CTCs that exhibit 10–20 µm characteristic length, bacteria (<1 µm) are significantly smaller and therefore challenging to focus using conventional inertial microfluidics. To overcome the size problem, we introduced a sheath flow at the inlet to "pinch" the bacteria-containing sample and demonstrated well-controlled Dean migration of bacteria towards the outer wall to achieve efficient bacteria recovery. Using the DFF principle, bacteria are separated from host blood cells in a label-free separation method with high recovery, even in low abundance bacteria situation. Ribosomal RNA detection can then be applied for direct identification of low abundance pathogens (~100 mL^{-1}) from blood without culturing or enzymatic amplification. Messenger RNA detection of antibiotic-responsive transcripts after brief drug exposure permits rapid susceptibility determination from bacteria with minimal culturing (~10^5 mL^{-1}). This novel combination of microfluidic cell separation with RNA-based molecular detection techniques represents significant progress towards faster diagnostics (~8 hours) to guide antibiotic therapy.

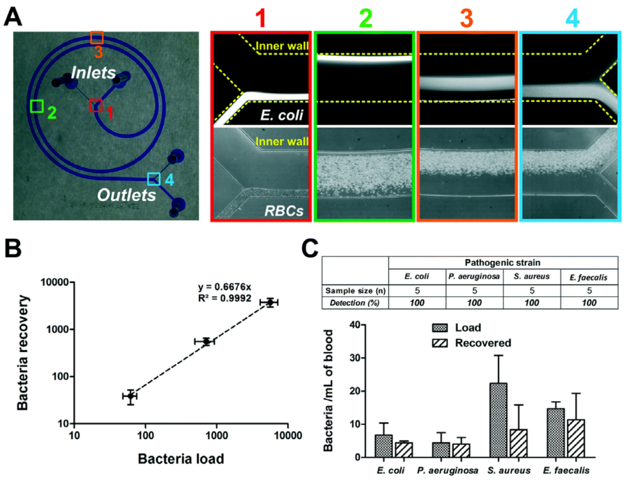

▲Figure 1: (A) Distribution of FITC-labeled E. coli and RBCs shows their differences along the separation channel. (B) Recovery plot indicates efficient bacterial recovery (>65%). (C) Histogram plot indicates the bacterial load and recovery for different pathogenic strains at clinically relevant concentrations (~10–50 cells mL^{-1}).

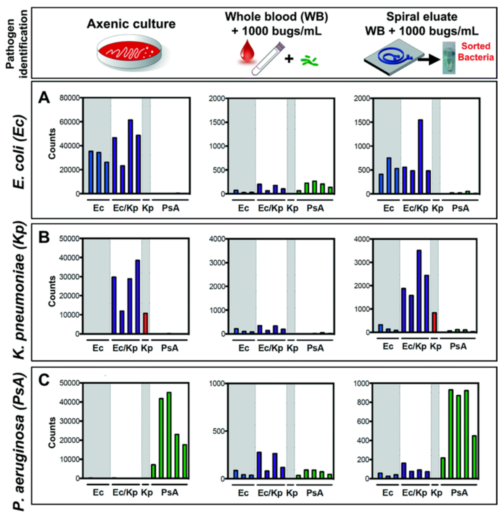

▲Figure 2: Pathogen identification from blood after DFF by rRNA recognition. (A) E. coli or (B) K. pneumoniae were either grown in axenic culture (left panel); in whole blood (middle); or in DFF-processed whole blood (right), before being detected by the NanoString assay using a probeset directed against rRNA from these three organisms.

FURTHER READING

- H. W. Hou, R. P. Bhattacharyya, D. T. Hung, and J. Han, *Lab on a Chip*, vol. 15, pp. 2297-2307, 2015.
- D. Di Carlo, D. Irimia, R. G. Tompkins, and M. Toner, *Proc. Natl. Acad. Sci. U. S. A.*, vol. 104, pp. 18892–18897, 2007.
- H. W. Hou, M. E. Warkiani, B. L. Khoo, Z. R. Li, R. A. Soo, D. S.-W. Tan, W.-T. Lim, J. Han, A. A. S. Bhagat, and C. T. Lim, *Sci. Rep.*, vol. 3, pp. 1259, 2013.

Nanofluidic Devices for Biologics Quality Assessment

S. H. Ko, W. Ouyang, T. Kwon, J. Han
Sponsorship: Integrated and Scalable Cyto-Technology Platform for Biopharmaceutical Manufacturing on Demand Project /DARPA

Biologics (protein drugs), which are applicable to the most effective means to treat serious diseases, are of great interest in the modern pharmaceutical industry. However, assuring their quality and safety is more difficult than it is for small molecule drugs due to their high sensitivity to external environment conditions, so developing analytical tools for exact and rapid quality assessment is essential. In this work, we have designed nanofluidic devices and demonstrated purity and bioactivity assessments for commercialized biologics using size-based separation and mobility-shift assay methods.

For the purity assessment, a slanted nanofilter array is used to demonstrate separation of the target (human growth hormone, or hGH) and impurities (molecular weight markers) based on size to reveal the presence of protein aggregation (potential cause of immune responses *in vivo*) or any fragments. Figure 1 shows the analysis of hGH with impurities. The device could resolve all the impurities although the low-molecular weight impurities (14.3 kDa and 3.5 kDa proteins) are not fully resolved. The bioactivity assessment is achieved by using positively modulated receptor as a probe molecule (growth hormone receptor or GHR(+)) to perform direct assay for assessing binding affinity (k_D). While GHR(+) is not concentrated, the complex GHR(+)-hGH is concentrated, with a stronger signal at higher hGH concentrations. Based on the fluorescence intensity of concentrated complex, the dose-response curve is plotted, indicating an apparent k_D of 1 nM, as shown in Figure 2.

The nanofluidic devices developed here have potential for drug (biologics) analysis. The devices have several advantages over conventional analytical tools, such as short operational time (less than 1 hour), operational simplicity, and small sample volume. Therefore, the nanofluidic devices are applicable for assuring quality and safety of biologics rapidly as point-of-care monitoring system.

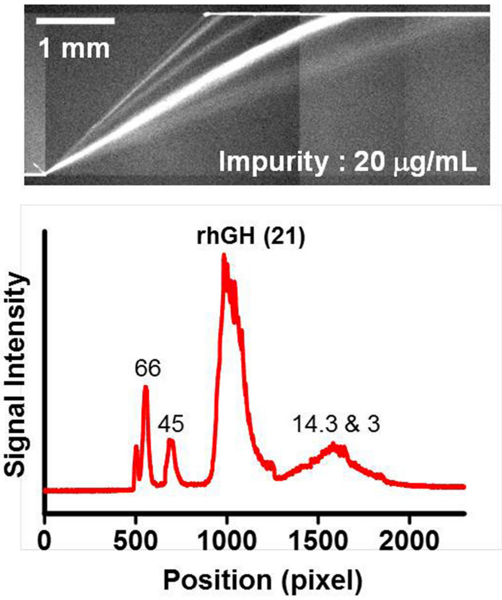

▲ Figure 1: Demonstration of purity assessment of hGH with molecular weight markers to simulate impurities using size-based separation (all samples are denatured by SDS, and the unit of molecular weight is kDa). Fluorescence profiles are measured along white dot line.

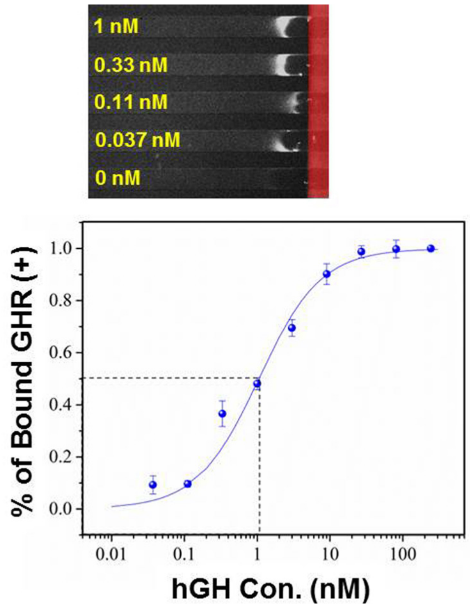

▲ Figure 2: Mobility-shift homogeneous assay for bioactivity assessment for hGH via receptor. The dose-response curve depending on hGh concentration shows 1 nM of k_D.

FURTHER READING

- S. H. Ko, W. Ouyang, D. Chandra, A. Y. Wang, P. Karande, W. Hancock, and J. Han, "A Nanofluidic Device for Rapid Biologics Quality Control," *Proc. 19th International Conference on Miniaturized Systems for Chemistry and Life Sciences*, Gyeongju, South Korea, pp. 329-331, 2015.
- W. Ouyang, S. H. Ko, A. Y. Wang, W. Hancock, and J. Han, "A Versatile Platform for Rapid Biologics Activity Assessment via Microfluidic Drug-Receptor Binding Assays," in *Proc. 19th International Conference on Miniaturized Systems for Chemistry and Life Sciences*, Gyeongju, South Korea, pp. 928-930, 2015.

Measuring Absolute Concentration of Particles in Suspension Using High Frequency B-mode Ultrasound Imaging

J. H. Lee, B. W. Anthony, D. S. Boning
Sponsorship (in part): Madrid-MIT M+Visión Consortium

Measuring particle concentration is one of the most essential procedures in life sciences, routinely performed in research laboratories as well as in clinics. For example, counts of blood cells are important parameters included in almost all blood tests. Several methods are available for measuring particle concentration. The most often used involves a hemocytometer, where the sample is placed in a chamber of known volume and particles are counted under an optical microscope. While the existing methods work well, they are not without limitations. One weakness is that the volumes analyzed by these methods are typically small. This limitation is especially problematic when the concentration is low because small analysis volumes lead to insufficient counts, which increases the measurement error. In addition, these methods are typically destructive in that the analyzed sample cannot be retrieved, which limits the volume that can be analyzed.

This work proposes an ultrasound-based concentration measurement method intended for dilute samples of micron-scale particles. Unlike the existing ultrasound-based methods, the proposed method is based on detecting individual particles in order to produce a direct particle count. It has been shown that when the scatterer size is similar to the wavelength of the ultrasound, individual scatterers can be distinguished in the B-mode image. While the number of scatterers in the image can be counted relatively easily, attaining the exact volume analyzed by the image as required to calculate the absolute concentration is not straightforward because the slice thickness of the image is unknown. The proposed method estimates the volume of a B-mode ultrasound image by examining the lateral spreading of individual echoes. In addition, by characterizing the backscatter coefficient of the echoes, this method can classify the different particle types and measure their concentrations separately. The method is entirely image-based and does not require prior characterization of the sample.

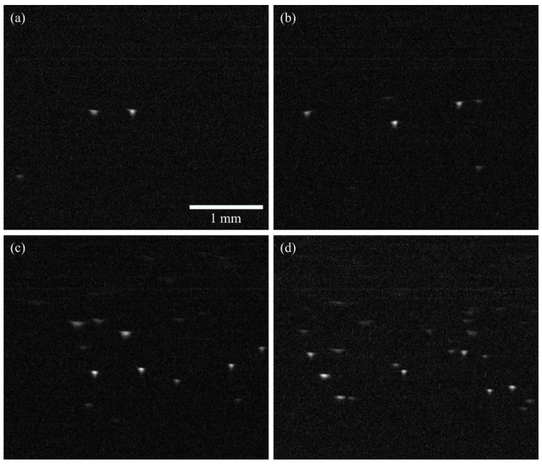

▲Figure 1: B-mode ultrasound images of 10 μm polystyrene microspheres suspended in distilled water. (a) 5 particles/μL, (b) 10 particles/μL, (c) 20 particles/μL, and (d) 50 particles/μL.

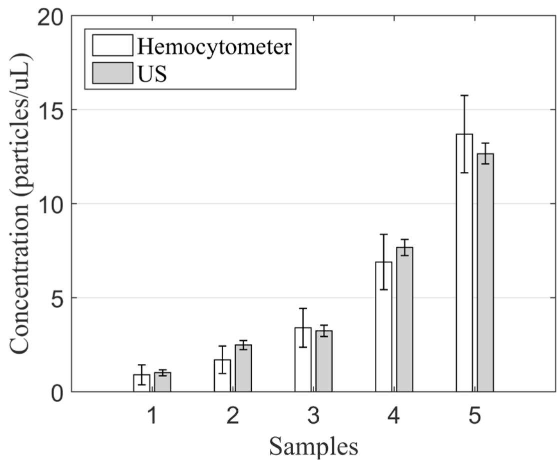

▲Figure 2: Concentration measurement results. The results from the proposed method are compared with reference measurements made with a Fuchs-Rosenthal hemocytometer.

FURTHER READING

- J. H. Lee, J. Jiménez, X. Zhang, D. S. Boning, and B. W. Anthony, "Ultrasound Image-Based Absolute Concentration Measurement Technique for Materials with Low Scatterer Concentration," presented at *2015 IEEE International Ultrasonics Symposium (IUS)*, Taipei, Taiwan, 2015.
- R. E. Baddour, M. D. Sherar, J. W. Hunt, G. J. Czarnota, and M. C. Kolios, "High-Frequency Ultrasound Scattering from Microspheres and Single Cells," *The Journal of the Acoustical Society of America*, vol. 117, no. 2, pp. 934–43, 2005.
- K. P. Mercado, M. Helguera, D. C. Hocking, and D. Dalecki, "Estimating Cell Concentration in Three-Dimensional Engineered Tissues Using High Frequency Quantitative Ultrasound," *Annals of Biomedical Engineering*, vol. 42, no. 6, pp. 1292–1304, 2014.

High-Speed Multiple-Mode Mass Sensing Resolves Dynamic Nanoscale Mass Distributions

S. Olcum, N. Cermak, S. C. Wasserman, S. R. Manalis
Sponsorship: U.S. Army Research Office, NCI

Simultaneously measuring multiple eigenmode frequencies of nanomechanical resonators can determine the position and mass of surface-adsorbed proteins and could ultimately reveal the mass tomography of nanoscale analytes. However, existing measurement techniques are slow (<1 Hz bandwidth), limiting throughput and preventing use with resonators generating fast transient signals. We develop a general platform for independently and simultaneously oscillating multiple modes of mechanical resonators (Figure 1), enabling frequency measurements that can precisely track fast transient signals within a user-defined bandwidth that exceeds 500 Hz. We use this enhanced bandwidth to resolve signals from multiple nanoparticles moving simultaneously through a suspended nanochannel resonator and show that four resonant modes are sufficient for determining their individual position and mass with an accuracy near 150 nm and 40 attograms throughout their 150 ms transit (Figure 2). We envision that our method can be readily extended to other systems to increase bandwidth, numbers of modes, or number of resonators.

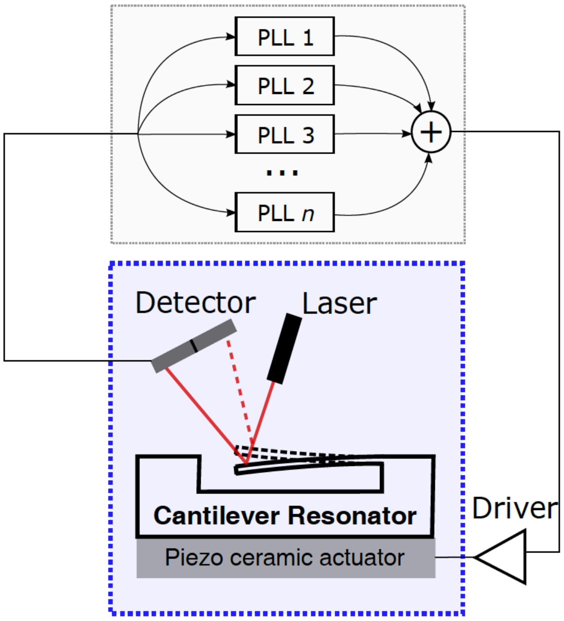

▲Figure 1: Schematic representation of the multi-mode resonator system operating in closed loop with multiple phase lock loops (one per resonant mode).

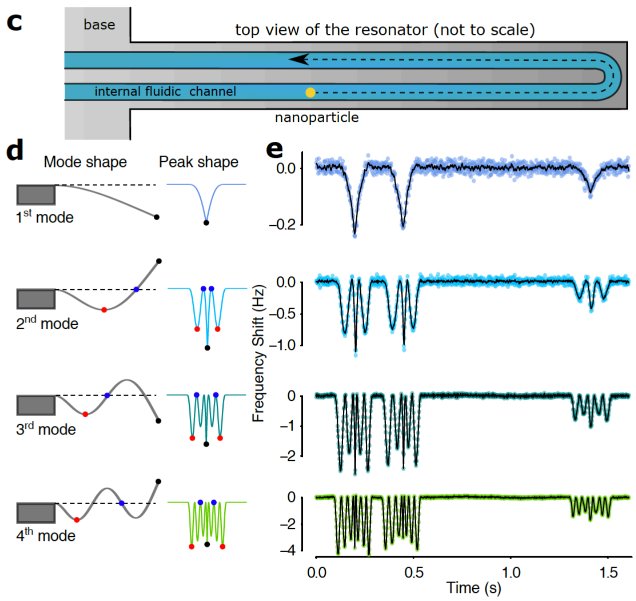

▲Figure 2: Schematic showing internal channel of resonator and bending profiles of first four resonant modes along with corresponding frequency deviations when particle with constant velocity travels through resonator. Bottom right shows frequency measurements of first four bending modes as two 150-nm and one 100-nm gold nanoparticle transit through resonator.

FURTHER READING

- S. Olcum N. Cermak S. C. Wasserman, and S. R. Manalis, "High-Speed Multiple-Mode Mass-Sensing Resolves Dynamic Nanoscale Mass Distributions," *Nature Communications*, vol. 6, pp. 7070, 2015.

Expansion Mini-Microscopy for the Identification of Pathogenic Bacteria

Y. S. Zhang, J.-B. Chang, M. M. Alvarez, G. Trujillo-de Santiago, J. Alemán, B. Batzaya, V. Krishnadoss, A. A. Ramanujam, M. Kazemzadeh-Narbat, F. Chen, P. W. Tillberg, M. R. Dokmeci, E. S. Boyden, A. Khademhosseini
Sponsorship: MIT-Tecnológico de Monterrey Nanotechnology Program, CONACyT, Fundación México en Harvard

Regretfully, even a modest but good optical microscope is frequently unavailable and unaffordable in remote and underprivileged areas. Expansion mini-microscopy (ExMM) is a novel form of microscopy, recently developed by our groups, in which specimens are physically (as supposed to optically) expanded and then observed by means of a low-cost mini-microscope (basically, a web camera with an inverted lens). Expansion microscopy and mini-microscopy have both been validated in different contexts. The technique of expansion microscopy was first introduced by Ed Boyden's group for physical expansion of human cells. Mini-microscopy was first introduced by Ali Khademhosseini´s group. The integration of these technologies is straightforward and will result in a simple and portable, but powerful and reliable diagnostic tool.

We are developing ExMM techniques to observe and identify common life-threatening pathogens. So far, Escherichia coli, a common cause of diarrhea in children and neonatal sepsis, has been taken as our first proof-of-principle model. In brief, ExMM can process a tissue or blood sample in successive steps. First, the sample is embedded in a polymeric pre-gel containing specific antibodies directed to the target pathogen (Figure 1A); a secondary antibody marked with a fluorophore and containing a covalently attached small DNA sequence is directed against the heavy chain of the primary antibody (Figure 1B); and monomers, containing a DNA complementary sequence (blue) (Figure 1C). The sample is trapped within the polymeric matrix by a photo-induced crosslinking reaction and then degraded with a proteinase enzyme, leaving the skeleton tagged with antibodies (or antibody fragments). Expansion of the polymeric matrix is achieved by addition of water and the structure defined by the fluorophores expand isotropically. The expansion is selective, meaning that only the surfaces tagged with antibodies (suspected pathogen) will expand. Finally, the sample is observed through a simple, inexpensive (~20 USD), and portable mini-microscope. Since specific antibodies can be used against different pathogens (i.e. E. coli can be antibody-marked in green and Streptococcus spp in red), the technique can conclusively and unequivocally identify the causative agent of an infection further facilitating proper intervention. More importantly, the technique does not require a trained microscopist or an expensive bench-top microscope, so we believe it will simplify, expedite, and improve the accuracy of diagnosis worldwide, and particularly in remote and underdeveloped regions.

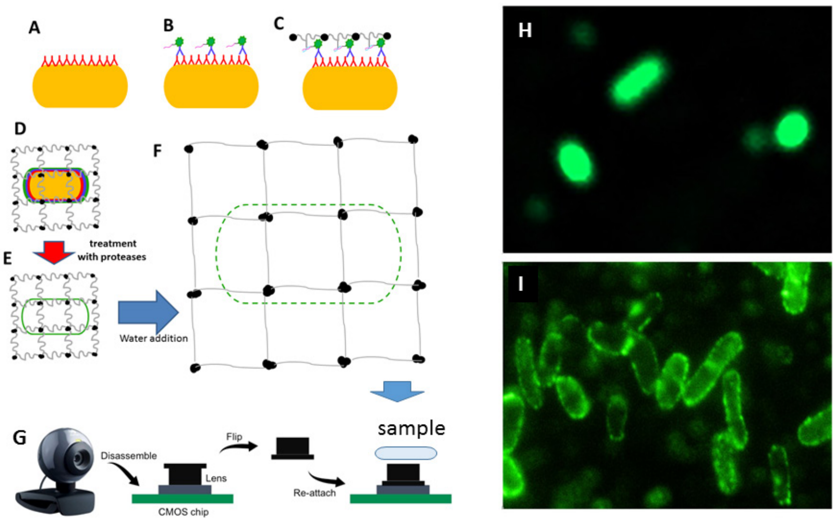

◀Figure 1: ExMM: (A) A pathogen is tagged with specific primary antibodies (red), (B) and secondary antibodies marked with a fluorophore (blue-green) and containing a small DNA sequence (pink). (C) The addition of monomers containing a DNA complementary sequence (blue), completes the expansion mix. (D) The sample is trapped within the polymeric matrix by photo-induced crosslinking. (E) Proteases are added to degrade the sample and the antibodies. (F) Expansion of the polymeric matrix is achieved by addition of water. (G) The mini-microscope is constructed by inverting the lens of a commercial web-camera. Images of *E. coli* captured with a benchtop microscope (H) before expansion, and (I) after expansion.

FURTHER READING

- F. Chen, P. W. Tillberg, and E. S. Boyden, "Expansion Microscopy," *Science*, vol. 19, pp. 543-548, January 2015.
- Y. S. Zhang, Y. S. Zhang, J.-B. Chang, M. M. Alvarez, G. Trujillo-de Santiago, J. Alemán, B. Batzaya, V. Krishnadoss, A. A. Ramanujam, M. Kazemzadeh-Narbat, F. Chen, P. W. Tillberg, M. R. Dokmeci, E. S. Boyden, and A. Khademhosseini, "Hybrid Microscopy: Enabling Inexpensive High-Performance Imaging through Combined Physical and Optical Magnifications," *Scientific Reports*, vol. 6, pp. 22691:1-10, March 2016.

High-Efficiency Capture of Pathogens in Chaotic Flows

G. Trujillo-de Santiago, G. Prakash, A. Risso, P. I. Sánchez-Rellstab, Y. S. Zhang, M. M. Alvarez, A. Khademhosseini
Sponsorship: MIT-Tecnológico de Monterrey Nanotechnology Program, CONACyT, Fundación México en Harvard

Infectious diseases, both of viral and bacterial origin, continue to be a health threat to millions of people in developed and underdeveloped countries. In cases of sepsis or viral infections such as Ebola disease and HIV, effective capture and removal of the pathogenic agent from the bloodstream is one potentially successful treatment strategy (i.e., pathogen blood cleansing). We are developing filter-less technologies for the direct capture of *Escherichia coli* (as a model pathogen) from the bloodstream. In a later stage of this project, we will work on the capture of viruses (i.e., Ebola virus-like-particles) using an analogous approach.

Our strategy is simple: We use a portable/disposable system for the continuous capture of bacterial particles circulating through a microfluidic chamber. The system is based on the specific recognition of proteins on *E. coli* membranes; it integrates the use of (a) anti-*E. coli* polyclonal antibodies, (b) magnetic nanoparticles (MNP), (c) a microfluidic chaotic flow system, and (d) a neodymium magnet. Anti-*E. coli* antibodies are covalently immobilized within commercial magnetic nanoparticles to fabricate nanoparticles that will bind *E. coli* bacteria (Figure 1B). Our experiments compare the performance of different immobilization strategies (amino-carboxylic covalent binding and streptavidin-biotin binding) and different magnetic nanoparticle sizes (range 30–800 nm). The heart and distinctive feature of our system is a microfluidic chamber where the *E. coli* binding particles and the bacteria are mixed by the action of a laminar chaotic flow produced by the alternating rotation of two cylinders (Figure 1C). The intimate contact induced by this chaotic laminar flow promotes bacteria capture by individual nanoparticles or nanoparticle clusters (Figure 1D). The trapped *E. coli* are concentrated by a simple magnet located downstream from the microchamber (Figure 1E).

This platform has key advantages over currently available methods, which are mostly based on the use of microfluidic channels or filtering membranes: (a) It is faster (overall capture times in the order of 1–5 minutes); (b) It offers superior capture due to the intimate mixing induced by the chaotic flow; (c) It is easy to use, which reduces labor efforts and eliminates the need for dedicated and costly infrastructure.

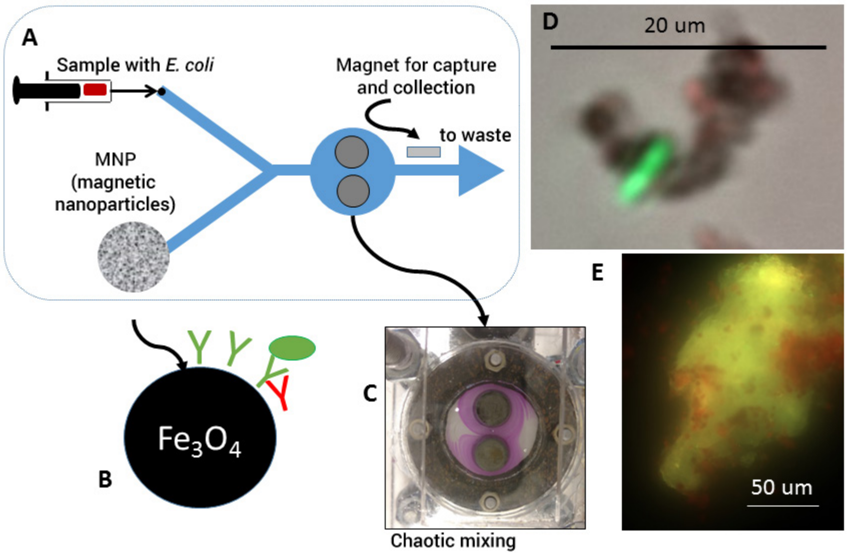

◀ Figure 1: Our pathogen capture system integrates magnetic nanoparticles (MNPs) functionalized with antibodies, a microfluidic chaotic chamber, and a static magnet. (A) General scheme. A sample spiked with *E. coli* bacteria is mixed with (B) MNPs functionalized with anti-*E. coli* antibodies (green Y). The presence of anti-*E.coli* antibodies can be validated by marking with a secondary antibody (red Y). (C) Mixing of the functionalized MNPs and the bacteria occurs under the action of a chaotic flow induced by the alternating rotation of two cylinders. (D) Zoomed view of a bacterium captured in an MNP cluster. (E) The action of the magnet concentrates the bacteria-loaded MNPs.

FURTHER READING

- WHO. Fact Sheets. "Infectious Diseases." [Online]. Available: http://www.who.int/topics/infectious_diseases/factsheets/en/.

Magnetic Nanoparticles for Wireless Manipulation of Neural Circuits

R. Chen, M. G. Christiansen, C. Loynachan, G. Romero, A. W. Senko, P. Anikeeva
Sponsorship: NSF, DARPA

Weak magnetic susceptibility and conductivity of biological matter suggest the application of alternating magnetic fields (AMF) with low amplitudes (~1-10s mT) and frequencies in the 100-kHz range for delivery of signals into deep-tissue targets. One can use nanomaterial transducers to convert the externally applied AMF into biological stimuli such as mechanical deformation or thermal perturbation. The latter can be achieved by magnetic nanoparticles 5-30 nm in diameter composed of biochemically stable and benign ferrites, such as iron oxide. When exposed to AMF with the abovementioned parameters, these MNPs undergo magnetization reversal, and the resulting hysteretic power loss is dissipated as heat.

Guided by the dynamic hysteresis model, we have previously engineered a palette of ferrites and identified the AMF conditions leading to high heating efficiencies in these nanomaterials. We have then applied the concept of magnetothermal stimulation to two biological systems: wireless excitation of neural activity and remote disaggregation of amyloid beta (Aβ) deposits characteristic of Alzheimer's disease. To enable AMF-driven neural excitation, we took advantage of a heat sensitive calcium channel TRPV1 (a capsaicin receptor), which is broadly expressed across the nervous system. We found that exposure to AMF in the presence of MNPs triggers TRPV1 and the corresponding influx of calcium ion into neurons leading to action potential firing (Figure 1). Externally controlled disruption of ~10-μm–sized Aβ aggregates into ~100s-nm fragments was observed when MNPs specifically targeted to Aβ via a coating with a short peptide (LPFFD) were exposed to AMF for 3-6 hrs (Figure 2).

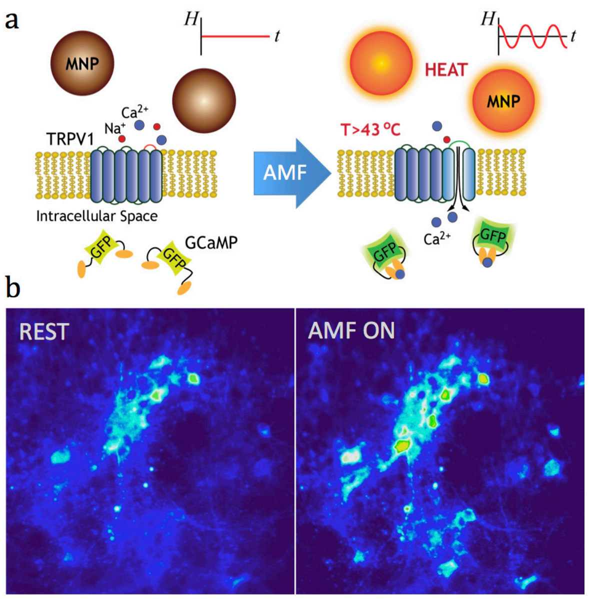

▲Figure 1: (a) Magnetothermal stimulation schematic. MNP = magnetic nanoparticle; TRPV1 = heat sensitive (calcium) ion channel; AMF = alternating magnetic field; GFP = green fluorescent protein; GCaMP6 = fluorescent calcium ion indicator. (b) AMF evokes activity in neurons in the presence of MNPs as recorded by GCaMP6 fluorescence increase.

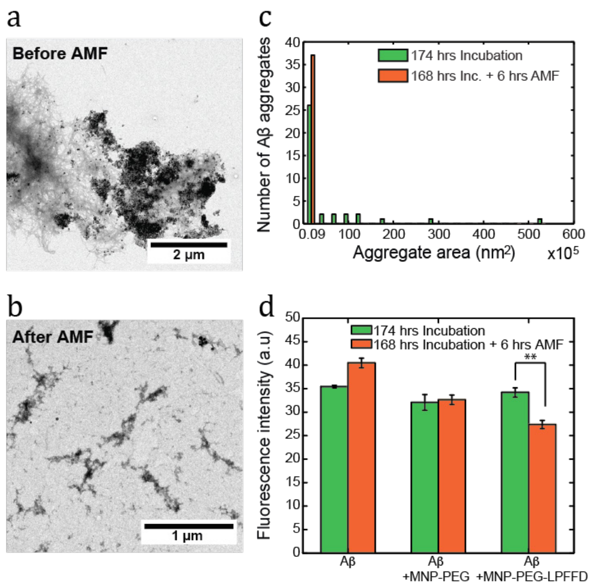

▲Figure 2: (a) Amyloid beta (Aß) aggregate decorated with MNPs. (b) Aggregate dissociated by magnetothermal stimulus transduced by MNPs. (c) Size distribution of aggregates as measured by transmission electron microscopy with and without exposure to AMF. (d) Fluorescence of the Aß stain thioflavin T indicates disruption of aggregates using targeted MNPs. PEG = poly(ethylene glycol); LPFFD = targeting peptide.

FURTHER READING

- R. Chen, M. G. Christiansen, and P. Anikeeva, "Maximizing Hysteretic Losses in Magnetic Ferrite Nanoparticles via Model-Driven Synthesis and Materials Optimization," *ACS Nano*, vol. 7, pp. 8990-9000, 2013.
- R. Chen, G. Romero, M. G. Christiansen, A. Mohr, and P. Anikeeva, "Wireless Magnetothermal Deep Brain Stimulation," *Science* 347, pp. 1477-1480, 2015.
- C. N. Loynachan, G. Romero, M. G. Christiansen, R. Chen, R. Ellison, T. T. O'Malley, U. P. Froriep, D. M. Walsh, and P. Anikeeva, "Targeted Magnetic Nanoparticles for Remote Magnetothermal Disruption of Amyloid-β Aggregates," *Adv. Health. Mater.*, vol. 4, pp. 2100-2109, 2015.

Circuits and Systems for Information Processing, Multimedia, Communication, Energy Management, and Sensing

Towards Real-Time Super-Resolution on Compressed Video

Z. Zhang, V. Sze
Sponsorship: MIT

High-resolution displays are increasingly popular, calling for faster algorithms to upsample the existing low-resolution video content. State-of-the-art super-resolution algorithms mainly address the visual quality of the output instead of real-time throughput. Even the fastest existing super-resolution algorithm, SRCNN, takes 0.4 second to process a single frame of size 256×256. This speed is far behind the requirement of a real-time super-resolution system, which should be capable of processing 30 frames per second on full HD videos (1920×1080).

We propose a framework called Free Adaptive Super-Resolution via Transfer (FAST) to accelerate any image-based super-resolution algorithm running on compressed videos. FAST leverages the similarity between adjacent frames in a video. Given the output of a super-resolution algorithm on one frame, FAST adaptively transfers the super-resolution to the adjacent frame so that we can avoid running the super-resolution algorithm on the adjacent frame. The transferring process has negligible computation cost because the required information including motion vectors, block size, and prediction residual is already embedded in the compressed video for free.

FAST also adapts to video content, which is composed of frames with varying block sizes. It adaptively enables and disables transfer for each block depending on the quality of motion compensation of the video encoder. Note that the blocks are non-overlapping so that the redundant computations for overlapping blocks in many existing super-resolution algorithms are avoided, which significantly reduce the complexity of the framework. The resulting artifacts are handled by low-complexity deblocking filters.

FAST was evaluated with existing state-of-the-art super-resolution algorithms on the common test sequences that were used in the development of the HEVC video compression standard. FAST accelerates all the tested super-resolution algorithms by up to an order of magnitude with acceptable quality loss of up to 0.2 dB. This result proves that FAST can accelerate any super-resolution algorithm, potentially enable running super-resolution algorithms to upsample streamed videos for large screens in real time.

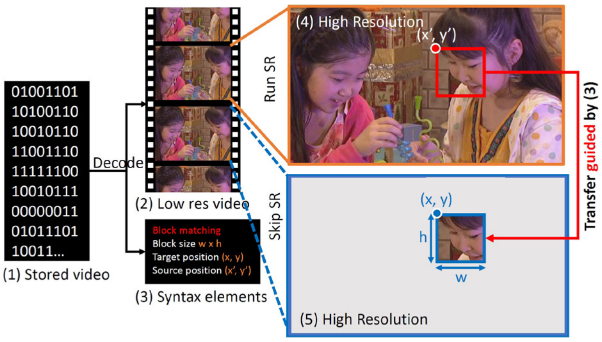

▲ Figure 1: Pipeline of FAST: From the compressed video (1), the video decoder decodes the low-resolution frames (2) and syntax elements (3). The SR algorithm is applied to the first frame to obtain a high-resolution output (4). FAST adaptively transfers it to the second frame (5).

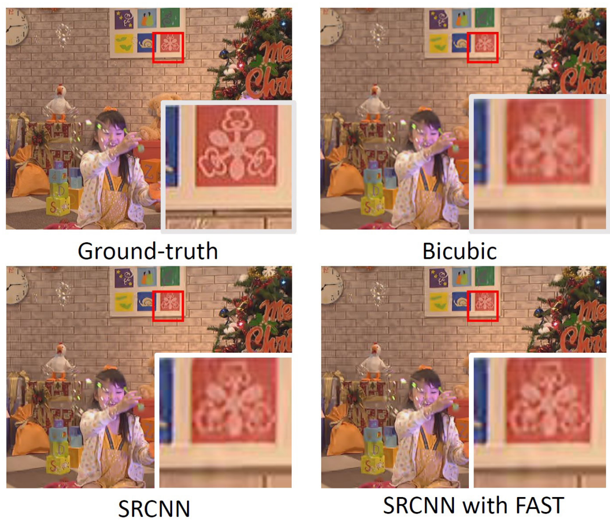

▲ Figure 2: FAST result: Running SRCNN with FAST preserves the rich high-frequency details that SRCNN generates compared to the blurry output of bicubic interpolation.

FURTHER READING

- C. Dong, C. C. Loy, K. He, and X. Tang, "Learning a Deep Convolutional Network for Image Super-Resolution," *European Conference on Computer Vision*, New York: Springer, pp. 189-199, 2014.
- C. Liu and D. Sun, "A Bayesian Approach to Adaptive Video Super Resolution," in *2011 IEEE Conference on Computer Vision and Pattern Recognition (CVPR)*, pp. 209-216, 2011.
- G. J. Sullivan, J. Ohm, T. K. Tan, and T. Wiegand, "Overview of the High Efficiency Video Coding (HEVC) standard," *IEEE Transactions on Circuits and Systems for Video Technology*, vol. 22, no. 12, pp. 1649-1668, December 2012.

Low-Power Hardware Accelerator for Object Detection with Deformable Parts Model

A. Suleiman, Z. Zhang, V. Sze
Sponsorship: Texas Instruments, DARPA

While fully autonomous cars are still in development, the advanced driver assistant systems (ADAS) is being improved and becoming standard in many cars. Using computer vision to support autonomy is one of the cheapest solutions compared to more complex approaches like Lidar. Increasing object detection accuracy is essential for these types of applications. In our previous project, we developed an object detection accelerator based on histogram of oriented gradients (HOG) features; it supports 12 scales per frame for accuracy and robustness, processes 1080HD videos to detect far objects, runs at 60fps in real time; which gives time to react in fast changing environment, and consumes only 45.3mW.

In this project, we present an object detection hardware accelerator that has higher detection accuracy by using deformable parts models (DPM). The chip processes 1080HD videos in real-time and supports multi-scale detection with a throughput of 30fps consuming only 58.6mW, and it is tested to run up to 60fps. The DPM algorithm is an extension of the HOG-based detection; both use similar HOG features. In DPM, the detection is done on two levels as shown in Figure 1: root and parts. Using the root template, the object is searched for as a whole in the image pyramid with the conventional sliding window approach. To enhance the detection accuracy, 8 different templates are defined for 8 parts of the object and each part is searched for separately at 2x image resolution relative to the root. Eventually, the root score and the 8 parts scores are added together with a deformation penalty. Being able to detect object parts and allowing parts movements by deformation increases the detection accuracy significantly, Figure 2. For example, when DPM and HOG-based detection are compared, the detection accuracy is doubled on INRIA person dataset.

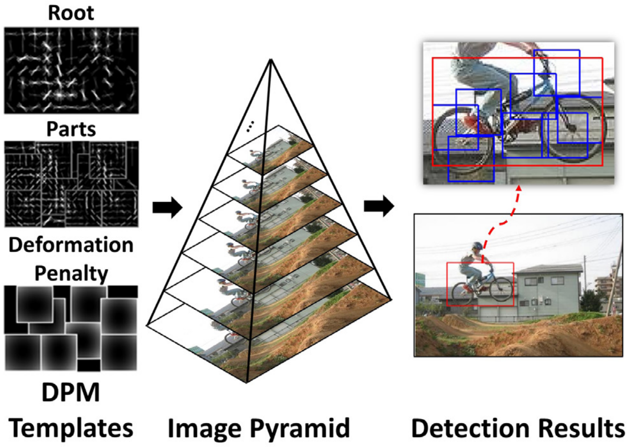

▲Figure 1: Detection with bicycle DPM templates. 8 part templates are defined at 2x resolution relative to the root. Each part has a deformation penalty. The darker regions indicate lower deformation cost.

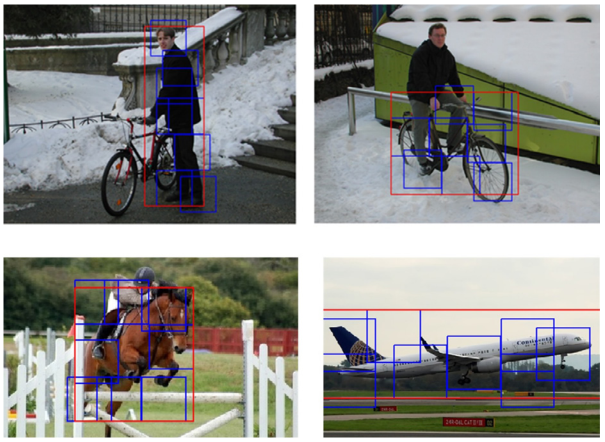

▲Figure 2: Detection examples with different object classes (person, bicycle, horse, and aeroplane). Red boxes highlight the object position, while blue boxes highlight the optimal position for each of the 8 parts.

FURTHER READING

- A. Suleiman, Z. Zhang, and V. Sze, "A 58.6mW Real-Time Programmable Object Detector with Multi-Scale Multi-Object Support Using Deformable Parts Model on 1920x1080 Video at 30fps," presented at *IEEE Symposium on VLSI Circuits*, Honolulu, HI, June 2016.
- A. Suleiman and V. Sze, "Energy-Efficient HOG-based Object Detection at 1080HD 60 fps with Multi-Scale Support," *IEEE Workshop on Signal Processing Systems*, pp. 1-6, October 2014.
- P. F. FelzenszwalR. B. Girshick, D. McAllester, and D. Ramanan, "Object Detection with Discriminatively Trained Part-Based Models," *IEEE Transactions on Pattern Analysis and Machine Intelligence*, vol. 32, pp. 1627-1645, September 2010.

Energy-Efficient Reconfigurable Accelerator for Deep Convolutional Neural Networks

Y.-H. Chen, T. Krishna, J. Emer, V. Sze
Sponsorship: DARPA YFA, CICS, Intel

Deep learning using convolutional neural networks (CNNs) give unprecedented accuracy on many computer vision tasks, such as object detection, recognition, and segmentation. These state-of-the-art CNNs are orders of magnitude larger than the CNNs used in the 1990s, when CNNs were first introduced, requiring not only a larger number of layers but also millions of filter weights in varying shapes. For instance, AlexNet uses 2.3 million weights (4.6MB of storage) and requires 666 million MACs per 227x227 image (13 kMACs/pixel). VGG16 uses 14.7 million weights (29.4 MB of storage) and requires 15.3 billion MACs per 224x224 image (306 kMACs/pixel).

The size of these CNNs poses both throughput and energy efficiency challenges to the underlying processing hardware. Specifically, large number of weights, filters, and channels results in substantial data movement, which consumes significant energy. Today, CNN processing is carried out mostly in data centers or by high-end GPUs, where power dissipation often limits the achievable throughput. In the future, CNN processing will also be carried out on embedded devices rather than in the cloud, due to privacy, latency, or communication bandwidth concerns; these battery-powered devices will have even tighter energy and power constraints. Therefore, specialized CNN accelerators, which give higher throughput and improved energy-efficiency over general purpose platforms, will be critical for the implementation of future vision systems.

This work describes a CNN accelerator that can deliver state-of-the-art accuracy with minimum energy consumption in the system (including DRAM) in real-time, by using two key methods: (1) efficient dataflow and supporting hardware (spatial array, memory hierarchy, and on-chip network) that minimize data movement by exploiting data reuse and support different shapes and (2) exploitation of data statistics to minimize energy through zeros skipping/gating to avoid unnecessary reads and computations and data compression to reduce off-chip memory bandwidth, which is the most expensive data movement.

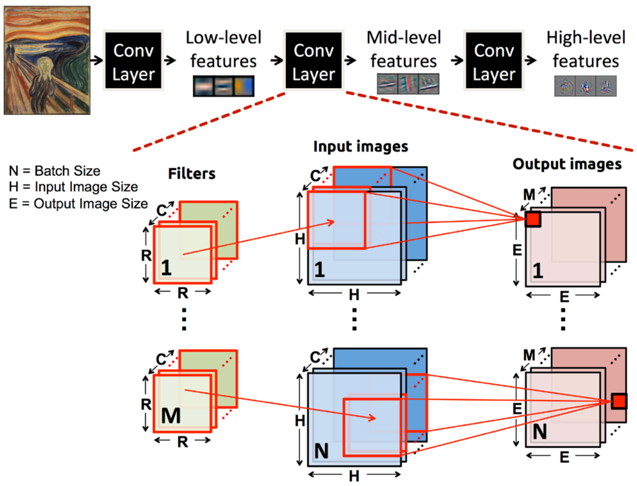

▲Figure 1: The CNN compute pipeline consists of many layers, each of which performs convolution-like processing to extract abstract features in the image.

CNN	LeNet	AlexNet	VGG16
Year	1989	2012	2014
# of Convolution Layers	2	5	13
# of weights	50k	2.3M	14.7M
Ratio (memory)	**1x**	**46x**	**294x**
# MACs	322k	666M	15.3G
Ratio (Computation)	**1x**	**2067x**	**47660x**

AlexNet

Layer	Filter Size (R)	# Filters (M)	# of Channels (C)	Stride
1	11x11	96	3	4
2	5x5	256	48	1
3	3x3	384	256	1
4	3x3	384	192	1
5	3x3	256	192	1

▲Figure 2: State-of-the-art deep CNNs require not only large number of layers but also millions of filter weights and varying shapes (i.e., filter sizes, # of filters, # of channels).

FURTHER READING

- A. Krizhevsky, I. Sutskever, and G. E. Hinton, "ImageNet Classification with Deep Convolutional Neural Networks," *Advances in Neural Information Processing Systems* 25, pp. 1097-1105, 2012.
- K. Simonyan and A. Zisserman, "Very Deep Convolutional Networks for Large-Scale Image Recognition," *CoRR*, abs/1409.1556, 2014.

Low-Power Security-Acceleration Core for the Internet of Things

U. Banerjee, C. Juvekar, A. P. Chandrakasan
Sponsorship: Analog Devices, Inc.

The Internet of Things (IoT) has introduced a vision of an Internet where all computing and sensing devices are interconnected. Digitally connected devices are encroaching on every aspect of our lives, including our homes, cars, offices, and even our bodies. Researchers estimate that there will be over 40 billion wireless connected devices by 2020. On one hand, the IoT enables fundamentally new applications, but on the other, these devices are attractive targets for cybercriminals, thus making IoT security a major concern. According to a report on the state of IoT security in 2015, 90% of IoT devices have collected personal data, but 70% of them used unencrypted network services.

Most commercial IoT transceivers either have no security implementations in hardware or only support symmetric key primitives like Advanced Encryption Standard (AES). To achieve end-to-end security in IoT networks, public key algorithms, like elliptic curve cryptography (ECC) are indispensable. Software implementations of these algorithms involve significant computational costs, and the power consumption presents a bottleneck in resource-constrained environments. In this work, we propose to design low-power security-acceleration hardware that interfaces with a standard micro-processor and supports ECC for key exchange and digital signatures, along with standard cryptographic components like AES (Figure 1), thus alleviating the security and efficiency trade-off observed in embedded devices.

Our work also focuses on optimizing network security protocols for efficient implementation in embedded devices. Standard implementations of these protocols tend to have a large communication overhead, which becomes an additional concern for battery-powered or energy-harvesting IoT devices. Therefore, our proposed hardware can not only secure private data using low power cryptographic computations, but also reduce energy consumption of the RF transceiver (Figure 2).

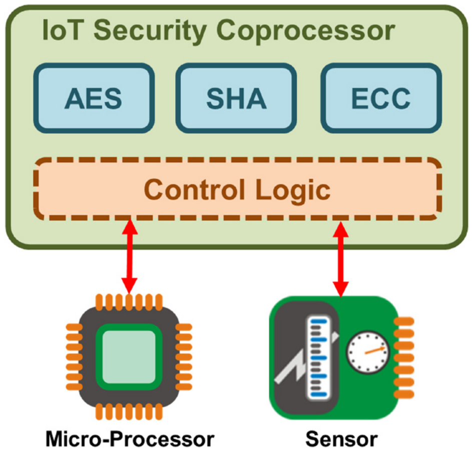

▲ Figure 1: Security coprocessor for IoT to accelerate cryptographic primitives like AES, SHA and ECC. The hardware accelerator, which interfaces with a micro-processor, can be used to implement standard transport layer security protocols.

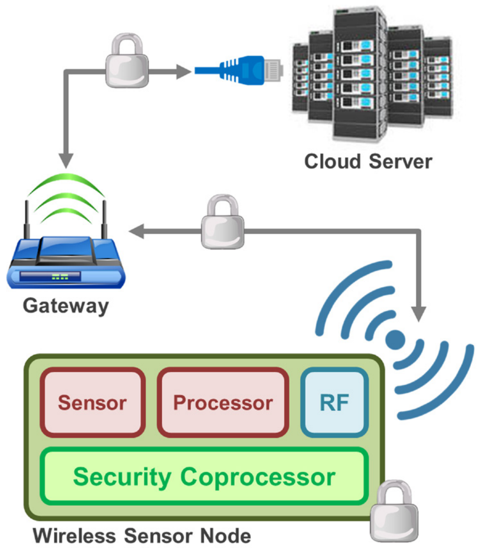

▲ Figure 2: Wireless sensor node using the proposed security coprocessor to send encrypted data all the way to the cloud. Application payloads are fully encrypted so that intermediate nodes can process and modify network addresses without gaining access to the actual data.

FURTHER READING

- D. Miessler, "The State of IoT Security," 2015. [Online]. Available: http://community.hpe.com/t5/Protect-Your-Assets/The-State-of-IoT-Security-2015/ba-p/6744413.
- P. Miranda, M. Siekkinen, and H. Waris, "TLS and Energy Consumption on a Mobile Device: A Measurement Study," *IEEE Symposium on Computers and Communications (ISCC)*, pp. 983-989, 2011.

Ultra Low-Power, High-Sensitivity Secure Wake-Up Transceiver for the Internet of Things

M. R. Abdelhamid, A. Paidimarri, A. P. Chandrakasan

Nanopower "Internet of Things" (IoT) devices deployed in short-range personal health devices, home automation systems and longer-range industrial monitoring systems all consume a large portion of energy on their wireless communication systems. However, long battery lifetimes or energy-harvested operation is desired in order to ease their adoption. In this work, we propose protocol optimizations for sensor-node driven communications. For base-station driven communication, we propose to achieve power reduction through an ultra-low-power wake-up receiver with optimizations in the protocols as well as the circuit design.

Wireless protocols such as Bluetooth low energy (BLE) are optimized for short-length packets with small preambles and reduced header sizes. However, low duty-cycle performance in the default connected-mode of operation is limited by periodic beacons and the requirement that the low-power sensor node absorbs the timing uncertainties and associated guard time intervals. As shown in Figure 1, the analysis of a commercial BLE radio performance shows that the average total power is much higher than the standby power of the radio, which presents opportunities for significant power reduction through protocol optimization. On the wake-up receiver chain, the design can exploit different trade-offs in the protocol to reach a sub-μW average power consumption while maintaining the specifications by the base-station. Therefore, the sensitivity/power trade-off of the receiver can be mitigated through an optimized protocol and system. Additionally, the tremendous growth of IoT devices allows open communication among all sorts of devices. With such a huge amount of data flowing through the network, security becomes a critical issue. Hence, we propose the wake-up transceiver system shown in the block diagram of Figure 2. The transceiver incorporates a transmitter that provides small amounts of data sporadically upon request and creates a two-way communication channel for secure wake-ups and transmissions.

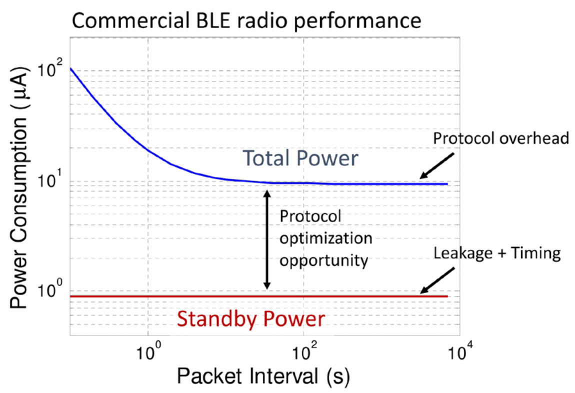

▲ Figure 1: Commercial BLE performance analysis.

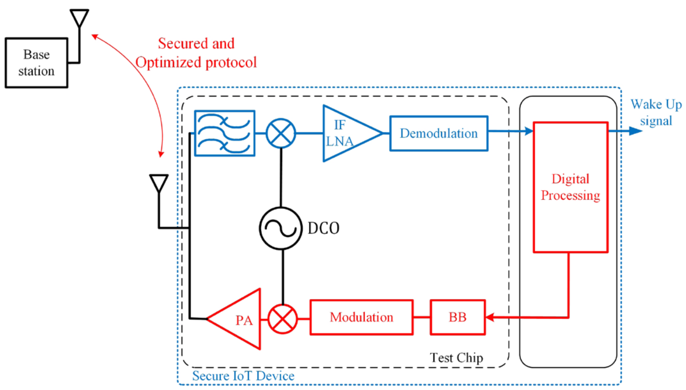

▲ Figure 2: Block diagram of the proposed wake-up transceiver.

FURTHER READING

- C. Salazar, A. Kaiser, A. Cathelin, and J. Rabaey, "A -97dBm-sensitivity Interferer-resilient 2.4GHz Wake-up Receiver using Dual-IF Multi-N-Path Architecture in 65nm CMOS," presented at *IEEE International Solid-State Circuits Conference*, San Francisco, CA, February 2015.
- O. Seunghyun, N. Roberts, and D. Wentzloff, "A 116nW Multi-band Wake-up Receiver with 31-bit Correlator and Interference Rejection," in *Proc. 2013 IEEE Custom Integrated Circuits Conference (CICC)*, pp. 1-4, 22-25, 2013.

A Noise-Efficient Chopper Amplifier Using a 0.2V-Supply Input Stage

F. M. Yaul, A. P. Chandrakasan
Sponsorship: Shell, Texas Instruments

Wireless sensor nodes often monitor low-bandwidth signals from sensors that may be small in amplitude. Examples include biopotential signals for medical applications and vibration and strain signals for industrial monitoring applications. Typically, a low-noise instrumentation amplifier (LNIA) is used to provide a high-impedance sensor interface with good common-mode rejection (CMR). Electroencephalogram (EEG) monitoring is one application where LNIA designers have targeted sub-microvolt input-referred noise over a sub-100Hz signal band. Prior work to improve the energy-efficiency of LNIAs includes chopping techniques, current-reuse through amplifier stacking, and low-voltage design reaching 0.45V.

This work explores the limits of supply voltage reduction and focuses on the input stage of the LNIA, which consumes the highest amount of bias current in order to reduce its input-referred noise. Supply voltage reduction has typically been limited by topological constraints such as transistor headroom requirements and signal swing, as a conventional differential pair input stage has at least three stacked devices.

We present a chopper amplifier that uses a 0.2V-supply for the input stage followed by a 0.8V-supply amplifier stage. The high input-stage current needed to reduce the input-referred noise is drawn from the 0.2V supply, significantly reducing power consumption. The 0.8V stage provides high gain and signal swing, improving linearity. Biasing and common-mode rejection (CMR) techniques for the 0.2V stage are also presented. The test chip was fabricated in a 0.18-μm CMOS process and achieves sub-μV_{RMS} input noise from 0.5-670Hz while also achieving sub-μW power consumption. The test chip was also used to measure EEG signals, demonstrating high-impedance low-noise sensor measurement capability.

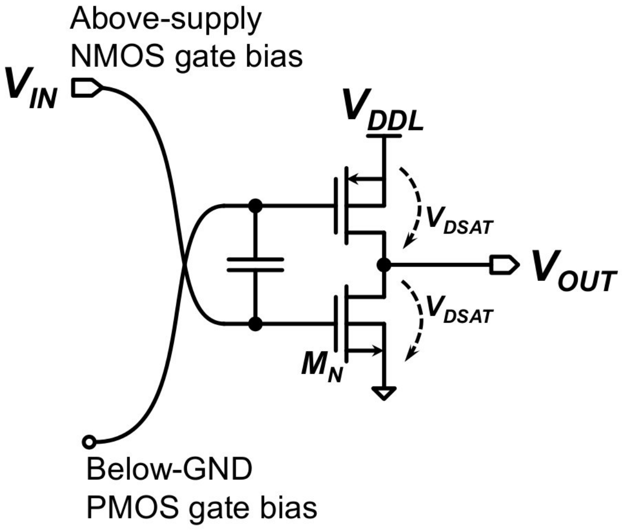

▲Figure 1: Supply-squeezed inverter concept. The supply voltage may be reduced to just $2V_{DSAT}$ while keeping both devices saturated.

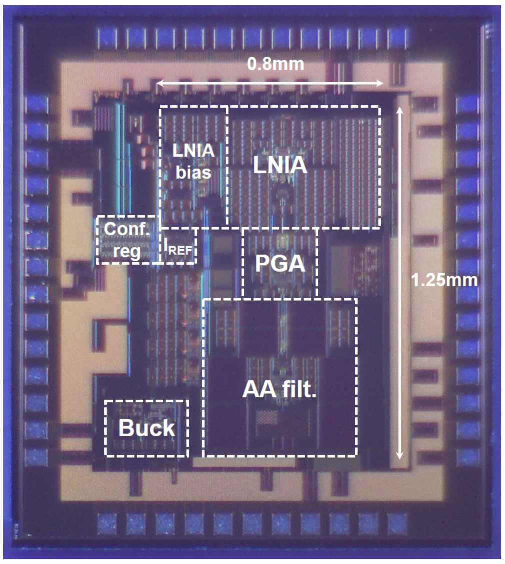

▲Figure 2: Die micrograph showing major circuit blocks in the system. The signal path occupies 1 mm^2.

FURTHER READING

- F. M. Yaul and A. P. Chandrakasan, "A Sub-μW 36nV/√Hz Chopper Amplifier for Sensors Using a Noise-Efficient Inverter-Based 0.2V-Supply Input Stage," *IEEE International Solid State Circuits Conference (ISSCC)*, San Francisco, CA, 2016.
- Y. P. Chen, D. Blaauw, and D. Sylvester, "A 266nW Multi-Chopper Amplifier with 1.38 Noise Efficiency Factor for Neural Signal Recording," *IEEE Symposium on VLSI Circuits*, pp. 1-2, June 2014.

Efficiency Maximization for Wireless Charging

N. Desai, A. P. Chandrakasan
Sponsorship: Hon Hai Precision Co., Ltd.

A large number of low-power sensors and wearable devices will operate in indoor environments in the near future. Wireless power transfer is well suited for powering such devices without increasing infrastructure costs. However, inductor-based wireless charging, which is a commonly used solution, suffers from a limited range. Since the receivers are low-power devices, they can also be recharged infrequently by a portable wireless power transmitter (that could be integrated into a smartphone, for example) with short bursts of energy. This is shown in Figure 1, with a wireless charging power amplifier (PA) integrated into a smartphone that powers a transmitter coil that is part of a resonant tank. The same near-field coil that implements wireless charging and/or NFC on most smartphones can potentially be multiplexed to turn the phone into a wireless power transmitter when required.

The receiver in Figure 1 is an Internet-of-Things (IoT) device that has a receiver coil built in, also part of a series tank that is resonant at the same frequency. A rectifier charges the battery on the device. The ac input characteristics of the rectifier can be modeled as an equivalent non-linear resistor whose value depends on both the input ac and output dc voltages since the rectifier is a non-linear device. As the battery on the receiver charges up, the ac input resistance of the rectifier increases.

Figure 2 illustrates the dependence of the end-to-end efficiency of a coupled resonator system similar to the one in Figure 1, but with the rectifier replaced by a load resistor for different coupling factors between the transmitter and receiver coils. The efficiency at a given coupling factor has a maximum at a finite value of the load resistance, which changes as the coupling factor changes. Since both the coupling factor and the load resistance seen by the receiver coil can change during charging, the latter due to the increasing battery voltage, the maximum-efficiency point needs to be tracked dynamically by the rectifier. This tracking ensures maximum average efficiency across the entire charging duration of the receiver battery.

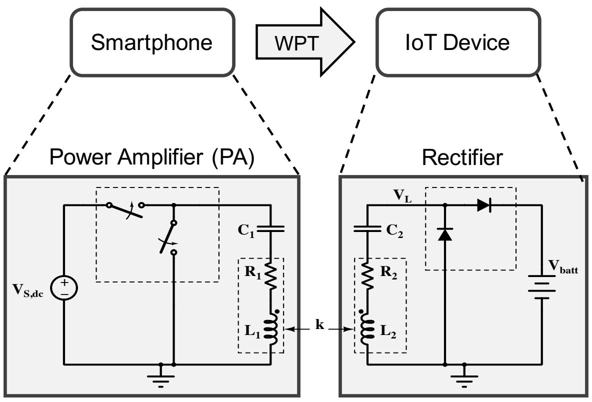

▲ Figure 1: System architecture of a portable wireless power transmitter charging a small IoT device.

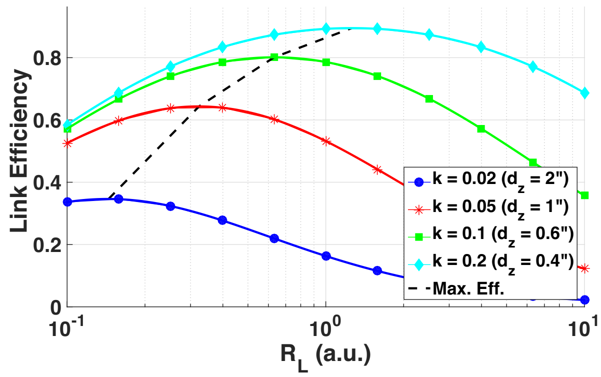

▲ Figure 2: Theoretical plot of system efficiency of wireless power transmitter using coupled resonators while both the load resistance and the coupling factor are changed.

FURTHER READING

- A. Karalis, J. D. Joannopoulos, and M. Soljačić, "Efficient Wireless Non-radiative Mid-range Energy Transfer," *Annals of Physics*, vol. 323, no. 1, pp. 34-48, January 2008.
- M. Zargham and P. G. Gulak, "The Circuit Theory Behind Coupled-mode Magnetic Resonance-based Wireless Power Transmission," *IEEE Transactions on Circuits and Systems – Part I: Regular Papers*, vol. 59, no. 9, pp. 2065-2074, September 2012.

Fully Integrated Thermal Energy Harvesting System with 50mV Start-Up

P. Garcha, M. Araghchini, M. Chen, N. Desai, D. El-Damak, J. Troncoso, D. Buss, J. H. Lang, A. P. Chandrakasan
Sponsorship: Texas Instruments

Energy harvesting allows us to use ambient sources of energy for powering small electronic systems. Such self-powered operation can be extremely useful in wearable electronics, remote sensor nodes, and other wireless sensor networks that are widely used for monitoring and sensing applications, as it eliminates the need for battery replacement. Most of the energy harvesters employ boost converters for stepping up voltages, which can operate from as low as 10 mV input voltage. However, they typically need > 200 mV in order to start up initially. Current solutions for achieving a low-voltage start-up require the use of bulky off-chip transformers. Our research goal is to provide a proof-of-concept for a fully integrated start-up system, which can cold-start from 50 mV using on-chip magnetics and also be used as a complete energy harvesting system for ultra low power applications.

Our approach involves designing on-chip transformers in Texas Instruments' flux gate technology (Figure 1) for use in a Meissner oscillator circuit (Figure 2). The much lower Q-factors of these on-chip transformers than their discrete counterparts pose new design and optimization challenges. Hence, we have derived analytical expressions that are well-suited for use with the on-chip magnetics in order to co-optimize the oscillator components.

An optimized depletion-mode MOS device was fabricated and tested with an off-chip transformer and found to start oscillating at much lower voltages than the state-of-the-art oscillators. An on-chip transformer design with the potential of low-voltage start-up has been identified, and will be fabricated in the near future to have an integrated Meissner oscillator circuit. We have also designed and taped-out a switched capacitor DC-DC circuit to be cascaded with the Meissner oscillator block. The switched capacitor chip will rectify and boost the voltage to >1 V to have a complete start-up system for energy harvesting.

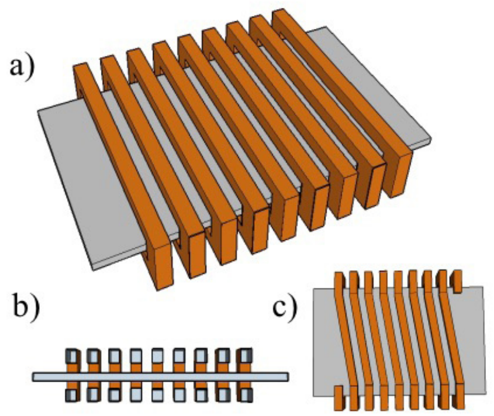

▲Figure 1: Flux gate inductor having a permalloy core (that sits above the top metal layer) with copper windings around it; a) 3D view, b) cross-sectional view, and c) bottom view.

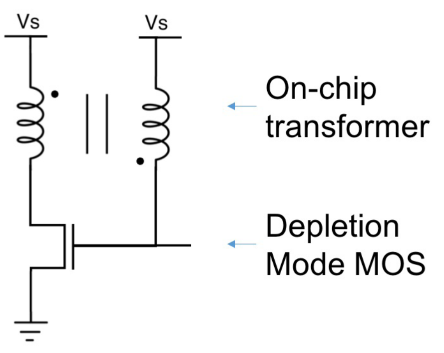

▲Figure 2: Meissner oscillator circuit, to be built with Texas Instruments' flux gate technology and specially fabricated MOS device, and co-packaged for an integrated proof-of-concept solution.

FURTHER READING

- A. Shrivastava, N. E. Roberts, O. U. Khan, D. David, B. H. Calhoun, and S. Member, "A 10 mV-Input Boost Converter With Inductor Peak Current Control and Zero Detection for Thermoelectric and Solar Energy Harvesting With Kick-Start," *IEEE Journal of Solid State Circuits*, vol. 50, no. 8, pp. 1820–1832, 2015.
- J. Luo, M. Boutell, and C. Brown, "LTC3108 - Ultralow Voltage Step-Up Converter and Power Manager," *Data Sheet*, vol. 23, no. 2, pp. 1–20, 2010.
- N. V. Desai and A. P. Chandrakasan, "A Bipolar ± 40 mV Self-Starting Boost Converter with Transformer Reuse for Thermoelectric Energy Harvesting," *Proc. 2014 Int. Symp. Low Power Electron. Des.*, pp. 221–226, 2014.

0.3V Biopotential Sensor Interface for Stress Monitoring

S. Orguc, H. S. Khurana, H.-S. Lee, A. P. Chandrakasan
Sponsorship: MIT

Miniaturized sensor nodes have a very tight power budget, especially in the case of implantables and health monitoring devices that require long operation lifetimes. Designing these sensor nodes with such a low power budget is a challenging problem, which requires careful design in both analog blocks and back-end digital signal processing blocks. In the present analog-front-end (AFE) solutions, theoretically more power can be saved at lower supply levels, but this comes at the cost of losing dynamic range, speed, and robustness. In order to further reduce the supply without significantly compromising these performance metrics, the analog architectures used in the signal acquisition should be re-designed.

The motivation of this work is to explore the limits of low-voltage design by using simplistic, yet robust circuit topologies. We present a 0.3V biopotential sensor interface (amplifier+ADC) that achieves state-of-the-art power efficiency and ensures enough circuit reliability with reduced dynamic range requirement. The system will provide diagnostic information about stress-related health problems by measuring electromyographic (EMG) signals.

Figure 1 shows the block diagram of the AFE. The AFE has large-signal cancellation ability in order to suppress the effect of unexpected motion-artifact signals coming from the environment and the sensor interface. Figure 2 illustrates the setup that we will use in future experiments.

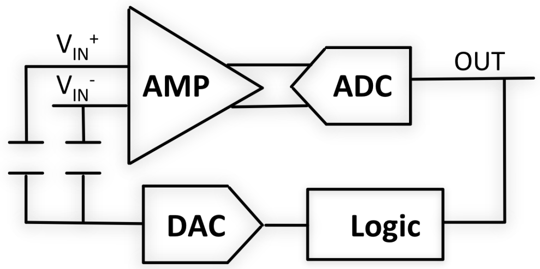

▲Figure 1: Block diagram of EMG signal acquisition AFE. The whole system works from 0.3V supply and has single-digit nanowatt power consumption.

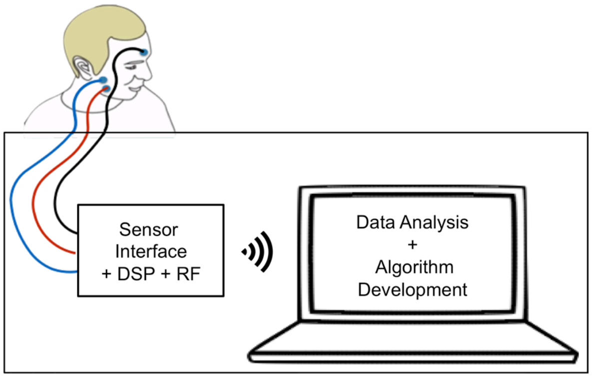

▲Figure 2: The test setup that will be used in the data collection. Once the data is digitized and processed, we will send it wirelessly to a computer for feature extraction and machine learning algorithm development.

FURTHER READING

- P. Harpe, H. Gao, R. van Dommele, E. Cantatore, and A. van Roermund, "A 3 nW Signal-acquisition IC Integrating an Amplifier with 2.1 NEF and a 1.5 fJ/conv-step ADC," *IEEE Int. Solid-State Circuits Conf. (ISSCC) Dig. Tech. Papers*, pp. 382–383, February 2015.
- Y.-P. Chen, D. Jeon, Y.Lee, Y. Kim, Z. Foo, I. Lee, N.B. Langhals, G. Kruger *et al*, "An Injectable 64 nW ECG Mixed-signal SoC in 65 nm for Arrhythmia Monitoring," *IEEE J. Solid-State Circuits*, vol. 50, no. 1, pp. 375–390, January 2015.

12-bit, 300MS/s CMOS Pipelined Analog-to-Digital Converter

T. Jeong, A. P. Chandrakasan, H.-S. Lee
Sponsorship: CICS, Korea Foundation for Advanced Studies

Among many analog-to-digital (ADC) architectures, pipelined ADC covers the widest performance space, and thus various applications adopt it. However, as CMOS technology scaling continues, implementing high-speed, high-accuracy pipelined ADCs has become more difficult. This is mainly due to technology scaling that causes low device intrinsic gain and reduced voltage headroom. Desired characteristics of op-amps for high-performance pipelined ADCs are having high-gain, low-noise, and wide-bandwidth. Low gain and bandwidth cause charge transfer error and nonlinearity in the ADC characteristic (Figure 1). In deep sub-micron technologies, high-gain, high bandwidth op-amps are usually implemented at the expense of high power consumption and increased complexity to overcome the low intrinsic gain and reduced headroom.

Numerous techniques have been reported in the literature to address this issue. One approach is to relax the required performance of op-amps. Digital calibration techniques have proposed to remove errors due to low-gain, low-speed op-amps. The drawback of these techniques is that continuous background digital calibration is necessary to track the gain and bandwidth drift due to the power supply or ambient temperature variations. The background calibration consumes a large amount of power. In addition, many background calibration techniques require certain input signal characteristics for the calibration to function properly and therefore are not suitable for general-purpose applications.

Techniques to avoid the usages of op-amps have also been proposed. Zero-crossing-based circuit (ZCBC) is one of the representative examples. In ZCBC-based pipelined ADCs, the ZCBC detects the instant when its input voltage crosses virtual ground rather than requiring it to be virtual ground. By doing so, ZCBC-based pipelined ADCs tend to be more power-efficient than op-amp-based pipelined ADCs. However, ZCBC-based pipelined ADCs entail considerable circuit complexity to deal with signal-dependent voltage drop across switches.

In this project, we seek to develop a digital calibration scheme for op-amp-based pipelined ADCs. The focus of this project is to develop a one-time digital calibration scheme that does not require continuous background calibration. The prototype is currently being designed in 28-nm CMOS technology.

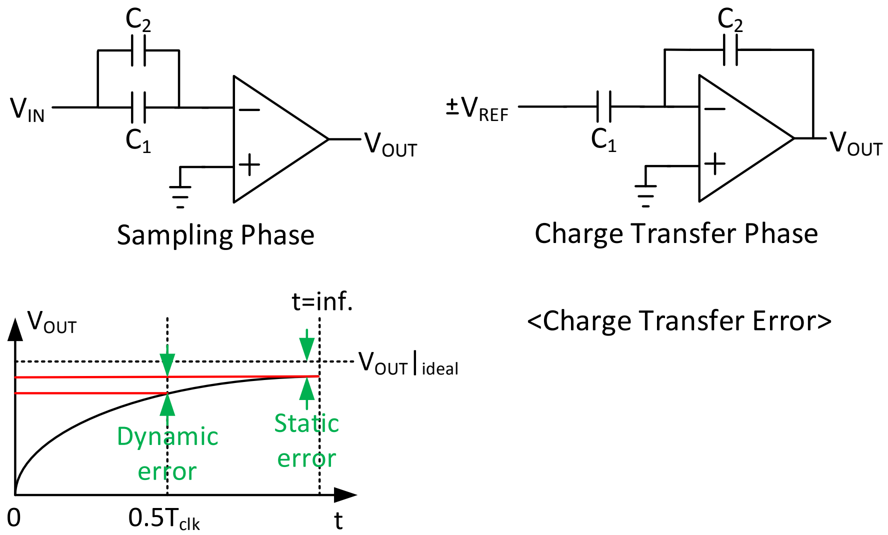

▲ Figure 1: Charge transfer error in switched-capacitor MDAC.

FURTHER READING

- B. Murmann, "ADC Performance Survey 1997-2015," [Online]. Available: http://web.stanford.edu/~murmann/adcsurvey.html.
- B. Murmann and B. E. Boser, "A 12-bit 75MS/s Pipelined ADC using Open-Loop Residue Amplification," *IEEE Journal of Solid-State Circuits*, vol. 38, pp. 2040-2050, December 2003.
- L. Brooks and H.-S. Lee, "A Zero-Crossing-Based 8-bit 200MS/s Pipelined ADC," *IEEE Journal of Solid-State Circuits*, vol. 42, pp. 2677-2687, December 2009.

A CMOS Flash ADC for GaN/CMOS Hybrid Continuous-Time ΔΣ Modulator

X. Yang, H.-S. Lee
Sponsorship: MIT/MTL Gallium Nitride (GaN) Energy Initiative, ONR

High-speed and low-resolution flash analog-to-digital converters (ADCs) are widely used in applications such as 60-GHz receivers, series links, and high-density disk drive systems, as well as in quantizers in delta-sigma ADCs. In this project, we propose a flash ADC with a reduced number of comparators by means of interpolation. One application for such a flash ADC is a GaN/CMOS hybrid delta-sigma converter. The GaN first stage exploits the high-voltage property of the GaN while the CMOS backend employs high-speed, low-voltage CMOS. This combination may achieve an unprecedented SNR/bandwidth combination by virtue of its high input signal range and high sampling rate. One key component of such an ADC is a flash ADC.

To take advantage of the high signal-to-thermal-noise ratio of the proposed system, the quantization noise must be made as small as possible. Therefore, a high-speed, 8-bit flash ADC is proposed for this system. Figure 1 shows the block diagram of the ADC architecture. 65 comparators are used to achieve the six most significant bits (MSBs). 64 interpolators are inserted between the comparators to obtain two extra bits. The input capacitance of this design is ¼ of the conventional 8-bit flash ADC. Therefore a higher operating speed can be achieved. We introduced gating logic so that only one interpolator is enabled during operation, which reduces power consumption significantly. A high-speed, low-power comparator with low noise and low offset requirements is a key building block in the design of a flash ADC. We chose a two-stage dynamic comparator, as in Figure 2, because of its fast operation and low power consumption. With the scaling of CMOS technology, the offset voltage of the comparator keeps increasing due to greater transistor mismatch. A popular offset cancellation technique is to digitally control the output capacitance of the comparator. However, this technique reduces the speed of the comparator because of the extra loading effect. In this project, we also propose a novel offset compensation method that eliminates the speed problem.

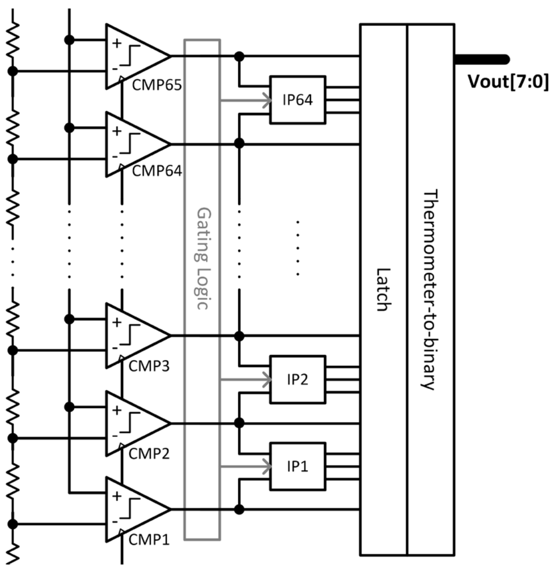

▲Figure 1: Flash ADC architecture, with 65 comparators and 64 2-bit interpolaters.

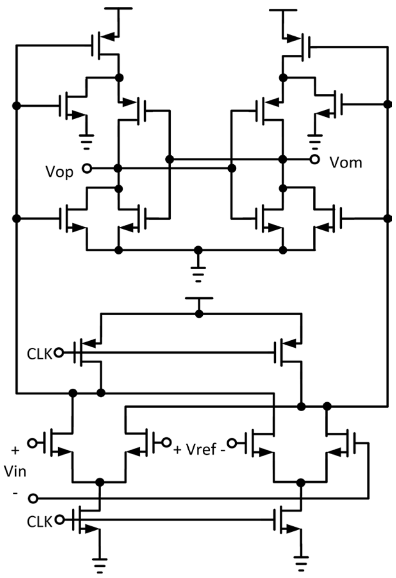

▲Figure 2: Schematic of the two-stage dynamic comparator.

FURTHER READING

- M. Miyahara, Y. Asada, D. Paik, and A. Matsuzawa, "A Low-Noise Self-Calibrating Dynamic Comparator for High-Speed ADCs," *Proc. IEEE Asian Solid-State Circuits Conf. (A-SSCC)*, pp. 269-272, November 2008.
- Y.-S. Shu, "A 6b 3GS/s 11mW Fully Dynamic Flash ADC in 40nm CMOS with Reduced Number of Comparators," *Symp. on VLSI Circuits Dig. Tech. Papers*, pp. 26-27, June 2012.
- M. Miyahara, I. Mano, M. Nakayama, K. Okada, and A. Matsuzawa, "A 2.2GS/s 7b 27.4mW Time-Based Folding-Flash ADC with Resistively Averaged Voltage-to-time Amplifiers," *IEEE Int. Solid-State Circuit Conf. (ISSCC) Dig. Tech. Papers*, pp. 388-389, February 2014.

High-Performance GaN HEMT Track-and-Hold Sampling Circuits

S. Chung, P. Srivastava, D. Piedra, X. Yang, T. Palacios, H.-S. Lee
Sponsorship: MIT/MTL Gallium Nitride (GaN) Energy Initiative, ONR

The performance of emerging applications in ultrafine medical imaging, extremely high-performance cable modem, and data server backbone networks is often limited by analog-to-digital converters (ADCs) whose performance is in turn limited at least partly by a track-and-hold sampling circuits (THSC). The low supply voltage of deeply scaled CMOS transistors determines the THSC input signal range, therefore becoming a fundamental barrier to the signal-to-noise ratio (SNR) of CMOS circuits.

This research ultimately aims to design ultra high-performance THSCs in GaN-on-Si technology, which monolithically integrates GaN HEMTs with Si-CMOS transistors. Operating GaN HEMTs at a high voltage (>30 V) allows a very large input swing (>16 V) and provides performance beyond the limit of CMOS THSCs. As a first step, we designed two GaN HEMT THSCs. The first THSC was fabricated in a commercial GaN foundry technology on SiC substrate, providing 98-dB SNR at 200-MS/s (Figure 1). The second THSC design was fabricated in a GaN technology that was developed at MTL on Si substrate, which operates at 1 GS/s thanks to a higher device transition frequency f_t and external gate-bootstrapping clock (Figure 2).

While these two GaN THSCs achieved high SNR at a given input frequency, they suffered from nonlinearity. We characterized how the static nonlinearity and dynamic memory effects of GaN HEMT THSCs affect the sampled output; we observed that the GaN HEMT dynamic on-resistance does not significantly degrade the THSC linearity because the capacitive load suppresses the impact of on-resistance variation on the sampled voltage. Although dynamic nonlinearity correction techniques are mature with RF power amplifiers (PAs) and improve PA linearity typically by 20-40 dB depending on signal bandwidth and modeling accuracy, these RF PA pre-distortion techniques cannot be directly applied to THSCs. Presently, we are working on a digital post-correction technique, which will demonstrate the accurate cancellation of both static and dynamic nonlinearity in GaN HEMT THSCs.

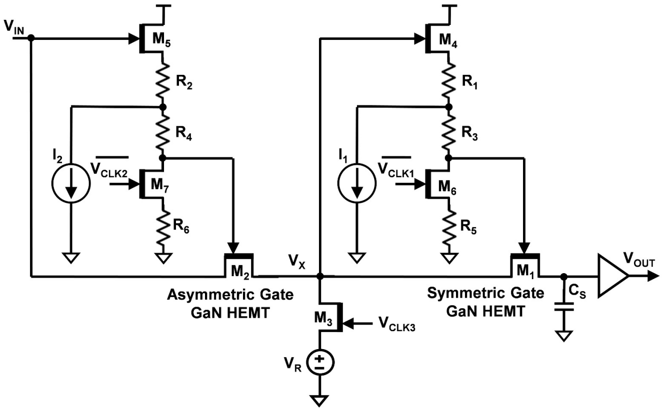

▲Figure 1: Pseudo-differential two-stage track-and-hold sampling circuit in 0.25-um GaN HEMT technology on SiC substrate, which demonstrates 200-MS/s 98-dB SNR and 240-MHz track-mode bandwidth with 20-V differential input signal swing.

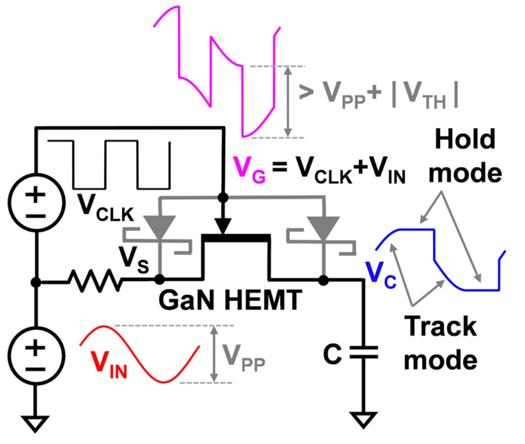

▲Figure 2: Track-and-hold sampling circuit with external gate-bootstrapping clock in a GaN technology developed at MTL on Si substrate, which provides over 700-MHz track-mode bandwidth and operates at 1 GS/s.

FURTHER READING

- S. Chung and H.-S. Lee, "A 200-MS/s 98-dB SNR Track-and-Hold in 0.25-um GaN HEMT," *Proc. of IEEE Custom Integrated Circuits Conference*, pp. 1-4, 2015.
- A. Zhu, P. J. Draxler, J. J. Yan, T. J. Brazil, D. F. Kimball, and P. M. Asbeck, "Open-loop Digital Predistorter for RF Power Amplifier Using Dynamic Deviation Reduction-based Volterra Series," *IEEE Transactions on Microwave Theory and Techniques*, vol. 56, no. 7, pp. 1524-1534, July 2008.

Broadband Inter-Chip Link Using a Terahertz Wave on a Dielectric Waveguide

J. Holloway, Z. Hu, R. Han
Sponsorship: ONR, Lincoln Laboratory

The development of data links between different microchips of an on-board system has encountered a speed bottleneck due to the excessive transmission loss and dispersion of the traditional inter-chip electrical interconnects. Although high-order modulation schemes and sophisticated equalization techniques are normally used to enhance the speed, they also lead to significant power consumption. Silicon photonics provide an alternative path to solving the problem, thanks to the excellent transmission properties of optical fibers. However, the existing solutions are still not fully integrated (e.g., off-chip laser source) and normally require process modification to the mainstream CMOS technologies. Here, we aim to utilize a modulated THz wave to transmit broadband data.

Similar to the optical link, the wave is confined in dielectric waveguides, with sufficiently low loss (~0.1dB/cm) and bandwidth (>100GHz) for board-level signal transmission (Figure 1). In commercial CMOS/BiCMOS platforms, we have previously demonstrated high-power THz generation with modulation, frequency conversion, and phase-locking capabilities. In addition, a room-temperature Schottky-barrier diode detector (in 130-nm CMOS) with <10pW/Hz$^{1/2}$ sensitivity (antenna loss excluded) is also reported. The proposed data link will leverage these techniques to achieve a >100Gbps/channel transmission rate with <1pJ/bit energy efficiency. As the first step of this project, we have designed a new broadband chip-to-fiber THz wave coupler. In contrast to previous couplers using off-chip antennas, our THz coupler is entirely implemented using the metal backend of a CMOS process and requires no post-processing (e.g., wafer thinning). The structure is also fully shielded, which prevents THz power leakage into the silicon substrate. Conventional on-chip radiators using ground shield work are the resonance type (e.g., patch antenna) and have only <5% bandwidth. In comparison, our design is based on a traveling-wave, tapered structure, which supports broadband transmission. A proof-of-concept is shown in Figure 1: two on-chip couplers are connected with a 2-cm waveguide using Rogers 3006 dielectric material. The entire back-to-back setup exhibits only ~11dB insertion loss across over 60-GHz bandwidth (Figure 2).

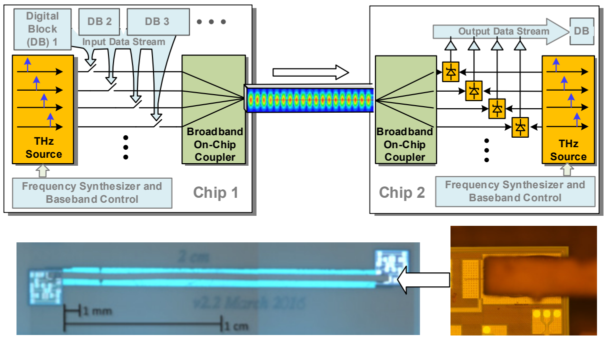

▲ Figure 1: (Top) High-speed, energy-efficient inter-chip transmission using guided terahertz wave. (Bottom) A test structure including a pair of back-to-back THz integrated couplers separated by a 2-cm dielectric waveguide using Rogers 3006.

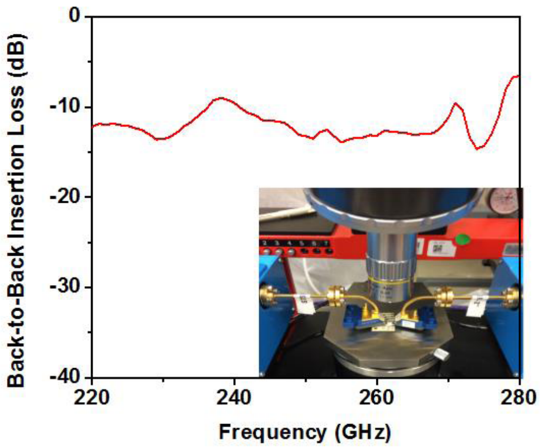

▲ Figure 2: The measured back-to-back insertion loss using a two-port network analyzer in the WR-3 band.

FURTHER READING

- C. Yeh, F. Shimabukuro, and P. H. Siegel, "Low-Loss Terahertz Ribbon Waveguides," *Applied Optics*, vol. 44, no. 28, pp. 5937-5946, October 2005.
- R. Han, C. Jiang, A. Mostajeran, M. Emadi, H. Aghasi, H. Sherry, A. Cathelin, and E. Afshari, "A 320GHz Phase-Locked Transmitter with 3.3mW Radiated Power and 22.5dBm EIRP for Heterodyne THz Imaging Systems," *IEEE Int. Solid-State Circuit Conf. (ISSCC)*, San Francisco, CA, 2015.
- R. Han, Y. Zhang, Y. Kim, D. Kim, H. Shichijo, E. Afshari, and K. K. O, "Active Terahertz Imaging Using Schottky Diodes in CMOS: Array and 860-GHz Pixel," *IEEE Journal of Solid-State Circuits (JSSC)*, vol. 48, no. 10, October 2013.

A Fast, Wideband THz CMOS Spectrometer Based on Dual-Frequency Comb Architecture

C. Wang, R. Han
Sponsorship: TSMC, Center for Integrated Circuits and Systems

Terahertz (THz) spectroscopy detects gaseous molecules using the unique characteristic absorption spectrum lines associated with their rotational modes. It is valuable in applications such as industrial noxious leakage monitoring and human breath analyses. A broadband, high-power THz source and sensitive detector are critical for THz spectroscopy. They enable faster spectrum sweeping and better identifications of molecules from samples with complex composition. However, the existing electronic THz spectrometers are still based on single-channel, narrowband transceiver architectures with slow sweeping speed. On the other hand, optical THz spectroscopy provides inadequate frequency resolution for gas spectroscopy and is not compact.

We propose a fast, wideband THz CMOS spectrometer using a THz-comb structure. When used in a chip-pair configuration (shown in Figure 1), the system simultaneously generates and detects 20 tunable signal tones, which seamlessly cover an ultra-broad band (225–315 GHz). The frequencies of the tones are equally spaced and are precisely controlled by a single input clock reference at lower frequency. Compared to that of the previous single-tone systems, the spectral sweeping time of the proposed scheme is greatly reduced. For each tone, a multi-functional THz circuit is proposed, which enables THz signal generation, radiation, and detection at the same time. Meanwhile, a feedback loop is introduced in this circuit, which greatly improves the THz power generation efficiency without deteriorating the stability. In simulation, 0.5-mW output power for each transmitted tone (~5mW for the total comb spectrum) and 15-dB conversion loss for each receiving channel are achieved. The strong output power and low noise heterodyne detection further increase the signal-to-noise ratio of the system (and hence the sweeping speed). The architecture of the spectrometer is highly scalable, and the frequency coverage can be extended by cascading more comb stages. This design uses a 65-nm bulk CMOS process.

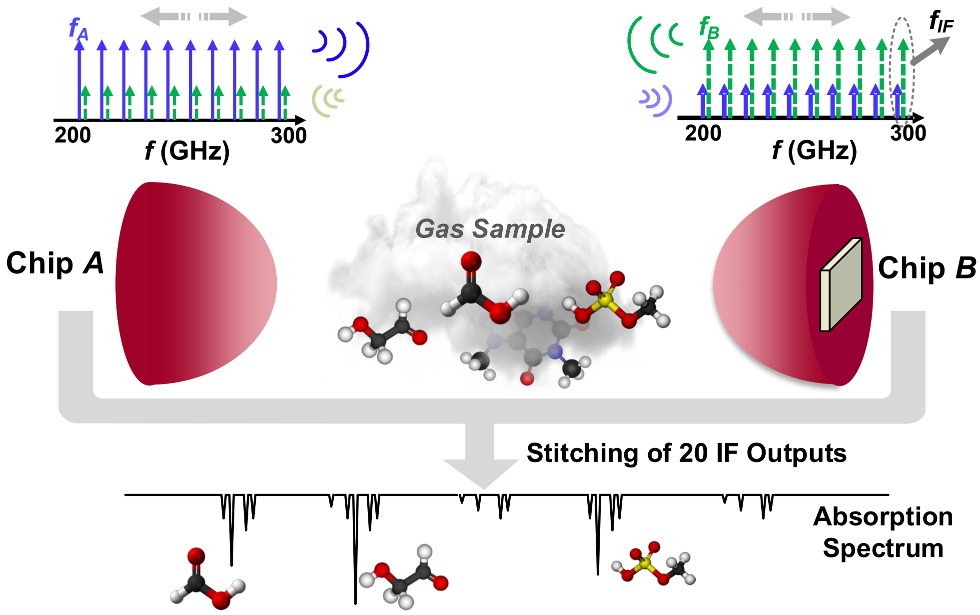

▲ Figure 1: System architecture of the proposed wideband THz CMOS spectrometer.

FURTHER READING

- C. F. Neese, I. R. Medvedev, G. M. Plummer, A. J. Frank, C. D. Ball, and F. C. De Lucia, "Compact Submillimeter/Terahertz Gas Sensor With Efficient Gas Collection, Preconcentration, and ppt Sensitivity," *Sensors Journal, IEEE*, vol. 12, pp. 2565-2574, 2012.
- H. Yi-Da, Y. Iyonaga, Y. Sakaguchi, S. Yokoyama, H. Inaba, K. Minoshima, F. Hindle, Y. Takahashi, *et al*, "Terahertz Comb Spectroscopy Traceable to Microwave Frequency Standard," *IEEE Transactions on Terahertz Science and Technology*, vol. 3, pp. 322-330, 2013.
- K. Schmalz, J. Borngräber, W. Debski, P. Neumaier, R. Wang and H. W. Hübers, "Tunable 500 GHz Transmitter Array in SiGe Technology for Gas Spectroscopy," *Electronics Letters*, vol. 51, pp. 257-259, 2015.

High-Power 1-THz Source Based on a Scalable 2D Radiating Mesh

Z. Hu, R. Han
Sponsorship: Analog Devices, Inc., IHP Germany

Terahertz waves, which possess unique penetration behaviors through non-polar materials, short wavelength (versus mm-waves), and interaction with the intrinsic motions of molecules, have profound potential in imaging, communication, spectroscopy, etc. Previously, room-temperature, silicon-based sources were able to provide only milliwatt-level radiation power in the low-THz range (0.2~0.5 THz). On the other hand, there is an increasing interest in solid-state microsystems operating in the mid-THz range (~1 THz) due to higher spatial resolution in imaging, more collimated beams (hence smaller path loss) in communications, and enhanced gas spectroscopy sensitivity via high-order rotational modes. Following this trend, this work aims to push the limit of electronics further – building a 1-THz coherent radiation source targeting an output power of ~1mW.

Our design, shown in Figure 1, is based on a scalable slot mesh structure that creates a 250-GHz oscillation for the transistor pair located inside each mesh unit, and then extracts and radiates the 4th harmonic component of the oscillation. Due to the weak high-frequency activity of the transistors, the loss overhead of the above operations needs to be as small as possible. To achieve this, a multi-functional electromagnetic structure is proposed that is based on the synthesis of complex wave patterns inside multiple slot waveguides. By applying certain boundary conditions and topology manipulation (e.g., bending the slots), radiations at fundamental and 3rd harmonic signals are cancelled among adjacent slots in the horizontal direction. Meanwhile, the radiation of the 2nd-harmonic signal is also canceled among adjacent slots in the vertical direction. Such configuration minimizes the loss, increases the radiation spectral purity, and creates the optimum conditions of the devices for maximum oscillation and frequency up-conversion.

Lastly, the generated standing waves at the 4th harmonic (~1 THz) are all in phase inside each horizontal slot sections, resulting in efficient, coherent radiation into free space. Due to the compactness of the design, each radiator unit occupies only λ/2×λ/2 area, which increases the radiation density and suppresses the side lobe formation. Using a 130-nm SiGe HBT process, we have designed a 1-THz source consisting of 330 coupled radiators. Figure 2 shows the simulated radiation pattern of the array, which predicts ~1.2mW radiated power, 34dBi beam directivity, and 2.8W effective isotropic radiated power.

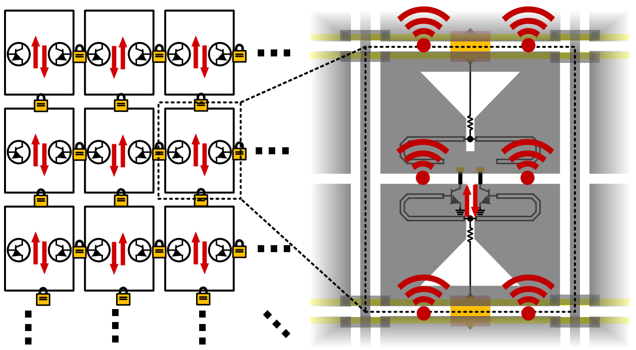

▲ Figure 1: The architecture of the radiator array: (left) the mutual coupling between cells and (right) a single cell with the locations of 1-THz radiation indicated.

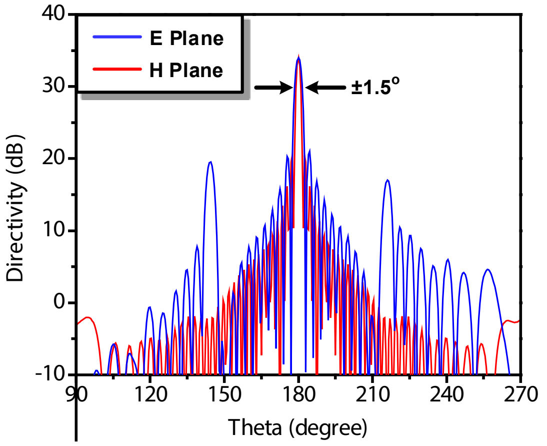

▲ Figure 2: The simulated radiation pattern of our array. The peak directivity is 34dBi (i.e., a beam collimation factor of 2500x).

FURTHER READING

- D. Mittleman, *Sensing with Terahertz Radiation*, vol. 85 New York:, Springer, 2013.
- R. Han *et al*, "A 320Ghz Phase-Locked Transmitter with 3.3 mW Radiated Power and 22.5 dBm EIRP for Heterodyne THz Imaging Systems," *International Solid-State Circuits Conference (ISSCC)*, 2015.
- O. Momeni and E. Afshari, "High Power Terahertz and Millimeter-wave Oscillator Design: A Systematic Approach," *IEEE Journal of Solid-State Circuits*, vol. 46, no. 3, pp. 583-597, 2011.

Design, Modeling, and Fabrication of Chemical Vapor Deposition-Grown MoS_2 Circuits with E-Mode Field-Effect Transistors for Large-Area Electronics

L. Yu, D. El-Damak, S. Ha, X. Ling, U. Radhakrishna, J. Kong, D. A. Antoniadias, A. P. Chandrakasan, T. Palacios
Sponsorship: NSF CIQM

The flexibility and the low temperature process for MoS_2 electronics has a great potential for realizing ubiquitous computing systems. Here we present an E-Mode field-effect transistor (FET) based on chemical vapor deposition (CVD) MoS_2 and computer-aided design (CAD) flow to realize this vision. On the device development side, the flow starts with the growth of MoS_2 using CVD, followed by device fabrication and characterization. The CAD flow includes (1) compact models of MoS_2 devices, (2) schematic design based on analytical and simulation results, and (3) layout with parameterized cells using cadence design environment. Then, the full chip layout is exported in GDS format for mask generation, and chip fabrication is performed. This design flow allows for technology-design co-optimization to realize the full potential of such emerging technology. It also allows for capturing the impact of the device parameters on the circuit performance, speeds up the layout process, reduces the number of iterations for system development, and allows for exploring the potential improvements on the system level with the predicted next generation device.

On the device side, the E-Mode device using CVD-grown large area MoS_2 is realized by a gate-first process: passive components are built and optimized before transfer of the atomically thin layer of MoS_2. Statistical distributions of threshold voltage, mobility, and subthreshold swing of E-mode MoS_2 confirm the high uniformity and high yield of this technology. Using our design flow, we built logic circuits such as multi-stage combinational and sequential circuits (AND, OR, XNOR, latch, NAND, NOR) and power circuits such as switch capacitance regulators. The logic circuits show correct functionality; the regulator generates output voltage regulated by switching frequency. Our device technology, modeling, and design flow bridges gaps between the development stages of MoS_2 to use the full potential of emerging technologies.

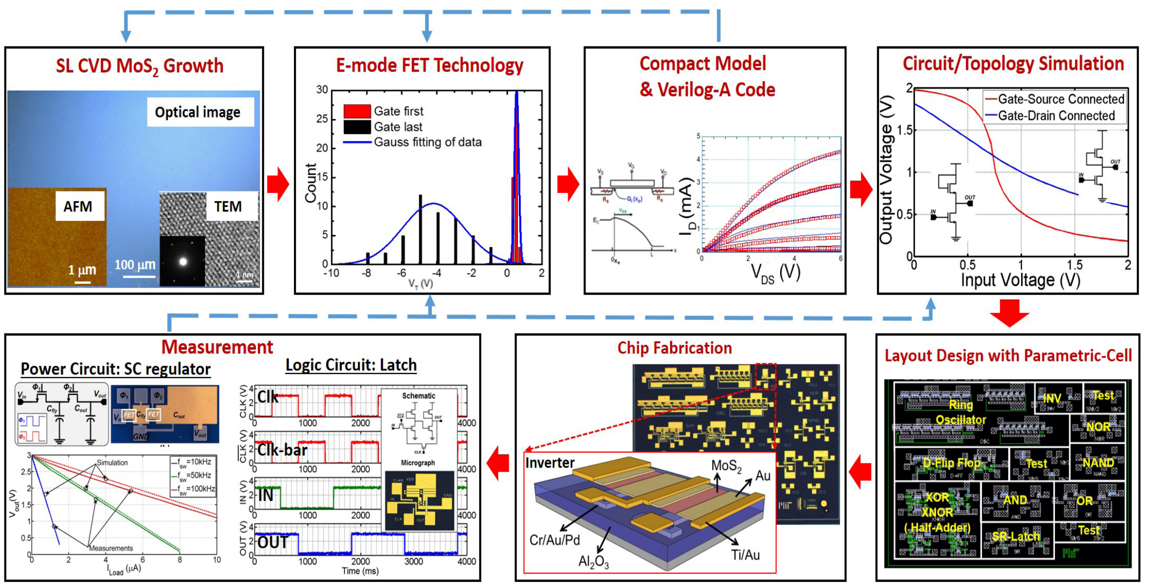

▲ Figure 1: The design flow of large-scale MoS_2 integrated circuit with highlight performance of various stages. The red arrows indicate the process procedure, and dashed blue arrow indicating the main feedback and iteration loops.

FURTHER READING

- L. Yu, D. El-Damak, S. Ha, X. Ling, Y. Lin, A. Zubair, Y.-H. Lee, J. Kong, A. Chandrakasan, and T. Palacios, "Enhancement-Mode Single-layer CVD MoS_2 FET Technology for Digital Electronics," *IEDM*, 2015.
- L. Yu, D. El-Damak, S. Ha, S. Rakheja, X. Ling, J. Kong, D. Antoniadis, A. Chandrakasan, and T. Palacios, "MoS_2 FET Fabrication and Modeling for Large-scale Flexible Electronics," *2015 Symposium on VLSI Technology Digest of Technical Papers*, pp. T144-T145, 2015.

Electronic Devices

On Apparent Electron Mobility in Si nMOSFETs from Diffusive to Ballistic Regimes

D. A. Antoniadis
Sponsorship: Ray and Maria Stata Chair

The Matthiessen-law combination of diffusive and ballistic mobility provides a framework to explain the decrease of apparent mobility in near-ballistic field-effect transistors (FETs). While this theory works well for III-V FETs reported to date, it under-predicts the mobility decrease in several Si experiments, raising concerns about FET performance in the near-ballistic regime. In this work, recent SOI planar and FinFET n-MOSFET I-V data are analyzed in detail, accounting for the effect of channel degeneracy. Assuming a channel-length independent mean free path (MFP), it is demonstrated that good agreement can be obtained with the conventional Matthiessen-law combination modified to include the effect of drain-channel backscattering recently proposed by Natori et al [1]. On the other hand, good agreement can also be obtained with the Matthiessen-law combination if the MFP is assumed to be channel-length dependent. The full range of $I_d(V_{gs}, V_{ds})$ is well modeled by incorporating either of these effects in a recent transmission-based compact model, but drastically different critical lengths for backscattering must be used in the Landauer formulation in the saturation region. It is also shown that this apparent anomaly is technology-dependent and its effect in overall device performance is discussed.

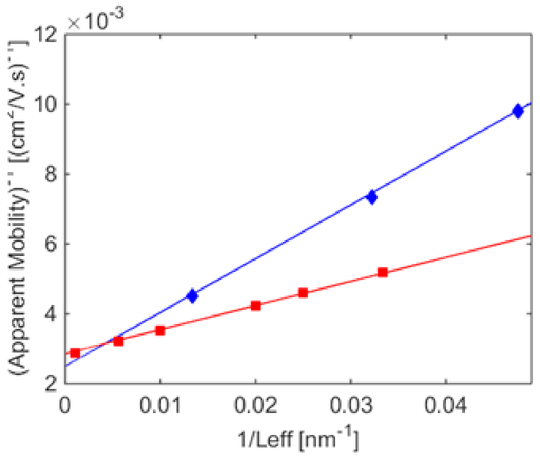

▲ Figure 1: Comparison of extracted apparent mobilities for the ETSOI (squares) where R=0.2 and FinFET (diamonds) where R=0.65, technologies. The channel degeneracies correspond approximately to N_s=6x10^{12} cm^{-2}, which occurs at V_{gs}=0.5 and 0.8 V, respectively. Mean free paths in both cases are assumed independent of channel length with values 19.7 and 26 nm respectively.

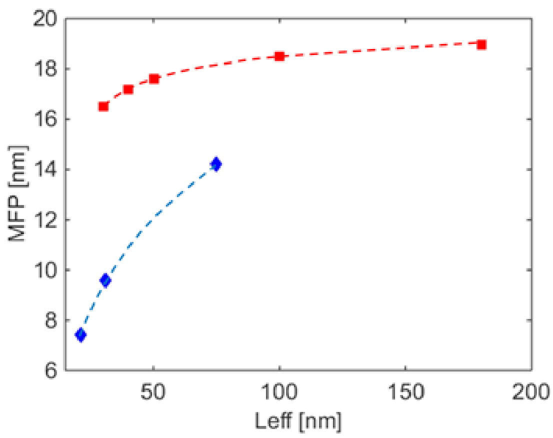

▲ Figure 2: MFP vs. L_{eff} for the ETSOI (squares) where and FinFET (diamonds) technologies. Channel degeneracy corresponds to N_s=6x10^{12} cm^{-2}. Dashed lines are guides to the eye only. The long-channel MFP from for the same degeneracy for these two technologies is 19.7 and 26 nm respectively.

FURTHER READING

- K. Natori, H. Iwai, and K. Kakushima, "Anomalous Degradation of Low Field Mobility in Short-channel Metal-oxide-semiconductor Field-effect Transistors," *Journal of Appl. Phys.*, vol. 118, no. 23, pp. 234502, 2015.

Gate Efficiency in InGaAs/GaAsSb Quantum-well Tunnel-FETs

T. Yu, U. Radhakrishna, J. L. Hoyt, D. A. Antoniadis
Sponsorship: NSF E3S

The tunnel field-emission transistor (TFET), in which carrier injection is determined by gate-controlled tunneling from the source to the channel, has been attractive as one of the promising candidates for future ultra-low-power applications. In this study, *inline-TFETs* with tunneling direction aligned to the gate electric field are designed, fabricated, and analyzed based on InGaAs/GaAsSb material. Using ultrathin InGaAs/GaAsSb quantum-wells (QWs), the device fabrication technology was developed and the tunneling properties of two successive generations of QWTFETs were investigated. In the first generation QWTFETs, the limitation of gate oxide quality on InGaAs and parasitic thermal currents manifested itself in degraded subthreshold swing (SS) of 140 mV/dec, as well as strongly temperature-dependent SS from 300 K to 77 K. The second generation QWTFETs with sub-nm InP cap between the gate oxide and InGaAs channel and revised structure design has demonstrated improved SS of 87 mV/dec at 300 K and temperature-independent SS below 140 K, indicating the achievable tunneling current steepness with the current device design.

Physical modeling and quantum simulations based on the low-temperature I-V characteristics were used to analyze the fundamental gate efficiency of the experimental QWTFETs to reveal the ultimate intrinsic tunneling steepness of the InGaAs/GaAsSb tunneling junction. The extracted gate efficiency around 55-64% is due to the coupling of the gate capacitance and tunneling junction capacitance and degrades significantly the attainable SS in the QWTFET. On the other hand, the implied intrinsic tunneling steepness of the InGaA/GaAsSb is around 30 mV/dec, almost identical to previously reported non-abruptness of the conduction/valence band-edge into the bandgap. The result indicates the possibility of achieving SS as low as 38 mV/dec in QWTFETs by improving gate efficiency (GE) by up to 78% with proposed optimized parameters based on simulation results.

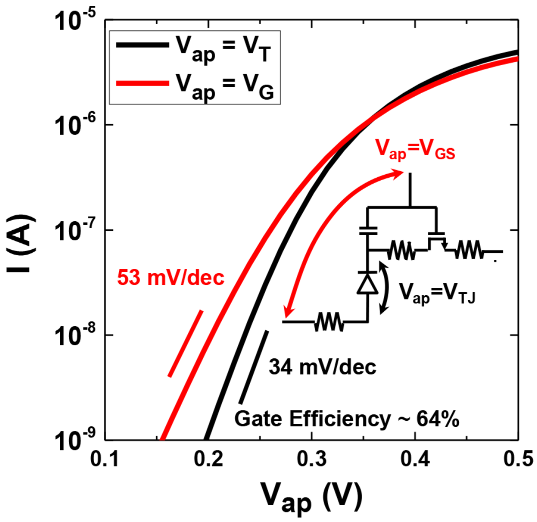

▲Figure 1: Comparison between the I-V characteristics with voltage applied at the gate and directly across the tunneling junction. The ratio of the subthreshold swings indicates a GE of ~64%.

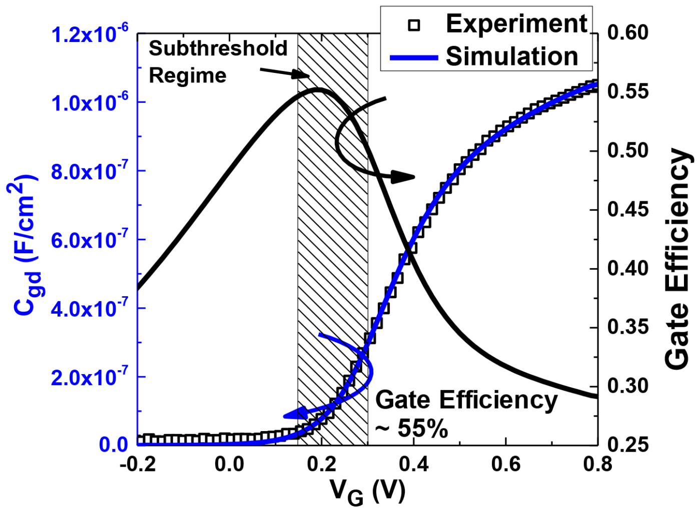

▲Figure 2: C-V and extracted GE based on the quantum simulation of the InGaAs/GaAsSb MOS capacitor. GE is defined by the change in first sub-band energy (ΔE_1) over the change in the gate potential (ΔqV_G). The extracted GE_{max} is ~55%, close to the value extracted from the model.

FURTHER READING

- (2012) International Technology Roadmap for Semiconductor. [Online]. Available: http://www.itrs.net/.
- A. M. Ionescu and H. Riel, "Tunnel Field-effect Transistors as Energy-efficient Electronic Switches," *Nature*, vol. 479, no. 7373, pp. 329–337, 2011.
- T. Yu, U. Radhakrishna, J. Hoyt, and D. Antoniadis, "Quantifying the Impact of Gate Efficiency on Switching Steepness of Quantum-well Tunnel-FETs: Experiments, Modeling, and Design Guidelines," *IEEE International Electron Devices Meeting (IEDM)*, pp. 22.4.1-22.4.4, December 2015.

Impact of Trap-Assisted Tunneling on the Performance of Tunnel Field-Effect Transistors

R. Sajjad, W. Chern, J. L. Hoyt, D. A. Antoniadis
Sponsorship: NSF E3S

Tunnel field-effect transistors (TFETs) are promising candidates for low-power logic applications. They have strong potential to reduce energy dissipation by relying on band-to-band tunneling (BTBT) for carrier injection to achieve steep turn-ON and thus reduce the logic circuit supply voltage. However, most experiments so far have failed to show subthermal switching.

In our model, we show that trap assisted tunneling (TAT) (Figure 1) due to surface interface traps is the principal mechanism of leakage current in TFETs. With a modified Shockley-Read-Hall formalism, we show that the TAT obscures the steepest part of the BTBT current for realistic trap densities. Through a multi-phonon process, an electron (or hole) can be emitted to a trap state, followed by tunneling into the conduction band (or the valence band for a hole), giving rise to the TAT. The minimum subthreshold swing (SS) is a combined result of the trap density, sharpness of the band edge (Urbach tail), and material parameters (Figure 2). We show that the TAT current is greatly enhanced with a high electric field in the tunnel barrier, in the same way as the desired BTBT current. Based on the detailed formalism, we build a physics-based compact model that is able to capture the SS, minimum current achievable at any given temperature, and the temperature-dependence of the transfer characteristics. All TFET device features such as negative differential resistance (NDR), superlinear ON current, and the drain control over the channel potential are captured through physical parameters. Our model a) matches closely with TFET experiments, b) captures the material and structural parameters that influence the TAT, and c) allows predictions of what trap density is needed to see subthermal switching.

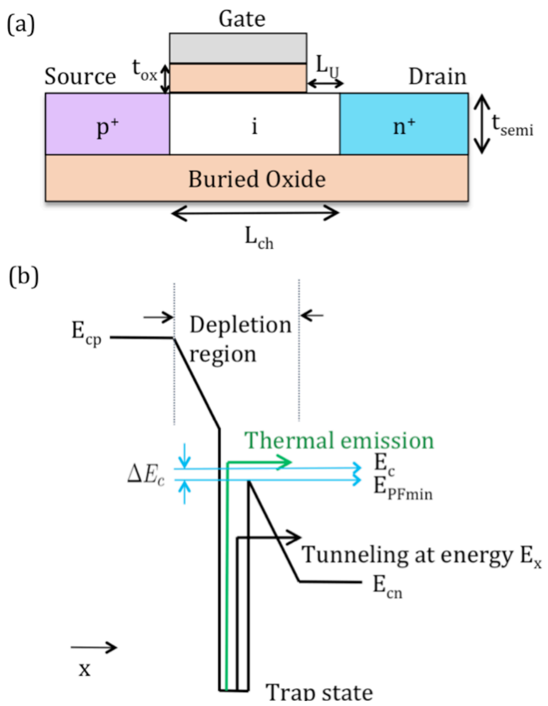

▲Figure 1: A schematic of a TFET and TAT.

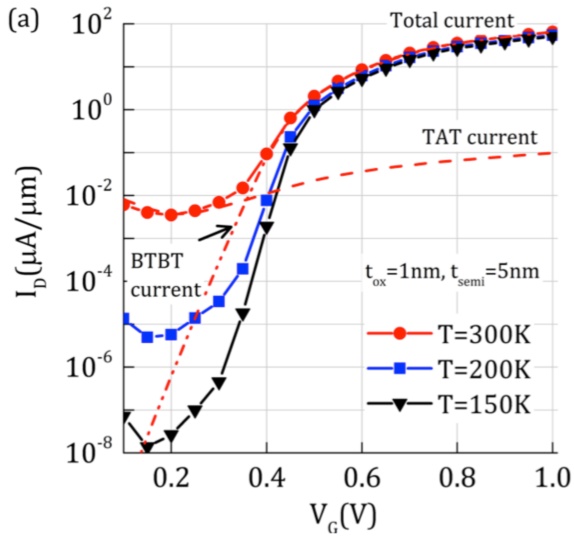

▲Figure 2: Total current in a homojunction III-V TFET in presence of TAT. The steepest part of the transfer curve is obscured by TAT.

FURTHER READING

• J. Furlan, "Tunneling Generation-recombination Currents in a-Si Junctions," *Progress in Quantum Electronics*, vol. 25, pp. 55-96, 2001.

Auger Generation as an Intrinsic Limit to Tunneling Field-Effect Transistor Performance

J. T. Teherani, S. Agarwal, W. Chern, P. M. Solomon, E. Yablonovitch, D. A. Antoniadis
Sponsorship: NSF E3S

Many in the microelectronics field view tunneling field-effect transistors (TFETs) as society's best hope for achieving > 10× power reduction for electronic devices; however, despite a decade of considerable worldwide research, experimental TFET results have significantly underperformed simulations and conventional metal-oxide semiconductor FETs (MOSFETs). To explain the discrepancy between TFET experiments and simulations, we investigate the parasitic leakage current due to Auger generation, an intrinsic mechanism that cannot be mitigated with improved material quality or better device processing. We expose the intrinsic link between the Auger and band-to-band tunneling rates, highlighting the difficulty of increasing one without the other. From this link, we show that Auger generation imposes a fundamental limit on ultimate TFET performance.

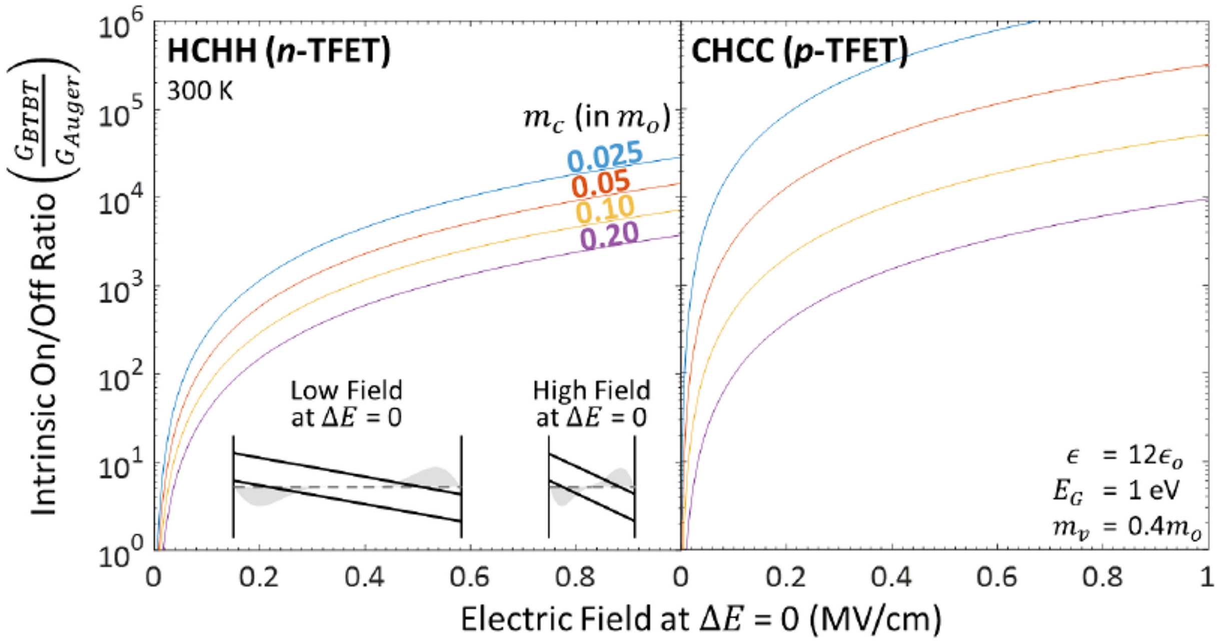

▲ Figure 1: Intrinsic on/off ratio of the band-to-band-tunneling (BTBT) and Auger rates at eigenstate alignment ($\Delta E=0$) as a function of the electric field. The BTBT rate decreases dramatically as the field decreases, and therefore, the ratio drops. The relative permittivity (ε) and heavy-hole mass (m_v) do not vary significantly among materials; hence, constant values indicated on the plot are used. A 1-eV band gap is also assumed. The ratio depends linearly on $1/E_G$ so decreasing the band gap by half will double the on/off ratio. The CHCC process is one where an electron-hole pair is spontaneously generated by a high energy electron; the HCHH process is the opposite where an electron-hole pair is generated by a high energy hole. The CHCC process (dominant in p-TFETs with high n-doping) gives a much better on/off ratio because the Auger generation rate is much lower for the CHCC process due to the light electron mass. The inset shows the energy-band diagram for two structures with different body thicknesses at $\Delta E=0$. The thinner structure requires a higher electric field to align the bands, which results in an improved on/off ratio due to increased BTBT at high fields. The electric field at $\Delta E=0$ will also be dependent on the doping profile and electrostatics of the device, in addition to body thickness.

Simulation Study of the Performance of Negative Capacitance Field-Effect Transistors Using a Physics-Based Compact Model

U. Radhakrishna, D. A. Antoniadis in collaboration with A. Khan and S. Salahuddin
Sponsorship: NSF NEEDS, ONR, LEAST, SRC STARnet Center, MARCO, DARPA

There is an increasing need for semiconductor logic devices that can operate at scaled power supply voltage in digital computing systems for overall energy efficiency in electronics. A fundamental limitation on the scaling of supply voltage in CMOS technology is the Boltzmann limit of 60 mV/decade on the sub-threshold swing (SS) of field-effect transistors (FETs). The concept of negative capacitance (NC) FETs (NCFETs) has been proposed to overcome this limitation by using a capacitor with a ferroelectric material (FE-oxide), connected in series with the gate dielectric of a regular MOSFET. The underlying mechanism for sub-60 mV/decade operation of a NCFET is the passive amplification of the gate voltage at the interface between the FE-oxide and the semiconductor channel yielding steep-SS as the ferroelectric NC state cancels the equivalent of all the positive capacitances in NCFETs.

The FE -oxide capacitor with Q-V characteristics showing the NC-regime (where $dQ_F/dV_F < 0$) in Figure 1-a is connected in series with the gate of a regular MOSFET to constitute the NCFET shown in Figure 1b. Simulations are conducted to study the performance of the NCFET by using the MVS-model calibrated against Intel 45-nm NFET connected to the FE-oxide capacitor as shown, including the scenario of FE-leakage through R_{FE}. Leakage shifts the Q-V characteristics by Q_0, stabilizing the FE-oxide in the positive-capacitance (PC) state, with the unintended consequence of decreasing the NCFET performance versus baseline MOSFETs. Work function engineering of the external and internal metal gates to shift the Q-V characteristics by V_{offset} as shown in Figure 1c-d restores the advantage of leaky-NCFETs in terms of steeper SS by stabilizing the FE-oxide close to the NC-regime (V_{offset}, Q_{offset}). Transient simulations for the triangular gate voltage on the NCFETs for leaky and non-leaky scenarios in Figure 2a-b show that the NC-state in segments AC and DF results in steeper-SS in the NCFET transfer characteristics versus baseline FETs, as Figure 2c-d shows. Leakage results in PC in the sub-threshold regime of the NCFET (in segments A'C' and H'F') yielding degraded SS. Leakage-aware design by work function engineering preserves lower SS along with higher I_{on} as seen in Figure 2e-f. The NCFET model implemented in Verilog-A can be a useful tool to design NCFET-parameters (t_{FE}, V_{offset}) and evaluate circuit-level performance of NCFETs.

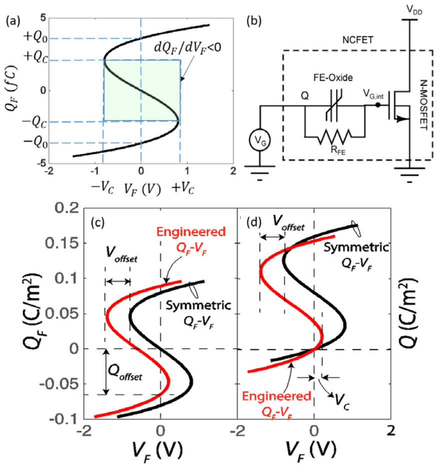

▲ Figure 1: (a) Q_F-V_F characteristics of a FE-oxide showing the NC-region. (b) The NC-state is stabilized with the gate-oxide of MOSFET forming the NCFET shown. (c)-(d) Leakage shifts the Q-V characteristics by Q_0 pushing it to the PC-state while LA-design by work-function engineering to shift the Q-V curves by V_{offset}, stabilizes the oxide to have charge of Q_{offset} closer to the NC-state.

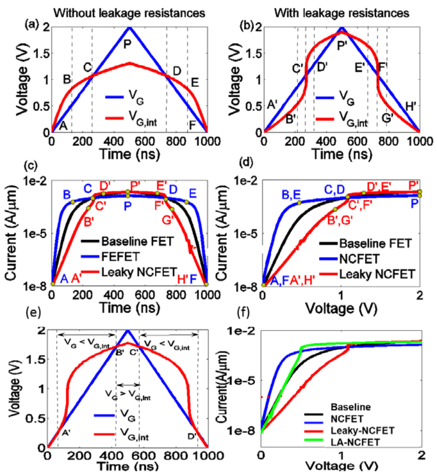

▲ Figure 2: (a)-(b) Internal gate-voltage ($V_{G,int}$) response to a triangular gate voltage in leaky and non-leaky scenarios showing amplification in certain segments. (c)-(d) NCFETs have steeper SS than the baseline while leakage eliminates this advantage. (e)-(f) LA-design preserves the NC-state stability in sub-threshold, yielding steeper SS to some extent and higher I_{on}.

FURTHER READING

- S. Salahuddin and S. Datta, "Use of Negative Capacitance to Provide Voltage Amplification for Low Power Nanoscale Devices," *Nano Letters*, vol. 8, no. 2, pp. 405–410, 2008.
- A. Khan, U. Radhakrishna, K. Chatterjee, D. Antoniadis, and S. Salahuddin, "A Simulation Study of Negative Capacitance Field-Effect Transistors: The Effects of Leakage through Ferroelectric Negative Capacitor," *IEEE Transactions on Electron Devices*, submitted for publication, 2016.

High Aspect Ratio InGaAs FinFETs with Sub-20 nm Fin Width

A. Vardi, J. A. del Alamo
Sponsorship: DTRA, NSF E3S, Lam Research

InGaAs is a promising candidate for channel material for CMOS technologies beyond the 10-nm node. In this dimensional range, only high aspect-ratio (AR) 3D transistors with a fin or nanowire configuration can deliver the necessary performance. Impressive fin- and nanowire-based InGaAs FinFET prototypes have recently been demonstrated. However, to date, InGaAs FinFETs with fin widths below 30 nm and channel aspect ratio better than unity have yet to be demonstrated. Furthermore, the channel sidewall slopes demonstrated so far are typically lower than 80°. At the point of insertion in a sub-10-nm node, InGaAs FinFETs with sub-10-nm fin widths and steep sidewalls will be required.

In this work, we present the first self-aligned InGaAs FinFETs with sub-20-nm fin width, high channel aspect ratio (H_c=40 nm), vertical sidewalls, gate lengths as short as 20 nm, and CMOS-type manufacturability. We use a top-down process based on reactive-ion etching (RIE) and digital etch. Our transistors are the most aggressively scaled InGaAs FinFETs to date.

The process is illustrated in Figure 1 and follows a flow developed for self-aligned planar InGaAs quantum-well MOSFETs. SEM images of sub-20-nm fin test structures are shown in Figures 1(a) and (b). Low-resistivity Mo is first sputtered as contact metal (R_{sh}=5 Ω/□), followed by SiO_2 CVD. The gate pattern is defined by E-beam lithography. The SiO_2 and Mo layers are then etched by RIE. After RIE mesa isolation, the top n⁺ InGaAs cap is wet-etched in a well-controlled manner (see Figure 1(c)). Fins are then patterned using 40-nm-thick HSQ and E-beam lithography and RIE etched (see Figure 1(d)-(e)). This yields fins as narrow as 20 nm with an aspect ratio of 8. The fins are highly vertical in the top ~70 nm (Figure 1(b)). Gate dielectrics composed of 0.5 nm of Al_2O_3 and 2.5 nm HfO_2 are deposited by ALD. Sputtered Mo is used as gate metal and patterned by RIE. The device is finished by via opening and pad formation. In this process, the HSQ that defines the fin etch is kept in place. This feature makes our FinFETs double-gate transistors with carrier modulation only on the sidewalls.

The electrical characteristics of a device with W_f=22 nm L_g=30 nm (AR= H_c/W_f=1.8) are shown in Figure 2(a)-(c). Well-behaved characteristics and good sidewall control are obtained. R_{on} is 170 Ω·µm, and a peak transconductance, g_m, of 1400 µS/µm is obtained at V_{DS}=0.5 V. This value is comparable to the highest g_m obtained so far in InAs FinFETs with W_f=40 nm (AR=0.23). Figure 2 (s) shows a benchmark plot comparing normalized g_m per fin footprint of InGaAs FinFETs realized to date as well as commercial Si FinFETs.

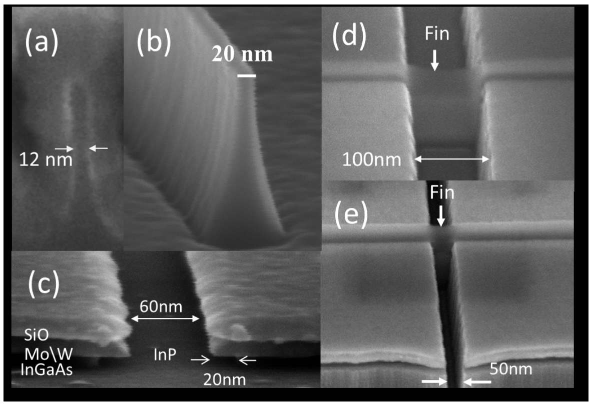

▲Figure 1: SEM image of self-aligned InGaAs FinFET. (a) cross section of gated fin, (b) stand-alone fin test structure, (c) gate area after recess, and (d) and (e) 100- nm and 50-nm gate length devices, respectively, after fin etch.

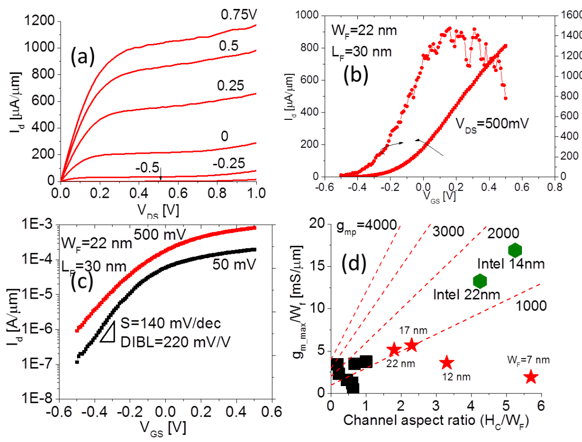

▲Figure 2: (a) output, (b) transfer and (c) subthreshold characteristics of self-aligned InGaAs FinFET with L_g=30 nm and W_f =22 nm. (d) g_m per fin footprint as a function of AR= H_c/W_f for InGaAs (black), this work (red) and Si (green) FinFETs. Trend lines show the physical g_m of equivalent planar device.

FURTHER READING

- J. Lin, D. A. Antoniadis, and J. A. del Alamo, "Sub-30 nm In As Quantum-Well MOSFETs with Self-Aligned Metal Contacts and Sub-1 nm EOT HfO_2 Insulator," *IEEE International Electron Devices Meeting*, pp. 757-760, 2012.
- A. Vardi, X. Zhao, and J. A. del Alamo, "Quantum-Size Effects in Sub 10 nm Fin Width InGaAs FinFETs," *IEEE International Electron Devices Meeting*, pp. 807-810, 2015.
- A. Vardi, J. Lin, W. Lu, X. Zhao, and J. A. del Alamo, "High Aspect Ratio InGaAs FinFETs with Sub-20-nm Fin Width," *VLSI Symposium*, pp 136-137, 2016.

An InGaSb Tri-gate MOSFET

W. Lu, J. A. del Alamo
Sponsorship: Lam Research Corporation, Samsung Electronics

Recently, III-V multi-gate metal-oxide semiconductor field-effect transistors (MOSFETs) have attracted great interest to replace silicon in future CMOS technology. This is due to the III-V semiconductor's outstanding carrier transport properties. Although impressive n-type transistors have been demonstrated on materials such as InAs and InGaAs, research in III-V p-channel devices is lacking. The antimonide system, such as InGaShas the highest hole mobility among all III-V compound semiconductors; its hole mobility can be further improved by applying compressive strain. Therefore, InGaSb is regarded as one of the most promising semiconductors to replace p-channel Si MOSFETs.

In this work, we have designed and demonstrated the first InGaSb p-channel FinFET. A FinFET is a nonplanar transistor in which the conducting channel sticks out of the wafer top in a similar way as the fin of a shark above the ocean surface. In a FinFET, the gate wraps around the fin, helping to reduce leakage current when the device is OFF and mitigating short-channel effects. The FinFET is the state-of-the-art transistor architecture in current Si CMOS technology and demonstration of III-V FinFETs is imperative.

In order to fabricate an InGaSb FinFET, we have developed two critical technologies. First, a high-aspect ratio dry etching process has been demonstrated. It can produce antimonide-based fins or nanowires as narrow as 15 nm with vertical sidewalls and low sidewall defects. Second, a Si-compatible nickelide ohmic contact scheme has been developed that offers an ultra-low contact resistivity of $3.5 \cdot 10^{-8}$ Ω-cm². With the aid of these two technologies, the first InGaSb p-channel FinFET has been fabricated with a narrowest fin width of 30 nm and total fin height of 150 nm, as shown in Figure 1. The output characteristics of a 30-nm wide FinFET with 100-nm gate length are shown in Figure 2. In this transistor, a transconductance, g_m, of 78 µS/µm is obtained. In devices of 100-nm fin width and 100-nm gate length, g_m of 122 µS/µm has been attained. This transconductance is about the same as in the best InGaSb planar MOSFETs. For the first FinFETs in this material system, this is a very encouraging result.

We are currently working on different approaches to achieve smaller device pitch and enhanced device characteristics. In particular, a passivation technology for InGaSb fin sidewalls is of great importance. Our research will be instrumental in mapping the potential of InGaSb for future CMOS nodes.

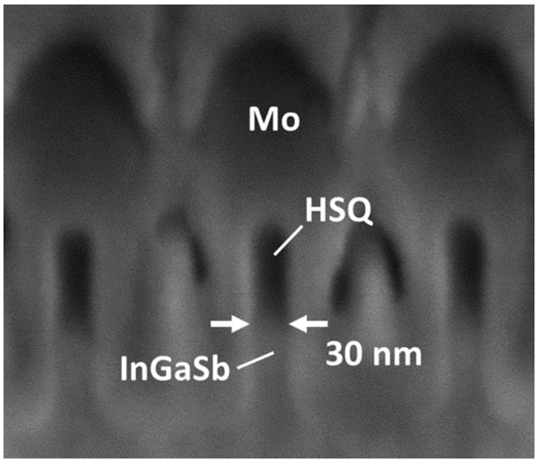

▲Figure 1: Focused-ion-beam cross-section image of a finished InGaSb FinFET with fin width of 30 nm.

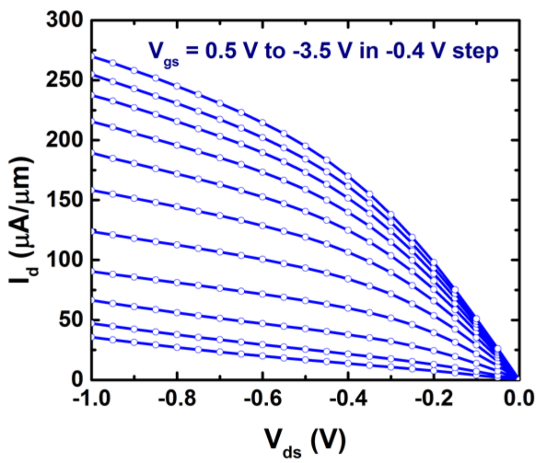

▲Figure 2: Output characteristics of an InGaSb p-channel FinFET with fin width of 30 nm and gate length of 100 nm.

FURTHER READING

- J. A. del Alamo, "Nanometer-scale Electronics with III-V Compound Semiconductors," *Nature*, vol. 479, pp. 317-323, 2011.
- W. Lu, J. K. Kim, J. F. Klem, S. D. Hawkins, and J. A. del Alamo, "An InGaSb p-Channel FinFET," *IEEE International Electron Devices Meeting*, pp. 819-822, 2015.
- L. W. Guo, W. Lu, B. R. Bennett, J. B. Boos, and J. A. del Alamo, "Ultra-low Resistance Ohmic Contacts for p-Channel InGaSb Field-Effect Transistors," *IEEE Electron Device Letters*, vol. 36, no. 6, pp. 546-548, 2015.

Si Donor Passivation in InGaAs MOSFETs

X. Cai, J. Lin, J. A. del Alamo
Sponsorship: DTRA, Lam Research Corporation

InGaAs is a promising n-channel material candidate for future CMOS technology due to its superior electron transport properties and low-voltage operation. While the process technology and performance of InGaAs metal-oxide semiconductor field-effect transistors (MOSFETs) continues to improve, there is increasing anxiety about the electrical reliability of this device technology. Issues of concern are reactive-ion etching (RIE) damage, ion contamination, radiation damage, trapping, etc. As F-based RIE is important for III-V device processing and F is known to passivate Si donors in n-InAlAs, a common material in InGaAs MOSFET heterostructures, it is important to verify and mitigate this potentially deleterious effect.

To investigate F^- induced donor passivation in our process, we have fabricated transmission line model (TLM) structures on a heterostructure that includes an n-InGaAs/n-InP/n-InAlAs (15/3/3 nm) cap, as shown in Figure 1. We use two different processes. A standard process that is the same as in our InGaAs MOSFET process uses sputtered Mo contacts etched by SF_6/O_2 RIE. In an alternative process, the Mo contacts are lifted-off, and there is no exposure to F.

Figure 2 shows the measurement results of the TLM structures before and after annealing at 350ºC for 1 min. The pre-anneal sample prepared by F-RIE exhibits a semiconductor sheet resistance (R_{sh}) of 176 Ω/□, 30% higher than that of the lift-off sample. After annealing, R_{sh} of the lift-off sample decreases somehow, while R_{sh} of the F-RIE sample increases by 3X to 543 Ω/□. This result is consistent with literature findings that during a thermal step, F diffuses and passivates donors in n-InAlAs. Our standard self-aligned InGaAs MOSFET fabrication process includes a 340ºC, 15-min thermal step after F-based RIE. Thus, we expect that F passivates Si donors in the n-InAlAs cap layer of the MOSFET and deteriorates device performance. Furthermore, F renders the device unstable as it tends to move around under an electric field.

Our work will be instrumental in enhancing the performance, reliability, and stability of future InGaAs MOSFETs.

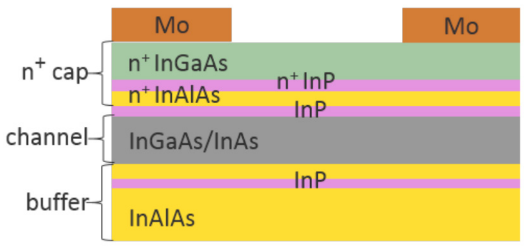

▲ Figure 1: Cross-sectional schematic of TLM structure.

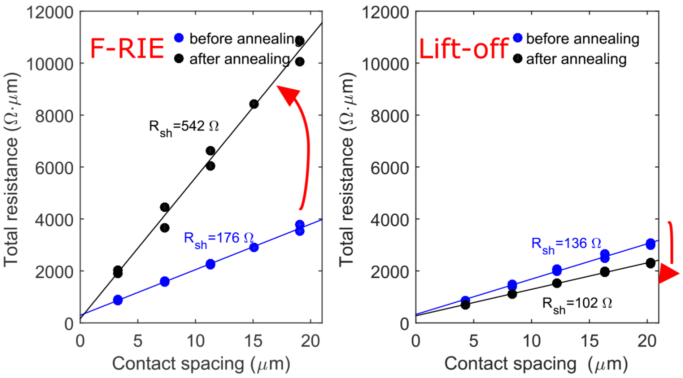

▲ Figure 2: TLM resistance versus measured contact distance before and after annealing on (left) samples that have undergone F-based RIE and (right) samples fabricated by lift-off in a F-free process.

FURTHER READING

- J. A. del Alamo, "Nanometer-scale Electronics with III–V Compound Semiconductors," *Nature*, vol. 479, no. 7373, pp. 317–323, November 2011.
- J. Lin, D. A. Antoniadis, and J. A. del Alamo, "A CMOS-compatible Fabrication Process for Scaled Self-aligned InGaAs MOSFETs," *CS Mantech*, pp. 239-242, May 2015.
- Y. Yamamoto, N. Hayafuji, N. Fujii, K. Kadoiwa, N. Yoshida, T. Sonoda, and S. Takamiya, "Donor Passivation in n-AllnAs Layers by Fluorine," *J. Electron. Mater.*, vol. 25, no. 5, pp. 685-690, May 1996.

Source/Drain Asymmetry in InGaAs Vertical Nanowire MOSFETs

X. Zhao, C. Heidelberger, E. A. Fitzgerald, J. A. del Alamo
Sponsorship: NSF E3S, Lam Research, SRC

CMOS technologies beyond the 5-nm node not only require a highly three-dimensional transistor structure but also benefit from incorporation of new channel materials. InGaAs is considered a promising material candidate while the vertical nanowire MOS field-effect transistor (MOSFET) has been shown to offer better scalability when compared at the circuit level with horizontal nanowire devices. The vertical nanowire InGaAs MOSFET is, therefore, an interesting device technology worth investigating. An intrinsic feature of vertical devices is the asymmetry between source and drain contacts, which is absent in intrinsically symmetric horizontal devices. To date, this source/drain asymmetry has been studied only theoretically.

This work demonstrates InGaAs vertical nanowire MOSFETs fabricated via a top-down approach that achieves state-of-the-art performance in terms of the balance between transport and electrostatics. The much-improved device electrostatics compared to those of an earlier device generation (Further Reading 2) stem mainly from a better oxide/semiconductor interface, enabled by improved atomic layer deposition (ALD) chamber conditioning. These devices and those of an earlier generation have enabled the first experimental study of the impact of source/drain asymmetry in vertical nanowire MOSFETs by comparing device characteristics with bottom electrode as the source (BES) and top electrode as the source (TES). Figure 1 shows key electrical figures of merit measured in both configurations in devices from this work and a previous generation (Further Reading 2). The ON-current characteristics, assessed by the transconductance, differ significantly when swapping source and drain. This is due to the inherently different top and bottom contacts. g_m asymmetry is visible in both the present and previous work. On the other hand, the asymmetry in subthreshold characteristics (notably drain-induced barrier lowering or DIBL), prominent in earlier devices, is eliminated in this work. This lack is explained by simulations that show that diameter non-uniformity along the transport direction leads to asymmetry in electrostatics. The improved InGaAs dry etch technology used in this work delivers a uniform nanowire cross section that improves over prior work, as shown in Figure 2.

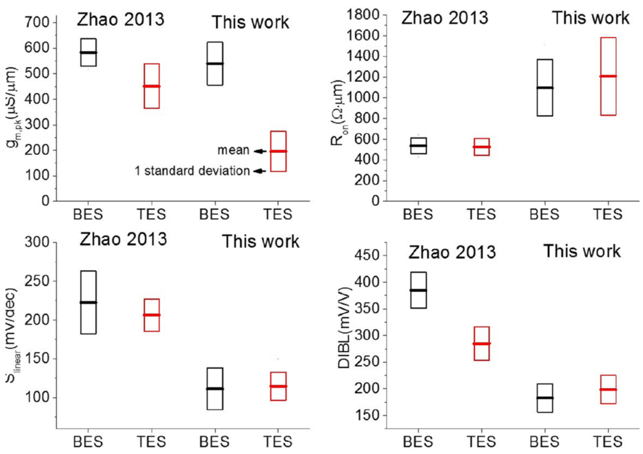

▲ Figure 1: Key electrical figures of merit of a number of devices measured in BES and TES configuration from our previous work in 2013 (below) and this work.

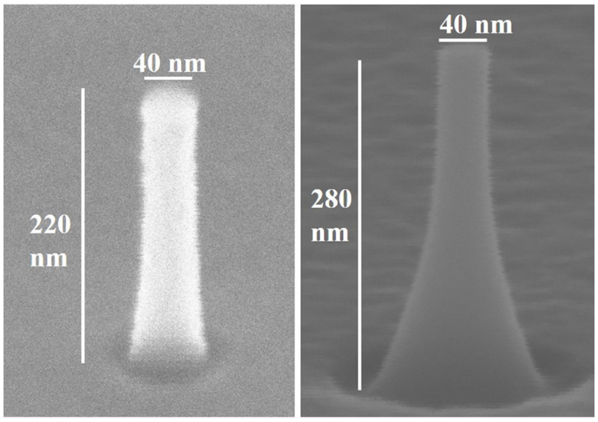

▲ Figure 2: Improved NW profile in this work (left) compared to our previous work referenced below (right).

FURTHER READING

- X. Zhao, J. Lin, C. Heidelberger, E. A. Fitzgerald, and J. A. del Alamo, "Source/Drain Asymmetry in Vertical InGaAs Nanowire MOSFETs," *IEEE Electron Device Letters*, to be published.
- X. Zhao, J. Lin, C. Heidelberger, E. A. Fitzgerald, and J. A. del Alamo, "Vertical Nanowire InGaAs MOSFETs Fabricated by a Top-down Approach," *International Electron Device Meeting Technical Digest*, pp. 695-698, 2013.
- X. Zhao and J. A. del Alamo, "Nanometer-Scale Vertical-Sidewall Reactive Ion Etching of InGaAs for 3-D III-V MOSFETs," *IEEE Electron Device Letters*, vol. 35, no. 5, pp. 521-523, May 2014.

Fabrication of Test Structures for Measuring Contact Resistance of Vertical Nanowires

D. Choi, J. A. del Alamo
Sponsorship: ILJU Academy and Culture Foundation Fellowship, NSF E3S, Lam Research

In modern transistors, the contact resistance to the source and drain has been increasing in importance as the device size has been decreasing. Although the traditional technique to measure contact resistance in planar devices, the transmission line method (TLM), is well developed, a similar technique for vertical nanowire (VNW) transistors, which are under intense investigation as next generation devices, does not exist. Our research aims to address this need.

Our test structure concept is based on a top-down nanowire fabrication approach. Once the nanowire has been etched, we need to form a thin insulating spacer on the surrounding field while preserving a clean nanowire sidewall. We are investigating hydrogen silsesquioxane (HSQ) to make this possible. The basic idea is that because HSQ is a negative electron-beam (e-beam) resist, adjusting the e-beam dose can control the final thickness after development.

To explore this concept, we have performed e-beam dose test experiments using HSQ on n+ InGaAs. The e-beam lithography pattern consists of a ten-by-ten array of test squares and a two-by-two array of reference squares (left in Figure 1). In each test pattern, the e-beam dose is increased from one end to the other.

An example of the final thickness of HSQ as a function of e-beam dose is shown in Figure 2 (black). For HSQ, FOX 16 (HSQ from Dow Corning) is used after mixed with methyl isobutyl ketone in a 2:1 ratio. The final thickness of HSQ in the exposed area increases as e-beam dose increases, and the film is hardened, as expected (right in Figure 1). Beyond a dose of around 300 μC/cm², the entire film thickness is hardened, and its final thickness saturates to the original thickness of the HSQ film. The threshold dose beyond which the final HSQ thickness is finite is about 80 μC/cm². The threshold dose is the criterion for sensitivity of HSQ; as the threshold dose increases, the sensitivity decreases.

The results of this calibration experiment suggest that to control the final thickness of HSQ through the e-beam dose, the linearly dependent portion of Figure 2 between about 80 μC/cm² to 300 μC/cm² should be used. Also, to control the final thickness easily, the slope of the linear portion of the curve needs to be reduced. We have explored processing conditions that enable this reduction. For example, Figure 2 shows data for various temperatures of a baking step after e-beam lithography. As the baking temperature increases, the slope increases, which is undesirable. We are currently exploring other process parameters to obtain improved thickness control of HSQ films. This technique should allow the fabrication of insulating layers of controlled thickness at the bottom of etched nanowires.

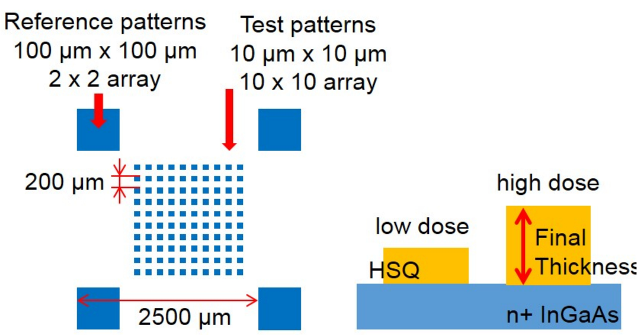

▲ Figure 1: Left: Test and reference patterns fabricated in this work. Right: Illustration of final thickness dependence of HSQ after low and high e-beam dose and subsequent development.

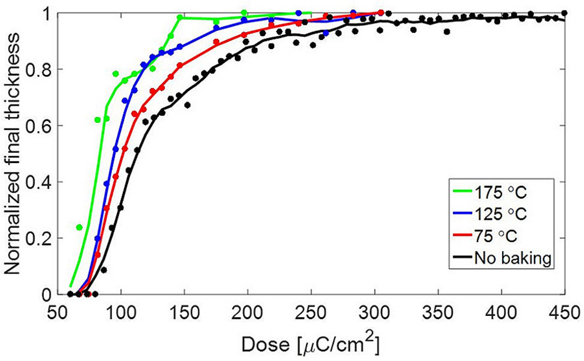

▲ Figure 2: Effect of temperature of baking after e-beam lithography on the final thickness of HSQ normalized to its initial value.

FURTHER READING

- M. Berg, J. Svensson, E. Lind, and L.-E. Wernersson, "A Transmission Line Method for Evaluation of Vertical InAs Nanowire Contacts," *Applied Physics Letters*, vol. 107, pp. 232102: 1-5, 2015.
- E. Memiševi, E. Lind, and L.-E. Wernersson, "Thin Electron Beam Defined Hydrogen Silsesquioxane Spacers for Vertical Nanowire Transistor," *Journal of Vacuum Science & Technology* vol. 32, no. 5, pp. 051211: 1-7, 2014.
- X. Zhao, J. Lin, C. Heidelberger, E. A. Fitzgerald, and J. A. del Alamo, "Vertical Nanowire InGaAs MOSFETs Fabricated by a Top-down Approach," *2013 IEEE International Electron Devices Meeting*, pp. 695-698, 2013.

Gallium Nitride Low-Voltage Devices and Technology Development for GaN Circuits

D. Piedra, T. Palacios
Sponsorship: Lincoln Laboratory, Masdar Institute of Science and Technology

Gallium nitride has found an active avenue in the application spaces of RF and power electronics for mid- to high-voltage areas. However, a somewhat unexplored area is that of low-voltage power electronics, where silicon, due to its high integration density, low cost, and years of technological maturity, still reigns supreme. In this project, we explore, through modeling and experimentation, the design space of low-voltage power electronics and gauge the feasibility of using GaN for such applications. We will see the limitation, which may restrict performance in this space, and examine what improvements would need to be made to have the biggest impact on device performance for low-voltage switching.

Using empirical results from devices designed for RF applications, we model to see if such devices could be competitive with Si low-voltage devices and to determine potential problems or limitations. The initial test device was an InAlGaN/GaN HEMT grown on SiC substrate. The fabricated devices had Lg=90 nm and an array of different gate widths.

Finally, we have fabricated and tested structures to satisfy the requirements of the passive components. We have fabricated capacitors using the dielectrics that are to be used in the device process as passivation or interlayer dielectric layers and confirmed that the employed thickness can meet capacitance and breakdown requirements. Also, an initial batch of thin film resistors has been fabricated from evaporated NiCr metal showing a resistivity of 36Ω/sq.

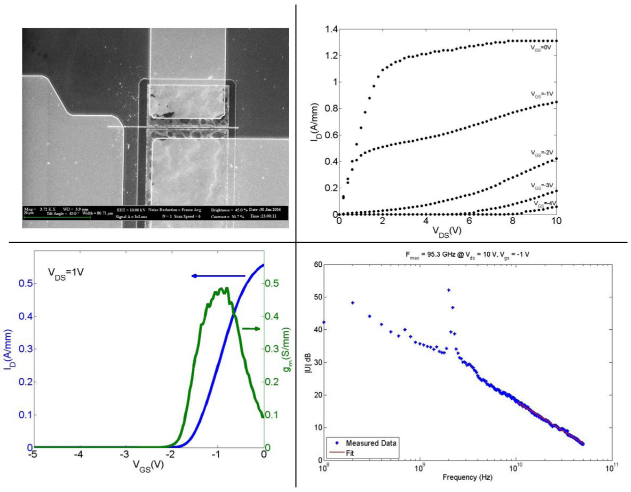

▲Figure 1: InAlGaN/GaN HEMT with Lg=90 nm and F_{max}=95.3 GHz. This device will serve as the initial test device to obtain empirical measurements on which to build the model for a low-voltage switching device.

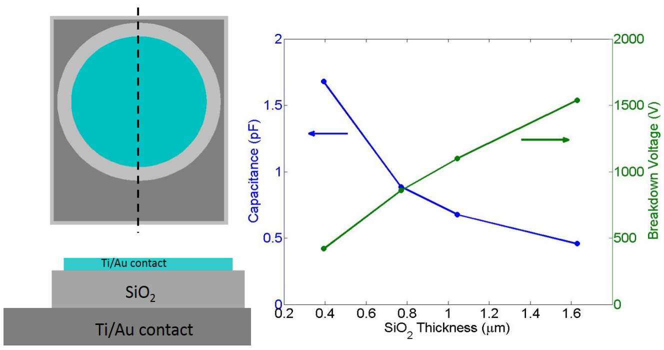

▲Figure 2: Test SiO_2 capacitors fabricated out of the device passivation and interlayer dielectric layers.

FURTHER READING

- D. S. Lee, X. Gao, S. Guo, and T. Palacios, "InAlN/GaN HEMTs with AlGaN Back Barriers," *IEEE Electron Device Letters*, vol. 32, no. 5, pp. 617-619, May 2011.
- D. S. Lee, X. Gao, S. Guo, D. Kopp, P. Fay, and T. Palacios, "300-GHz InAlN/GaN HEMTs with InGaN Back-Barrier," *IEEE Electron Dev. Letters*, vol. 32, no. 11, pp. 1525-1527, November 2011.

Vertical GaN Power Transistors on Bulk GaN Substrate

M. Sun, T. Palacios
Sponsorship: ARPA-E SWITCHES

The ideal power switch combines a high breakdown voltage and a low on-resistance, R_{on}. Gallium nitride, GaN, due to its high critical field and electron mobility, has superior R_{on} compared to Si for a given breakdown voltage. Now lateral GaN transistors on Si substrates, with operating voltage less than 650 V, are commercially available. The main drawback of the lateral geometry is, however, that the transistor area is proportional to the breakdown voltage. In addition, numerous material interfaces are exposed to high electric fields. For higher-voltage high-current applications, the device size increases dramatically. A vertical device would significantly reduce the die size, as this size would not depend on the breakdown voltage.

The most studied vertical GaN transistor, the current aperture vertical electron transistor (CAVET), has made significant progress in performance, but it still faces great challenges. The CAVET structure requires a p-doped current- blocking layer buried in the n-doped GaN layer. Activating the p-dopant magnesium in GaN has been found very challenging. Also, it needs a high-quality regrowth of the AlGaN/GaN layer, making it expensive. Our work has developed a novel vertical Junction Field Effect Transistor (JFET) structure to address the challenge mentioned above. As shown in Figure 1, the current flows from the drain to source vertically through a sub-micron-channel, which is surrounded by the metal gate pads. Below the threshold voltage, the channel electrons are depleted due to the work-function difference between the gate metal and GaN. Figure 2 shows the transfer characteristics of the new vertical GaN JFET with channel length 0.4 µm. The current on/off ratio is ~ 10^{11}. The device shows a 0.5-V threshold voltage, defined at $I_{on}/I_{off} = 10^5$. The subthreshold swing of the device is less than 100 mV/dec. The hysteresis is very small, which demonstrates the excellent material quality of the wet etched sidewall. The VFET broke down at V_d = 450 V measured at V_{gs} = 0 V.

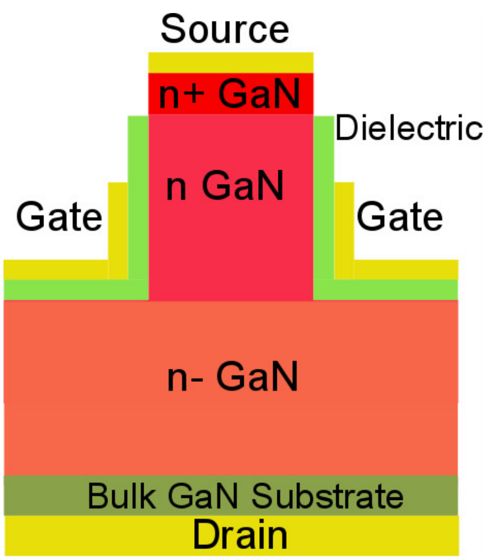

▲Figure 1: Structure of a Vertical GaN JFET on bulk GaN substrate.

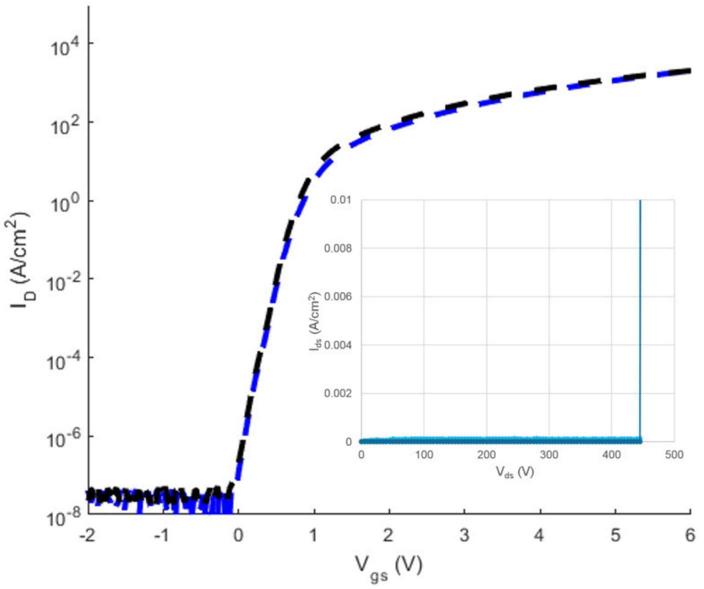

▲Figure 2: Transfer IV characteristics of a vertical GaN JFET with 0.4-µm channel length. The drain voltage is 10 V. The inset figure shows the breakdown curve at V_{gs} = 0 V.

FURTHER READING

- H. Amano, "Progress and Prospect of the Growth of Wide-Band-Gap Group III Nitrides: Development of the Growth Method for Single-Crystal Bulk GaN," *Japanese Journal of Applied Physics*, vol. 52, pp. 050001, 2013.
- S. Chowdhury, "Current Status and Scope of Gallium Nitride-based Vertical Transistors for High-power Electronics Application," *Semiconductor Science and Technology*, vol. 28, pp. 074014, 2013.

Origin of Off-State Leakage in GaN Vertical Power Diodes

Y. Zhang, M. Sun, T. Palacios
Sponsorship: ARPA-E SWITCHES

GaN transistors and diodes are excellent candidates for high-power electronics. Currently, both lateral and vertical GaN devices are being considered. Specifically, vertical devices have attracted increased attention, due to several potential advantages over lateral devices: 1) higher breakdown voltage (BV) without enlarging chip size, 2) superior reliability, and 3) enhanced thermal performance. Recently, high-performance GaN vertical devices have been demonstrated on GaN, sapphire and Si substrates with over 3.7 kV BV and lower leakage than GaN lateral devices.

Off-state leakage current is a key factor determining the device BV, power circuit loss and, potentially, reliability. However, the physical mechanisms and the design space of the leakage current in GaN vertical devices are still unknown.

In this work, we fabricated GaN vertical diodes on different substrates and then unveiled the leakage mechanism by analytical analysis and TCAD simulation. Finally, the design space of leakage current in GaN vertical devices was derived and benchmarked with GaN lateral, Si, and SiC devices.

GaN vertical p-n diodes were fabricated on GaN, sapphire, and Si substrates with similar doping levels in p-GaN and n-GaN drift layers (Figure 1). To identify the bulk leakage mechanism, correlations between leakage current I and the average electric field in the drift layer (E_{av}) were studied. According to the I *vs.* E_{av} relationship, variable-range-hopping through dislocations was identified as the main off-state leakage mechanism for GaN vertical diodes on different substrates. The behavior of leakage current for vertical devices as a function of dislocation density and electric field was derived by TCAD simulations, after careful calibration with experimental and literature data. The designed GaN vertical diodes demonstrate 2-4 orders of magnitude lower leakage current while supporting 3-5 times higher electric field, compared to GaN lateral, Si and SiC devices (Figure 2).

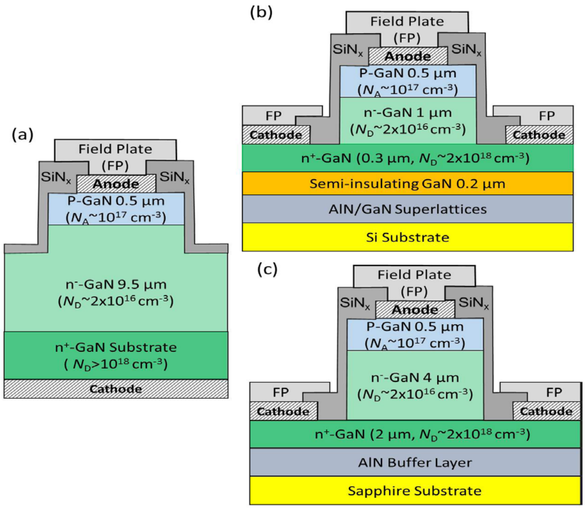

▲Figure 1: Schematic of GaN vertical p-n diodes on (a) GaN, (b) Si, and (c) sapphire substrates, fabricated at MIT MTL.

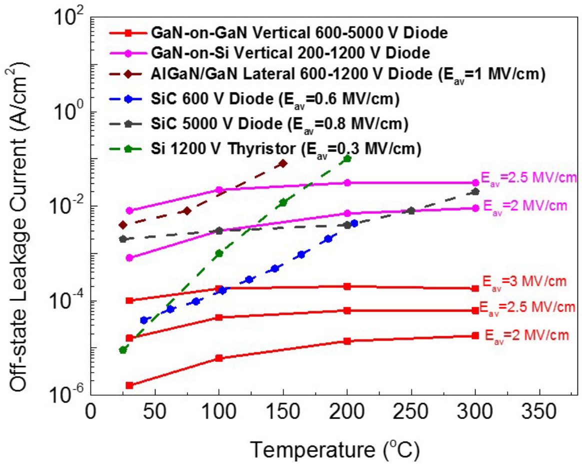

▲Figure 2: Off-state leakage current vs. temperature of the designed GaN-on-GaN vertical diodes and GaN-on-Si vertical diodes, benchmarked with the reported lateral GaN diodes, SiC 600 V and 5000 V diodes, and Si 1200 V thyristors.

FURTHER READING

- Y. Zhang *et al*, "Design Space and Origin of Off-state Leakage in GaN Vertical Power Diodes," *Proceedings of 2015 IEEE International Electron Devices Meeting (IEDM)*, pp. 35.1-35.4, Washington DC, USA, December, 2015.
- Y. Zhang *et al*, "Origin and Control of Off-State Leakage Current in GaN-on-Si Vertical Diodes," *IEEE Transactions on Electron Devices*, vol. 62, pp. 2155-2161, 2015.
- Y. Zhang *et al*, "GaN-on-Si Vertical Schottky and pn Diodes," *IEEE Electron Device Letters*, vol. 35, pp. 618-620, 2014.

Near-Junction Thermal Management in GaN HEMTS via Wafer Bonding

R. M. Radway, T. Palacios
Sponsorship: Masdar Institute of Science and Technology

Gallium nitride (GaN)-based high electron mobility transistors (HEMTs) offer excellent performance for use in power conversion, high-frequency power amplifiers, and radar applications. However, operating temperatures effectively limit output power to 5W/mm from the reported maximum of 40W/mm. Thermal management is, therefore, critical for reliable high-power use. Our current research focuses on developing effective thermal models and scalable fabrication techniques to aid in solving these thermal management problems in GaN HEMT design.

Using an analytical solution for temperature rise in multilayered epitaxial structures, we evaluated several standard GaN-on-silicon, GaN-on-silicon carbide (SiC), and GaN-on-diamond epitaxial structures as well as novel structures formed via waferbonding. Going beyond structure, we modeled thermal conductivity reduction and thermal-boundary resistances for the materials in question. In determining these parameters, we considered non-classical effects due to scale and material quality. Phonon mean free path reduction due to diffuse boundary scattering decreases thermal conductivities of thin epitaxial layers. We calculated thermal-boundary resistances using a diffuse mismatch model, but these values are highly dependent on interfacial material quality; interfaces between low-quality material near growth origination will have higher resistivities than those further from nucleation due to GaN crystal dislocations caused by lattice mismatch. These constraints suggest that thermally optimal interfaces are formed by directly bonding high-quality materials from the final layers of epitaxial growth to thermally conductive substrates such as SiC (Figure 2).

We examined several designs based on GaN-SiC direct bonding, etching away of poor material and interfaces, and subsequent device fabrication on the high-quality material remaining. The novel structure shown below improved thermal performance compared to a standard epitaxial structure (Figures 1 and 2). We are currently researching methods for wafer bonding of GaN and SiC to achieve this efficient design. Plasma surface activation shows promise, and we are focused on using these bonding techniques for device fabrication, with the end goal of experimental verification of simulated improvements.

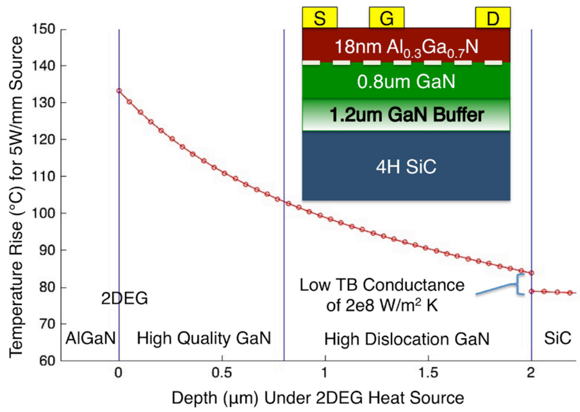

▲Figure 1: GaN-on-SiC structure grown via MBE; simulated temperature rise of vertical locations under the right edge of gate with device dissipation 5W/mm.

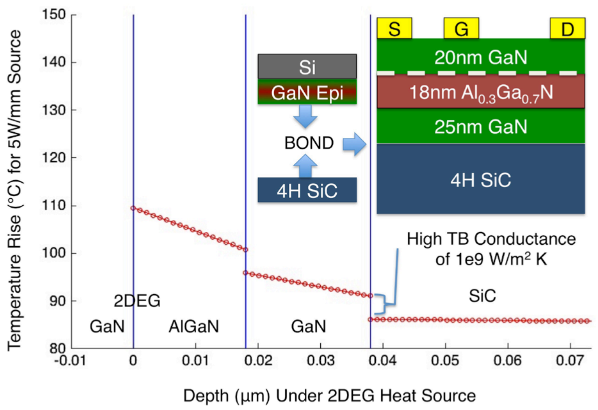

▲Figure 2: Novel GaN-on-SiC structure fabricated via wafer bonding; simulated temperature rise of vertical locations under the right edge of gate with device dissipation 5W/mm.

FURTHER READING

• K. R. Bagnall, Y. S. Muzychka, and E. N. Wang, "Analytical Solution for Temperature Rise in Complex Multilayer Structures with Discrete Heat Sources," *IEEE Transactions on Components, Packaging and Manufacturing Technology*, vol. 4, no. 5, pp. 817-830, 2014.

Impact of the Inverse Piezoelectric Effect on Micro-Raman Thermography in GaN HEMTs

K. R. Bagnall, E. N. Wang
Sponsorship: MIT/MTL Gallium Nitride (GaN) Energy Initiative, SMART LEES

Gallium nitride (GaN) high electron mobility transistors (HEMTs) are one of the most promising compound semiconductor technologies for solid-state high-frequency power amplifier (PA) and high-voltage power conversion applications. However, the high power densities present in GaN HEMTs often lead to high channel temperatures, which must be accurately characterized and managed to maximize device reliability and performance. Over the last fifteen years, micro-Raman thermography has emerged as one of the most reliable and popular techniques for measuring the channel temperature in GaN HEMTs with high spatial (~1 μm) and temporal (~10 ns) resolution.

Despite the many advantages of micro-Raman thermography, temperature measurements based on the change in Raman peak position associated with the Stokes (phonon emission) process are also affected by the thermoelastic and inverse piezoelectric (IPE) effects. A number of studies have shown that using the pinched-off state as the unpowered reference for micro-Raman thermography effectively removes the impact of IPE-induced strain/stress. Yet quantitative values of the strain, stress, and electric field components derived from micro-Raman spectroscopy measurements of GaN HEMTs biased in the pinched-off state disagree in sign and order of magnitude with those predicted by electro-mechanical modeling.

Using both electro-mechanical device modeling and very high precision micro-Raman spectroscopy, we are investigating the response of the Raman spectrum of the GaN buffer in GaN HEMTs to strain, stress, and electric field induced in the pinched-off state. Thus far, our work has shown that experimental data from previous studies predict the in-plane stress and vertical electric field to be an order of magnitude larger than our electro-mechanical model. We believe that these discrepancies can be resolved by considering the impact of the electric field on the optical phonon frequencies apart from the IPE effect, which we aim to demonstrate experimentally for the first time.

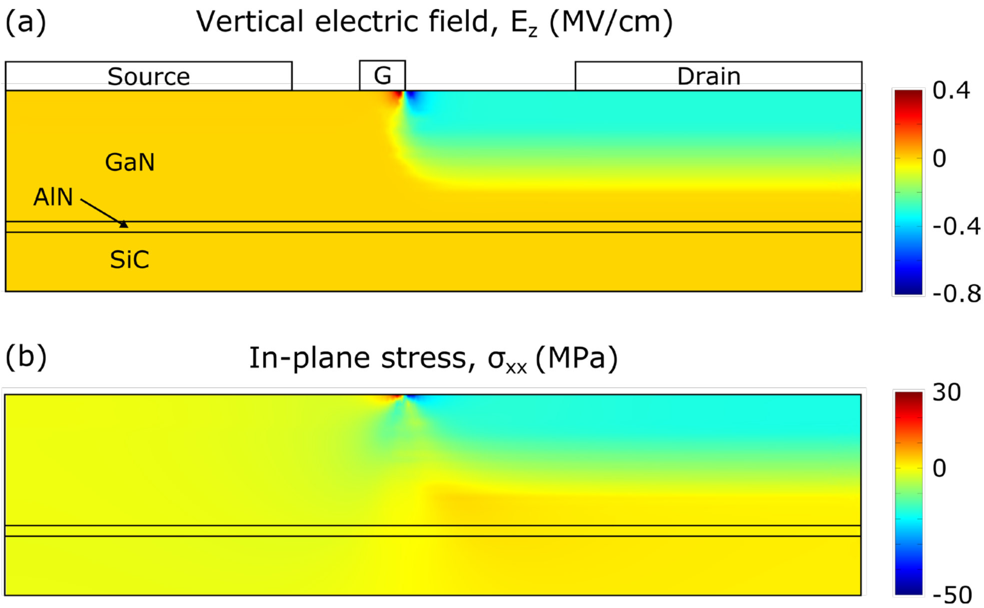

▲ Figure 1: (a) Vertical electric field and (b) in-plane stress predicted by a semiconductor device electro-mechanical model of a GaN HEMT under bias in the pinched-off state. The vertical electric field component in the gate-drain access region is negative, resulting in a compressive in-plane stress.

FURTHER READING

- A. Sarua, H. Ji, M. Kuball, M. J. Uren, T. Martin, K. J. Nash, K. P. Hilton, and R. S. Balmer, "Piezoelectric Strain in AlGaN/GaN Heterostructure Field-effect Transistors Under Bias," *Applied Physics Letters*, vol. 88, pp. 103502, 2006.
- K. R. Bagnall and E. N. Wang, "Experimental Characterization of Inverse Piezoelectric Strain in GaN High Electron Mobility Transistors via Micro-Raman Spectroscopy," *Review of Scientific Instruments*, vol. 87, pp. 061501:1-23, June 2016.

Imaging Current Distributions and Temperature Profiles in GaN HEMTs using Nitrogen Vacancy Centers in Nanodiamonds

C. Foy, K. R. Bagnall, M. E. Trusheim, A. Lauri, E. N. Wang, D. R. Englund
Sponsorship: EFRC Center for Excitonics, NSF

Gallium nitride (GaN) high-electron-mobility transistors (HEMTs) are a leading solid-state technology for microwave power amplifiers for a range of applications. However, the high power densities in GaN HEMTs often lead to electronic junction temperatures in excess of 200 °C. Such high temperatures accelerate device degradation. In this work, we introduce a wide-field temperature and magnetic measurement technique with simple instrumentation and calibration procedures for GaN electronics characterization. This technique is based on nanoscale spin-based thermometry using NV centers in nanodiamonds.

NV centers, under ambient conditions, enable optically detected magnetic resonance (ODMR) and can provide sub-wavelength imaging. These properties allow the NV to make highly localized simultaneous measurements of temperatures and magnetic fields. Such measurements are accomplished by determining the NV's ground state spin electron levels, which respond to the changes in the NV's local magnetic and thermal environment. Determining the position of these electron spin sublevels is accomplished by measuring the ODMR spectra on standard microscopes.

We deposited NVs onto the surface of an ungated GaN-on-sapphire HEMT so that they are within ~30 nm of the HEMT channel. In Figure 1 we measure the magnetic field and temperature across an NV by applying the model described previously and observe an increase of 67 °C and 3.4 G as 10 V and 42 mA are applied across the ungated GaN HEMT. These wide-field temperature measurements allow us to determine the location and value of the peak junction temperature of the GaN-on-sapphire HEMT. The current density distribution is then subsequently calculated from the magnetic field distribution. NV centers offer robust, wide-field temperature and current measurements with simple instrumentation and are a promising addition to the repertoire of thermal and magnetic imaging.

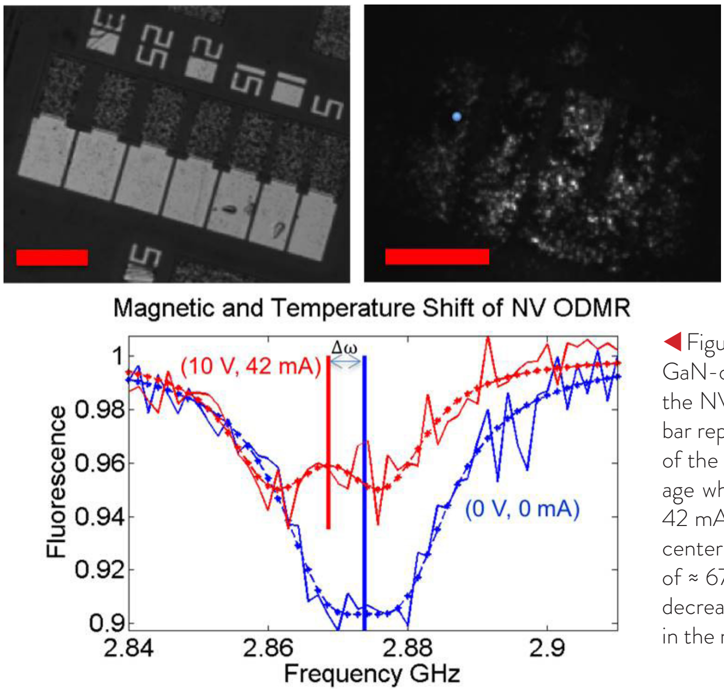

◀ Figure 1: Top Left: Bright field image of a series of ungated GaN-on-sapphire HEMTs. Top Right: Fluorescence image of the NV centers on top of the ungated GaN HEMTs. The scale bar represents 100 μm in both images. Bottom: ODMR curves of the NV located at the point marked in the fluorescence image when the device is unpowered (blue curve) and 10 V and 42 mA are applied (red curve). The change in frequency of the center of the ODMR curve (Δω) represents a temperature rise of ≈ 67 °C across the NV center. Further, the broadening and decrease in amplitude of the distribution represent an increase in the magnetic field of 3.4 G across the NV.

FURTHER READING

- S. Steinert, F. Dolde, P. Neumann, A. Aird, B. Naydenov, G. Balasubramanian, F. Jelezko, and J. Wrachtrup, "High Sensitivity Magnetic Imaging Using an Array of Spins in Diamond," *Review of Scientific Instruments*, vol. 81, no. 4, pp. 043705, April 2010.
- G. Kucsko, P. C. Maurer, N. Y. Yao, M. Kubo, H. J. Noh, P. K. Lo, H. Park, and M. D. Lukin, "Nanometre-scale Thermometry in a Living Cell," *Nature*, vol. 500, no. 7460, pp. 54, August 2013.

Negative-Bias Temperature Instability in GaN Power Field-Effect Transistors

A. Guo, J. A. del Alamo
Sponsorship: MIT/MTL Gallium Nitride (GaN) Energy Initiative, NDSEG Research Fellowship

Gallium nitride (GaN) field-effect-transistors (FETs) are promising for replacing silicon in power electronics. For high-voltage applications, GaN-high electron mobility transistors with insulated-gate (GaN MIS-HEMTs) are especially attractive because the added insulator suppresses gate leakage and allows for larger gate swing, both essential for high-voltage performance. However, reliability issues surrounding GaN MIS-HEMTs are major roadblocks for technology commercialization. For example, threshold voltage (V_T) instability as a result of negative gate stress at elevated temperature (referred to as negative-bias temperature instability, or NBTI) is a serious concern. NBTI is studied in silicon transistors but much less well understood in GaN MIS-HEMTs. Addressing this issue is challenging because the many layers and interfaces of a MIS-HEMT structure make identifying the physical origin of NBTI difficult. Here, we study GaN metal-oxide-semiconductor FETs (MOSFETs) (Figure 1), which allow us to focus on stability issues associated with the oxide and the oxide/GaN interface.

We used a benign characterization scheme, also utilized in our earlier studies on positive-bias temperature instability (PBTI). We carried out experiments with gate stress ($V_{GS,stress}$) between -1 V and -70 V, stress time (t_{stress}) between 1 and 10,000 seconds, and temperature (T) between -40°C and 175°C. Our study shows that NBTI in GaN MOSFETs progresses through three regimes. Figure 2 shows this progression. A device was subjected to $V_{GS,stress}$ = -10 V at T = 175°C for 10,000 s. As t_{stress} increases, V_T first shifts negative, then positive, and then negative again. At the end, we see a negative V_T shift that is non-recoverable after thermal detrapping.

After many detailed experiments, we identified three mechanisms responsible for V_T shift of GaN MOSFETs due to NBTI. Under low-stress (regime 1), a small, negative V_T shift that is completely recoverable is observed. This shift can be modeled using a well-established oxide-trapping model. We then conclude that electron detrapping from pre-existing oxide traps is likely to be responsible for this shift. For mid-stress (regime 2), a recoverable positive V_T shift is observed. We attribute this behavior to trapping in the GaN channel. The high vertical electrical field in the channel under the gate edges causes electron trapping in deep levels within the GaN band gap, which appears as a temporarily increased doping level. For high-stress (regime 3), there is an additional negative V_T shift that is non-recoverable and that is accompanied by permanent subthreshold swing degradation. These observations strongly suggest the generation of interface states. Our findings should be instrumental in understanding the instability of GaN MIS-HEMTs.

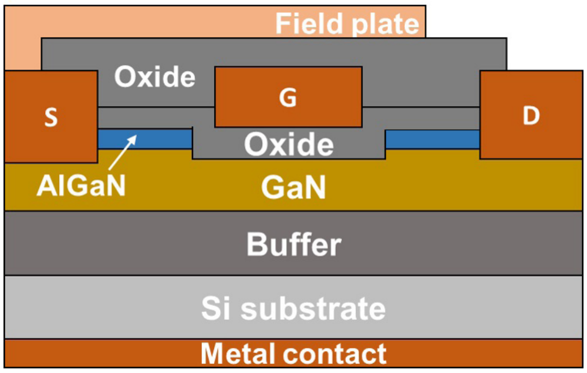

▲ Figure 1: GaN MOSFET structure studied in this work.

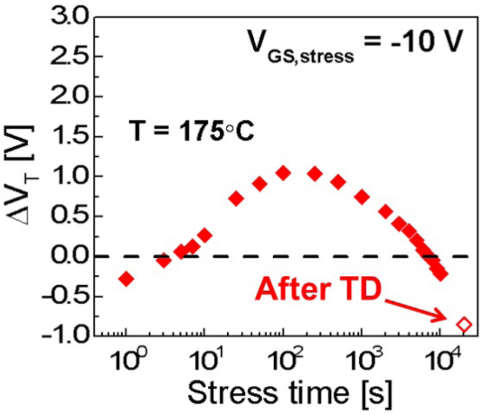

▲ Figure 2: Stress time evolution of ΔV_T for GaN MOSFETs with SiO_2/Al_2O_3 as gate dielectric for $V_{GS,stress}$ = -10 V at 175°C. Filled symbols are the total ΔV_T extracted 1 sec after stress, and open symbol are the non-recoverable ΔV_T after a thermal detrapping (TD) step.

FURTHER READING

- A. Guo and J. A. del Alamo, "Negative-Bias Temperature Instability (NBTI) of GaN MOSFETs," *IEEE International Reliability Physics Symposium*, Pasadena, CA, 2016.
- A. Guo and J. A. del Alamo, "Positive-Bias Temperature Instability (PBTI) of GaN MOSFETs," *IEEE International Reliability Physics Symposium*, Monterey, CA, 2015.

Progressive Breakdown in High-Voltage GaN Field-Effect Transistors

S. Warnock, J. A. del Alamo
Sponsorship: Texas Instruments

As the demand for more energy efficient electronics increases, GaN field-effect transistors (FETs) have emerged as promising candidates for high-voltage power management applications. Though GaN has excellent material properties, there are still many challenges to overcome before GaN power transistors are ready for commercial deployment. One of the concerns is gate dielectric reliability as a result of high-voltage stress. In particular, after prolonged high-voltage gate bias stress, the dielectric will suffer from catastrophic breakdown beyond which the transistor is no longer operational.

Our research is directed to providing fundamental understanding behind the physics of time-dependent dielectric breakdown (TDDB) of the gate dielectric in GaN metal-insulator-semiconductor high-electron-mobility transistors (MIS-HEMTs), the most promising transistor structure for power electronics. We focus here in particular on a regime of breakdown known as progressive breakdown, or PBD. As this condition at times takes place soon before the complete breakdown of the gate dielectric, studying PBD could provide valuable insight into the hard breakdown (HBD) physics. Figure 1 shows the evolution of the gate current, I_G, in a typical constant-voltage TDDB experiment. We can observe first a decrease in current due to trapping and then an increase in what is known as stress-induced leakage current (SILC). The inset shows that near the final catastrophic breakdown (or HBD), I_G becomes noisy, a condition known as progressive breakdown (PBD). The time at which the noise appears is denoted as time-to-first-breakdown, t_{1BD}.

Figure 2 shows the statistical distribution of both hard breakdown and first breakdown in a number of transistors. TDDB statistics are typically shown on a Weibull plot, where F is the cumulative device failure for a given time. The nearly parallel slopes for t_{1BD} and HBD suggest the two have a common physical origin.

Through experiments such as these, we hope to gain an understanding of the fundamental mechanisms behind dielectric breakdown as well as build models that allow us to predict device lifetime under realistic operating conditions.

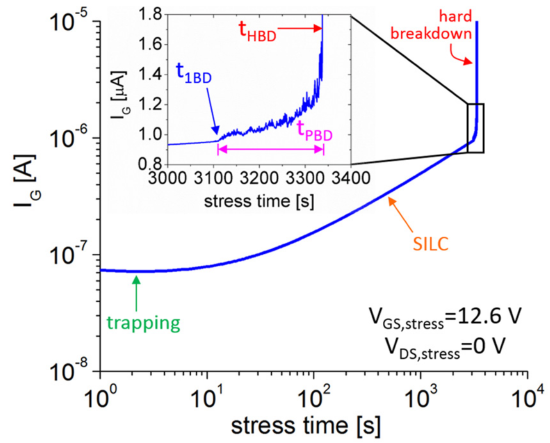

▲ Figure 1: Gate current as function of stress time during constant $V_{GS,stress}$ TDDB experiment. FET is held at $V_{GS,stress}$=12.6 V until device breaks down. $V_{DS,stress}$=0 V. Inset shows detail of I_G evolution right before HBD. Clear onset of noise in I_G marks the start of PBD.

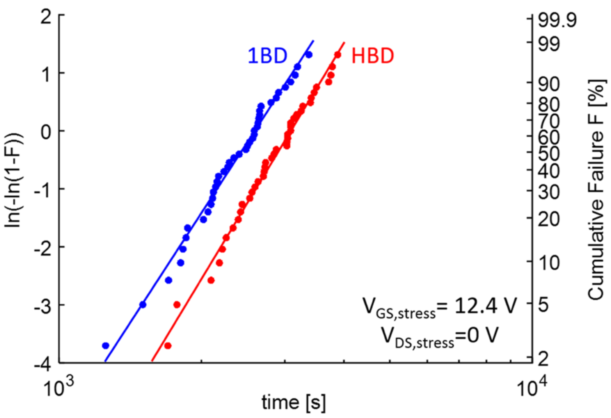

▲ Figure 2: Weibull plot of t_{1BD} and t_{HBD}. $V_{GS,stress}$=12.4 V, $V_{DS,stress}$=0 V. Nearly parallel statistics for t_{1BD} and HBD suggest a unified degradation mechanism.

FURTHER READING

- S. Warnock and J. A. del Alamo, "Stress and Characterization to Assess Oxide Breakdown in High-Voltage GaN Field-Effect Transistors," *Compound Semiconductor Manufacturing Technology Conference (CS MANTECH)*, pp. 311-314, 2015.
- S. Warnock and J. A. del Alamo, "Progressive Breakdown in High-Voltage GaN MIS-HEMTs," *IEEE International Reliability Physics (IRPS) Conference*, Pasadena, CA, pp. 4A-6-1-4A-6-6, 2016.

Gate Stack Degradation of InAlN/GaN HEMTs for RF Applications

Y. Wu, J. A. del Alamo
Sponsorship: National Reconnaissance Office

First demonstrated in the 1990s, GaN transistors have become commercially available in recent years. Compared with other commonly used materials such as Si and GaAs, GaN devices can operate at higher voltages and frequencies, thus enabling significant improvements in power efficiency and a dramatic reduction in size.

In contrast to the conventional GaN HEMT with AlGaN as barrier layer, the use of an InAlN barrier yields, for the same layer thickness, a higher spontaneous polarization-induced charge at the barrier/GaN interface. This enables aggressive barrier thickness scaling and therefore greater gate length scaling. As a result, InAlN/GaN HEMTs are extremely promising for very high frequency applications. However, unlike the better understood AlGaN/GaN system, the dominant degradation mechanisms in InAlN/GaN HEMTs are not well established. Our project aims to study the leading degradation modes of InAlN/GaN HEMTs under different stress conditions with the ultimate goal of constructing models to predict device lifetime.

After exploring various stress conditions, we have identified a common pattern of degradation in which a significant increase in gate leakage current takes place together with a drain current decrease (see Figure 1). Further study revealed two degradation mechanisms at play: one is responsible for the rapid degradation of gate and drain currents (first few seconds in Figure 1) as well as a positive shift of threshold voltage (first few seconds in Figure 2). Pure thermal stress experiments (not shown here) have led us to believe that the rapid degradation could be caused by gate sinking, essentially a reaction at the gate metal/semiconductor interface that reduces the Schottky barrier height. In transmission electron microscopy images of stressed devices, we have also observed the appearance of a disordered region in the semiconductor channel under the gate metal, which is consistent with our hypothesis. A second degradation mechanism is responsible for the longer-term continued degradation of the currents (Figure 1) as well as the negative shift of V_T (Figure 2). This mechanism could be trapping and/or the creation of new traps.

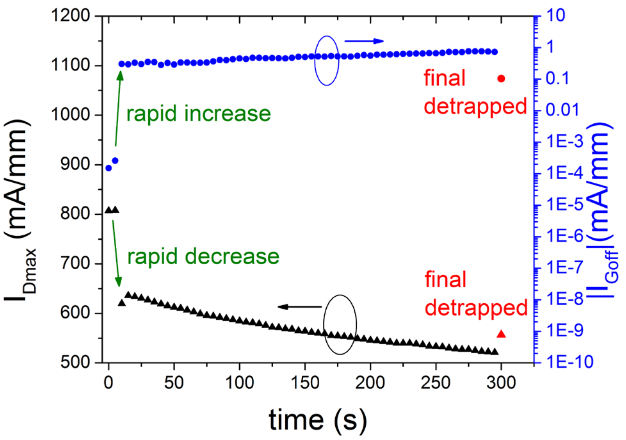

▲ Figure 1: Evolution of I_{Dmax} (@ V_{DS} = 4 V, V_{GS} = 2 V) and I_{Goff} (@ V_{DS} = 0.1 V, V_{GS} = -2 V) under high-power stress. During the first few seconds, a rapid drain current decrease and a gate current increase occur. Following this, device degradation continues at a much slower rate.

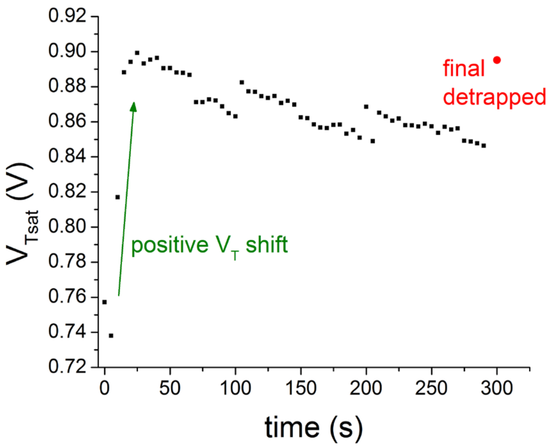

▲ Figure 2: Evolution of threshold voltage under high-power stress. An initial increase takes place within the first few seconds. After that, V_T shifts in the negative direction.

FURTHER READING

- Y. Wu, C.-Y. Chen, and J. A. del Alamo, "Electrical and Structural Degradation of GaN HEMTs Under High-power and High-temperature DC Stress," *Journal of Applied Physics*, vol. 117, no. 2, pp. 025707, January 2015.

Characterization of Graphene/GaN Heterojunction Diodes for Graphene-on-GaN Hot Electron Transistor

A. Zubair, A. Nourbakhsh, J. Y. Hong, J. Kong, M. Dresselhaus, T. Palacios
Sponsorship: U.S. Army Research Office

Hot electron transistors (HETs) are promising devices that may enable high-frequency operation that currently CMOS cannot provide. In an HET, carrier transport is due to injection of hot electrons from an emitter to a collector, which is modulated by a base electrode. Therefore ultra-thin base electrodes are needed to facilitate ultra-short transit time and high performance for a THz operation range. In this regard, graphene, the thinnest conductive membrane in nature, is considered the best candidate for the base material in HETs.

We previously demonstrated a vertical graphene-on-GaN HET with a record current density and current saturation. Nevertheless, the device showed a relatively high turn-on voltage due to relatively thick barrier. To reduce the turn-on voltage and enhance the tunneling current, a thinner emitter-base barrier is needed. In this work, we use a 1 nm/ (5 nm or 7.4 nm) AlN/InAlN heterostructure instead of the 15 nm/3 nm AlGaN/GaN barrier that was used previously. The current-voltage characteristics show that the turn-on voltage decreases significantly with barrier thickness (Figure 2 (a)). The measured current density (~10 A/cm² at 2V) in the modified graphene-GaN HET is comparable to the values reported in the literature for all-GaN HETs. Our capacitance-voltage (C-V) study of graphene/AlN/InAlN/GaN structures shows good interface between graphene and AlN/InAlN barrier. The C-V measurement (Figure 2(b)) shows a clear transition from depletion to accumulation for a typical GaN-based capacitor. The valleys at the accumulation region correspond to the graphene quantum capacitance, which is in series with the barrier capacitance. The presence of this feature indicates strong Fermi-level modulation in graphene near its Dirac point.

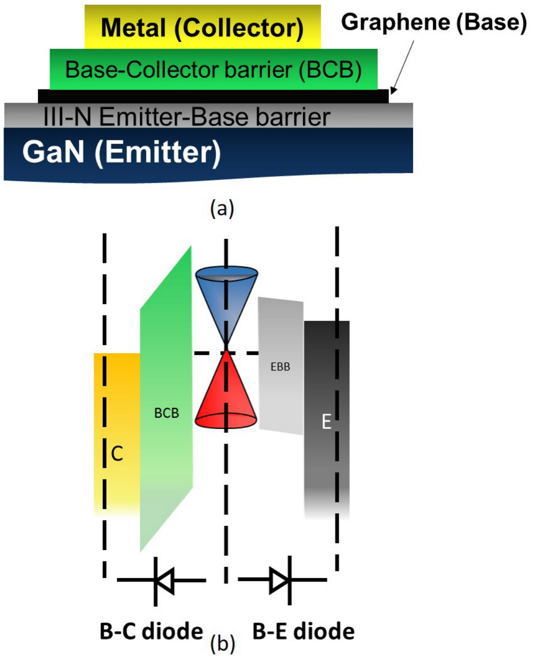

▲Figure 1: (a) Schematic cross section of a typical graphene-on-GaN hot electron transistor. (b) Qualitative energy band diagram of an HET showing base-emitter and base-collector diode components.

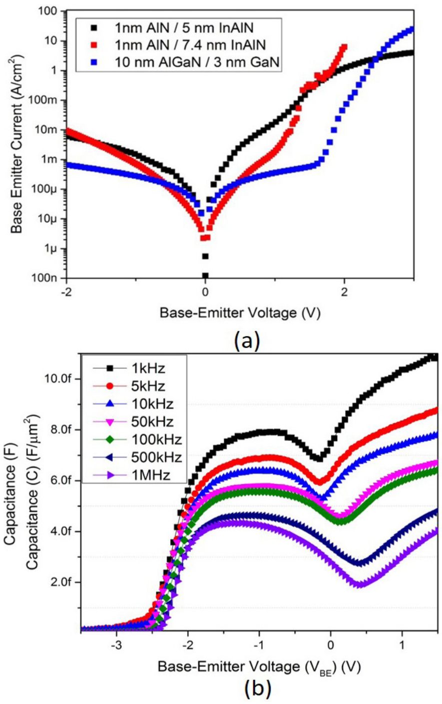

▲Figure 2: (a) Base-emitter transport characteristics of graphene/GaN heterojunction diode for different barrier thickness. (b) Capacitance-voltage characteristics of graphene/GaN heterojunction.

FURTHER READING

- C. A. Mead, "Operation of Tunnel Emission Devices," *Journal of Appl. Phys.*, vol. 32, pp. 646, 1961.
- S. Vaziri, G. Lupina, C. Henkel, A. Smith, M. Ostling, J. Dabrowski, G. Lippert, W. Mehr, M. Lemme, "A Graphene-Based Hot Electron Transistor," *Nano Letters*, vol. 13, 1435-1439, 2013.
- S. Dasgupta, A. Nidhi, J. Speck, U. Mishra, "Experimental Demonstration of III-Nitride Hot Electron Transistor with GaN Base," *IEEE Electron Device Letter*, vol. 32, pp. 1212–1214, 2011.

Monolayer MoS_2 FETs with Sub-10-nm Channel Formed by Directed Self-Assembly

A. Nourbakhsh, A. Zubair, A. Tavakkoli K. G., R. Sajjad, X. Ling, M. Dresselhaus, J. Kong, K. K. Berggren, D. A. Antoniadis, T. Palacios
Sponsorship: ONR, U.S. Army Research Office

2D crystals of layered transition metal dichalcogenides such as molybdenum disulfide (MoS_2) are ideal candidates for aggressive miniaturization of field-effect transistors (FETs) to the single-digit-nanometer scale. Beyond having a large bandgap, chemical stability, and compatibility with CMOS processes, this class of materials can benefit from their atomically thin body with dangling-bond-free surfaces. Because of this and their ultra-small body thickness, the transistor subthreshold swing (SS) and drain-induced barrier-lowering (DIBL) coefficient in such films can be significantly smaller than for conventional thin-body semiconductors. In particular, monolayer-MoS_2 (ML-MoS_2), because of its bandgap of 1.8 eV yields high I_{on}/I_{off} ratio FETs, while its low dielectric constant, ε_s = 4-7, and atomically thin body, t ≈ 0.7 nm, facilitate the reduction of characteristic scaling length.

We previously reported a 15-nm channel length MoS_2 FET using monolayer graphene as the source/drain (S/D) contacts. Here, by exploiting the semiconducting to metallic phase transition in MoS_2, we demonstrate a 7.5-nm transistor channel length by patterning of ML-MoS_2 in a periodic chain of homojunction semiconducting- (2H) and metallic-phase (1T') MoS_2 regions. The 2H- to 1T'-phase transition occurs by exposing 2H-MoS_2 to *n*-butyl lithium solution. Sub-10-nm 1T'/2H MoS_2 patterning is achieved by directed self-assembly of block copolymers (BCP: PDMS/polystyrene) technique, as shown in Figure 1. Figure 2 shows the transfer characteristics of the MoS_2 transistor chain at different V_d values and the model fit to the data using the MIT Virtual Source model (MVS). The transistor chain shows I_{on}/I_{off} ≈10^6 with I_{off} ≈100 pA/µm. Modeling of the resulting characteristics reveals that the 2H/1T' MoS_2 homojunction has a resistance of 75 Ω.µm while the 2H-MoS_2 exhibits low-field mobility of ~8 cm^2/V.s and carrier injection velocity of ~10^6 cm/s.

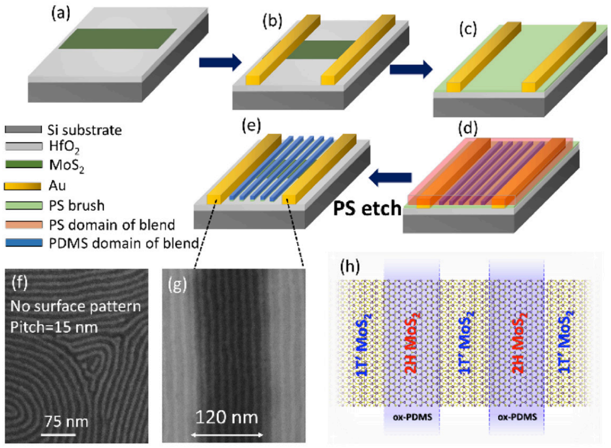

▲Figure 1: (a-e) Schematics depicting the different steps of the DSA of BCP on MoS_2 FETs. (f, g) SEM images show PDMS lines with 15-nm pitch after polystyrene etch on surfaces with no guide pattern as well as surfaces with Au lines as directional guides. (h) Schematic short channel FET comprised of a 2H-MoS_2 channel contacted to two adjacent metallic 1T'-MoS_2 regions forming S/D contacts.

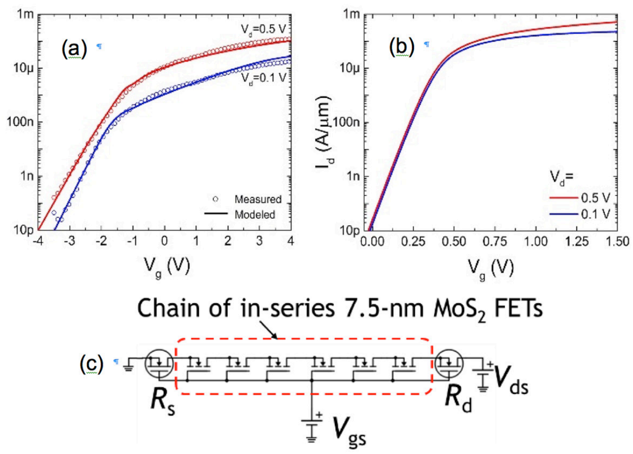

▲Figure 2: (a) Id-Vg of a 6-transistor array at different V_d values and MVS fit of the experimental data. (b) Performance prediction of a single transistor with a double-gate structure, EOT of 0.5 nm, and with the same device parameters but assuming excellent contact resistance (R_s=R_d=100 Ω.mm). Threshold voltage is adjusted to +0.5V for this plot. (c) Circuit configuration used MVS modeling.

FURTHER READING

- A. Nourbakhsh, A. Zubair, S. Huang, X. Ling, M. Dresselhaus, J. Kong, S. De Gendt, and T. Palacios, "15-nm Channel Length MoS_2 FETs with Single-and Double-gate Structures," *2015 Symposium on VLSI Technology*, pp. 28-29, 2015.
- D. Voiry, S. Yalcin, B. Branch, G. Gupta, A. Mohite, and M. Chhowalla, "Phase-engineered Low-resistance Contacts for Ultrathin MoS_2 Transistors,"*Nature Materials*, vol. 3, pp. 1128-1134, August 2014.

A MoS_2/WSe_2 van der Waals Heterojunction Tunnel Diode

A. Nourbakhsh, A. Zubair, M. S. Dresselhaus, T. Palacios
Sponsorship: U.S. Army Research Office, ONR

Two-dimensional (2D) crystals based on atomically thin films of layered semiconductors, such as the family of transition metal dichalcogenides (MX_2: MoS_2, WSe_2, $SnSe_2$, etc.), offer an attractive platform for various optoelectronic applications. The unique crystal properties of atomically thin 2D crystals make them particularly attractive for heterojunction devices, which can potentially overcome some of the problems that conventional heterostructure devices face. A very promising field of application for van der Waals (vdW) heterostructures of 2D crystals is as band-to-band tunneling (BTBT) devices for low-power applications. Such vdW heterostructures can benefit from atomically sharp interfaces and no dangling bonds. These features are crucial for tunneling devices that suffer from impurities and interfacial defects.

To obtain a better understanding of BTBT in MoS_2/WSe_2 hetero-diode, the energy band diagram of the MoS_2/WSe_2 heterostructure was calculated and compared in the out-of-plane and in-plane directions to evaluate the possibility of BTBT in different regions and directions (Figure 1). The results show that the effective heterojunction bandgap at the edge of the overlapped region of *n*-MoS_2 and *p*-WSe_2 in the horizontal direction is significantly smaller than their bandgap in the overlapped region, in the out-of-plane direction (40 meV *vs.* 750 meV). These results indicate that the BTBT occurs dominantly at the edge rather than, as is commonly believed, the overlapped region of the MoS_2/WSe_2 heterojunction.

Next, a MoS_2/WSe_2 heterodiode was designed and fabricated. We observe, for the first time, room-temperature negative differential resistance (NDR) in a heterodiode comprised of 2nm-WSe_2 stacked on 10-nm MoS_2. The presence of NDR is attributed to the lateral BTBT at the edge of the MoS_2/WSe_2 heterojunction. The diode shows an average conductance swing voltage of 75 mV/dec with a high curvature coefficient of 62 V^{-1} (Figure 2). This work represents the remarkable potential of 2D crystals-based heterostructures for high-performance tunneling devices.

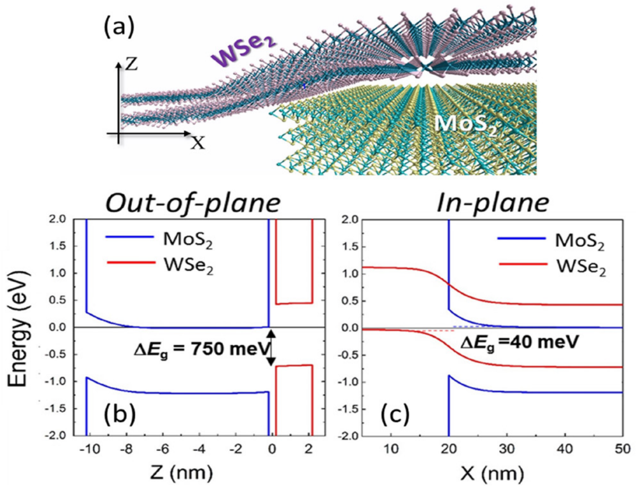

▲ Figure 1: (a) Schematic of a MoS_2/WSe_2 heterostructure. (c) Calculated band diagrams of 10 nm-MoS_2/ 2 nm-WSe_2 heterojunctions in the out-of-plane and in-plane directions. The WSe_2 charge density is $5\times10^{18}/cm^3$, the MoS_2 charge density is $1\times10^{19}/cm^3$, and the MoS_2/WSe_2 gap is 4 Å, assuming the vdW gap between the two films.

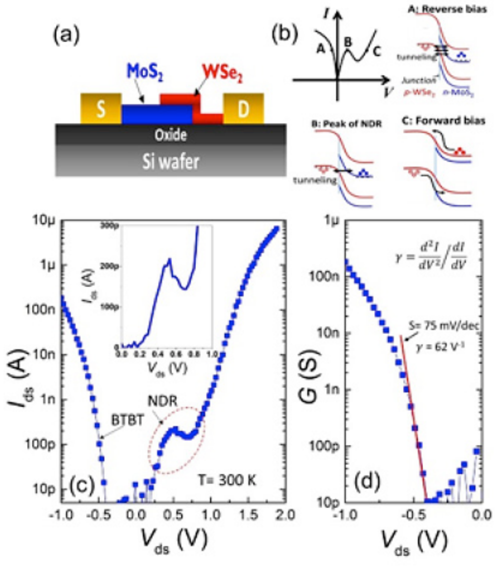

▲ Figure 2: (a) Schematic of a MoS_2/WSe_2 hetero- diode (b) Schematic band diagrams of a MoS_2/WSe_2 junction at different bias regimes. (c) Absolute current, I_{ds}, and (d) conductance, $G=I_{ds}/V_{ds}$, versus V_{ds} of a 10-nm MoS_2/2 nm WSe_2 heterodiode. The inset in (c) shows $I_{ds}-V_{ds}$ at the NDR region with a linear scale.

FURTHER READING

- D. Jena, "Tunneling Transistors Based on Graphene and 2-D crystals," *Proceedings of the IEEE*, vol. 101, pp. 1585-1602, 2013.
- C. H. Lee, G.-H. Lee, A. M. van der Zande, W. Chen, Y. Li, M. Han, X. Cui, G. Arefe, C. Nuckolls, T. F. Heinz, J. Guo, J. Hone, and P. Kim, "Atomically Thin p-n Junctions with Van der Waals Heterointerfaces," *Nature Nanotechnology*, vol. 9, pp. 676-681, 2014.

MoS_2-Based Two-Dimensional Radio Frequency Rectifiers

X. Zhang, J. Grajal de la Fuente, U. Radhakrishna, A. Zubair, A. Nourbakhsh, X. Ling, X. Ji, L. Zhou, J. Kong, M. Dresselhaus, T. Palacios
Sponsorship: ARL

The development of autonomous flexible electronic systems is still not possible, even though thin-film electronics have experienced rapid progress recently. One of the key missing components is a flexible rectifier that can operate fast enough to enable wireless communication and RF energy harvesting. The critical frequency for these applications is 2.45 GHz, since our smart phones, GPS, Bluetooth, Wi-Fi, and many other communication systems all utilize this radio frequency. In this work, we are developing a MoS_2-based Schottky diode rectifier and improving its cut-off frequency to GHz range.

The cutoff frequency of a Schottky diode can be determined by $f_T = 1/2p*R_s*C_j$, where R_s is the series resistance and C_j is the junction capacitance. Figure 1 illustrates the structure of our MoS_2 device structure. Both Au and Pd exhibit n-type behavior as MoS_2 metal contacts. Gold deposited at high vacuum is good for Ohmic contact, while the Pd metal enables Schottky contact with MoS_2 with a built-in potential around 0.7 eV. The band alignment diagram of MoS_2 and Pd metal contacts is also illustrated in Figure 1.

To study the high frequency performance of the MoS_2 Schottky diode, we did S-parameter measurements by using a vector network analyzer. The S parameter of the diode was converted to Z-parameter and the real/imaginary part of the diode impedance was plotted in Figure 2. The cutoff frequency can be determined by the crossing point of the Re{Z} and Im{Z} curves. At a forward bias of 2.5V, the cutoff frequency can reach ~500MHz (Figure 2). The equivalent circuits of the internal part of a MoS_2 Schottky diode can be modeled as a junction resistance R_s in shunt with a junction capacitance C_j. At radio frequency, the impedance of the junction capacitance $1/jwC_j$ will roughly "short" the impendence of R_j. Therefore, at radio frequency, the series resistance R_s, instead of R_j, is the most significant limiting factor.

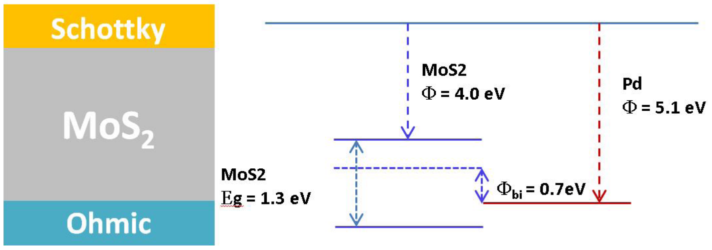

▲ Figure 1: Illustration of MoS_2 device structure and band alignment diagram.

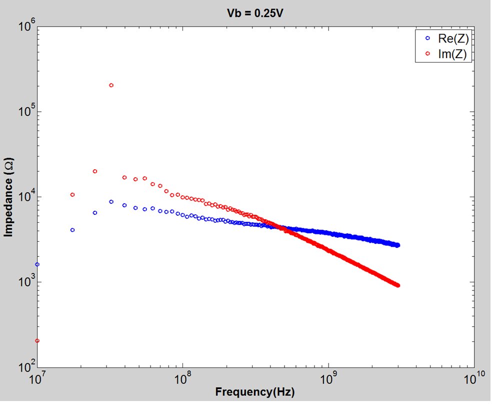

▲ Figure 2: The real (red dots) and imaginary (blue dots) part of the impedance of the MoS_2 diode. The cutoff frequency f_T can be determined by the crossing point of the Re{Z} and Im{Z}.

FURTHER READING

- Q. H. Wang, K. Kalantar-Zadeh, A. Kis, J. N. Coleman, M. S. Strano, "Electronics and Optoelectronics of Two-dimensional Transition Metal Dichalcogenides," *Nature Nanotechnology*, vol. 7, pp. 699-712, 2012.
- N. Shinohara, "Rectennas for Microwave Power Transmission," *IEICE Electronics Express*, vol. 10, no. 21, pp. 1-13, 2013.

Control of Heating Dynamics in Superconducting Thin-Film Niobium Nitride Nanowires by Resistive Shunting

E. Toomey, A. McCaughan, Q. Zhao, K. K. Berggren
Sponsorship: IARPA, AFOSR, NSF, Intel

We have demonstrated the use of resistive shunting on thin-film NbN nanowires to control the heating dynamics of a three-terminal superconducting device. The nanocryotron (nTron) is a T-shaped device consisting of a channel, which can be switched from the superconducting state to the normal state by the injection of hot quasiparticles from the gate through the channel once the gate current exceeds the critical current density. Unlike Josephson junctions, this device can be fabricated from a single thin-film layer, produces large output voltages (>100 mV), and offers a third terminal for gate modulation, which can be triggered by a single flux quantum input. However, the heating dynamics of the nTron limit its speed and power efficiency while also preventing precise control of the phase difference between its terminals.

To overcome these limitations, we have investigated the impact of resistive shunting on thin-film NbN constrictions as a model for controlling the thermal dynamics of the nTron. Using the RCSJ model to approximate the phase-slip center in these superconducting nanowires as a weak link, we have simulated the suppression of hysteresis that results from increased damping of the constriction as the magnitude of shunt resistance decreases. We also evaluated the change in Joule heating power at the time of switching to demonstrate the decrease in hotspot formation caused by the diversion of bias current to the shunt. Experimentally, we have confirmed these results and characterized the change in switching and retrapping current distributions to determine the appropriate shunt resistance needed to preserve coherence in the resistive state. Extending this knowledge to the nTron could change its operation from a Joule-heated state governed by hotspots to a non-hysteretic, coherent mode controlled by single vortex crossings. We expect to use our results for applications such as reading out the discrete number of fluxons in a superconducting loop for single-flux quantum logic.

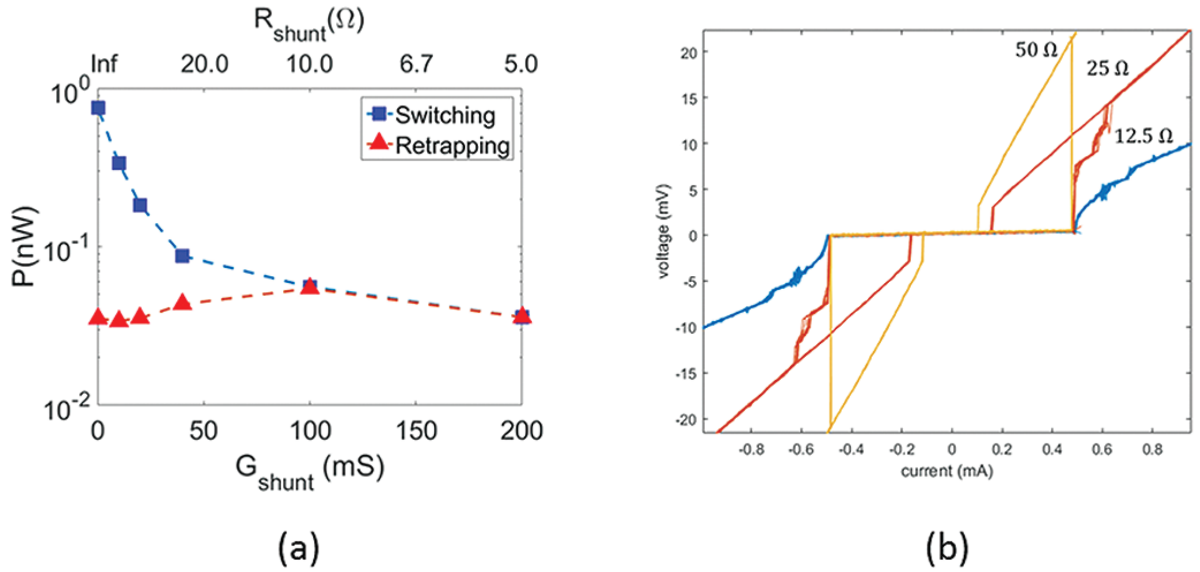

▲ Figure 1: (a) Simulated switching and retrapping power of a shunted nanowire. Power at switching decreases with decreasing shunt resistance. (b) Experimentally observed suppression of hysteresis as a function of shunt resistance for thick-film NbN (R_{sheet} = 59 Ω/square). Full suppression is seen at R_s = 12.5 Ω.

FURTHER READING

- M. W. Brenner, D. Roy, N. Shah, and A. Bezryadin, "Dynamics of Superconducting Nanowires Shunted with an External Resistor," *Phys. Rev.* vol. 85, no. 22, pp. 224507, June 2012.
- S.-Z. Lin and L. N. Bulaevskii, "I–V Characteristics of Short Superconducting Nanowires with Different Bias and Shunt: A Dynamic Approach," *Journal of Phys. Condens. Matter*, vol. 26, no. 15, pp. 155703, April 2014.

Energy: Photovoltaics, Energy Harvesting, Energy Storage, Fuel Cells

Improving Photovoltaic Conversion Using Spectral Conversion

D. M. Bierman, A. Lenert, W. R. Chan, B. Bhatia, I. Celanovic, M. Soljačić, E. N. Wang
Sponsorship: S3TEC, DOE

A single-junction PV cell generating electrical power through incident sunlight is limited by the Shockley-Queisser limit, which for any bandgap is far below the limiting efficiency of converting work from sunlight. By introducing an intermediate component that absorbs sunlight and re-emits a tailored thermal radiation spectrum towards a single junction PV cell, solar thermophotovoltaics (STPVs) promise to bridge the gap between these two disparate limits.

For STPVs to succeed, a detailed understanding of the energy flow via radiation and heat conduction is key. We have been working to enhance the performance of a single-junction PV by incorporating a spectral converter. The spectral converter consists of a multi-walled carbon nanotube (MW-CNT) area for complete thermalization of incident sunlight, a one-dimensional Si/SiO_2 photonic crystal for spectrally selective thermal emission, and a tandem rugate/interference filter. The PV cell used in the study is a low-bandgap InGaAsSb (E_g = 0.55 eV) cell.

While absolute efficiencies are still low relative to more mature technologies, our peak measured efficiency of 6.8% is above all others reported for STPVs. We have shown improved device conversion efficiency as well as reduced parasitic heat generation as a result of the spectral converter. This is the first time that the performance at the device level of a single junction PV cell has been enhanced due to the presence of a spectral converter.

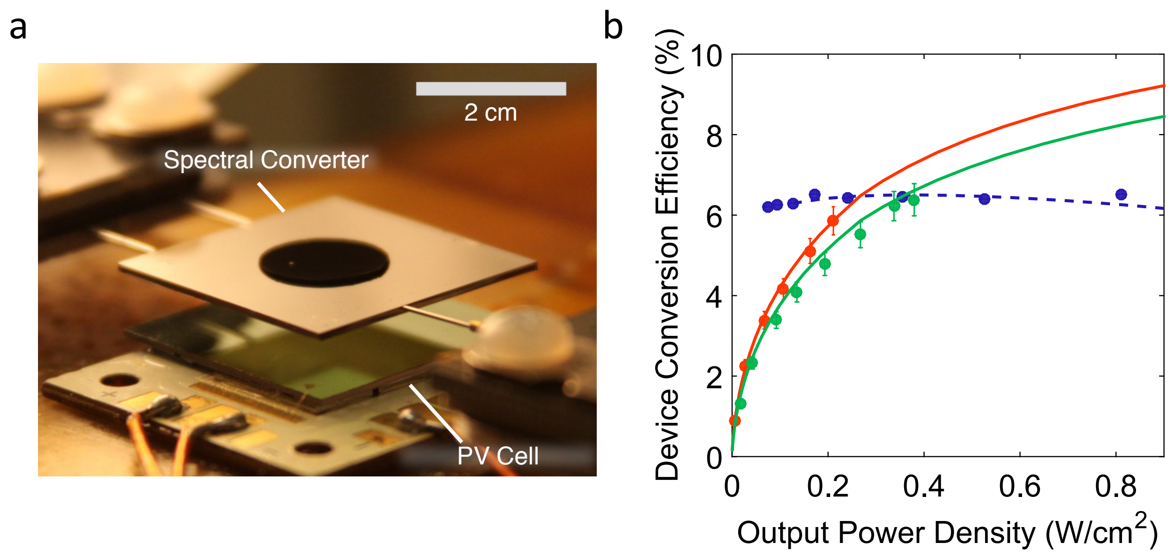

▲ Figure 1: (a) Optical image of STPV device. Top surface has small MW-CNT area for photon absorption and tungsten-coated surface to reduce heat loss through thermal emission. Bottom surface (not shown) produces spectrally selective thermal emission spectrum through one-dimensional photonic crystal and rugate/interference filter. (b) Performance of device shows that STPVs can enhance performance of PV cell by introducing intermediate absorption/re-emission process.

FURTHER READING

- W. Shockley and H. J. Queisser, "Detailed Balance Limit of Efficiency of P-N Junction Solar Cells," *Journal of Appl. Phys.*, vol. 32 no. 3, pp. 510, 1961.
- P. Würfel and U. Würfel, *Physics of Solar Cells: From Basic Principles to Advanced Concepts*, Hoboken: John Wiley & Sons, 2009.

Oxidative Chemical Vapor Deposition of Polymers for Printable and Flexible Photovoltaics

W. J. Jo, K. K. Gleason
Sponsorship: Eni S.p.A, Samsung Electronics, Institute for Soldier Nanotechnologies

A variety of solar energy conversion systems has emerged as attractive candidates to establish fossil fuel-free energy networks. Among these, organic solar cells offer the promise of a lightweight, flexible, large-area, and cost-effective photovoltaic technology. Traditionally, organic photovoltaic devices (OPVs) have been fabricated with thermal evaporation or solution-based techniques, but these two methods are suitable for only low molecular weight or soluble materials. In order to apply high molecular weight and insoluble polymers to OPVs, we explore the use of oxidative vapor deposition (oCVD) for the polymer deposition.

As Figure 1 shows, oCVD is a solvent-free conformal vacuum-based technique to enable thin-film fabrication of insoluble polymers at moderate vacuum (~ 0.1 Torr) and low temperature (25–150°C). Moreover, oCVD carries the well-cited processing benefits of vacuum processing, such as parallel and sequential deposition, well-defined thickness control, large-area uniformity, and inline integration with other standard vacuum processes (e.g., vacuum thermal evaporation).

Based on the aforementioned technical advantages from oCVD, various insoluble polymers are successfully applied to OPVs. First, polyselenophene donor layers are integrated into OPVs for the first time with 0.4 % of power conversion efficiency. Second, ternary OPVs employing polythiophene donor layers has been realized to increase the power conversion efficiency up to 2.4%. Third, a new concept of neutral hole transporting layers (HTLs) is achieved by integrating patterned Cl^--doped poly(3,4-dimethoxy-thiophene) (PDMT) HTLs into OPVs via oCVD. Due to this novel polymer's neutrality, high transparency, good conductivity, and appropriate energy levels, the power conversion efficiency and lifetime of OPVs are remarkably boosted compared to those of OPVs depending on the commercial hole transporting polymer, acidic PEDOT:PSS [poly(3,4-ethylenedioxythiophene):polystyrene sulfonate] (Figure 2). Finally, we are currently studying hyper-conductive PEDOT for printable and flexible electronics by using a vacuum-based polymer vapor printing technique – oxidative chemical vapor deposition (oCVD) combined with *in situ* shadow masking.

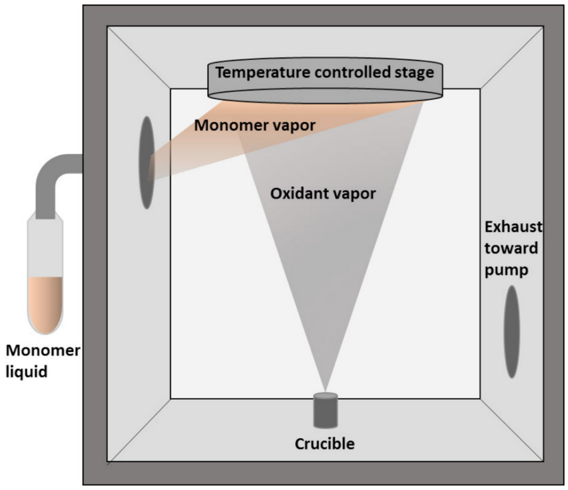

▲Figure 1: Schematic of oCVD reactor.

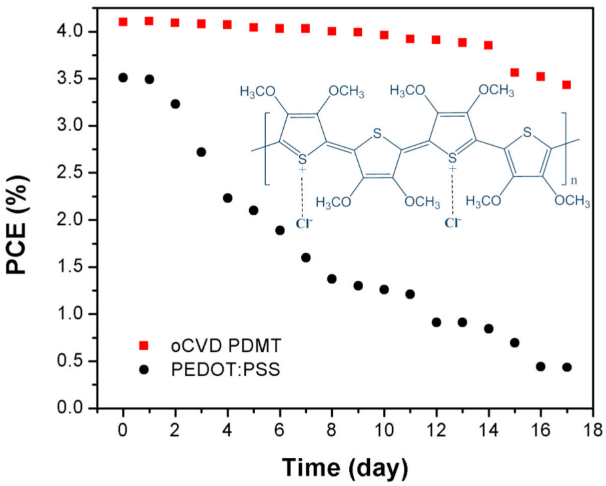

▲Figure 2: Evolution of power conversion efficiency with respect to storage time under N_2 atmosphere.

FURTHER READING

- W. J. Jo, J. T. Nelson, S. Chang, V. Bulović, S. Gradečak, M. S. Strano, and K. K. Gleason, "Oxidative Chemical Vapor Deposition of Neutral Hole Transporting Polymer for Enhanced Solar Cell Efficiency and Lifetime," Advanced Materials, 2016.
- W. J. Jo, D. C. Borrelli, V. Bulović, and K. K. Gleason, "Photovoltaic Effect by Vapor-Printed Polyselenophene," *Organic Electronics*, vol. 26, pp. 55-60, 2015.

High-Efficiency Photovoltaic Devices using Nanocavity Array

W. L. Kwan, A. El-Faer, X. Li, S.-G. Kim
Sponsorship: SUTD-MIT Program

We have demonstrated in our earlier results that metal-dielectric nanocavity arrays can improve broad-band light absorption due to the enhancement in the cavity, waveguide, and surface plasma polariton resonance modes around the nanocavity. This project aims to utilize this absorber structure for applications in photovoltaic devices with soft absorber materials like organic and perovskite materials, which have limited carrier lifetime and thereby require ultra-thin film thickness for efficiency charge extraction. However, light absorption is insufficient if the absorber layer is too thin, and a compromise between complete light absorption and charge extraction is often needed, resulting in mediocre energy harvesting efficiencies.

The nanocavity array we fabricated can alleviate the need for thicker absorber film by enhancing broad-band absorption in the absorber material. Figure 1(a) shows the results of a finite-difference time-domain (FDTD) simulation that the absorption in a poly(3-hexylthiophene-2,5-diyl):phenyl-C61-butyric acid methyl ester (P3HT:PCBM) film is enhanced by the nanocavity structure (SEM image in Figure 1(b)). The enhanced absorption can also be clearly seen in the photograph of a thin gold film deposited on the nanocavity array in Figure 1(c). Most of the visible light is absorbed, leaving a black appearance on the surface of the substrate. A prototype device is under fabrication to demonstrate higher solar energy harvesting efficiency.

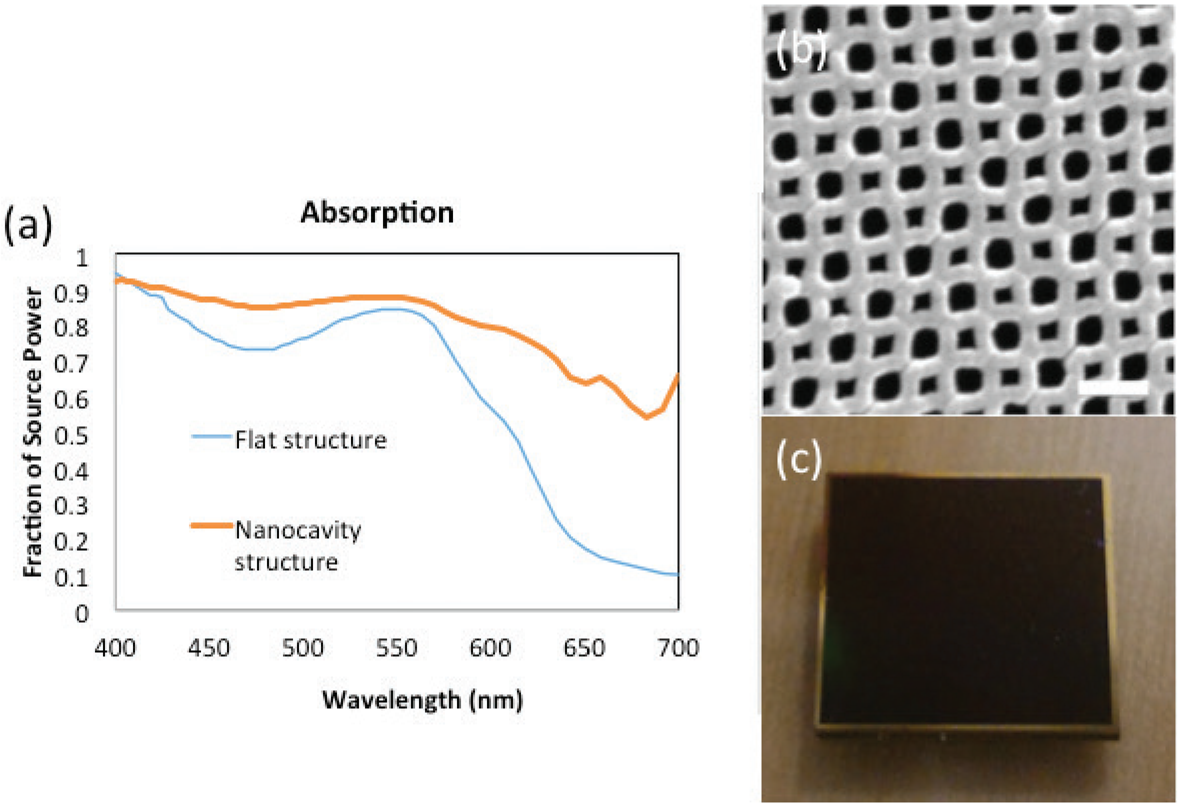

▲Figure 1: (a) FDTD simulation results on the absorption spectrum of P3HT:PCBM films on a flat surface and nanocavity structure. (b) SEM image of Al_2O_3 nanocavity array coated with gold. The scale bar is 1mm. (c) Photograph of a silicon substrate with Al_2O_3 nanocavity array coated with gold.

FURTHER READING

- J. B. Chou, D. P. Fenning, Y. Wang, M. A. M. Polanco, J. Hwang, A. El-Faer, F. Sammoura, J. Viegas, M. Rasras, A. M. Kolpakl, Y. Shao-Hom, and S.-G. Kim, "Broadband Photoelectric Hot Carrier Collection with Wafer-scale Metallic-semiconductor Photonic Crystals," 42nd *IEEE Photovoltaic Specialist Conference (PVSC)*, New Orleans, LA, 2015.

Germanium-on-Silicon Heteroepitaxy for High-Efficiency Photovoltaic Devices

B. R. Albert, L. C. Kimerling, J. Michel
Sponsorship: ARPA-E

While III-V based photovoltaic cells demonstrate high energy-conversion efficiencies, their widespread adoption is limited by the prohibitive cost per device area. Substantial cost reduction of germanium lattice-matched III-V cells can be realized by replacement of the Ge substrate with a thin layer of Ge deposited on silicon. To maintain efficient energy conversion, the Ge-on-Si "virtual substrate" must be single crystalline with a threading dislocation density (TDD) low enough to not affect carrier lifetimes in the epitaxially deposited III-V layers.

Lateral overgrowth and film coalescence create a more suitable, planar Ge film for III-V growth in large areas. Fabrication of a continuous Ge surface from a patterned Ge film demands complete coalescence during lateral overgrowth. Due to the high surface energy of the Ge/SiO_2 interface, lateral overgrowth does not readily occur. Ge mesa arrays were staggered to eliminate regions entirely dependent on overgrowth from mesa corners. A staggered arrangement decreased the growth time until complete coalescence by at least 50% as compared to a regular gridded array. The rate of overgrowth over isolated SiO_2 lines was observed to increase for smaller line widths up to 1.5 µm.

Etch pit studies of coalesced structures employing faceted Ge growth around SiO_2 walls arranged as grids and isolated lines indicated a local increase in the TDD in the vicinity of Ge film edges while decreasing to 1 x 10^7 cm^{-2} further away in the film. A significant improvement in TDD reduction by avoidance of dislocation pile-up is expected by these same models if blanket Ge is instead grown, followed by etching and filling of trenches with poly-Ge separated by a thin layer of SiO_2. A 1-µm thick Ge film is expected to exhibit a TDD of 1 x 10^5 cm^{-2}. At this density level, the performance of high-efficiency III-V photovoltaic cells will be unaffected.

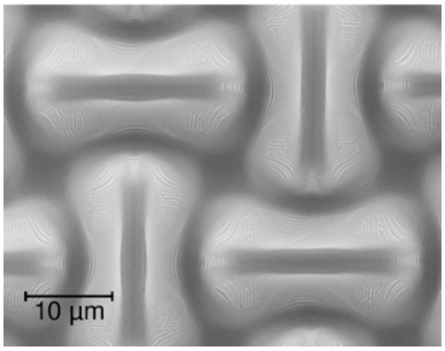

▲ Figure 1: Ge lateral overgrowth over SiO_2 isolated walls.

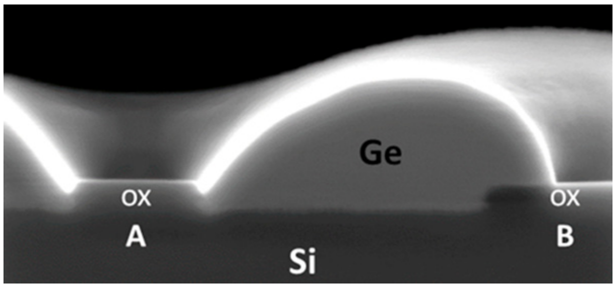

▲ Figure 2: Overgrowth at zero and negative concavity Ge film perimeters.

Solid-State Infrared-to-Visible Upconversion Sensitized by Colloidal Nanocrystals

M. Wu, D. N. Congreve, M. W. B. Wilson, J. Jean, N. Geva, M. Welborn, T. Van Voorhis, V. Bulović, M. G. Bawendi, M. A. Baldo
Sponsorship: EFRC Center for Excitonics

Optical upconversion is a process that converts two or more low-energy photons into a single high-energy photon. Upconversion from the infrared to the visible is useful in photovoltaics, photodetection, bioimaging and three-dimensional displays. In photovoltaic applications specifically, an optical upconversion layer can capture sub-bandgap photons, increasing the efficiency of a conventional single-junction solar cell beyond the Shockley–Queisser limit.

To upconvert light at relatively low intensities, a promising approach is the sensitized triplet-triplet annihilation (TTA). It utilizes a sensitizer and an annihilator. The sensitizer absorbs incident light and transfers the energy as spin-triplet excitons to the annihilator. When two triplets meet in the annihilator, they form a single higher-energy spin-singlet exciton via TTA. Blue-shifted light is emitted when the singlets relax. It has been, however, difficult to identify effective molecular sensitizers that absorb in the infrared. Efficient demonstrations to date have been mostly conversion among visible wavelengths. Furthermore, the majority of them are in solution, while a solid-state architecture is necessary for solar and detection applications.

Here, we report a solid-state thin film for infrared-to-visible upconversion that employs lead sulfide colloidal nanocrystals as a sensitizer; see Figure 1. Upconversion is achieved from pump wavelengths beyond $\lambda = 1\,\mu m$ to emission at $\lambda = 610$ nm (Figure 2). When excited at $\lambda = 808$ nm, two excitons in the sensitizer are converted into one higher energy state in the emitter at a yield of 1.2±0.2%. Upconversion efficiency reaches the maximum at an absorbed intensity equivalent to less than one sun. We demonstrate that colloidal nanocrystals are an attractive alternative to existing molecular sensitizers, given their small exchange splitting, wide wavelength tunability and broadband infrared absorption. This solid-state architecture for upconversion may prove useful for enhancing the capabilities of solar cells and photodetectors.

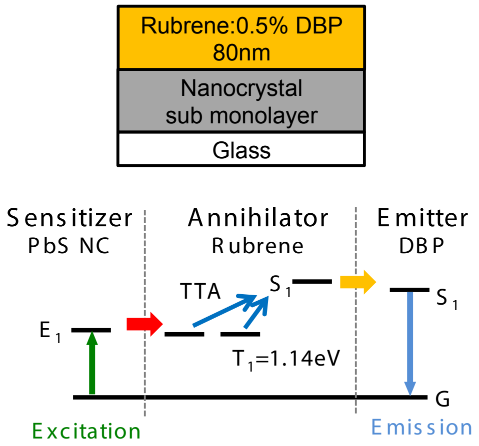

▲Figure 1: Thin-film device structure (top) and energy diagram (bottom) illustrating TTA-based upconversion sensitized by PbS colloidal nanocrystals (NC). DBP: dibenzotetraphenylperiflanthene.

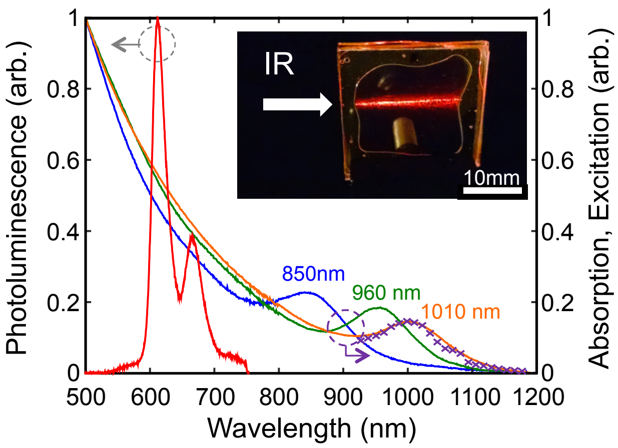

▲Figure 2: Nanocrystal absorption labeled by first excitonic peaks, DBP photoluminescence (red), and excitation spectra (purple crosses) for λ=1010nm NC. Inset: photograph of a device under λ=808nm excitation.

FURTHER READING

- M. Wu, D. N. Congreve, M. W. B. Wilson, T. Van Voorhis, V. Bulović, M. G. Bawendi, M. A. Baldo *et al*, "Solid-State Infrared-to-Visible Upconversion Sensitized by Colloidal Nanocrystals," *Nature Photonics*, vol. 10, pp. 31-34, 2016.
- T. N. Singh-Rachford and F. N. Castellano, "Photon Upconversion Based on Sensitized Triplet-Triplet Annihilation," *Coordination Chemistry Reviews*, vol. 254, pp. 2560-2573, 2010.
- T. F. Schulze and T. W. Schmidt, "Photochemical Upconversion: Present Status and Prospects for Its Application to Solar Energy Conversion," *Energy & Environmental Science*, vol. 8, pp. 103-125, 2015.

Solar Water Splitting with Metallic-Semiconductor Photonic Crystals

X. H. Li, A. Elfaer, J. Chou, S.-G. Kim
Sponsorship: Masdar Flagship Program

The major challenges for current solar energy harvesting techniques are the limitations in high-efficiency energy conversion and large-scale energy storage. Directly converting solar energy into storable chemical fuels can solve these problems. A promising method is utilizing photoelectric hot electron generation to split water and produce hydrogen fuel. Titanium-oxide-based photocatalytic systems have been widely used in photon-driven hot electron generation. However, the efficiency of the present design is limited due to the low absorption of visible light. Here we report hot electron collection by wafer-scale Au/TiO_2 metallic-semiconductor photonic crystals (MSPhC), with a broadband photoresponse below the bandgap of TiO_2. Multiple absorption modes supported by the 2D micro-cavity structure of the MSPhC extend the photon-metal interaction time and fulfill broadband light absorption. Surface plasmon absorption mode gives access to enhanced electric field oscillation and hot electron generation at the interface between Au and TiO_2. As demonstrated in Figure 1a, the generated hot electrons with enough energy to overcome the Au/TiO_2 Schottky barrier could be collected for water splitting.

Figure 1b shows the micro-cavity arrays with depth of 1 μm and diameter of 500 nm. We deposited thin layers of TiO_2 and Au to form the Schottky junction. Finite-difference time-domain simulation results in Figure 2a show that thinner Au layers can promote broadband light absorption, which might be beneficial for hot electron generation. Experimental results of the photoresponse in Figure 2b show a peak at around 590 nm, which is below the TiO_2 bandgap. We also tried to achieve multi-band photoresponse by depositing gold nanorods on MSPhC. In order to understand the generation and injection of hot electrons through plasmon decay, we are currently working on modeling and measuring momentum distribution of plasmon-induced hot electrons in metal nanostructures such as gold nanorods.

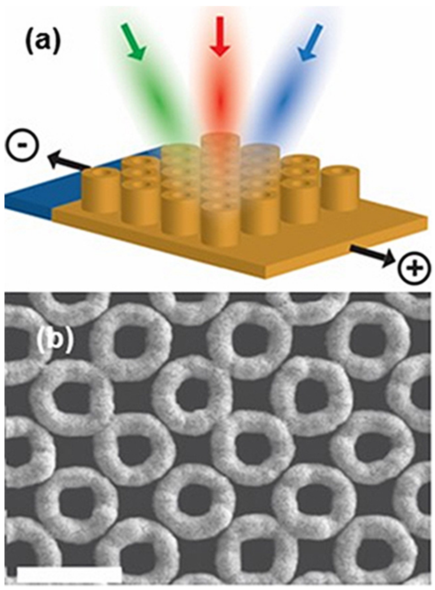

▲Figure 1: (a) Schematic of 2D micro-cavity arrays of MSPhC. (b) Top view photo of MSPhC via SEM. Scale bars are 1 μm.

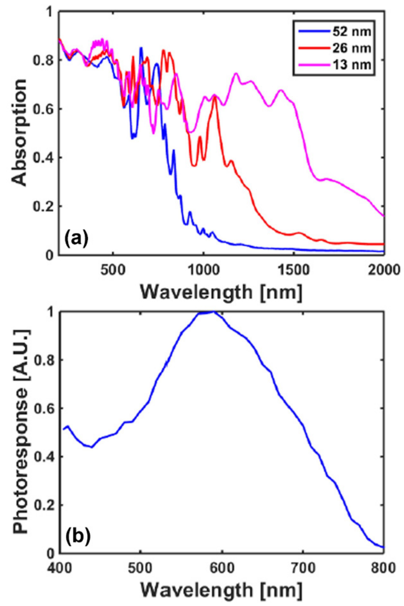

▲Figure 2: (a) Simulated absorption spectra of MSPhC for various Au thickness. (b) Photoresponse of MSPhC centered at 590 nm.

FURTHER READING

- J. B. Chou, D. P. Fenning, Y. Wang, M. A. M. Polanco, J. Hwang, F. Sammoura, J. Viegas, M. Rasras, A. Kolpak, S. H. Yang, and S.-G. Kim, "Broadband Photoelectric Hot Carrier Collection with Wafer-Scale Metallic-Semiconductor Photonic Crystals," *42nd IEEE PVSC*, New Orleans, LA, 2015.
- Y. Wang, J. B. Chou, and S.-G. Kim, "Simulation Study of Metallic Photonic Crystal for Enhanced Hot Electron Transfer in Electrochemical Cells," presented at *MRS Fall Meeting*, Boston, MA, 2015.
- A. Elfaer, Y. Wang, X. H. Li, J. B. Chou, and S.-G. Kim, "Gold Nanorods Coated Metallic Photonic Crystal for Enhanced Hot Electron Transfer in Electrochemical Cells," *MRS Advances*, FirstView, pp. 1-7, 2015.

Optimizing Stability and Capacity for Lithium-Air Batteries

T. Batcho, D. Kwabi, D. Perego, R. Omampuliyur, Y. Shao-Horn, C. V. Thompson
Sponsorship: Skoltech Center for Electrochemical Energy Storage

Lithium-air batteries hold promise for the next generation of electric vehicles and other applications. By reacting oxygen directly with lithium ions to form Li_2O_2 on discharge, they can achieve energy densities 3-5 times higher than current lithium-ion batteries. However, a number of challenges exist for implementing lithium-air batteries, including poor rate capability, poor cyclability, high overpotentials upon charging, and electrode and electrolyte instability. We seek to address these issues by developing new electrode materials and architectures and performing studies of Li_2O_2 formation under various discharge conditions.

Aligned arrays of carbon nanotubes (CNTs) provide ideal conductive scaffolding materials for Li_2O_2, while having high void space and low mass. CNTs of 5-10 nm in diameter are grown in aligned forests on catalyst deposited silicon wafers. These forests can be delaminated and placed directly into our cell. We observed near ideal gravimetric capacities and high volumetric capacities. However, carbon has been found to decompose in lithium-air cells and promote electrolyte decomposition. This leads to poor cycling performance and high overpotentials on charge. To avoid these effects, we coated materials such as TiN onto CNTs using atomic layer deposition to chemically passivate the carbon surface. These coated CNTs are capable of supporting Li_2O_2 growth (Figure 1). We are currently working on optimizing conductivity of the deposited films and testing electrochemical performance during charge and cycling.

Another challenge in designing Li-O_2 is obtaining optimal volumetric discharge capacity, which can be achieved by promoting the growth of large toroidal deposits of Li_2O_2 as opposed to thin films, which electrically passivate and cut off cell discharge prior to full void space filling of the electrode. We seek to study the mechanisms of nucleation and growth in order to control these processes. For this study we used carbon paper electrodes for greater reproducibility and facility in modeling. We test these electrodes with potentiostatic discharges, which use a fixed driving force. We can then adapt existing models for electrodeposition to our system to extract rates of surface nucleation and growth based on current transients (Figure 2). By further studying the dependence of these rates on solvent type, potential, and electrode surface, we can find optimal conditions for greater cell capacity and better understand mechanisms of Li_2O_2 evolution.

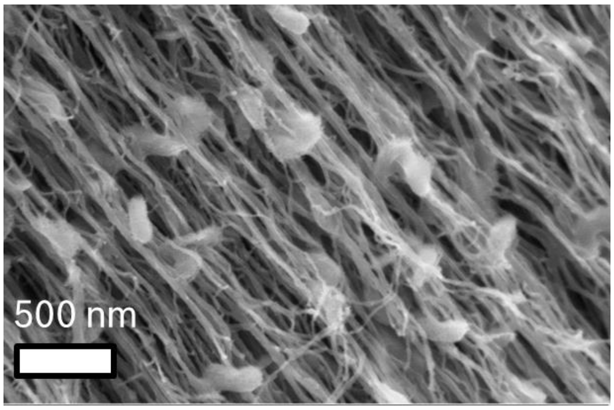

▲ Figure 1: SEM micrograph of toroidal Li_2O_2 formation on CNTs deposited with a coating of TiN.

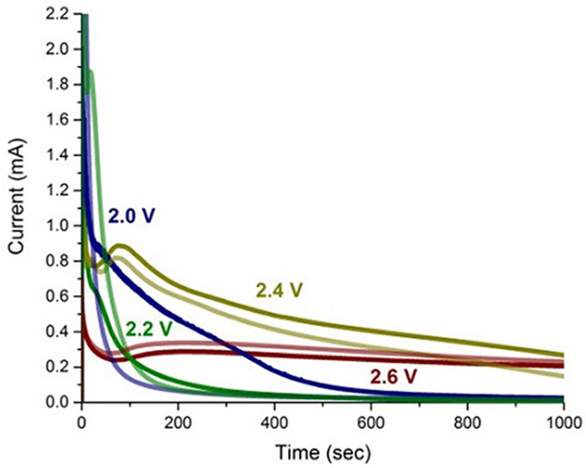

▲ Figure 2: Current transients from potentiostatic discharges at a range of potentials in 0.1 M $LiClO_4$ DMSO. Peaks occur at longer times at higher potentials (lower overpotentials), suggesting slower nucleation/growth rates.

FURTHER READING

- R. R. Mitchel, B. M. Gallant, Y. Shao-Horn, and C. V. Thompson, "Mechanisms of Morphological Evolution of Li_2O_2 Particles during Electrochemical Growth," *Journal of Physical Chemistry Letters*, vol. 4, no. 7, pp. 1060, March 2013.
- B. M. Gallant, R. R. Mitchell, D. G. Kwabi, J. Zhou, L. Zuin, C. V. Thompson, and Y. Shao-Horn, "Chemical and Morphological Changes of Li–O2 Battery Electrodes upon Cycling," *The Journal of Physical Chemistry C*, vol. 116, no. 39, pp. 20800–20805, October 2012.

Mechanical Stresses in Lithium Phosphorus Oxynitride-Coated Germanium Thin-Film Electrodes

A. Al-Obeidi, D. Kramer, R. Moenig, C. V. Thompson
Sponsorship: SMART

In the electronics and health industry, there has been a strong trend toward miniaturized devices for use in wearable electronics, medical implants, and wireless communication. The reduced energy consumption of microsystems makes it possible to integrate microbatteries directly onto electronic chips. Solid-state microbatteries are ideally suited for such applications since they can be integrated on microchips while offering improved safety (no liquid electrolytes and thermal runaway), performance (higher voltages, wider range of operating temperatures), and lifetime. The simplest and most common form of a solid-state battery is a planar solid-state thin-film battery. For the anode, germanium is an ideal candidate since it offers large volumetric capacities (7366 A h l^{-1}) compared to lithium (2065 A h l^{-1}) while being compatible with conventional semiconductor processing techniques. However, use of germanium is limited by the significant volumetric and structural changes that occur during cycling. In order to explore the relationship between electrochemistry and the mechanical stresses, in situ stress measurements on germanium thin-film electrodes coated with lithium phosphorus oxynitride (LiPON) were performed.

It was found that LiPON, a rigid solid electrolyte, suppresses morphological evolution and results in reproducible cycle-to-cycle stress behavior. The repeatable behavior observed in LiPON-coated films allows more direct characterization of electrochemical processes governing lithiation and delithiation. Cycling at various rates (Figure 1) revealed that the lithiation capacity of coated electrodes increased at slower cycling rates, saturating at about 1200 A h kg^{-1} when using rates slower than 1 C. Cycling below 100 mV resulted in the formation of c-$Li_{15}Ge_4$, which appeared as a sharp drop in the compressive nominal stress to values close to zero (Figure 2, points 1-2). Overlithiation of this phase resulted in a linear compressive increase in stress (Figure 2, points 2-3). These results indicate that c$Li_{15}Ge_4$ has a higher density than its a-Li_xGe precursor. Delithiation of c-$Li_{15}Ge_4$ seems to consist of two successive events: the formation of an intermediate phase followed by a rapid release of lithium from this intermediate phase, which resulted in the amorphization of the electrode. While crystalline $Li_{15}Ge_4$ develops a lower maximum nominal tensile stress than its amorphous counterpart, extraction of lithium from c$Li_{15}Ge_4$ requires more energy and therefore reduces the energy efficiency of a cell.

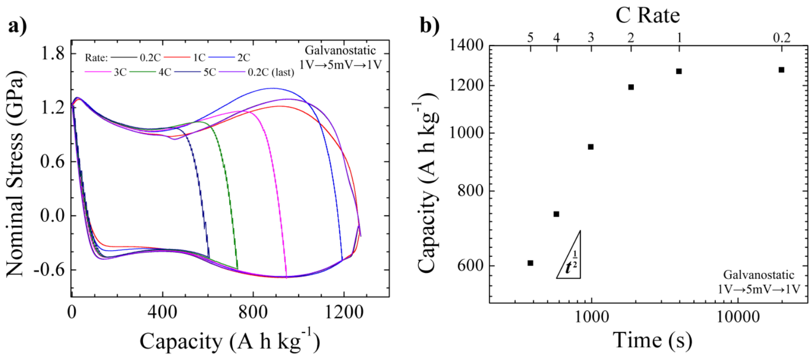

▲ Figure 1: Nominal stress vs. capacity plots for a LiPON-coated 170-nm germanium film cycled galvanostatically (1 V ⟶ 5mV ⟶ 1 V) at different C rates. The data for the final scan at 0.2 C (purple) overlaps with that of the initial 0.2 C scan (black). The 1 C rate corresponds to 115 μA cm^{-2}.

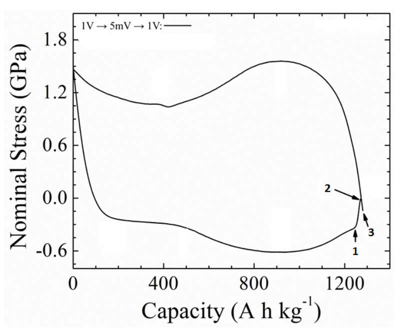

▲ Figure 2: Nominal stress-capacity plots for conditions that lead to the formation of crystalline $Li_{15}Ge_4$ of a LiPON-coated 170-nm-thick germanium electrode cycled galvanostatically at 13.3` μA (i.e., 0.2 C, 23 μA cm^{-2}).

FURTHER READING

- Z. Choi, D. Kramer, and R. Mönig, "Correlation of Stress and Structural Evolution in Li4Ti5O12-based Electrodes for Lithium Ion Batteries," *Journal of Power Sources*, vol. 240, pp. 245, 2013.
- A. Al-Obeidi, D. Kramer, R. Mönig, and C. V. Thompson, "Mechanical Stresses and Crystallization of Lithium Phosphorous Oxynitride-coated Germanium Electrodes During Lithiation and Delithiation," *Journal of Power Sources*, vol. 306, pp. 817, 2016.

Fabrication of Ruthenium Oxide-Coated Si Nanowire-Based Supercapacitors

W. Zheng, Q. Chen, D. Wang, C. V. Thompson
Sponsorship: SMART

Supercapacitors are electrochemical devices that have high power density and long cycle life. Pseudo-capacitors are a type of supercapacitor that involves reversible surface reduction/oxidiation reactions. Among all the pseudo-capacitive materials, ruthenium oxide is the most promising due to its high specific capacitance, excellent cyclability, and high conductivity. While researchers have been developing supercapacitors based on ruthenium oxide or its composite with other materials such as carbon nanotubes (CNTs), there has been little study on ruthenium oxide-Si composite electrodes. In earlier work, we demonstrated the feasibility of using metal assisted chemical etching (MACE) to fabricate Si nanowires for on-chip MOS capacitors. Here we use an ordered vertical array of Si nanowires from a similar wet etching process named metal-assisted anodic etching (MAAE) to fabricate on-chip supercapacitors.

Atomic layer deposition (ALD) is used to deposit ruthenium oxide on silicon nanowires due to its conformal coating of high aspect ratio structures. The use of ALD also provides precise control of the ruthenium oxide film thickness. As pseudo-capacitive reactions occur at the surface of ruthenium oxide, the high aspect ratio Si nanowire structures coated with ruthenium oxide has a high surface area of accessible ruthenium oxide per area of substrate surface, which thus leads to a high energy storage capacitance. We have developed an ALD process for coating of ruthenium oxide on Si nanowires generated by MAAE. The composite structure showed a con-tinuous coating of well-distributed particles (Figure 1). High-resolution transmission electron microscopy characterization and x-ray diffraction analysis confirmed that most nanoparticles were in the form of elemental ruthenium. We are currently investigating the electrochemical performance of this composite material in an aqueous electrolyte using a three-electrode setup. The preliminary data showed that the specific capacitance scaled well with the length of silicon nanowires in this aqueous electrolyte (Figure 2). Meanwhile, we are fabricating solid-state micro-supercapacitors based on use of solid electrolytes. We are interested in studying the performance dependence of the solid-state device on both Si nanowire aspect ratios and ALD cycle numbers.

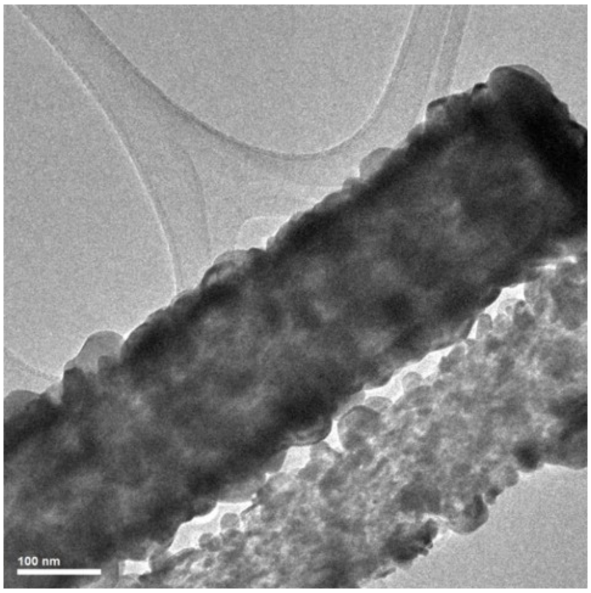

▲Figure 1: TEM image of Si nanowires after ALD coating of ruthenium oxide.

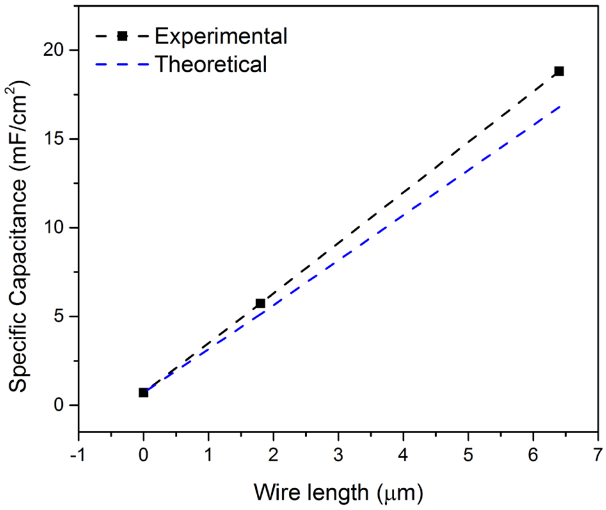

▲Figure 2: Specific capacitance as function of Si nanowire lengths. The black line shows linear fit to experimental data; the blue line shows theoretical projection of the specific capacitance with nanowire lengths.

FURTHER READING

- S. W. Chang, J. Oh, S. T. Boles, and C. V. Thompson, "Fabrication of Silicon Nanopillar-based Nanocapacitor Arrays," *Appl. Phys. Letters*, vol. 96, pp. 153108, 2010.
- S. W. Chang, V. P. Chuang, S. T. Boles, C. A. Ross, and C. V. Thompson, "Densely-packed Arrays of Ultrahigh-aspect-ratio Silicon Nanowire Fabricated Using Block Copolymer Lithography and Metal-assisted Etching," *Adv. Funct. Mater.*, vol. 19, pp. 2495, 2009.
- C. Q. Lai, W. Zheng, W. K. Choi, and C. V. Thompson, "Metal Assisted Anodic Etching of Silicon," *Nanoscale*, vol. 25, pp. 11123, 2015.

Electro-Chemo-Mechanical Studies of Perovskite-Structured Mixed Ionic-Electronic Conducting $SrSn_{1-x}Fe_xO_{3-x/2+\delta}$

C. S. Kim, S. R. Bishop, N. H. Perry, H. L. Tuller
Sponsorship: Skolkovo Foundation

High efficiency and fuel flexibility make solid oxide fuel cells (SOFCs) attractive for conversion of fuels to electricity. Reduced operating temperatures, desirable for reduced costs and extended operation, however, result in significant losses in efficiency. This loss has been traced primarily to slow cathode surface reaction kinetics. In this work, we extend previous studies on the promising mixed ionic and electronic conducting perovskite-structured $SrTi_{1-x}Fe_xO_{3-x/2+\delta}$ (STF) materials system whose exchange kinetics were correlated with the minority electron charge density by replacing Ti with Sn, due to its distinct band structure and higher electron mobility.

Oxygen nonstoichiometry and the defect chemistry of the $SrSn_{1-x}Fe_xO_{3-x/2+\delta}$ (SSF) system were examined by thermogravimetry as a function of oxygen partial pressure in the temperature range of 973-1273 K. Marginally higher reducibility was observed compared to corresponding compositions in the STF system. The bulk electrical conductivity was measured in parallel to examine how changes in defect chemistry and electronic band structure, associated with the substitution of Ti by Sn, impact carrier density and ultimately electrode performance. Bulk chemical expansion was measured by dilatometry as a function of oxygen partial pressure, while surface kinetics were examined by means of AC impedance spectroscopy. The electro-chemo-mechanical properties of SSF were found not to differ significantly from the corresponding composition in STF. Key thermodynamic and kinetic parameters for $SrSn_{0.65}Fe_{0.35}O_{2.825+\delta}$ (SSF35) were derived, including the reduction enthalpy, electronic band gap, anion Frenkel enthalpy, oxygen vacancy migration energy, and electron and hole mobilities. Though slightly shifted by the larger size of Sn, the defect equilibria and the cathode area specific resistance differed only in a limited way from that in STF. This was attributed to properties being largely dominated by Fe and not by the substitution of Ti with Sn.

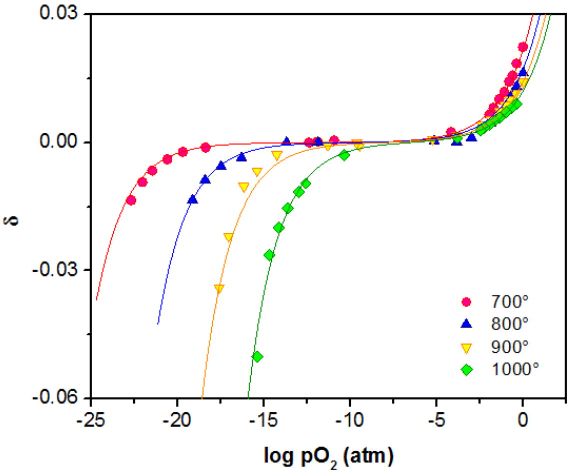

▲Figure 1: Oxygen nonstoichiometry δ as a function of pO_2 and temperature for SSF35.

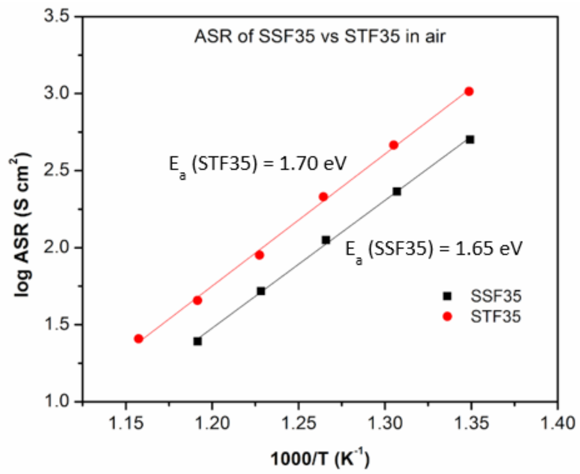

▲Figure 2: Comparison of temperature dependence of area specific resistance (ASR) of SSF35 and STF35 thin film electrodes.

FURTHER READING

- W. Jung and H. L. Tuller, "A New Model Describing Solid Oxide Fuel Cell Cathode Kinetics: Model Thin Film $SrTi_{1-x}Fe_xO_{3-\delta}$ Mixed Conducting Oxides, a Case Study," *Advanced Energy Materials*, vol. 1, pp. 1184–1191, 2011.

Utilization of $BaSnO_3$ and Related Materials Systems for Transparent Conducting Electrodes

M. Campion, S. R. Bishop, H. L. Tuller
Sponsorship: NSF

Efficient transparent electrode materials are vital for applications in smart window, LED display, and solar cell technologies. These materials must possess a wide band gap for minimal optical absorption in the visible spectrum while maintaining a high electrical conductivity. Tin-doped indium oxide (ITO) has been the industry standard for transparent electrodes, but the use of the rare element indium has led to a search for better material alternatives. $BaSnO_3$ represents a promising alternative due to its high electron mobility and resistance to property degradation under oxidizing conditions, but the mechanisms by which processing conditions and defect chemistry affect the final material properties are not well understood.

This work seeks to better understand the relationships between processing, defect chemistry, and material properties of $BaSnO_3$ in order to better establish the consistent and controllable use of $BaSnO_3$ as a transparent electrode. To accomplish these goals, methods such as *in-situ* resistance and impedance monitoring during annealing will be applied. In addition, a variety of novel methods such as the *in-situ* monitoring of optical transmission (shown in Figure 1) during annealing and the *in-situ* monitoring of resistance during physical vapor deposition will be utilized to investigate $BaSnO_3$. Direct measurements of the key constants for the thermodynamics and kinetics of oxidation in donor-doped $BaSnO_3$ will be experimentally determined for the first time. This increase in understanding will provide a predictive model for determining the optical properties, carrier concentrations, and electron mobilities in $BaSnO_3$.

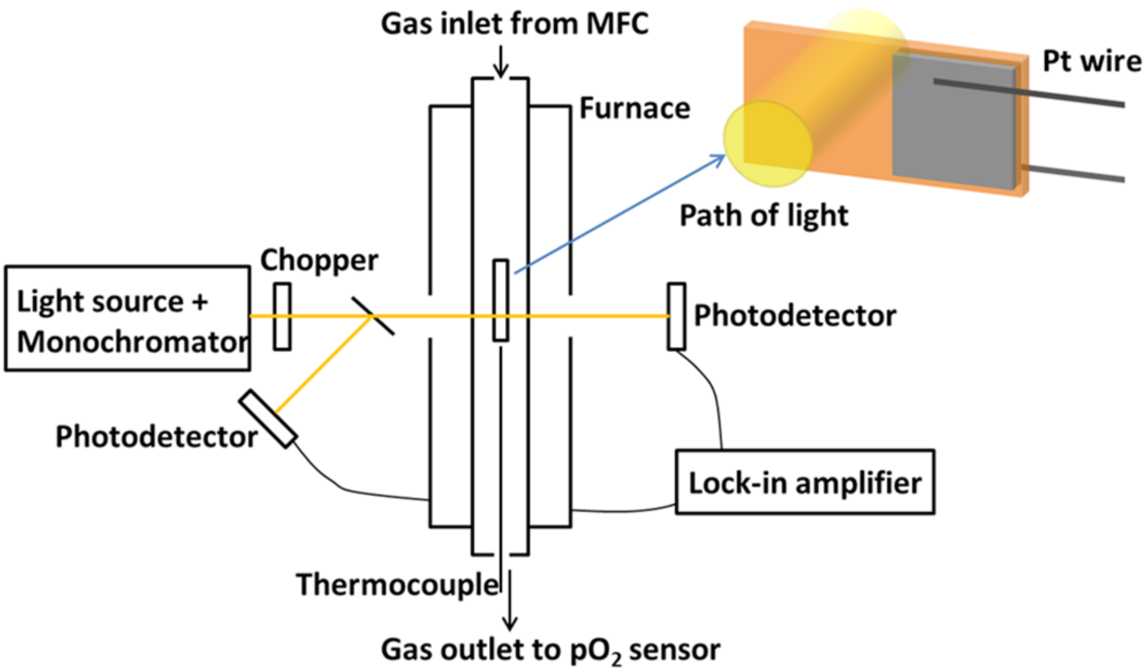

▲ Figure 1: Schematic of experimental setup to be used for simultaneous in-situ measurement of the optical transmission and electrical conductivity of thin film $BaSnO_3$ samples during annealing under controlled atmosphere and temperature.

FURTHER READING

- D. O. Scanlon, "Defect Engineering of BaSnO3 for High-performance Transparent Conducting Oxide Applications," *Phys. Rev.* vol. 87, no. 16, pp. 161201, April 2013.
- J. J. Kim, S. R. Bishop, N. J. Thompson, D. Chen, and H. L. Tuller, "Investigation of Nonstoichiometry in Oxide Thin Films by Simultaneous *in Situ* Optical Absorption and Chemical Capacitance Measurements: Pr-Doped Ceria, a Case Study," *Chemistry of Materials*, vol. 26, pp. 1374-1379, 2014.

Oxygen Reduction Kinetics and Defect Chemistry of Layered Praseodymium Cuprate-Based Materials

C. S. Kim, K. Mukherjee, S. R. Bishop, H. L. Tuller in collaboration with Y. Hayamizu, S. Istomin
Sponsorship: Skolkovo Foundation

Layered cuprate compounds with mixed ionic electronic conductivity are promising candidate materials for cathodes in intermediate-temperature solid oxide fuel cells. There have been reports of anisotropic oxygen diffusion in materials with the K_2NiF_4 (T) and Nd_2CuO_4 (T') crystal structures, with facile transport along the rock-salt layers. These material systems also exhibit anisotropic thermal and chemical expansion properties, potentially important for long-term device stability. However, in practice, it is difficult to independently control the crystal structure, doping, and grain orientation to understand their effects on cathode performance. Additionally, the lanthanide cuprates exhibit a third phase (T*), a hybrid of the T and T' phases, with important implications for the ionic and electronic conductivity.

In this work, we aim to understand the correlation between defect chemistry and surface exchange kinetics. Oxygen nonstoichiometry of Pr_2CuO_4 with varying amounts of Sr and Ce doping is studied as a function of oxygen partial pressure and temperature by thermogravimetry. Fitting the nonstoichiometry data to defect models enables the derivation of thermodynamic parameters as well as defect carrier concentrations. Dopants added to praseodymium cuprate were found to considerably extend the range of oxygen nonstoichiometry. Thins films of corresponding compounds were prepared by pulsed-laser deposition onto single-crystal YSZ substrates. Alloys with the same crystal structure and doping but with different film orientations were also successfully synthesized through the use of seed layers on YSZ (Figure 1). Using electrochemical impedance spectroscopy to measure the area-specific resistance (ASR), we found a significant improvement in the oxygen surface-exchange rate as a result of both donor and acceptor doping (Figure 2). However, the activation energies are very different, indicative of different rate-determining steps in each case. Also, contrary to expectations, the effect of film orientation (fast oxygen diffusion axis vs. slow diffusion axis) had only a relatively weak effect on the ASR. The reason for this weak correlation between the film orientation and the ASR is under investigation.

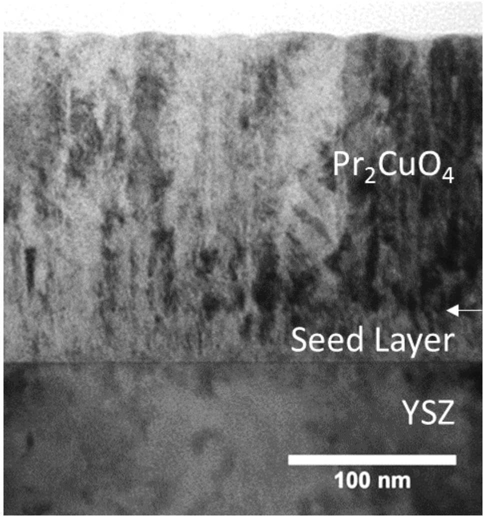

▲ Figure 1: Cross-sectional TEM of a Pr_2CuO_4 thin film grown epitaxially on a YSZ substrate. The columnar grains are a result of tetragonal film on cubic substrate resulting in two possible in-plane orientations.

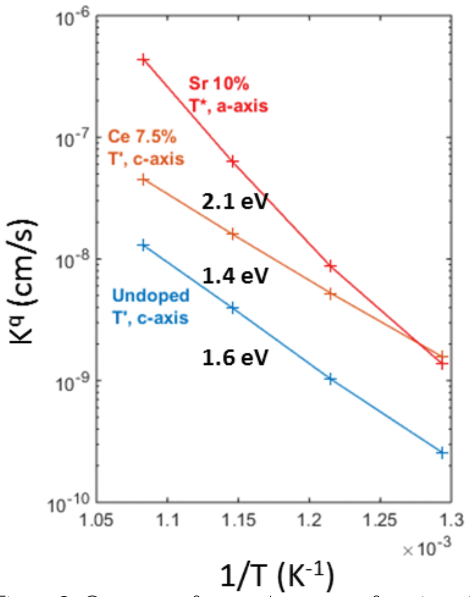

▲ Figure 2: Oxygen surface exchange as a function of inverse temperature in Pr_2CuO_4 thin films as determined from the area-specific resistance by electrochemical impedance spectroscopy. The activation energies are listed.

FURTHER READING

- M. Burriel, G. Garcia, J. Santiso, J. A. Kilner, R. J. Chater, and S. J. Skinner, "Anisotropic Oxygen Diffusion Properties in Epitaxial Thin Films of $La_2NiO4+\delta$," *Journal of Materials Chemistry*, vol. 18, pp. 416-422, 2008.
- G. N. Mazo, Y. A. Mamaev, M. Z. Galin, M. S. Kaluzhskikh, and A. K. Ivanov-Schitz, "Structural and Transport Properties of the Layered Cuprate Pr_2CuO_4," *Inorganic Materials*, vol. 47, pp. 1218–1226, 2011.
- H. Y. Hwang, S.-W. Cheong, A. S. Cooper, L. W. Rupp Jr., B. Batlogg, and G. H. Kwei, "Crystallographic Evolution, T'→T*→T, in $Pr_{2-x}Sr_xCuO_{4-\delta}$," *Physica C: Superconductivity*, vol. 192, pp. 362–371, 1992.

Investigation of Fuel Cell Cathode Performance in Solid Oxide Fuel Cells: Application of Model Thin Film Structures

J. J. Kim, D. Chen, N. H. Perry, S. R. Bishop, H. L. Tuller
Sponsorship: DOE

An improved fundamental understanding of oxygen nonstoichiometry (δ) and surface exchange kinetics in solid oxide fuel cell (SOFC) cathodes is considered critical for achieving enhanced device performance and longevity, especially at reduced operating temperatures. Although numerous research activities have been focused on elucidating the oxygen reduction reaction (ORR) mechanisms at the cathode, their conclusions remain unsatisfactory and controversial. The ORR at mixed conducting oxide thin film cathodes consists of oxygen adsorption, dissociation, charge-transfer, incorporation, and migration of charge carriers. The kinetic parameters associated with the overall ORR, such as the diffusion coefficient (D) and surface exchange coefficient (k), are strongly influenced by δ in the oxides. On the other hand, oxygen defect generation is often associated with valence changes in the transition metal or rare earth ions within the oxides and corresponding changes in lattice constant (chemical expansion). This phenomenon may lead to stresses sufficient to support crack initiation and/or delamination, impacting the device's long-term stability. Because many advanced oxide materials used in SOFCs experience significant changes in δ during operation at elevated temperatures and under reducing/oxidizing conditions, the ability to diagnose a material's behavior *in situ* is, therefore, important.

Our group recently demonstrated that δ in $Pr_{0.1}Ce_{0.9}O_{2-\delta}$ (10 PCO) thin films could be reliably derived by utilizing chemical capacitance extracted from electrochemical impedance spectroscopy (EIS) measurements. Furthermore, we introduced a non-contact optical means for *in situ* recording of transient redox kinetics, as well as the equilibrium Pr oxidation state and, in turn, δ in 10 PCO thin films, by monitoring the change in absorption spectra upon change in pO_2 or temperature. Recently, these optical techniques have been extended by our group to examination of the perovskite SOFC electrode $Sr(Ti,Fe)O_{3-\delta}$. In this study, we are investigating cathode kinetics and nonstoichiometry of two model oxide thin films, $Sr(Ti,Fe)O_{3-\delta}$ (STF) with La doping and $(Pr,Ce)O_{2-\delta}$ (PCO), by simultaneously utilizing *in situ* and *in operando* optical absorption spectroscopy and EIS as a function of temperature, pO_2 and electrical potential. We are also investigating changes in surface chemistry and their impact on electrode impedance by atomic force microscopy (AFM), x-ray photoelectron spectroscopy (XPS), and low-energy ion scattering spectroscopy (LEIS).

FURTHER READING

- D. Chen, S. R. Bishop, and H. L. Tuller, "Non-stoichiometry in Oxide Thin Films Operating Under Anodic Conditions: A Chemical Capacitance Study of the Praseodymium-cerium Oxide System," *Chemistry of Materials*, vol. 26, no. 22, pp. 6622-6627, 2014.
- N. H. Perry, D. Pergolesi, S. R. Bishop, and H. L. Tuller, "Defect Chemistry and Surface Oxygen Exchange Kinetics of La-doped $Sr(Ti,Fe)O_{3-a}$ in Oxygen-rich Atmospheres," *Solid State Ionics*, vol. 273, pp. 18-24, 2015.
- J. J. Kim, S. R. Bishop, N. J. Thompson, D. Chen, and H. L. Tuller, "Investigation of Nonstoichiometry in Oxide Thin Films by Simultaneous in Situ Optical Absorption and Chemical Capacitance Measurements: Pr-doped ceria, a Case Study," *Chem. Mater.*, vol. 26, pp. 1374-1379, January 2014.

Coupling of Oxide Catalyst Chemistry with Durability and Conversion Efficiency for Biomass Reforming

V. Mortola, S. R. Bishop, H. L. Tuller in collaboration with M. Shetty, Y. Roman
Sponsorship: Basic Energy Sciences/DOE

The transportation sector currently relies heavily on non-renewable fossil-based fuels to meet its energy requirements. Alternative energy sources need to be developed to meet the projected energy demand in the future in a sustainable and environmentally conscious manner. Bio-oils, generated via biomass fast pyrolysis, represent an attractive avenue for the production of renewable fuels and chemicals. We are investigating $MoO_{3-\delta}$, a promising catalyst for bio-oil upgrading, that selectively transforms various phenolic compounds into aromatic hydrocarbons with high yields using low H_2 pressures by hydrodeoxygenation (HDO). While it is clear that both ionic (oxygen vacancies) and electronic defects (e.g., $Mo^{5+/3+}$), in both the oxide catalyst and oxide support (e.g., TiO_2, ZrO_2 and Al_2O_3), play controlling roles in the catalytic reactions, surprisingly little is known about how operating conditions (temperature, dopants/impurities, and atmosphere (pO_2, pH_2O, pH_2, carbon activity, etc.)) impact the concentration or the diffusivities of these key defects, or how they influence the reaction kinetics. In this project, we combine catalysis with defect chemical and impedance spectroscopic approaches to achieve a deeper understanding of the role that defects in metal oxide catalysts and supports play in influencing catalytic selectivity, efficiency, stability, and reaction rates.

FURTHER READING

- T. Prasomsri, M. Shetty, K. Murugappan, and Y. Roman-Leshkov, "Insights into the Catalytic Activity and Surface Modification of MoO_3 During the Hydrodeoxygenation of Lignin-derived Model Compounds into Aromatic Hydrocarbons Under Low Hydrogen Pressures," *Energy Environ. Sci.*, vol. 7, pp. 2660, 2014.
- T. Prasomsri, T. Nimmanwudipong, and Y. Roman-Leshkov, "Effective Hydrodeoxygenation of Biomass-derived Oxygenates into Unsaturated Hydrocarbons by MoO_3 Using Low H_2 Pressures," *Energy Environ. Sci.*, vol. 6, pp. 1732, 2013.

Synthesis of CRUD and its Effects on Pool and Subcooled Flow Boiling

C. P. Coyle, B. A. Phillips, S. P. Lowder, J. Buongiorno, M. Bucci, T. McKrell
Sponsorship: DOE, Office of Nuclear Energy

Chalk River Unidentified Deposits (CRUD) are a naturally occurring porous, hydrophilic layer that forms on fuel rods during nuclear reactor operation. Unique features of these deposits are the characteristic boiling chimneys, as shown in Figure 1. It has been hypothesized that the presence of these chimneys, by providing a clear path for vapor escape, can further enhance boiling properties such as critical heat flux and heat transfer coefficient.

An investigation of such effects has been conducted by preparing a porous, hydrophilic layer with boiling chimneys on indium-tin-oxide-coated sapphire heaters. A porous matrix emulating CRUD, shown in Figure 2, was created using layer-by-layer deposition of 100-nm silica nanoparticles to form porous, hydrophilic thick films. Photolithography was used to manufacture posts that were then dissolved to create characteristic boiling chimneys. MTL facilities were used to deposit gold pads on the heater, plasma clean heaters, create and remove photoresist posts, and confirm film thickness using the Dektak profilometer. Features such as thickness, wettability, pore size, and chimney diameter and pitch were verified. During pool and flow boiling testing, IR thermography and high-speed video were used to obtain temperature profiles of the active heater area to quantify properties such as heat transfer coefficient, nucleation site density, bubble departure frequency, and bubble departure diameter.

Data from pool and subcooled flow boiling tests has shown that the heat transfer coefficient increases with increasing layer thickness and chimney diameter while the chimney pitch has relatively no effect. The observed increase results from greater nucleation site densities and greater bubble departure frequencies, meaning the surface is able to remove more heat through the creation of more bubbles per unit area and per unit time. The bubble parameters also followed expected trends with mass flux and imposed heat flux.

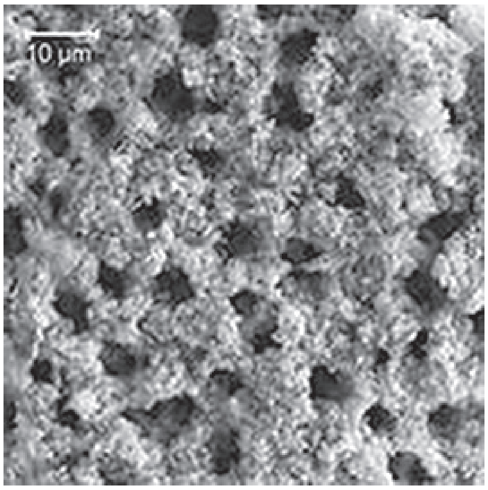

▲ Figure 1: SEM image of actual reactor CRUD (note the micro-scale boiling chimneys).

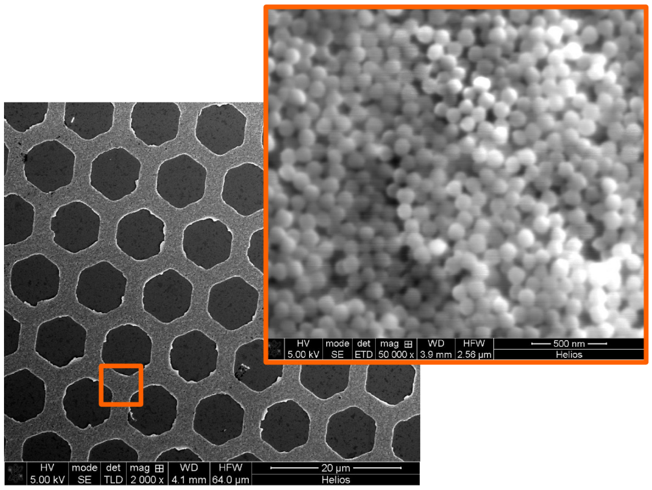

▲ Figure 2: SEM image of synthetic CRUD with a zoom-in of the nanoporous CRUD matrix in between the boiling chimneys.

MEMS, Field-Emitter, Thermal, and Fluidic Devices

Development of a Tabletop Deep Reactive-Ion Etching System for MEMS Development and Production

P. A. Gould, M. D. Hsing, K. K. Gleason, M. A. Schmidt
Sponsorship: MTL

A general rule of thumb for new semiconductor fabrication facilities (fabs) is that revenues from the first year of production must match the capital cost of building the fab itself. With modern fabs routinely exceeding $1 billion to build, this rule serves as a significant barrier to entry for research and development and groups seeking to commercialize new semiconductor devices aimed at smaller market segments that require a dedicated process. To eliminate this cost barrier, we are working to create a suite of tools that will process small (~1") substrates and cost less than $1 million. This suite of tools, known colloquially as the 1" Fab, offers many advantages over traditional fabs. By shrinking the size of the substrate, we trade off high throughputs for significant capital cost savings while incurring substantial savings in material usage and energy consumption. This substantial reduction in the capital cost will drastically increase the availability of semiconductor fabrication technology and enable experimentation, prototyping, and small-scale production to occur locally and economically. To implement this suite of 1" Fab tools, our current research has been focused primarily on developing a deep reactive-ion etching (DRIE) system. DRIE tools are used to create highly anisotropic, high aspect-ratio trenches in silicon—a crucial element in many MEMS processes that will benefit from a 1" Fab platform. A labeled image of the 1" Fab DRIE system is shown in Figure 1. The load lock and wafer lift assembly allow up to 2" wafers and pieces to be easily loaded and processed, and the modularized design of the processing chamber means that the (currently DRIE) system can be easily adapted to produce other plasma-based etching and deposition tools (such as PECVD and RIE). Using the switched-mode Bosch Process, the 1" Fab DRIE system currently can achieve silicon etch rates up to 6 µm/min with vertical sidewall profiles, an estimated photoresist selectivity greater than 75:1, and etch depth non-uniformity to less than 2% across the substrate. Several examples of anisotropic etches performed with our system are included in Figure 2. Presently, we are working to refine the thermal design of the system and optimize recipes for high-aspect ratio etching.

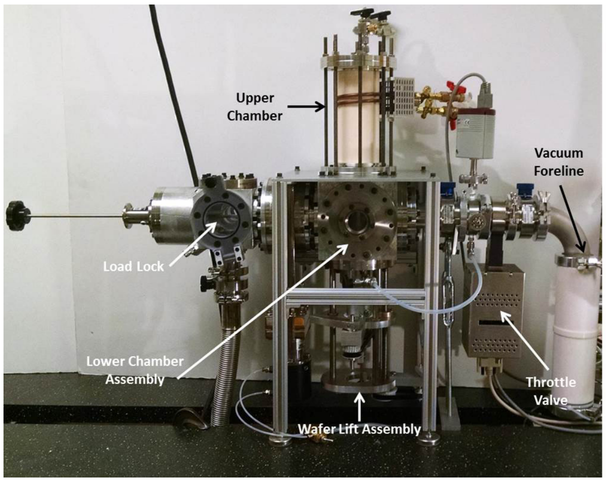

▲Figure 1: View of the basic components of the 1" Fab DRIE system.

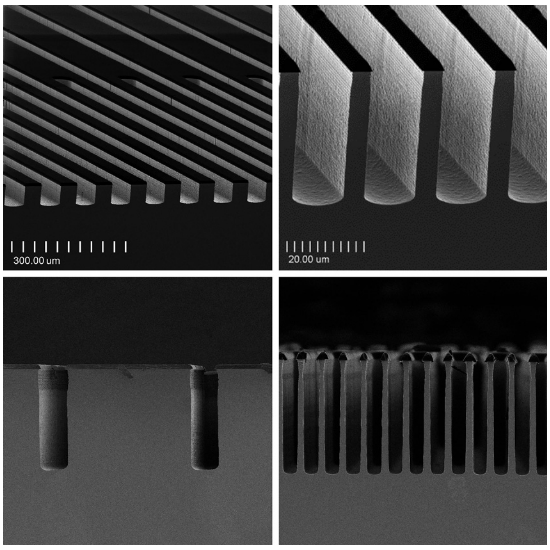

▲Figure 2: Examples of anisotropic etches performed using the Bosch process in the 1" Fab DRIE.

FURTHER READING

- S. Heck, S. Kaza, and D. Pinner. (2011, Autumn) "Creating Value in the Semiconductor Industry" [Online]. Available: http://www.mckinsey.com/~/media/McKinsey/dotcom/client_service/Semiconductors/PDFs/MOSC_1_Value_creation.ashx.
- P. A. Gould, M. D. Hsing, H. Q. Li, K. K. Gleason, and M. A. Schmidt, "An Ultra-low Cost Deep Reactive Ion Etching (DRIE) Tool for Flexible, Small Volume Manufacturing," *Solid-State Sensors, Actuators and Microsystems (TRANSDUCERS)*, pp. 2268-2271, 2015.

Resonant Body Transistor with MIT Virtual Source (RBT-MVS) Compact Model

B. Bahr, D. Weinstein, L. Daniel
Sponsorship: NSF NEEDS

High-Q mechanical resonators are crucial components for filters and oscillators that are essential for RF and analog circuits. It is highly desirable for resonators to scale to GHz-frequencies and beyond to meet today's challenging requirements in terms of speed and data rates. Furthermore, aggressive scaling requirements call for monolithic integration with CMOS circuits to allow for a smaller footprint and reduced parasitics and power consumption. Micro-electromechanical (MEM) resonators represent a potential solution for frequency and footprint scaling, along with monolithic integration in CMOS.

A resonant body transistor (RBT) is a MEM resonator with a field-effect transistor (FET) incorporated into the resonator structure. The FET is intended for active sensing of the mechanical vibrations through piezoresistive modulation of the channel mobility. RBTs also rely on electrostatic internal dielectric transduction for actuation, by means of MOS capacitors (MOSCAPs). Such sensing and actuation enable these devices to easily scale to multi-GHz frequencies, while being compatible with CMOS manufacturing technologies.

Compact modeling for these devices is essential to gain a deeper insight into the tightly coupled physics of the RBT while emphasizing the effect of the different parameters on the device performance. It also grants circuit designers and system architects the ability to quickly assess the performance of prospective RBTs, while minimizing the need for computationally intensive coupled-multi-physics finite element method (FEM) simulations.

The RBT compact model is developed as a set of modules, each representing a physical phenomenon. Mechanical resonance, FET sensing, MOSCAP driving, and thermal modules are the most notable. The modules are interconnected through a set of nodes (namely, mechanical nodes and a thermal node) to represent the coupling between the different physics. This modular approach enables the seamless expansion of the RBT model either by incorporating new physics, adding driving or thermal sources, or mechanically coupling multiple RBTs together. A modified version of the MIT Virtual Source (MVS) model is used to implement both the electrostatic driving (as a MOSCAP) as well as the piezoresistive active FET sensing. The full model is developed in Verilog-A and available on nanohub.org.

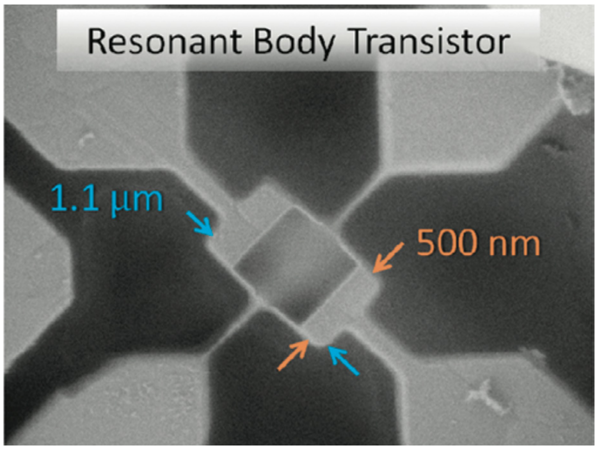

▲Figure 1: The first RBT, developed by D. Weinstein and S. Bhave in 2009 at Cornell University.

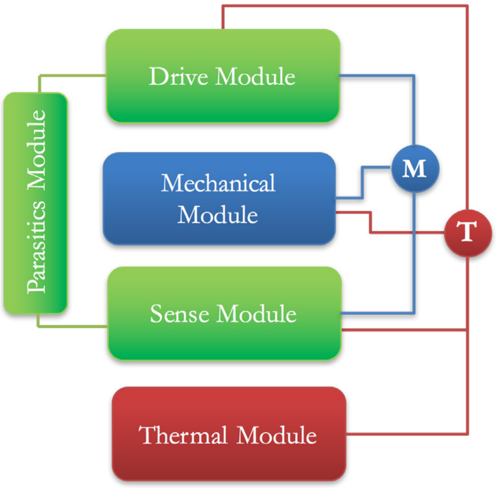

▲Figure 2: Modular RBT model, with each physical phenomenon represented by a module. Different modules are connected through a mechanical node (M) and thermal node (T).

FURTHER READING

- D. Weinstein and S. Bhave, "The Resonant Body Transistor," *Nano Letters*, pp. 1234–1237, 2010.
- B. Bahr, D. Weinstein, and L. Daniel, "RBT-MVS Model" [Online]. Available: nanohub.org: https://nanohub.org/publications/72/1.
- B. Bahr, D. Weinstein, and L. Daniel, "URBT-MVS Model" [Online]. Available: nanohub.org: https://nanohub.org/publications/132/1.

Piezoelectric Micro-Machined Ultrasonic Transducer Array for Medical Imaging

K. M. Smyth, C. G. Sodini, S.-G. Kim
Sponsorship: Medical Electronic Device Realization Center, Analog Devices, Inc.

Diagnostic medical ultrasound imaging is becoming increasingly widespread because it is relatively inexpensive, portable, compact, and non-invasive compared to other diagnostic scanning techniques. However, commercial realization of advanced imaging trends will require cost-effective, large-scale arrays of miniaturized elements, which are expensive to fabricate with the current bulk piezoelectric transducers. At high volume, micro-fabricated transducers based on micro-electro-mechanical (MEMS) technology are an array-compatible and low-cost option.

The piezoelectric micro-machined ultrasonic transducer (pMUT) is a promising alternative to previously proposed capacitive MUT devices since it does not suffer from electrostatic transduction limitations, including potentially unsafe high bias voltage, and non-linearity. With more effective transformation via the piezoelectric effect, pMUTs have already demonstrated viability for deep penetration imaging via high acoustic pressure output. However, insufficient modeling has produced pMUT devices that often fall short of predictions, resulting in low electromechanical coupling and reduced bandwidth. With an improved modelling framework and optimization, pMUT based arrays have the potential for efficient, low-power, and high-pressure operation necessary for wearable applications.

Based on a high force-output figure of merit, a 31-mode, lead zirconate titanate (PZT)-based pMUT plate cell design is selected. Our previous work developed and validated an analytical, electro-acoustic model of the single cell through experiment and finite element simulation. By leveraging and building on the validated single-cell model, we further optimized parallelized multi-cell elements to achieve high acoustic power and power efficiency. These elements are incorporated into 1D arrays (Figure 1) to demonstrate basic beamforming and image collection capabilities of a pMUT-based ultrasound system.

Current work focuses on fabrication of the pMUT arrays (Figure 2) using common micro-fabrication techniques including a PZT sol-gel deposition process. Beyond fabrication, the project aims to generate proof-of-concept images to demonstrate the commercial viability of pMUT-based array systems.

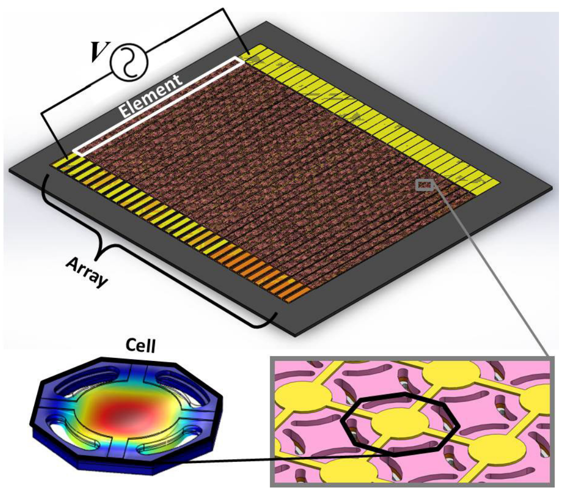

▲ Figure 1: Rendering of 1D pMUT array (top) in which each element consists of many small pMUT cells (bottom right). Deflection of single cell based on piezo-acoustic finite element model simulated in COMSOL (bottom left).

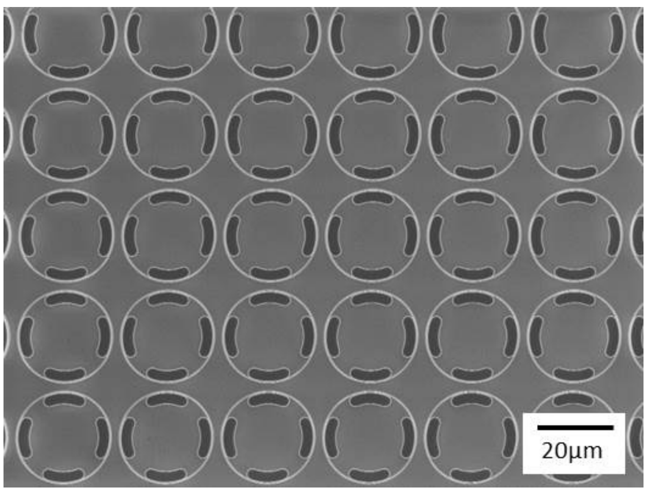

▲ Figure 2: Scanning electron microscope image of partially completed pMUT cells currently undergoing fabrication.

FURTHER READING

- K. Smyth, S. Bathurst, F. Sammoura, and S.-G. Kim, "Analytic Solution for N-electrode Actuated Piezoelectric Disk with Application to Piezoelectric Micromachined Ultrasonic Transducers," *IEEE Trans. Ultrason. Ferroelectr. Freq. Control*, vol. 60, no. 8, pp. 1756–1767, August 2013.
- K. Smyth and S.-G. Kim, "Experiment and Simulation Validated Analytical Equivalent Circuit Model for Piezoelectric Micromachined Ultrasonic Transducers," *IEEE Trans. Ultrason. Ferroelectr. Freq. Control*, vol. 62, no. 4, pp. 744–765, April 2015.

MEMS Energy Harvesting from Low-Frequency and Low-Amplitude Vibrations

R. Xu, S.-G. Kim
Sponsorship: MIT-SUTD International Design Center

Vibration energy harvesting at the microelectromechanical system (MEMS) scale will promisingly advance exciting applications such as wireless sensor networks and the Internet of Things by eliminating troublesome battery-changing or power wiring. On-site energy generation could be an ideal solution to powering a large number of distributed devices usually employed in these systems. To enable the envisioned battery-less systems, a fully assembled energy harvester at the size of a quarter-dollar coin should generate robustly 10^1~10^2 μW of continuous power from ambient vibrations (mostly less than 100 Hz and 0.5 g acceleration) with wide bandwidth. We are inching close to this goal in terms of power density and bandwidth, but not in terms of low-frequency and low-amplitude operations.

Most reported vibration energy harvesters use a linear cantilever resonator to amplify the energy absorption from weak ambient vibrations. While such structures are easy to model, design, and build, they typically have unusably narrow bandwidths. In contrast, nonlinear resonators have a different dynamic response and greatly increase the bandwidth by hardening or softening the resonance characteristic. Our previous research with nonlinear resonating bridge-structure-based energy harvesters achieved 2.0 mW/mm^3 power density with >20% power bandwidth. However, they were operated with input vibrations of >1 kHz at 4 g, which practically limits the use of this technology for harvesting energy from real environmentally available vibrations. Many believed this is an inherent limitation imposed on the MEMS-scale structures.

We approached this problem with a buckled-beam-based bi-stable nonlinear oscillator. Compared to mono-stable nonlinear oscillations, we found bi-stable oscillations could bring more dynamics phenomena to help reduce the operating frequency. An electromechanical lumped model has been built to simulate the dynamics of the buckled clamped-clamped beam-based piezoelectric energy harvesters. The two oscillation modes, intra-well and inter-well with respect to the double-well energy potential of the bi-stable system, have been predicted. The characteristic spring softening and spring stiffening responses corresponding to the simulations were observed by testing a meso-scale prototype. The testing results also verify the theoretical prediction on low-frequency operation, showing a shifted response of bi-stable configuration, which generates more power than the mono-stable configuration at lower frequencies. A MEMS mechanical bi-stable oscillator has also been fabricated to verify the operating frequency and amplitude of the new design (Figure 1). The multi-layer bridge structure has employed compressive residual stress in the micro-fabricated thin films to induce buckling and lower the operation frequencies. The dynamic responses were measured by a laser Doppler vibrometer (Figure 2). The wide-band nonlinear response shows a one-order-of-magnitude lower frequency range at low g's. The fully functional piezoelectric devices are under fabrication.

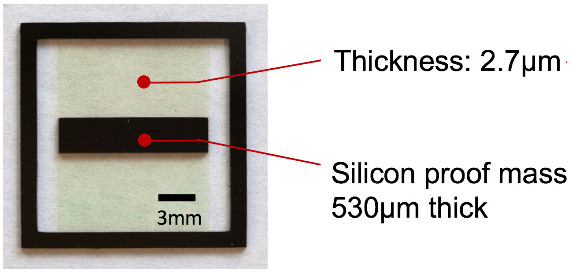

▲Figure 1: Top view of the fabricated MEMS prototype (the aspect ratio of the clamped-clamped plate is 4444:1). The plate vibrates out-of-plane during excitation.

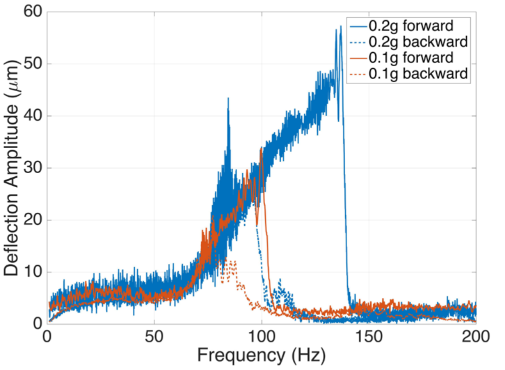

▲Figure 2: Frequency response of the MEMS prototype. The tilted peak shows the spring stiffening response with a wide bandwidth. The tests were done at 0.1g and 0.2g.

FURTHER READING

- R. Xu and S.-G. Kim, "MEMS Energy Harvesting from Low-frequency and Low-g Vibrations," *2015 MRS Spring Meeting*, San Francisco, CA, 2015.
- R. Xu and S.-G. Kim, "Low-Frequency, Low-G MEMS Piezoelectric Energy Harvester," *PowerMEMS 2015*, Boston, MA, 2015.

Wearable Energy Harvesters Based on Aligned Mats of Electrospun Piezoelectric Nanofibers

D. Olvera-Trejo, L. F. Velásquez-García
Sponsorship: U.S. Army

Battery recharging and replacement are still challenging after several decades of developing energy sources for portable and wireless devices. For this reason, new power sources have become essential for current and future stand-alone devices. Energy harvesters are an attractive alternative for supplying power in these systems.

We are developing wearable energy harvesters based on electrospun piezoelectric nanofibers as transducing elements. The proposed harvesting device consists of a set of flexible interdigitated electrodes on a flexible substrate; the electrodes are coated with aligned piezoelectric nanofibers. Each time the substrate is stretched or bent, the piezoelectric nanofibers produce voltage and charge that can be used to feed low-power devices. Our energy harvesters could be integrated into garments, allowing people to carry less weight and volume in batteries, which is particularly advantageous on long journeys and when located far from the electrical grid.

The piezoelectric nanofibers of our energy harvester are made of poly(vinylidene difluoride), i.e., PVDF, using the electrospinning technique. In electrospinning, a solution rich in long-chain polymers that is subject to a high electrostatic field ejects a jet that is thinned to a submicron diameter due to the interaction of the electric field and surface tension effects on the fiber (Figure 1). Highly aligned fiber deposition on the interdigitated electrodes of the energy harvester is necessary to achieve high efficiency. With this goal in mind, we developed a custom rotating collector system that allows control of the alignment and diameter of the deposited nanofibers. The collected fibers tend to be more aligned and exhibit smaller fiber diameters when the collector drum rotates at thousands of revolutions per minute (Figure 2). Current work focuses on controlling the morphology of the PVDF fibers and nanofiber mats, as well as on testing nanofiber harvester prototypes using a custom apparatus and benchtop electronics.

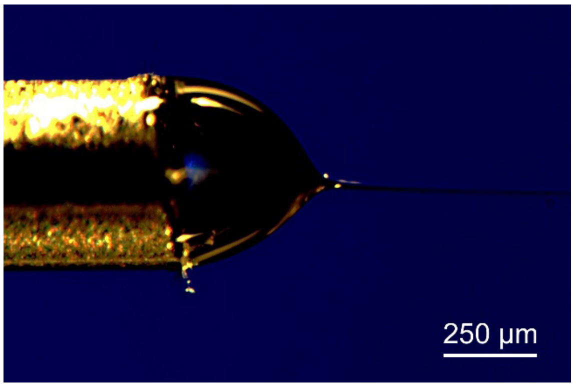

▲Figure 1: Electrospinning emitter in operation. A fine jet of liquid is electrohydrodynamically ejected from the emitter tip due to the high electric fields present there; the jet is stretched into a nanofiber due to the surface tension and electrostatic forces it experiments while traveling to the collector electrode.

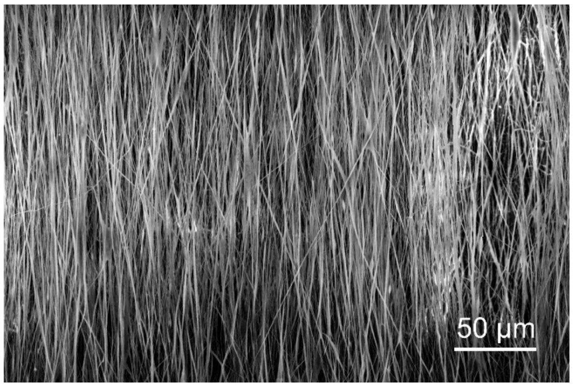

▲Figure 2: SEM micrograph of aligned PVDF nanofibers deposited on a rotating drum collector.

FURTHER READING

- P. J. Ponce de Leon, F. A. Hill, E. V. Heubel, and L. F. Velásquez-García, "Parallel Nanomanufacturing via Electrohydrodynamic Jetting from Microfabricated Externally-fed Emitter Arrays," *Nanotechnology*, vol. 26, no. 22, pp. 225301, June 2015.

Thin, Flexible, and Stretchable Tactile Sensor Based on a Deformable Microwave Transmission Line

M. E. D'Asaro, D. B. Sheen, J. H. Lang
Sponsorship: NSF CSNE

Over the past decade, there have been numerous publications on tactile sensors and skins aimed at replicating the human sense of touch in applications such as robotics, healthcare, and prosthetics. A variety of technologies are used, with the dominant ones being piezoresistive and capacitive, but both of these technologies have limitations due to mechanical fragility, complex fabrication, and the need for large numbers of connections to external electronics. We have developed another sensing technology that is mechanically robust, simple to fabricate, and requires only one connection to external electronics.

The new sensor, shown in Figure 1, consists of a flexible and stretchable 1.6-mm-thick microstrip transmission line with conductors made of stretchable silver-based conductive cloth and a dielectric made of soft silicone rubber (PDMS). When pressure is applied to the line, the dielectric is deformed, causing a local impedance discontinuity in the line. We have developed an algorithm that can reconstruct the deformation of the line as a function of position, based on the measured impedance of the line across a wide frequency range (30 MHz to 6 GHz).

To characterize the sensor and algorithm, the sensor was precisely deformed using a custom-designed jig based on a micrometer head while its impedance was measured in real time with a vector network analyzer. The analyzer was connected to a computer. in which the output was processed to display a plot of the reconstructed deformation, also in real time. To correct for imperfections in fabrication, any deformation present with the sensor at rest was subtracted from the responses with pressure applied. Three different pressures were applied at each of three locations, and the responses were combined to create Figure 2. Note that the reconstruction algorithm is derived entirely from physical theory and was calibrated to the measured velocity factor of the line but was not otherwise tuned to match the individual device.

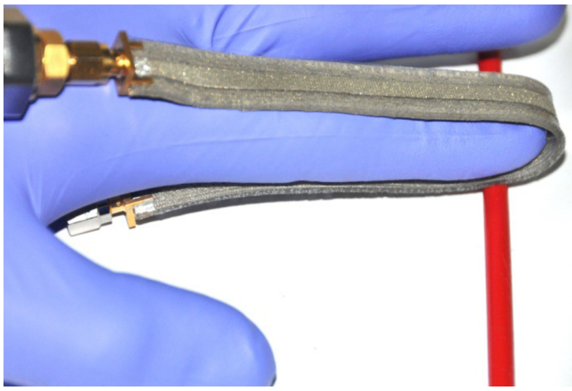

▲Figure 1: Sensor, mounted on nitrile glove. The sensor is flexible, stretchable, and rugged and is fabricated from silver cloth and silicone rubber.

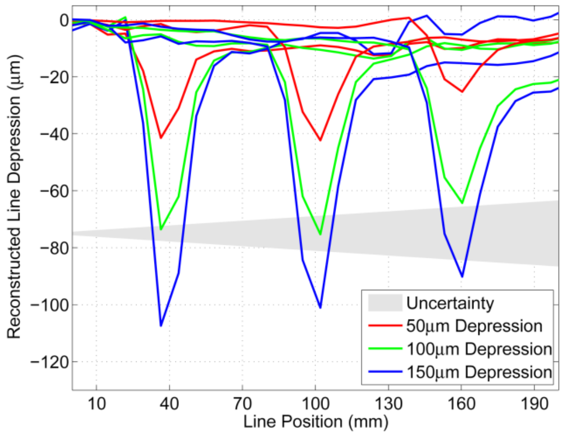

▲Figure 2: Response of the sensor to depressions applied at 40 mm, 100 mm, and 160 mm. The sensor is accurate in position to within a single data point (7.3 mm) and in depression to within 30% at 40 mm.

FURTHER READING

- M. E. D'Asaro, D. B. Sheen, and J. H. Lang, "Thin Flexible and Stretchable Tactile Sensor Based on a Deformable Microwave Transmission Line," *Hilton Head 2016 Workshop on Solid-State Sensors, Actuators and Microsystems*, June 2016.
- C. Lucarotti, C. M. Oddo, N. Vitiello, and M. C. Carrozzo, "Synthetic and Bio-Artificial Tactile Sensing: A Review," *Sensors*, vol. 13, no. 2, pp. 1435-1466, January 2013.
- M. L. Hammock, A. Chortos, B. C.-K. Tee, J. B.-H. Tok, and Z. Bao, "25th Anniversary Article: The Evolution of Electronic Skin (E-Skin): A Brief History, Design Considerations, and Recent Progress," *Advanced Materials*, vol. 25, no. 42, pp. 5997-6038, October 2013.

Close-Packed Silicon Microelectrodes for Scalable Spatially Oversampled Neural Recording

J. Scholvin, J. P. Kinney, J. G. Bernstein, C. Moore-Kochlacs, N. Kopell, C. G. Fonstad, E. S. Boyden
Sponsorship: Simons Center for the Social Brain at MIT, Paul Allen Family Foundation, NYSCF, NIH, NSF

The extracellular recording of brain activity in the mammalian brain provides an important tool for understanding neural codes and brain dynamics. Extracellular electrodes with recording sites that are closely packed can enable spatial oversampling of neural activity, which facilitates data analysis; such oversampling becomes important when we aim to scale up the number of neurons used for recording.

We designed and implemented close-packed silicon microelectrodes (Figure 1) to enable the spatially oversampled recording of neural activity (Figure 2) in a scalable fashion, using a tight continuum of recording sites along the length of the recording shank, rather than discrete arrangements of tetrode-style pads or widely spaced sites. This arrangement, thus, enables spatial oversampling continuously running down the shank, so that sorting of spikes recorded by the densely packed electrodes can be facilitated for all the sites of the probe simultaneously.

We use MEMS microfabrication techniques to create thin recording shanks, and a hybrid lithography process that allows a dense array of recording sites, which we connect with submicron dimension wiring. We have performed neural recordings with our probes in the live mammalian brain. Figure 2 illustrates the spatial oversampling potential of close packed electrode sites.

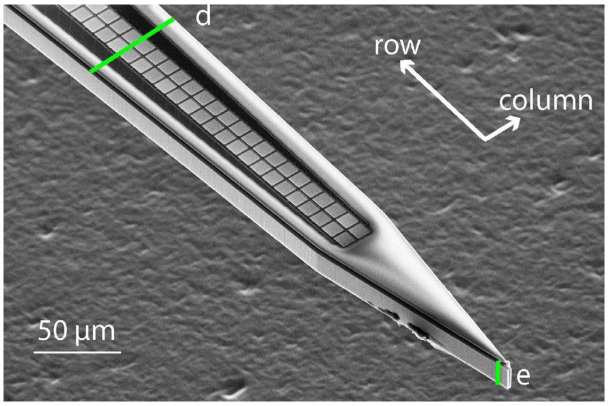

▲Figure 1: Close-up of the tip section of a recording shank, showing the two columns and a dense set of rows. The close packed pads are visible as light squares in the center of the shank. Insulated metal wires connect to individual sites, running next to recording sites along length of shank and visible as dark lines flanking rows of light squares. The shank itself is ~50-60 µm wide (d) and 15 µm thick (e) in the regions shown.

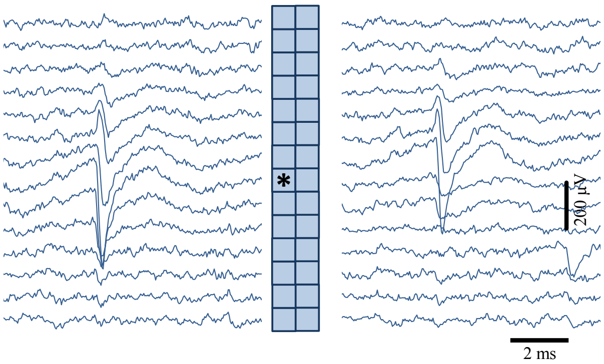

▲Figure 2: *In vivo* recorded data for a single spike across 28 pads (2 columns by 14 rows). The spatial oversampling enables the spike to be picked up by many nearby recording sites (9 x 9 µm pads, at a 10.5 µm pitch), to facilitate automated data analysis.

FURTHER READING

- J. Scholvin, J. P. Kinney, J. G. Bernstein, C. Moore-Kochlacs, N. Kopell, C. G. Fonstad, and E. S. Boyden, "Close-Packed Silicon Microelectrodes for Scalable Spatially Oversampled Neural Recording," *IEEE Trans. Biomed. Eng.*, vol. 63, no. 1, pp. 120–130, 2016.
- B. D. Allen, C. Moore-Kochlacs, J. Scholvin, J. P. Kinney, J. G. Bernstein, S. B. Kodandaramaiah, N. J. Kopell, and E. S. Boyden, "Towards Ground Truth in Ultra-dense Neural Recording," in *Computational and Systems Neuroscience (Cosyne)*, 2016.

Extreme Heat Flux Thermal Management via Thin-film Evaporation

S. Adera, D. S. Antao, R. Raj, E. N. Wang
Sponsorship: ONR, NSF GRFP

Thermal management is a primary design concern for numerous power-dense equipment such as power amplifiers, solar energy convertors, and advanced military avionics. During operation, these devices generate large amounts of waste heat (>1 kW/cm²) from sub-millimeter areas. These concentrated heat loads are spatially and temporally non-uniform and cause hotspots which are localized regions with extreme heat flux and exceedingly high temperature that can adversely impact device performance and reliability.

In this study, we demonstrate an extreme heat flux thermal management solution targeted towards cooling hotspots. Our test devices utilize well-defined silicon micropillar arrays which were fabricated via contact photolithography and deep-reactive-ion-etching for passive fluidic transport (i.e., capillary-wicking). Resistive thin-film heaters were integrated on the back side of our test device via electron-beam evaporation and acetone lift-off to emulate the heat generated by actual electronic chips during operation. The heaters which were used to measure temperature in addition to providing heating were calibrated prior to experiments in a convection oven. The hotspots (640×620 μm²) were spatially distributed over the microstructured surface (1×1 cm²). Uniform background heating was provided by heating the entire microstructured surface using a 1×1 cm² thin-film heater. Experiments were conducted in a temperature-controlled stainless steel environmental chamber which was maintained at saturated temperature and the corresponding pressure.

We dissipated ≈6 kW/cm² from a single hotspot without background heating before the microstructured surface dried out (Figure 1a). Dryout occurs due to liquid starvation when the viscous losses exceed the capillary pressure generated owing to the meniscus shape. We activated concurrent hotspots on our test devices over the 1×1 cm² microstructured surface and examined the hotspot dryout heat flux. Our experiments show that this hotspot dryout heat flux decreased monotonically when concurrent hotspots were present on the microstructured surface (left ordinate, Figure 1b). The dryout heat flux, which was ≈6 kW/cm² when a single hotspot (H2) was present, decreased to ≈4 kW/cm² per heater when two hotspots (H1/H3) were present (left ordinate, Figure 1b). This dryout heat flux decreased further to ≈3 kW/cm² per heater when three hotspots (H1/H2/H3) were present (left ordinate, Figure 1b). When a 10 W/cm² and 20 W/cm² uniform background heating was superposed with a hotspot, the hotspot dryout heat flux, which was ≈6 kW/cm² without background heating, decreased to ≈4 kW/cm² and ≈3 kW/cm², respectively (left ordinate, Figure 1c). Despite the decrease in the hotspot dryout heat flux, the total heating power increased when concurrent hotspots were created (right ordinate, Figure 1b) or when uniform background heating was superposed with a hotspot (right ordinate, Figure 1c). Our experiments show that thin-film evaporation is a promising thermal management solution for the next generation of power amplifiers and radio-frequency devices which generate extreme heat fluxes in excess of 1 kW/cm². The insights gained from this study can be used to improve the design of wicking structures which are commonly used in phase-change-based thermal management devices such as heat pipes and vapor chambers.

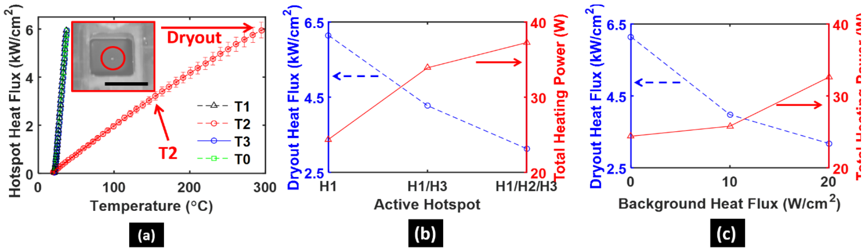

◀ Figure 1: (a) Heat flux as a function of temperature as measured by the different sensors (H1, H2, H3, and H0). A dry island formed at the hotspot H2 (inset, scale bar = 10 mm) when viscous losses exceed capillary pressure. Hotspot temperature (T2) was measured at the location where the heat was generated using heater H2. Local temperatures 3 mm away from the hotspot (T1 and T3) were measured using H1 and H3. Background temperature (T0) which is the average temperature of the entire 1×1 cm² microstructured surface was measured using H0. (b) The presence of concurrent hotspots decreased the hotspot dryout heat flux (blue, left ordinate), but increased the total heating power (red, right ordinate). (c) When the hotspot (H2) was superposed with a 10`W/cm² and 20`W/cm² uniform background heat flux, the hotspot dryout heat flux decreased (blue, left ordinate), but the total heating power increased (red, right ordinate).

FURTHER READING

- I. Mudawar, "Assessment of High-heat-flux Thermal Management Schemes," *IEEE Trans. Compon. Packag. Technol.*, vol. 24, pp. 122-141, 2001.
- A. Bar-Cohen and P. Wang, "Thermal Management of On-chip Hot Spot," *J. Heat Transfer*, vol. 134, pp. 051017, 2012.
- J.-M. Koo, *et al*, "Integrated Microchannel Cooling for Three-dimensional Electronic Circuit Architectures," *J. Heat Transfer*, vol. 127, pp. 49-58, 2005.

Prediction and Characterization of Dry-Out Heat Flux in Micropillar Wick Structures for Thermal Management Applications

Y. Zhu, D. S. Antao, Z. Lu, S. Somasundaram, T. J. Zhang, E. N. Wang
Sponsorship: ONR, Masdar Institute of Science and Technology, SMART

Thin-film evaporation in wick structures for cooling high-performance electronic devices is attractive because it harnesses the latent heat of vaporization and does not require external pumping. However, optimizing the wick structures to increase the dry-out heat flux is challenging due to the complexities in modeling the liquid–vapor interface and the flow through the wick structures. In this work, we developed a model for thin-film evaporation from micropillar array wick structures (Figure 1) and validated the model with experiments. The model numerically simulates liquid velocity, pressure, and meniscus curvature along the wicking direction by conservation of mass, momentum, and energy based on a finite volume approach. Specifically, the three-dimensional meniscus shape, which varies along the wicking direction with the local liquid pressure, is accurately captured by a force balance using the Young–Laplace equation. The dry-out condition is determined when the minimum contact angle on the pillar surface reaches the receding contact angle as the applied heat flux increases.

With this model, we predict the dry-out heat flux on various micropillar structure geometries (diameter, pitch, and height) in the length scale range of 1–100 µm and discuss the optimal geometries to maximize the dry-out heat flux (seen in Figure 2). We also performed detailed experiments to validate the model predictions, which all show good agreement. This work provides many insights into the role of surface structures in thin-film evaporation and also offers important design guidelines for enhanced thermal management of high-performance electronic devices.

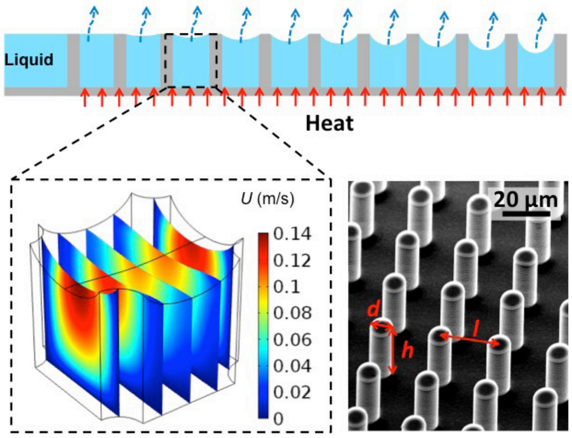

▲ Figure 1: Side view schematic (top) of capillary-pumped liquid film that evaporates on a hydrophilic micropillar array surface, where a uniform heat flux is applied. The fluid velocity and liquid-vapor interface shape is solved in a unit cell (bottom left). A representative SEM image of a fabricated silicon micropillar array (bottom right) with diameter ***d***, pitch ***l***, and height ***h***.

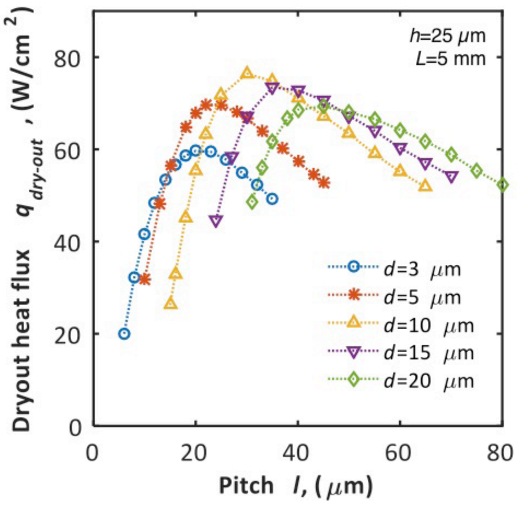

▲ Figure 2: The dry-out heat flux $q_{dry-out}$ for various micropillar geometries. The micropillar height ***h*** is 25 µm, and the receding contact angle of the evaporating liquid on the solid substrate is 15°.

FURTHER READING

- Y. Zhu, D. S. Antao, Z. Lu, S. Somasundaram, T. J. Zhang, and E. N. Wang, "Prediction and Characterization of Dry-out Heat Flux in Micropillar Wick Structures," *Langmuir*, vol. 32, pp. 1920-1927, 2016.
- Y. Zhu, D. S. Antao, K. H. Chu, S. Chen, T. J. Hendricks, T. J. Zhang, and E. N. Wang, "Surface Structure Enhanced Microchannel Flow Boiling," *Journal of Heat Transfer*, vol. 138, pp. 091501, 2016.

Enhanced Water Desalination in Electrochemical System

B. Kim, S. Choi, S. Ko, J. Han in collaboration with B. Al-Anzi, J. White, S. V. Pham
Sponsorship: Kuwait-MIT Center Signature Research Project / KFAS (Kuwait Foundation for the Advancement of Sciences)

Currently, reverse osmosis (RO) is considered the leading technology for desalination, and the operational efficiency of RO has been significantly improved over the last two decades with a thorough energy analysis. On the other hand, electrical desalination can be more advantageous in certain applications due to the diversity of allowed feed conditions, operational flexibility, and the relative low capital cost needed (the size of a system is generally small). Yet electrical desalination techniques such as electrodialysis (ED) have not been modeled in full detail, partially due to scientific challenges involving the multiphysics nature of the process. In addition, while current ED relies on bipolar ion conduction, removing one pair of a cation and an anion simultaneously, one final but most important point is that desalination achieved by means of an anion exchange membrane (AEM) and a cation exchange membrane (CEM) should be considered separately and independently (Figure 1a). Based on the intrinsically different ion transport near AEM and CEM, our group previously presented a novel process of ion concentration polarization (ICP) desalination (Figure 1b), which can basically enhance the amount of salt reduction, by examining unipolar ion conduction through both experiments and numerical modeling (Figure 1b). Since our experimental works are done in a model system for scalable electrochemical systems, the microfluidic device (Figure 1c) enables more scientific knowledge about ion transport phenomena through visualization. Meanwhile, the high-throughput module (stacked layer system, Figure 1d) enables us to realize a practical operation and evaluate the system's performance. Along with the ICP desalination, we also employed an ED system as a model to investigate the mass transport effects of embedded microstructures between the ion exchange membranes. In this work, therefore, we aim to perform a high-level analysis of ion transport near IEMs in order to enhance water desalination in electrochemical system.

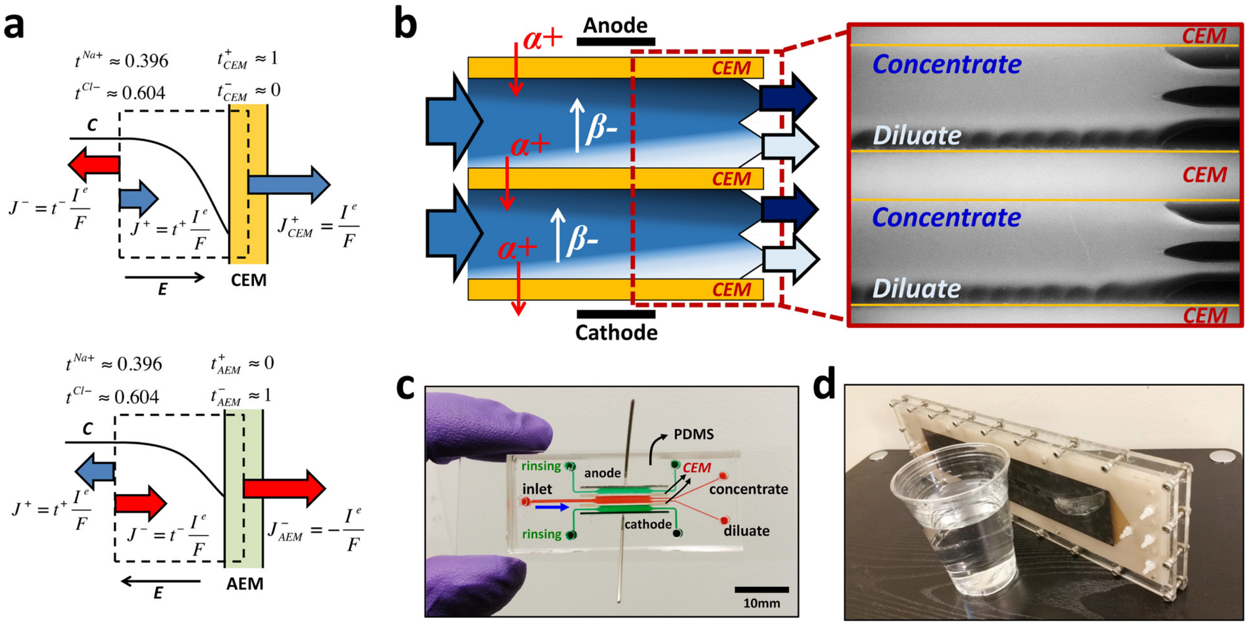

▲ Figure 1: Water desalination in electrochemical system; (a) Schematic diagram of counter-ion/co-ion transport near CEM/AEM, (b) schematics and fluorescent images of ICP desalination, photo of (c) microfluidic and (d) high-throughput devices.

FURTHER READING

- R. Kwak, G. Guan, W. K. Peng, and J. Han, "Microscale Electrodialysis: Concentration Profiling and Vortex Visualization," *Desalination*, vol. 308, pp. 138-146, 2013.
- R. Kwak, V. S. Pham, B. Kim, L. Chen, and J. Han, "High-Throughput Salt/Bio-Agent Removal by Ion Concentration Polarization for Water Desalination," in *International Conference on Miniaturized Systems for Chemistry and Life Sciences*, pp. 660-662, 2013.
- B. Kim, R. Kwak, H. J. Kwon, V. S. Pham, S. E. Kooi, G. Lim, and J. Han, "Purification of Ultra-High Salinity Produced Water by Multi-Stage Ion Concentration Polarization," *International Conference on Miniaturized Systems for Chemistry and Life Sciences*, pp. 160-162, 2014.

Fabrication of Core-Shell Microparticles Using 3-D Printed Microfluidics

D. Olvera-Trejo, L. F. Velásquez-García
Sponsorship: Tecnológico de Monterrey/MIT Nanotechnology Program

Coaxial electrospraying is an electrohydrodynamic process that creates core-shell microparticles by atomization of a coaxial electrified jet composed of two immiscible liquids. Coaxial electrospraying has several advantages over other microencapsulation technologies including higher encapsulation efficiency and more uniform size distribution. Coaxial electrosprayed compound microparticles can be used in exciting applications such as feedstock microencapsulation, controlled drug release, and self-healing composites.

Unlike traditional, i.e., uniaxial, electrospraying that has been investigated for over 100 years and of which many MEMS implementations exist, coaxial electrospraying was first described in 2002 and no microfabricated coaxial electrospray source had been reported due to the inherent three-dimensionality and complexity of its hydraulic system.

Stereolithography (SLA) is a layer-by-layer additive manufacturing process that creates solid objects via photopolymerization of a resin using ultraviolet light. Additive manufacturing started as a visualization tool for mesoscaled objects, but recent developments in the resolution and capabilities of 3-D printing suggest that these manufacturing processes could address the complexity, three-dimensionality, and material requirements of many microsystems. In particular, high-resolution SLA can be used to manufacture freeform microfluidics at a small fraction of the cost per device, infrastructure cost, and fabrication time of a typical silicon-based microfluidic system.

We developed SLA 3-D printed coaxial electrospray sources with one or two emitters that are fed by two helical channels (Figure 1). Each emitter spout is designed to produce a coaxial flow and to enhance the electric field on the liquid meniscus. Using these devices, we produced uniform core-shell microparticles using deionized water as the inner liquid and sesame oil as the outer liquid (Figure 2). The size of the droplets can be modulated by controlling the flow rates fed to the emitters. Electrical characterization of the devices demonstrates that the emitters operate uniformly. Current research efforts focus on demonstrating massively multiplexed sources with uniform array operation.

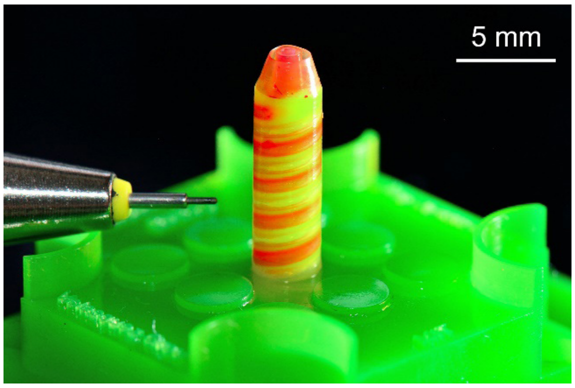

▲ Figure 1: 3-D printed coaxial electrospray device next to a 0.3-mm-diameter mechanical pencil; the different colors of the liquids supplied to the device evidence the helical channels that feed the emitter nozzle.

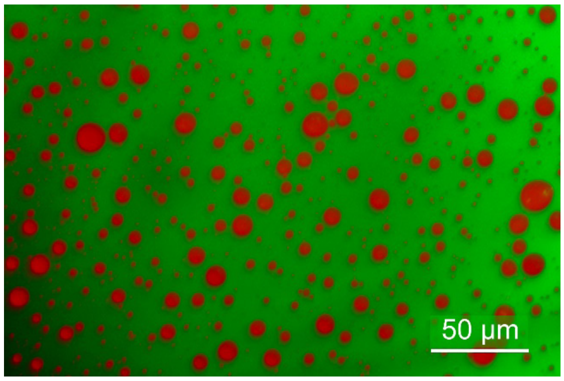

▲ Figure 2: Optical image from a fluorescent microscope of core-shell droplets (core is water dyed with Rhodamine B, shell is sesame oil) immersed in water dyed with fluorescein. The compound particles were produced by one of our 3-D printed coaxial electrospray sources. The oil shell covering each red-colored core of the droplets prevents their mixing with green-colored water.

FURTHER READING

- L. F. Velásquez-García, "SLA 3-D Printed Arrays of Miniaturized, Internally-fed, Polymer Electrospray Emitters," *Journal of Microelectromechanical Systems,* vol. 24, no. 6, pp. 2117-2127, December 2015.
- D. Olvera-Trejo and L. F. Velásquez-García, "3-D Printed Microfluidic Devices for Electrohydrodynamic Generation of Core-shell Microparticles," in *Technical Digest 17th Solid-State Sensor, Actuator and Microsystems Workshop*, pp. 176 – 179, 2016.

3-D Printed Massively Multiplexed Electrospray Sources

L. F. Velásquez-García
Sponsorship: U.S. Army

Electrospray is a electrohydrodynamic phenomenon that produces from a meniscus a stream of micro/nanoparticles that, depending on the properties of the liquid and the process conditions, can be droplets, ions, or fibers. The low spread in size and specific charge of the emitted particles makes the use of electrospray attractive in applications such as combustors, maskless micro/nanomanufacturing, and nanosatellite propulsion. However, the throughput of an electrospray emitter is very low, limiting the applicability of single-emitter electrospray sources to a few practical cases, e.g., mass spectrometry of biomolecules.

An approach to increase the throughput of an electrospray source without increasing the size variation of the emission is implementing arrays of electrospray emitters that operate in parallel. Miniaturization of the electrospray emitters results in less power consumption and lower onset voltage; in addition, using micro-fabrication, monolithic arrays of miniaturized emitters with large array size and emitter density can be made. Researchers have demonstrated a variety of MEMS multiplexed electrospray sources that operate uniformly. Although these devices work satisfactorily, they present a number of issues: (i) the device architecture is often a compromise between what should be made based on the modeling and what can be made given the limitations of traditional microfabrication, sacrificing device performance; (ii) a change in any of the in-plane features of the design requires the redesign and fabrication of one or more lithography masks while causing added costs and time delays; (iii) these devices are fairly expensive because they are made in a multi-million semiconductor-grade cleanroom with advanced tools that are operated by highly trained staff, which restricts their application to high-end applications and research.

We recently demonstrated the first 3-D printed multiplexed electrospray sources in the literature (Figure 1). The devices were fabricated with stereolithography and have associated two orders of magnitude less fabrication cost per device, fabrication time, and manufacturing infrastructure cost compared to a silicon MEMS multiplexed electrospray source. The 3-D printed devices include features not easily attainable with other microfabrication methods, e.g., tapered channels and threaded holes. Through the optimization of the fabrication process, arrays with as many as 236 internally fed electrospray emitters (236 emitters in 1 cm²) were made, i.e., a twofold increase in emitter density and a sixfold increase in array size compared with the best reported values from multiplexed, internally fed, electrospray sources made of polymer. The characterization of devices with a different array size suggests a uniform emitter operation (Figure 2).

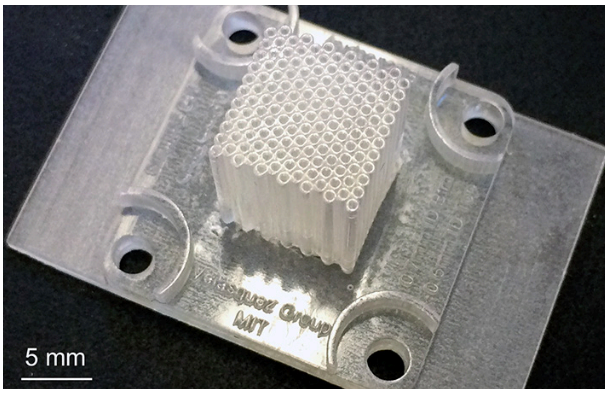

▲ Figure 1: A 3-D printed planar array of 143 tapered, internally fed electrospray emitters in 1 cm² (143 emitters/cm², hexagonal packing) The emitters are fed by 12 mm long tapered internal channels with 400 μm diameter at the emitter spouts.

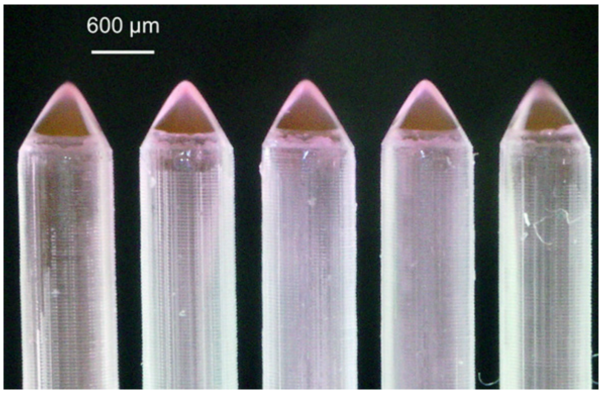

▲ Figure 2: External row of 5 emitters part of a 49-emitter planar array (70 emitters/cm², square packing). The scalloping on the exterior of the emitters, due to the layer-by-layer manufacturing, is visible.

FURTHER READING

- B. Gassend, L. F. Velásquez-García, A. I. Akinwande, M. Martínez-Sánchez, "A Microfabricated Planar Electrospray Array Ionic Liquid Ion Source with Integrated Extractor," *J. Microelectromech. Syst.*, vol. 18, no. 3, pp. 679-694, June 2009.
- F. A. Hill, E. V. Heubel, P. J. Ponce de Leon, L. F. Velásquez-García, "High-Throughput Ionic Liquid Ion Sources Using Arrays of Microfabricated Electrospray Emitters with Integrated Extractor Grid and Carbon Nanotube Flow Control Structures," *J. Microelectromech. Syst.*, vol. 23, no. 5, pp. 1237-1248, October 2014.
- L. F. Velásquez-García, "SLA 3-D Printed Arrays of Miniaturized, Internally-fed, Polymer Electrospray Emitters," *J. Microelectromech. Syst.*, vol. 24, no. 6, pp. 2117 – 2127, December 2015.

Optimization of Capillary Flow through Open Microstructured Arrays

P. Ponce de Leon, L. F. Velásquez-García
Sponsorship: DARPA

Liquid propagation through porous microstructures has received significant attention due to the importance of precisely controlling flow in microfluidic systems. Periodic surface structures, e.g., arrays of open micropillars or open microchannels, sometimes can be used to control the flow in a microsystem, introducing benefits such as direct access to the porous structure, device reusability, and resilience against clogging. In an open fluidic structure, the liquid is not actively pumped, e.g., using an upstream pressure signal; instead, the microstructured surface passively drives the liquid via capillary action. However, the same surfaces driving the flow via surface tension's pull simultaneously impede it by way of viscous resistance. Therefore, optimization of the geometry of the microstructured surface is required to maximize the flow rate it transports.

We developed semi-analytical models that describe the dynamics of capillary flow against gravity in (i) vertical arrays of open microchannels with rectangular cross-section and (ii) arrays of open micropillars with square packing and square cross section. We also extended our analysis to capture the shear-thinning behavior typical of many non-Newtonian fluids. Our models indicate the existence of multiple flow rate maxima with respect to pore size. One maximum, which occurs only in micropillar arrays, arises from the trade-off between capillary pressure and viscous resistance. The two other maxima, which occur for both micropillar and microchannel arrays, are related to meniscus and gravitational effects and only appear at low aspect-ratio (i.e., in channels/gaps between adjacent pillars that are about as wide as they are deep) and high Bond number, respectively. Experimental capillary rise data demonstrate that incorporating first-order gravitational effects and the impact of meniscus curvature improved flow rate predictions relative to models that neglect these factors (Figures 1 and 2; in both figures the working liquid is 1% PEO in 40/60 ethanol/water). Experimental capillary rise data also confirm the existence and location of a flow maximum with respect to the width of an open-microchannel; operating at any of the maxima decreases the sensitivity of flow rate to geometric variation, allowing for more robust microfluidic systems. Finally, we demonstrated electrospray emission from the edge of a microstructured surface as an example of an application of the porosity geometries we investigated in this study; the supply-limited regime of the current-voltage characteristics of these devices are in agreement with the literature on electrospray droplet emission, opening the possibility to implement arrays of externally-fed electrohydrodynamic jetting emitters that can operate continuously while producing droplets or nanofibers using suitable working liquids.

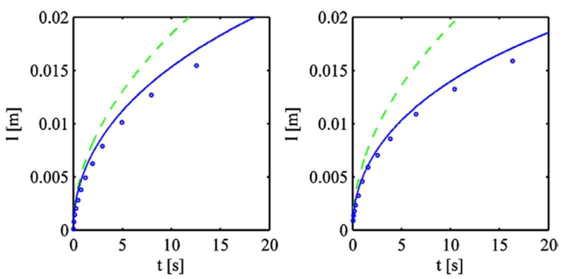

▲Figure 1: Height of rising liquid front vs. time for various open-microchannel geometries. In each subplot the blue circles are measured data points. The solid blue line shows the predictions of our model, and the dashed green line shows predictions neglecting gravitational and meniscus-permeability effects. Left – microchannels 139 µm deep, 149 µm wide, 101-µm thick walls; right – microchannels 141 µm deep, 211 µm wide, 289-µm thick walls.

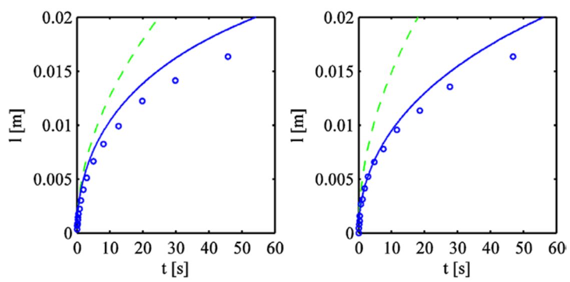

▲Figure 2: Height of rising liquid front vs. time for various open-micropillar array geometries. In each subplot the blue circles are measured data points, the solid blue line shows the predictions from our data, and the dashed green line shows predictions of the model proposed by Xiao *et al*, ***Langmuir,*** 2010. Left – micropillars 140 µm tall, 93 µm wide, 157 µm gap; right – microchannels 143 µm tall, 289 µm wide, 211 µm gap.

FURTHER READING

- F. A. Hill, E. V. Heubel, P. J. Ponce de Leon, and L. F. Velásquez-García, "High-throughput Ionic Liquid Ion Sources Using Arrays of Microfabricated Electrospray Emitters with Integrated Extractor Grid and Carbon Nanotube Flow Control Structures," *Journal of Microelectromech. Syst.,* vol. 23, no. 5, pp. 1237-1248, October 2014.
- P. J. Ponce de Leon, F. A. Hill, E. V. Heubel, and L. F. Velásquez-García, "Parallel Nanomanufacturing via Electrohydrodynamic Jetting From Microfabricated Externally-fed Emitter Arrays," *Nanotechnology,* vol. 26, no. 22, pp. 225301-1 – 225301-10, June 2015.
- P. J. Ponce de Leon, and L. F. Velásquez-García, "Optimization of Capillary Flow Through Open-microchannel and Open-micropillar Arrays," *Journal of Physics D – Applied Physics,* vol. 49, no. 5, pp. 055501-1 – 055501-13, February 2016.

Chip-Scale Electrostatic Vacuum Ion Pump with Nanostructured Field Emission Electron Source

A. Basu, L. F. Velásquez-García
Sponsorship: DARPA

Cold-atom interferometry of alkali atoms can be used in a variety of high-precision sensors and timing devices such as atomic clocks, gyroscopes, accelerometers, magnetometers, and gravimeters. These devices require ultra-high vacuum (UHV, pressure < 10^{-9} Torr) to operate; therefore, chip-scale versions require miniaturized UHV pumps resilient to alkali metal vapors that consume power at levels compatible with device portability. In a macro-sized chamber, UHV-level vacuum can be maintained using a conventional magnetic ion pump, where electrons that swirl around the magnetic lines of a magnet create ions by impact ionization of neutral molecules, which in turn sputter a Ti getter. While scaled-down versions of magnetic ion pumps have been reported, these are incompatible with miniaturized cold-atom interferometry systems because (i) a reduction in the pump size increases the required threshold magnetic field for electron trapping, and (ii) the larger magnetic field associated with a miniaturized ion pump can interfere with the operation of the cold-atom sensor, yielding flawed readings. Non-evaporable getter (NEG) pumps are used in some cold-atom interferometry systems, e.g., commercial chip-scale atomic clocks; however, NEG pumps are unable to pump noble gases such as He and N2 that are present in the chamber, and they inefficiently pump alkali vapors.

We are developing vacuum ion pumps compatible with chip-scale cold-atom interferometry devices. The proposed field emitter array (FEA)-based magnet-free ion pump architecture is shown in Figure 1. In this pump design, a helical electron collector pulls the electrons toward itself, forcing them to first travel beyond the height of the electron collector, to then get pushed back due to the electrostatic mirror effect of the annular-shaped ion collector. Therefore, the trajectory of the electrons is significantly increased compared to a pump design with a parallel-capacitor electrode configuration, augmenting the probability of impact ionization. The FEA consists of arrays nano-sharp silicon tips, each surrounded by a self-aligned gate electrode; we have shown that these FEAs do not degrade in the presence of Rb vapor.

Figure 2 shows the semi-log plot of the minus time derivative of the pressure versus time during pump-down, with the horizontal axis denoting the time since the beginning of each pump-down cycle; in these experiments, the pressure inside the chamber reached values as low as ~7×10^{-7} Torr. Each data point in the plot represents an average of the minus time derivative of the pressure considering all pump-down cycles. The R^2 of the linear fit of the data evidences that our reduced-order model accurately explains the dynamics of the pump. The slope of the linear fit of the data estimates the experimental pumping time constant at about 161 seconds.

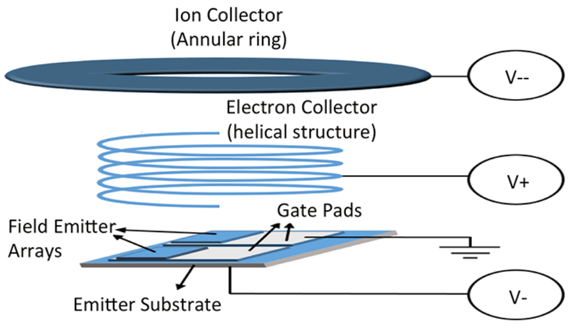

▲Figure 1: Schematic of the FEA-based, magnetic-less ion pump architecture.

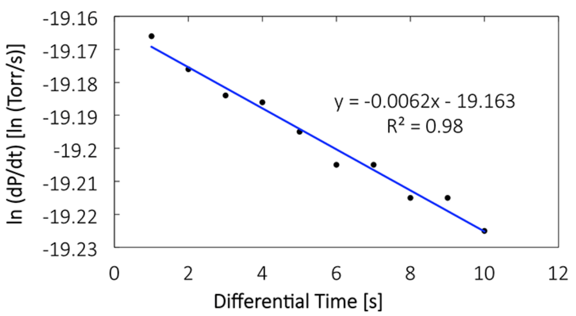

▲Figure 2: Semi-log plot of the negative of the time derivative of the chamber pressure vs. time. From the slope of the linear fit, τ = 161.2 s.

FURTHER READING

- A. Basu, M. A. Perez, and L. F. Velásquez-García, "Nanostructured Silicon Field Emitter Array-based High-vacuum Magnetic-less Ion Pump for Miniaturized Atomic Spectroscopy Sensors," *Technical Digest of the 18th International Conference on Solid-State Sensors, Actuators, and Microsystems (Transducers 2015)*, Anchorage AK, pp. 1021-1024, June 2015.
- A. Basu, M. A. Perez, and L. F. Velásquez-García, "Miniaturized, Electrostatic, High-vacuum Ion Pump Using a Nanostructured Field Emission Electron Source," *15th International Conference on Micro and Nanotechnology for Power Generation and Energy Conversion Applications (PowerMEMS 2015)*, Boston, MA, December 2015; *Journal of Physics Conference Series*, vol. 660 pp. 012027-1 – 012027-5, 2015.
- A. Basu and L. F. Velásquez-García, "Electrostatic Ion Pump with Nanostructured Si Field Emission Electron Source and Ti Particle Collectors for Supporting Ultra-high Vacuum in Miniaturized Atom Interferometry Systems," *Journal of Micromechanics and Microengineering*, 2016.

Nanotechnology and Nanomaterials

Variation Modeling in IC Technology

H. Chen, D. S. Boning
Sponsorship: Exxon Mobil First-Year Energy Fellowship

Integrated circuit (IC) fabrication at the nanoscale is never deterministic. As the scale of microelectronic devices decreases dramatically, even small variations in the IC manufacturing process lead to significant uncertainty in the behavior of electronic devices as well as in the IC as a whole. In order to predict the variations in fabrication, various silicon IC optimization and analysis approaches have been proposed, and they are playing important roles in the IC industry. To accurately model the IC, these methods rely on testing data from the devices and circuits. However, IC testing is not free. Hundreds of test structures, such as ring oscillators, must be carefully designed, fabricated, and measured; the cost is considerable.

We are developing new techniques to model and predict variations, especially spatial variations, in IC manufacturing based on a small number of measurements. Wafer-level and die-level spatial variation data can be considered as a two-dimensional function *f(x, y)* in which *x* and *y* are spatial coordinates of the measurement points. A Bayesian approach with frequency domain analysis is proposed to give a maximum a posteriori (MAP) estimation of the coefficients of the two-dimensional discrete cosine transform under noise. An algorithm is designed to reduce the number of frequency components to speed up the computation in large-scale problems. We also propose another fast variation estimation method based on low-rank matrix completion that transforms the estimation into an optimization problem with respect to the matrix of the variation data. We use a nuclear norm relaxation and singular value thresholding algorithm to solve this optimization problem. Penalty terms are carefully designed to take into account the different types of devices on the same die. An example is shown in Figures 1 and 2, where contact resistance data across a test chip is recovered using less than half of the measurement points. Further research will apply these methods to industrial data. Time series manufacturing data will also be studied to give an insight into the trend of variation over a large timespan.

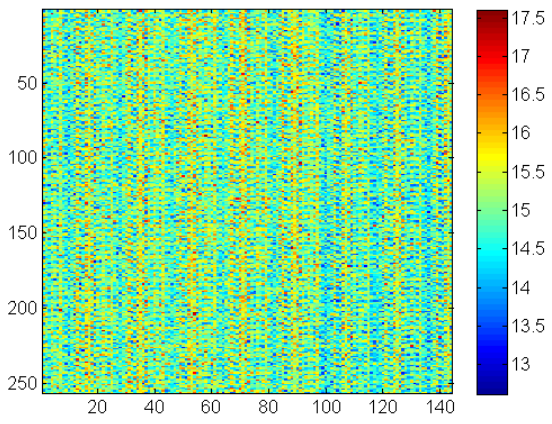

▲Figure 1: Contact resistance data (Ohms) with 256×144 measurement points.

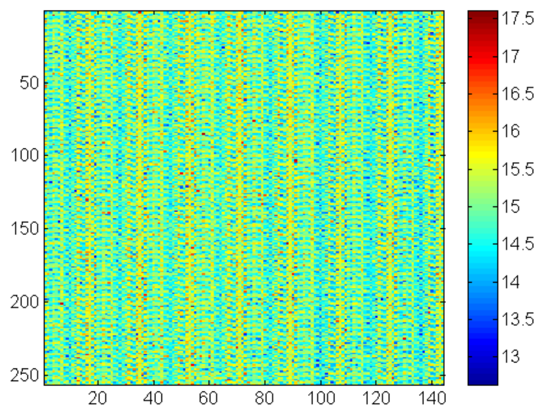

▲Figure 2: Recovered matrix with 40% measurement points randomly sampled.

FURTHER READING

- K. Balakrishnan and D. S. Boning, "Measurement and Analysis of Contact Plug Resistance Variability," *Custom Integrated Circuits Conference 2009. CICC '09*, pp. 415-422, 2009.

Characterization and Modeling of Pattern Dependencies in Spin-Coating for Advanced Packaging Technology

C. Lang, D. S. Boning
Sponsorship: Taiwan Semiconductor Manufacturing Company

Re-distribution layers (RDLs) are packaging layers dedicated to connecting separate integrated circuit (IC) chips or die to each other and to external I/O ports in advanced packaging technologies. These layers can be made smaller than the bulky metal traces in conventional substrate packaging, reducing electrical delay and power consumption. Electrochemical plating and dielectric spin-coating (DSC) can be used in wafer-scale processes to fabricate these chip-to-chip interconnects for advanced 2.5D packaging. However, non-uniformities in the underlying topography lead to surface variations in the resulting dielectric. As multiple layers are fabricated, these variations compound and can result in a structure with significant electrical parasitics.

In this study, we model and predict the non-uniformities in the DSC process caused by the underlying topographies. If these non-uniformities can be predicted, design rules can be defined that limit the resulting surface variation and enable multi-level RDL fabrication. We design test vehicles (TVs) that represent topographies common in RDLs, most notably the step heights and layout patterns of the RDL copper interconnects. Using these TVs, we experimentally determine the surface variation in the dielectric after spin coating, as a function of line heights, widths, and spacings, in addition to process variables. We model the resulting dielectric surface as a two-dimensional convolution between the underlying topography and an appropriately chosen impulse response (see Figure 1). The form of the impulse response is experimentally determined, and we predict the model coefficients based on the line height, coating thickness, and other process variables.

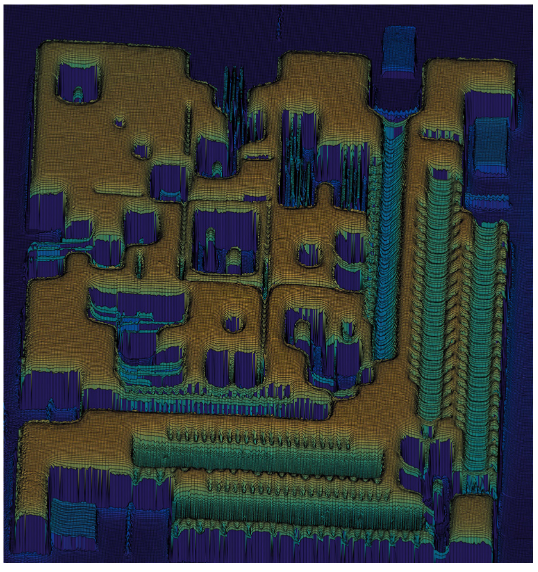

▲Figure 1a: Experimental surface after spin coating.

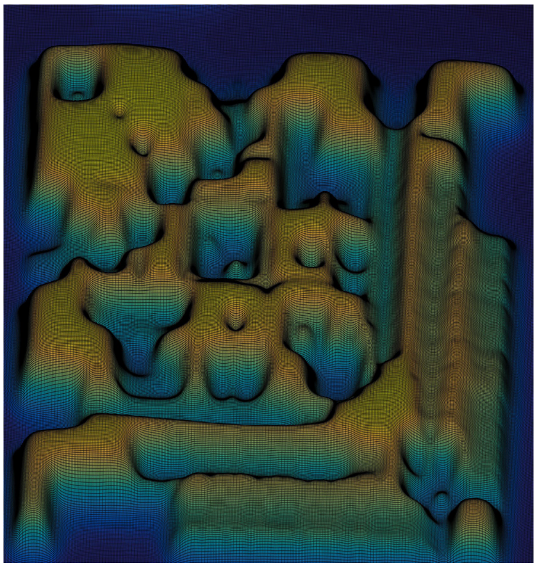

▲Figure 1b: Predicted surface using 2D convolution model.

FURTHER READING

- L. E. Stillwagon and R. G. Larson, "Leveling of Thin Films Over Uneven Substrates During Spin Coating," *Physics of Fluids*, pp. 1937-1944, November 1990.

Tensor Recovery for Stochastic Simulation of Nanoscale Devices and Circuits with Many Process Variations

Z. Zhang, T.-W. Weng, L. Daniel
Sponsorship: NSF NEEDS, AIM Photonics

Process variations have become a “red-brick” problem that prevents the semiconductor industry progressing forward. A random fluctuation at the atomic scale can cause a large impact on the performance of nanoscale and device simulations. In order to increase chip yields, the uncertainties caused by process variations must be well estimated and controlled before a final fabrication. In traditional EDA tools, such a task is done by Monte Carlo-type simulators. Recently, stochastic spectral methods have emerged as a promising alternative. They are much more efficient than Monte Carlo simulators for certain design cases, but their efficiency can degrade as the number of process variations increases.

Our approach can efficiently handle design problems with 50 to 60 uncorrelated random parameters. We represent the huge number of device/circuit simulation samples in stochastic collocation by a tensor, which is a representation of a high-dimensional data array. Then, similar to the matrix case, we can exploit the low-rank structure of a tensor to reduce the storage and computational cost, as shown in Figure 1. Combining this low-rank property with the sparse property in high-dimensional generalized polynomial-chaos expansion, we have suggested a low-rank and sparse tensor recovery model. This optimization model allows us to estimate the huge number of unknown simulation samples based on a small number of available simulation results. Therefore, the computational cost can be reduced from an exponential one to a linear one.

This approach has been successfully applied to solve stochastic modeling and simulation problems in MEMS design and in CMOS IC design. For the CMOS ring oscillator with 57 uncorrelated process variations in Figure 2, stochastic collocation using a standard deterministic numerical integration requires 1.6E27 simulation samples, whereas our tensor recovery approach only needs 300 simulation samples to construct a highly accurate (with 1% relative error) stochastic model for the oscillator frequency.

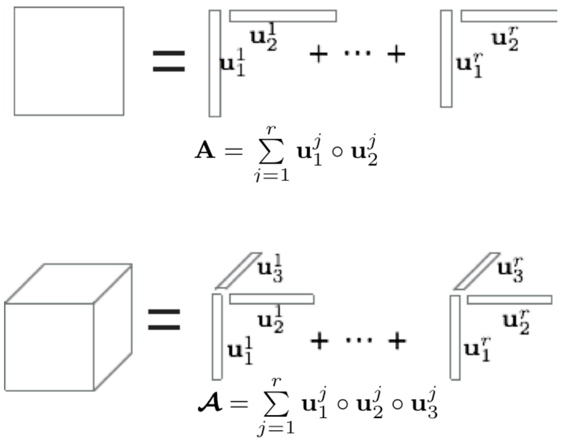

▲Figure 1: Low-rank decomposition of a matrix (top); and low-rank decomposition of a tensor (bottom). The low-rank decomposition allows representation of high-dimensional data arrays using a few vectors.

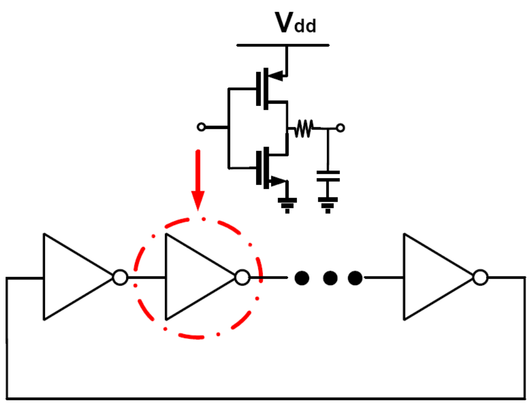

▲Figure 2: A CMOS ring oscillator. This circuit has 57 independent random parameters describing the variations of transistor threshold voltage, gate oxide thickness, channel length, and width.

FURTHER READING

- Z. Zhang, I. M. Elfadel, and L. Daniel, “Uncertainty Quantification for Integrated Circuits: Stochastic Spectral Methods,” *Proc. Int. Conf. Computer-Aided Design*, pp. 803-810, 2013.
- Z. Zhang, T.-W. Weng, and L. Daniel, “A Big-Data Approach to Handle Process Variations: Uncertainty Quantification by Tensor Recovery,” *Proc. IEEE Workshop on Signal and Power Integrity*, pp. 1-4, 2016.
- Z. Zhang, L. Daniel, K. Batselier, H. Liu, and N. Wong, “Tensor Computation: A New Framework for EDA,” *IEEE Trans. CAD of Integrated Circuits and Systems*, submitted, 2016.

Chemical Sensors Based on GaAs Nanowires and oCVD Polymers

X. Wang, S. Ermez, H. Goktas, S. Gradečak, K. K. Gleason
Sponsorship: Shell

Room temperature gas sensing has always been an intriguing topic in the areas of oil industry, air condition monitoring, and healthcare. The motivation for a room temperature gas detector is that the traditional metal oxide sensor, although with a very high resistive response, requires high operational and manufacturing temperature. Our group has developed several types of room temperature gas sensors based on oxidative chemical vapor deposition (oCVD) polymers and nanostructures such as gold nanoparticles and aligned carbon nanotubes (A-CNT). Here we introduce a new chemical sensor based on GaAs nanowires and oCVD polymers. With a higher resistive signal than the CNT sensor and a lower noise than the polymer-Au nanoparticle sensor, this compact gas detector shows prospects for numerous applications.

The structure of the GaAs-oCVD sensor is comprised of a GaAs nanowire array and an oCVD coating layer. GaAs nanowire arrays with different density are grown via self-seeded nanowire growth mechanism using metal-organic chemical vapor deposition (MOCVD). A layer of oCVD polymer, usually a type of polythiophene, is further conformally coated on the GaAs nanowire arrays. Two metal electrodes are used to measure the resistive change after exposure to analytes. Our sensors show remarkable sensitivity to a variety of organic vapors with good selectivity. One potential application of this device could be a sensing element in a wireless sensor network with appropriate reading circuits.

FURTHER READING

- X. Wang, S. Hou, H. Goktas, P. Kovacik, F. Yaul, A. Paidimarri, N. Ickes, A. P. Chandrakasan, and K. K. Gleason. "Small-Area, Resistive Volatile Organic Compound (VOC) Sensors Using Metal–Polymer Hybrid Film Based on Oxidative Chemical Vapor Deposition (oCVD)," *ACS applied materials & interfaces* 7, no. 30, pp. 16213-16222, 2015.
- X. Wang, A. Ugur, H. Goktas, N. Chen, M. Wang, N. Lachman, E. Kalfon-Cohen, W. Fang, B. L. Wardle, and K. K. Gleason, "Room Temperature Resistive Volatile Organic Compound Sensing Materials Based on a Hybrid Structure of Vertically Aligned Carbon Nanotubes and Conformal oCVD/iCVD Polymer Coatings," *ACS Sensors* 1, no. 4, pp. 374-383, 2016.
- S. Ermez *et al*, "Self-seeded III-V Nanowire Growth by Metal-organic Chemical Vapor Deposition," *Crystal Growth and Design*, vol. 15, no. 6, pp. 2768–2774, 2015.

Cost-Effective and Scalable Sub-10 nm Patterning via Initiated Chemical Vapor Deposition

D. H. Kim, H. S. Suh, P. Moni, S. Xiong, L. E. Ocola, P. Nealey, K. K. Gleason
Sponsorship: NSF

Making smaller patterns in a cost-effective way has always challenged the semiconductor industries. The current 14-nm patterning process, commercially enabled by multiple photolithography, is reaching the limit in pattern resolution and manufacturing cost. Last year, the use of 7-nm patterns in a working chip by extreme ultraviolet (EUV) lithography with a wavelength of 13.5 nm was announced, but it remains in lab-scale because of its high-cost process and low productivity coming from the EUV light source. Directed self-assembly (DSA) has garnered great interest as a promising technology with no need to use such an expensive light source. The DSA enables control of the orientation and alignment of nanoscale domains of block copolymers (BCPs) thermodynamically for producing periodic nanostructures. However, the number of BCPs and the process window of DSA to permit sub-10-nm patterns are very limited by conventional spin coating.

Instead, we introduced initiated chemical vapor deposition (iCVD), a solvent-free process, to the DSA process for forming an effective topcoat on BCP (Figure 1). In iCVD, monomer and initiator vapors flow into a vacuum chamber. The resistively heated hot filaments in the chamber break the initiator into free radicals. Subsequently, polymeric film growth begins on cooled substrates through free-radical polymerization of monomer. Because iCVD is a solvent-free and low- temperature process, it is able to deposit polymeric films on fragile substrates such as polymers, papers, and textiles without affecting the substrates. These features of iCVD allow the scalable deposition of an ultrathin topcoat on a highly segregating (high χ) BCP for sub-10-nm patterning. During the thermal annealing of DSA, the iCVD topcoat inhibits the collapse of the perpendicular orientation of BCP domains completely and then generates sub-10-nm line and space patterns underneath the iCVD topcoat. As a result, the iCVD topcoat creates sub-10-nm patterns from chemical guide strips of DSA with relatively low resolution patterns (pitch: ~40 nm), as seen in Figure 2. Spectroscopic studies reveal that iCVD forms the unique interface between BCPs and the topcoat, which is a mixed interface made by grafting and intermolecular entanglements. This unusual interface is not observed in a spun-cast topcoat.

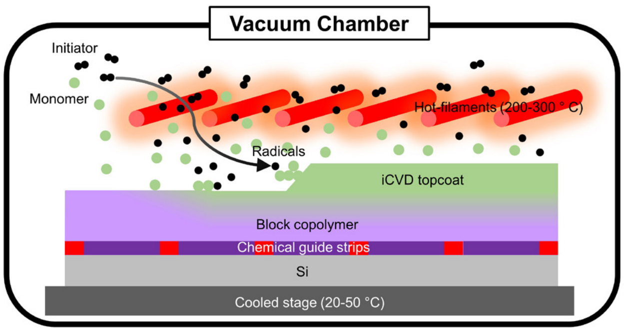

▲Figure 1: The iCVD process to deposit a polymeric topcoat on block copolymers for creating sub-10-nm patterns in conjunction with DSA.

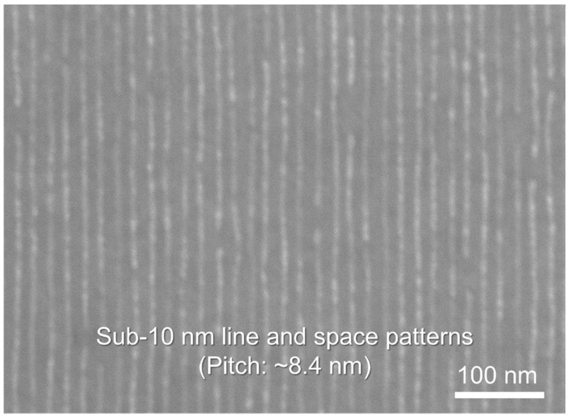

▲Figure 2: Scanning electron microscopic images taken from sub-10-nm line and space patterns with a pitch, ~8.4 nm underneath iCVD topcoat. The scale bars are 100 nm.

FURTHER READING

- O. Kim, H. H. Solak, M. P. Stoykovich, N. J. Ferrier, J. J. de Pablo, and P. F. Nealey, "Epitaxial Self-assembly of Block Copolymers on Lithographically Defined Nanopatterned Substrates," *Nature*, vol. 424, pp. 411–414, 2003.
- J. L. Yagüe, A. M. Coclite, C. Petruczok, and K. K. Gleason, "Chemical Vapor Deposition for Solvent-Free Polymerization at Surfaces," *Macromol. Chem. Phys.* vol. 214, pp. 302–312, 2013.

Free-standing Nano-Gratings as Phase-Shifting Devices for Electron Optics

Y. Yang, R. G. Hobbs, C.-S. Kim, K. K. Berggren
Sponsorship: Gordon and Betty Moore Foundation

Nanofabricated phase-shifting devices for electron optics are of interest for a variety of applications, such as beam splitters for electron interferometry and holography, holograms for electron vortex beam generation, and phase plates for contrast enhancement in electron microscopy. Nano-fabricated gratings provide more flexible control of diffraction angle and orbital angular momentum of diffracted electron beams compared to crystalline electron diffraction "gratings" and can be used at a variety of electron energies. For the applications given above, it is crucial to understand shifts in the phase of the electron beam imposed by these phase-shifting devices. Here we report a nanofabricated two-dimensional transmission grating for electron beams and its characterization with electron diffraction in a transmission electron microscope (TEM) at various electron energies.

The electron transmission gratings were fabricated from silicon nitride membrane (5-10 nm) TEM grids (*SiMPore Inc.*).High-resolution electron beam lithography (EBL) was used to define the grating pattern. After resist development, pattern transfer to the silicon nitride membrane was achieved with reactive-ion etching (RIE). Finally, the silicon nitride gratings were coated with approximately 10 nm of metal (gold or aluminum) to prevent charging in the experiment. Nano-gratings were characterized in a FEI Tecnai TEM in selected-area diffraction mode (Figure 1(a)). The electron energy was varied from 120 keV to 40 keV so that the membrane imposed different phase shifts to the electron beam, hence modulating the intensities of diffracted beams. The electron beam phase shifts were estimated by fitting experimentally measured intensities of diffracted beams to theoretical calculations. It was found that the membrane imposed the same phase shift as that of a 40-nm-thick membrane made of a material with a 20-V mean inner potential. The phase shift was found to be 2.2-3.5π for electrons with 120-40 keV energy.

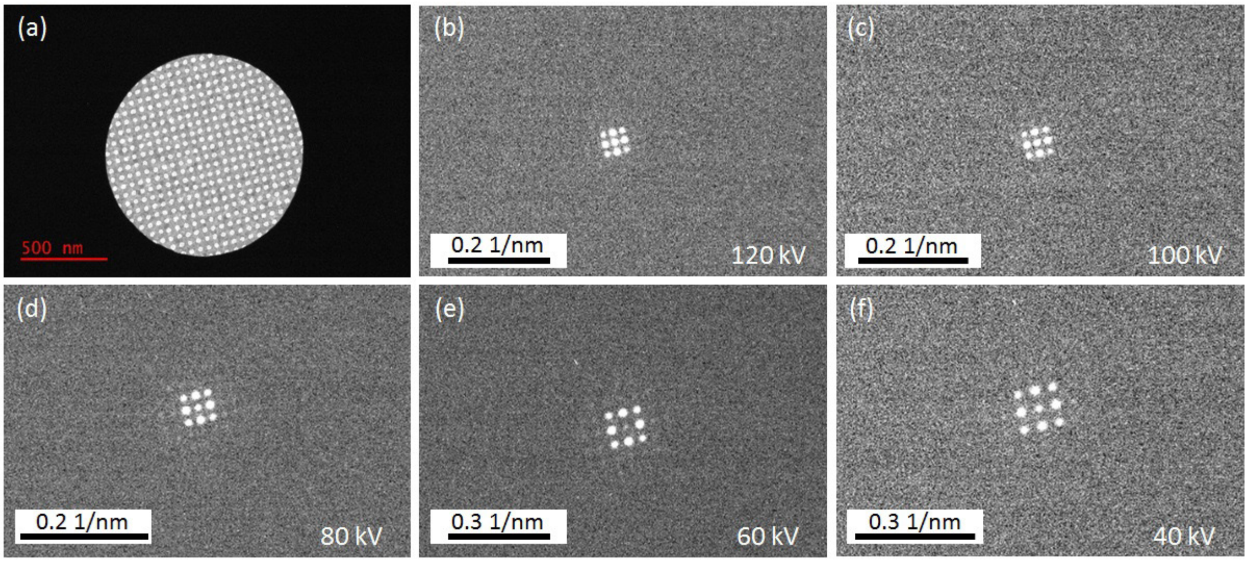

▲ Figure 1: Selected area TEM image and electron diffraction patterns of a nanofabricated transmission grating. (a) A two-dimensional mesh grating patterned from a 10-nm-thick silicon nitride membrane by EBL and RIE, followed by 10-nm gold coating to prevent charging during imaging and diffraction. The grating pitch is 50 nm. A selected area aperture is inserted to select a circular area with ~ 1-μm diameter. (b-f) Selected-area electron diffraction patterns from the mesh grating shown in (a), with electron energies from 120 keV to 40 keV. The TEM acceleration voltages are labeled. The diffract patterns are taken with a large camera length (4.8 m) to zoom into the center beam, while relatively high-angle electron diffraction from polycrystalline gold is not shown.

FURTHER READING

- J. Verbeeck, H. Tian, and P. Schattschneider, "Production and Application of Electron Vortex Beams," *Nature*, vol. 467, pp. 301-304, 2010.
- G. Gronniger, B. Barwick, H. Batelaan, T. Savas, D. Pritchard, and A. Cronin, "Electron Diffraction from Free-Standing, Metal-Coated Transmission Gratings," *Applied Physics Letters*, vol. 87, pp. 124104, 2005.
- P. Kruit, R. G. Hobbs, C-S. Kim, Y. Yang, V. R. Manfrinato, J. Hammer, S. Thomas, P. Weber, B. Klopfer, C. Kohstall, T. Juffmann, M. A. Kasevich, P. Hommelhoff, and K. K. Berggren, "Designs for a Quantum Electron Microscope," *Ultramicroscopy*, vol. 164, pp. 31-45, 2016.

Scanning Electron Microscopy with a Reflected Electron Beam

N. Abedzadeh, R. G. Hobbs, C.-S. Kim, K. K. Berggren
Sponsorship: Gordon and Betty Moore Foundation

Although electron microscopy has enabled imaging of biological specimens with near-atomic scale resolution, the damage that the electron beam imparts to these samples has been an unavoidable disadvantage that still limits the scope and throughput of the technique. Interaction-free measurement using a quantum electron microscope (QEM) is a scheme proposed to reduce or eliminate damage to biological samples. One possible path to realization of a QEM is to construct an electron resonator like that shown in Figure 1, including a diffractive electron optic such as a grating mirror in which Mach Zehnder-type splitting and re-coupling occur between the zero-order and first-order diffracted beams.

This project was broken into two sub-tasks: 1) design and construction of an electron mirror enabling simultaneous imaging of both the upper and underside of a sample with an electron beam, and 2) design and fabrication of a reflective diffraction grating for electrons, whereby a potential equivalent to the electron energy is applied to the grating. The diffraction grating functions both as the mirror and as the element that splits and re-couples the diffracted beams (see Figure 1). Finally, we will characterize diffraction from the grating by obtaining multiple images of the underside of a sample using zero-order and first-order diffracted beams.

Figure 2 shows the first demonstration of simultaneous imaging of the top and bottom surfaces of a sample in a SEM with a flat, unpatterned mirror surface. Figure 2 (a) shows that after the voltage applied to the mirror and lens system is tuned, the incident electron beam scans the top surface while the reflected beam scans the underside of the sample, resulting in the image shown in Figure 2 (b). The resolution of the reflected image is currently limited by the long working distance used in the SEM and astigmatism induced by the lens and mirror setup. The next step in this project is to reduce the working distance by rearranging the system configuration and to repeat the experiment with a grating mirror.

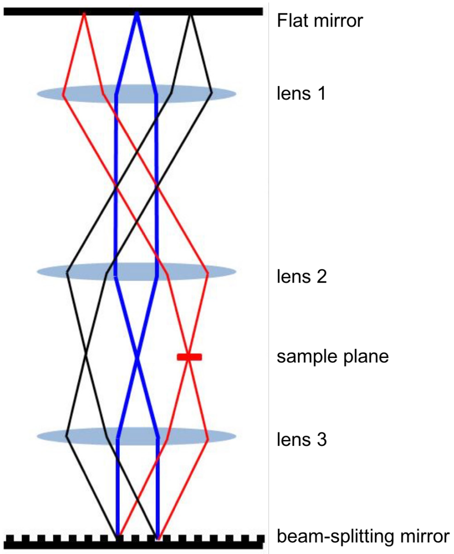

▲ Figure 1: Schematic representation of the electron cavity considered for the QEM: diffractive mirror approach with grating mirror.

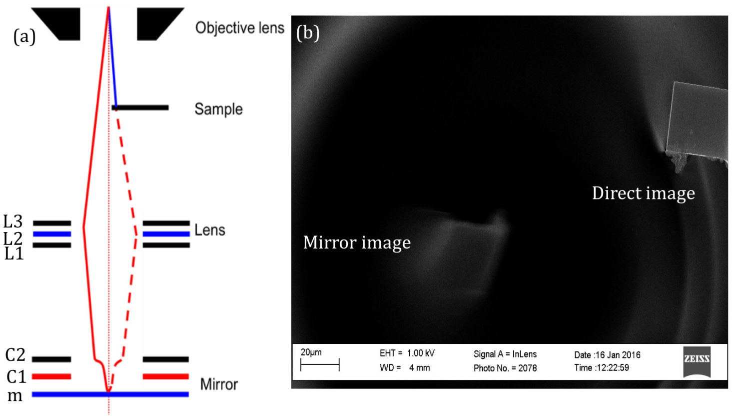

▲ Figure 2: (a) Schematic of setup used to image top and bottom surfaces of a sample simultaneously. Voltages applied to electrodes from bottom to top: V_m=-1050 V, V_{c1}=+6095 V, V_{c2}=0 V, V_{L1}=0 V, V_{L2}=-800 V, and V_{L3}=0 V. Energy of incident electron: 1 keV. (b) SEM image of top and bottom surfaces of a sample simultaneously using the in-lens secondary electron detector. The scale bar is 20 µm.

FURTHER READING

- W. P. Putnam and M. Fatih Yanik, "Noninvasive Electron Microscopy with Interaction-free Quantum Measurements," *Physical Review A*, vol. 80, pp. 040902, October 2009.
- P. Kruit, R. G. Hobbs, C-S. Kim, Y. Yang, V. R. Manfrinato, J. Hammer, S. Thomas, P. Weber, B. Klopfer, C. Kohstall, T. Juffmann, M. A. Kasevich, P. Hommelhoff, and K. K. Berggren, "Designs for a Quantum Electron Microscope," *Ultramicroscopy*, vol. 164, pp. 31-45, March 2016.

A Microfabricated Mach-Zehnder Interferometer for Electrons

A. Agarwal, C-S. Kim, R. G. Hobbs, D. Van Dyck, K. K. Berggren
Sponsorship: Gordon and Betty Moore Foundation

Electron interferometers, necessary for electron holographic microscopy, are usually constructed with a biprism as the beamsplitter. Interferometers that use diffraction from crystalline or nanofabricated gratings to split and recombine the beam offer the possibility of interferometry in a standard scanning electron/transmission electron microscope (SEM/TEM) but require precise and difficult alignment of the position and orientation of the gratings. To address this challenge, we designed an interferometer for a TEM based on a monolithic three-crystal grating fabricated by focused ion-beam milling of a single crystal of silicon, as shown in Figure 1(a).

We used parallel- and convergent-beam electron diffraction (PBED and CBED) to characterize the gratings. In PBED, diffraction spots arising from the first and second crystals overlap in the back focal plane, thus proving that the gratings are well aligned (Figure 1(b)). CBED yields a diffraction pattern with an array of satellite spots, as shown in Figure 1(c). Unlike conventional CBED, which looks at disks at or close to the back focal plane, we focused the diffraction pattern by controlling the intermediate lens (IL) and moving to the second crossover plane, where the diffracted beams from the first and second crystals are focused at horizontally displaced spots. We can build up the experimental pattern from Figure 1(c) by taking all diffraction orders into account.

We also fabricated a three-crystal grating with 23-µm separation between the crystals (Figure 2) to ensure that the first-order diffracted beam from the first crystal separates from the zero-order beam in the plane of the second crystal; this gives two independent arms of the Mach-Zehnder interferometer (drawn schematically in Figure 2). We imaged the beam separation on the second crystal and overlap on the third (Figure 2), but dynamical diffraction effects obscured the expected interference fringes. We are optimizing our design parameters (beam convergence angle, grating separation) to minimize these effects.

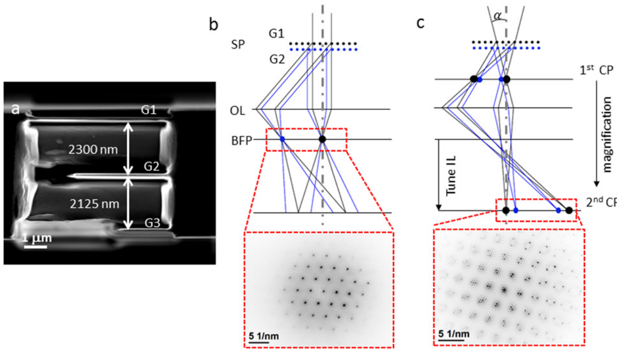

▲Figure 1: (a) Monolithic three-crystal grating fabricated from Si (110) by FIB. (b) Ray diagrams and experimentally observed DPs for PBED and (c) CBED. Black and blue rays represent diffraction from G1 and G2, respectively. (G1: first grating, G2: second grating, SP: sample plane, OL: objective lens, BFP: back focal plane, CP: crossover plane, α: convergent angle).

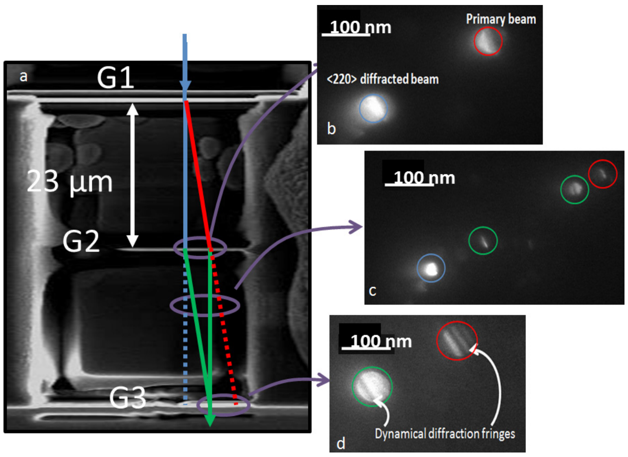

▲Figure 2: (a) 23-µm separation multi-grating with schematic of a Mach-Zehnder interferometer. First grating splits incident electron beam into primary and diffracted beam, which are recombined by second grating. By tilting sample holder so that grating is in 2-beam condition and varying objective lens current to change imaging plane, we imaged beam (b) in plane of second, (c) between second and third and (d) on third crystal, demonstrating beamsplitting and recombination.

FURTHER READING

- L. Marton, J. A. Simpson and J. A. Suddeth, "Electron Beam Interferometer," *Phys. Rev.* vol. 90, pp. 490, 1953.
- G. Gronniger, B. Barwick and H. Batelaan, "A Three-grating Electron Interferometer," *New Journal of Physics*, vol. 8, pp. 224, 2006.

Lithographically Patterned Nanostructures for Geometric Control of Coiled-Coil Protein Placement and Alignment

M. Bedewy, W. M. Park, A. E. Keating, K. K. Berggren
Sponsorship: DuPont

Developing methods to tailor nanoscale surface features has received significant attention recently, in particular for applications requiring control of living cell behavior. Engineering nanoridges to regulate cells in cardiac tissue constructs or using nanotubes to direct growth of motor neuron cells are two examples. Although various nanofabrication methods are capable of producing surfaces with anisotropic structure and properties at the nanoscale, most of these nanoengineered surfaces are made of synthetic and non-organic materials that are not necessarily biocompatible. Moreover, engineered surfaces do not mimic the atomic scale morphology and interactions of the native protein-based environment of the extracellular matrix. Hence, controlled functionalization of nanostructured surfaces with proteins is desired for advanced biointerfaces. While block copolymer micelle nanolithography and scanning probe methods have been used for this purpose, they are limited to spherical nanoparticles and randomly oriented protein binding.

In this work, we used electron beam lithography (EBL) to create arrays of designed nanoscale feature geometries and pattern topologies down to the 10-nm scale. Patterns are transferred to gold by deposition and lift-off. Silicon substrates are functionalized with a monolayer of methoxy polyethylene glycol (PEG) silane to prevent the nonspecific binding of proteins on non-patterned areas of the substrate. Purified coiled-coil tropomyosin proteins are then selectively immobilized on the surface by leveraging the formation of a thiol bond between the cysteine group at one end of the protein and the lithographically patterned gold. Atomic force microscopy was used to assess the protein structure and location, and scanning electron microscopy was also used to characterize the surface, after proteins were tagged with Au nanoprobes. Combining the versatility of EBL and the specificity of bottom-up protein binding makes this approach attractive for scalable production of nanobiointerfaces in high-sensitivity medical diagnostics and regenerative medicine.

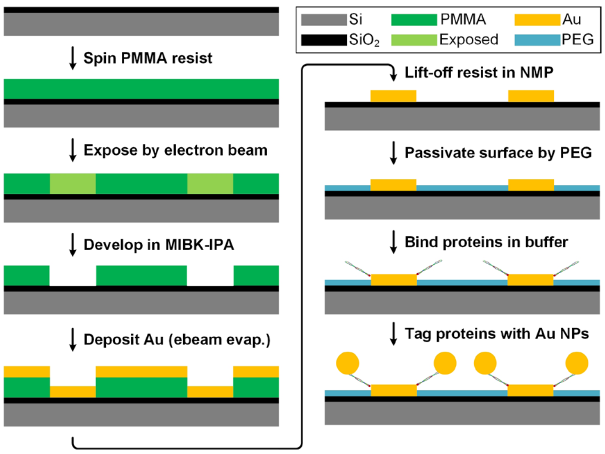

▲Figure 1: Process schematic showing fabrication of gold nanostructures by EBL and lift-off and attaching of PEG silane. Samples are incubated with proteins in buffer and in solution with gold nanoprobes for protein tagging.

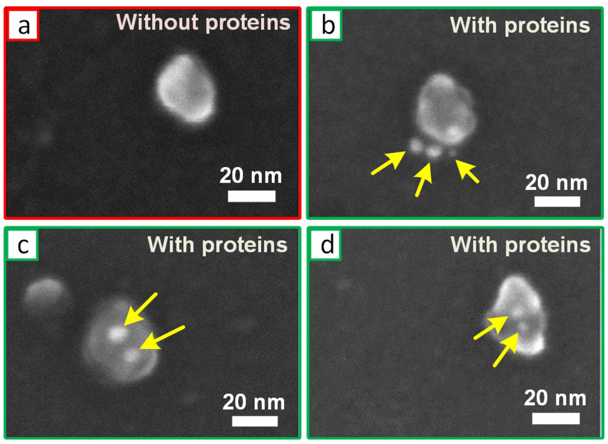

▲Figure 2: Scanning electron micrographs showing initial results for protein localization on 20-nm gold posts created by EBL. (a) gold nanopost without proteins. (b-d) gold nanoposts with proteins and nanoparticle tags.

FURTHER READING

- J.-B Chang, Y. H. Kim, E. Thompson, Y. H. No, N. H. Kim, J. Arrieta, V. R. Manfrinato, A. E. Keating, and K. K. Berggren, "The Orientations of Large Aspect-Ratio Coiled-Coil Proteins Attached to Gold Nanostructures," *Small*, vol. 12, pp. 1498–1505, 2016.
- A. W. Reinke, R. A. Grant, and A. E. Keating, "A Synthetic Coiled-Coil Interactome Provides Heterospecific Modules for Molecular Engineering," *Journal of Am. Chem. Soc.* vol. 132, pp. 6025-6031, 2010.
- V. R. Manfrinato, L. Zhang, D. Su, H. Duan, R. G. Hobbs, E. A. Stach, and K. K. Berggren, "Resolution Limits of Electron-Beam Lithography Toward the Atomic Scale," *Nano Letters*, vol. 13, pp. 1555-1558, 2013.

Multidirectional Block Copolymer Alignment: Shear-Induced Alignment by Mismatch of Thermal Coefficients of Expansion

S. M. Nicaise, A. Tavakkoli K. G., K. GadelraA. Alfredo-Katz, C. A. Ross, K. K. Berggren
Sponsorship: TSMC

Here we show shear-aligned BCP cylinders induced by a SiO_2 top-coat. The fabrication process involves four steps: (1) spin-coating a thin film of cylinder-forming BCP, poly(styrene-*b*-dimethylsiloxane) (PS-*b*-PDMS, 16 kg mol^{-1}) on Si; (2) deposition of ~100 nm of SiO_2 on the BCP; (3) thermal annealing of samples for 1 and 10 minutes, inducing oriented assembly; and (4) SiO_2 removal in 1% hydrofluoric acid and reactive-ion etching to leave PDMS cylinders. During annealing, the SiO_2 (coefficient of thermal expansion (CTE) ~0.5 ppm/°C) expanded less than the silicon (CTE ~2.6 ppm/°C). The resulting strain aligned the BCP cylinders perpendicular to scribes and cracks in the SiO_2.

The degree of alignment varied with annealing temperature and distance from hand-scribes. In Figure 1, we plotted the greatest distance from the scribe for which we observed ordering and alignment. BCP ordering increased with proximity to the crack, likely due to higher shear-stress at the SiO_2 free edge, as determined via finite-element simulation of the BCP-SiO_2 and –Si interfaces. Longer annealing time and higher annealing temperature resulted in improved long-range alignment and reduced defects. Furthermore, rapid orientation was achieved in as little as one minute of annealing. Different BCP orientations were achieved using crossed hand-scribes (Figure 2). Overall, this method shows promise to improve local orientational control as well as the long-range order of BCPs.

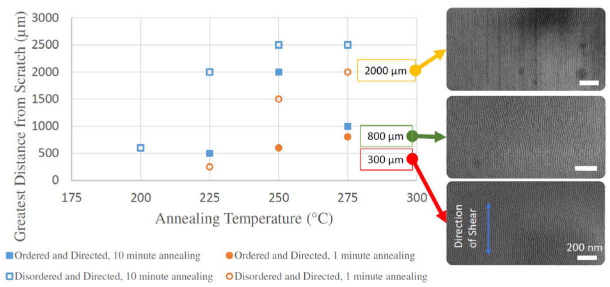

▲ Figure 1: Maximum observed distance (away from scribe) of ordering and direction vs. annealing temperature and time. Also, example scanning-electron micrographs of the aligned BCP at chosen distances.

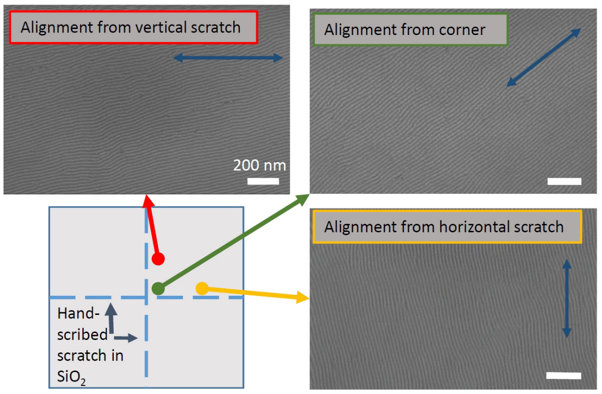

▲ Figure 2: The cartoon shows a cross hand-scribed in the SiO_2. The scanning electron micrographs show controlled shear-aligned BCP cylinders in directions perpendicular to the scribes on a single substrate.

FURTHER READING

- D. E. Angelescu, J. H. Waller, D. H. Adamson, P. Deshpande, S. Y. Chou, R. A. Register, and P. A. Chaikin, "Macroscopic Orientation of Block Copolymer Cylinders in Single-Layer Films by Shearing," *Advanced Materials*, vol. 16, pp. 1736-1740, 2004.
- Z. Qiang, L. Zhang, G. E. Stein, K. A. Cavicchi, and B. D. Vogt, "Unidirectional Alignment of Block Copolymer Films Induced by Expansion of a Permeable Elastomer during Solvent Vapor Annealing," *Macromolecules*, vol. 47, pp. 1109-1116, 2014.
- J. W. Eischen, C. Chung, and J. H. Kim, "Realistic Modeling of Edge Effect Stresses in Bimaterial Elements," *Trans. ASME*, vol. 112, pp. 16-23, 1990.

Rule-Based Patterning of a Multi-State System by Block Copolymer Self-Assembly

H. Do, H. Choi, J.-B. Chang, C. A. Ross, K. K. Berggren
Sponsorship: NSF, Taiwan Semiconductor Manufacturing Company

Lithographic confinement can direct the self-assembly of block copolymers (BCPs) to achieve highly ordered nanoscale patterns. Previously, we have demonstrated that BCP cylinders can form a multi-state system with ladder-shaped structures rather than a single-state system with concentric rings inside a confinement when the bending angle of the confinement is 90° or more. In this work, we describe a design rule to determine the individual state of the ladder-shaped structures by controlling alignment direction. This work could lead to a new patterning method that enables higher-throughput pattern generation.

We fabricated topographic templates consisting of square cells with one to four openings using electron-beam lithography of hydrogen silesquioxane resist. Figure 1 shows five different types of the square confinements and the measured probability of horizontal alignment, denoted as the 0 state. The templates were chemically functionalized with a hydroxyl-terminated polystyrene brush. Next, 45.5 kg/mol polystyrene-*b*-polydimethylsiloxane BCP (PS-*b*-PDMS) was spin cast on the templated substrate, and the sample was solvent annealed using a 5:1 mixture of toluene and heptane at room temperature for 5 h. The upper PDMS layer and PS matrix were removed using CF_4 and O_2 plasma treatment, respectively. Templates without openings produced ladder-shaped BCP patterns inside the square cell with equal probability of horizontal and vertical alignment. When one or more openings were introduced, the alignment directions were controlled by a majority rule determined by the number of horizontal and vertical openings.

Using five design rules, we fabricated an array of connected binary states where the two states were defined as horizontally (0 state) and vertically (1 state) aligned structures. Two examples of complex 4 by 4 binary patterns each composed of 16 independently controlled binary states are shown in Figure 2. After BCP self-assembly, binary states formed inside the template matched the desired binary patterns.

In the future, the possibility of propagating template information across multiple tiles will be investigated.

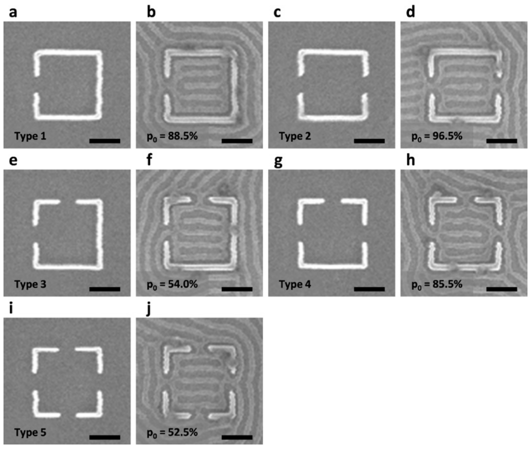

▲ Figure 1: Scanning electron microscope images of square confinement with different number of openings and resulting block copolymer patterns. Probability of horizontal alignment (0 state) for each type was measured. Binary states were determined by a design rule based on majority rule. Scale bars, 200 nm.

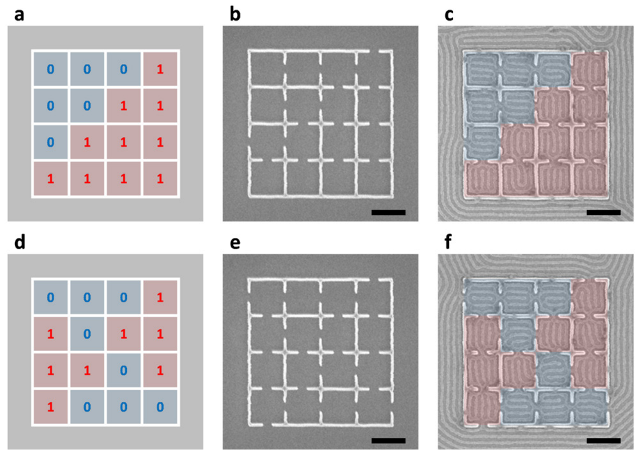

▲ Figure 2: Fabrication of binary state arrays. (a, d) Diagram of desired 4 x 4 binary state arrays. (e) Templates fabricated by rule-based design. (c, f) Resulting block copolymer patterns matching the desired binary states. Red indicates 0 state, and blue indicates 1 state. Scale bars, 200 nm.

FURTHER READING

- J. Y. Cheng, A. M. Mayes, and C. A. Ross, "Nanostructure Engineering by Templated Self-assembly of Block Copolymers," *Nature*, vol. 3, pp. 823-828, 2004.

Mapping Deep-Ultraviolet Plasmons in Lithographically Defined Aluminum Nanostructures

S. A. Goodman, R. G. Hobbs, V. R. Manfrinato, Y. Yang, L. Zhang, E. A. Stach, K. K. Berggren
Sponsorship: Gordon and Betty Moore Foundation, DOE EFRC

An electron beam induces collective oscillations of the free-electron gas in a material that take the form of surface plasmons (SPs) or volume plasmons (VPs). SPs are transverse and propagate at the material surface whereas VPs are longitudinal and propagate in the bulk of the material. Due to their longitudinal nature, VPs do not couple to light and must be excited by charged particle beams. Here, we demonstrate nanometer-scale mapping of SP and VP modes across these nanostructures using spatially resolved electron energy loss spectroscopy (EELS) with a scanning transmission electron microscope (STEM). Figure 1a shows a high-angle annular dark field STEM image of a 12-nm-diameter Al nanodisk. To create an EELS map of this nanodisk, a focused electron beam with a sub-nanometer-sized probe is raster-scanned across the sample (Figure 1b). Electrons passing through the material undergo various energy-loss pathways including plasmon excitation. An EEL spectrum (Figure 1c) is recorded at each 1-nm^2 pixel; the spectrum represents the number of electrons plotted versus energy-loss and contains Al SP peaks (2-8 eV), the Al VP peak (15 eV), and the Al_2O_3 VP peak (23 eV). Figure 1d shows three superimposed EELS maps obtained at each plasmon energy, providing a nanometer-scale representation of the local electric field density across the nanodisk. As demonstrated by the EELS map and plasmon intensity profile (Figure 1e), the Al VP mode is localized at the center of the particle while the Al SP mode is localized at the particle boundary. With SP resonances that can be tuned from the visible to the UV and a VP resonance in the deep-UV, Al is a promising material for high-energy plasmonics. The ability to map the spatial distribution of plasmon modes in Al nanodisks opens up a pathway for new optics, emitters, and hot-carrier-based chemistry in the UV range.

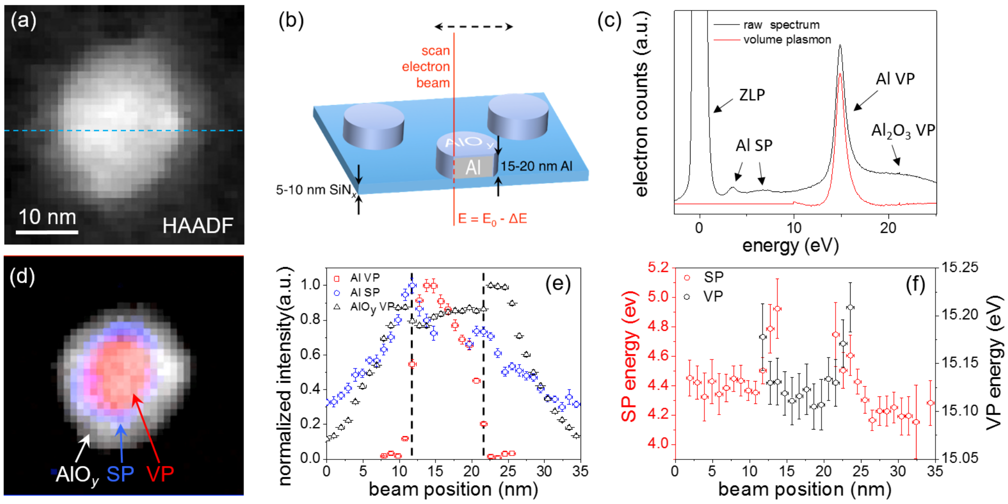

▲ Figure 1: EELS mapping of plasmon modes. (a) High-angle annular dark-field image of 12-nm-diameter Al nanodisk fabricated on 5-nm-thick SiN_x TEM grid. Scale bar also applies to (d). Blue dashed line represents path of electron beam in (e, f). Images and EEL spectra were acquired on aberration-corrected Hitachi HD2700C STEM at Brookhaven National Lab. (b) Electron beam is raster scanned across nanodisk, and EEL spectrum is recorded at each pixel. (c) Example EEL spectrum representing number of electrons vs. energy loss. Raw spectrum contains zero loss peak (ZLP), Al SP peaks, Al VP peak, and VP peak of Al_2O_3. Background is subtracted to obtain isolated Al VP peak (in red). (d) Superposition of three EELS maps acquired at energy of Al dipolar SP1, Al VP, and Al_2O_3 VP. (e) Normalized SP1 and VP intensities plotted as function of electron beam position. Dashed lines show two SP1 maxima, indicating position of particle boundary. (f) Energy of SP1 and VP modes vs. beam position.

FURTHER READING

- R. H. Ritchie, R. Hamm, J. Turner, H. Wright, J. Ashley, and G. Banks, "Physical Aspects of Charged Particle Track Structure," *US Department of Energy Publications*, January 1989.
- R. H. Ritchie, "Plasma Losses by Fast Electrons in Thin Films," *Phys. Rev.*, vol. 106, no. 5, pp. 874–881, June 1957.
- R. G. Hobbs, V. R. Manfrinato, Y. Yang, S. A. Goodman, L. Zhang, E. A. Stach, and K. K. Berggren, "High-Energy Surface and Volume Plasmons in Nanopatterned Sub-10 nm Aluminum Nanostructures," *Nano Letters*, vol. 16, no. 7, pp. 4149-4157, July 2016.

Bias-Sputtered Few-Nanometer-Thick Niobium Nitride for Superconducting Devices

A. Dane, A. McCaughan, D. Zhu, Q. Zhao, C-S. Kim, N. Calandri, F. Bellei, K. K. Berggren
Sponsorship: NASA Space Technology Research Fellowship

Few-nanometer-thick films of low temperature superconducting materials have become increasingly important for sensitive photonic devices. Hot electron bolometers, superconducting nanowire single photon detectors (SNSPDs), microwave kinetic inductance detectors, and transition edge sensors are all broadband, highly sensitive photo-detectors that are fabricated from thin films of low-temperature superconducting materials.

Improvements to materials synthesis and exploration of material-dependent properties of these devices have so far taken a back seat to advancing the performance of individual devices through electrical design. In particular, while the performance of individual few-nanometer-thick niobium nitride (NbN) SNSPDs has produced detectors with near-unity quantum efficiency and tens of picoseconds of jitter, the yield of these devices remains a major issue. As optical systems demand longer nanowire devices and arrays of devices, previously ignored yield issues must be addressed.

We have explored reactive DC magnetron sputtering of few-nanometer-thick NbN without intentional substrate heating and the performance of superconducting devices made from NbN. We find that for films with thicknesses typical of those used to fabricate SNSPDs, the addition of a 50 watt substrate bias and the ion bombardment that results during film deposition significantly reduce the film resistivity, increase the Tc, decrease the film roughness, and change the film's surface morphology. This material shows promise for fabricating SNSPDs with better yield and efficiency at easy-to-access temperatures. Many fabrication methods and structures become practical when the substrate is not heated.

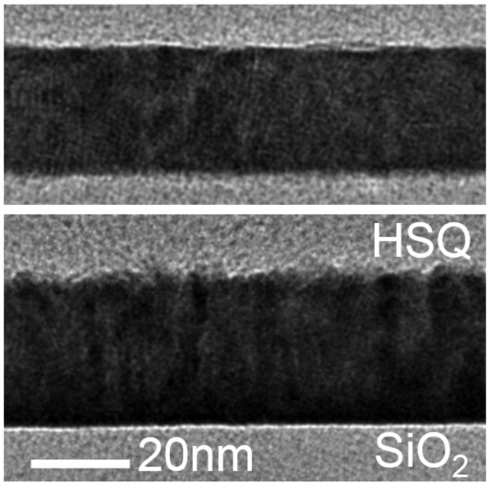

▲ Figure 1: Transmission electron microscope image of ~30-nm-thick NbN deposited by reactive magnetron sputter deposition without intentional heating. During the deposition a 50-watt RF bias was used to encourage ion bombardment and surface diffusion for the film shown on top.

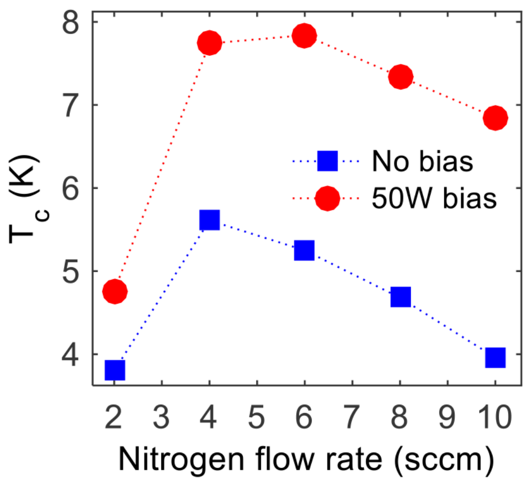

▲ Figure 2: The addition of a 50-watt RF bias increases the superconducting critical temperature of 5-nm- thick NbN films for different chamber conditions. The maximum T_c is seen to increase by about 2K.

FURTHER READING

- A. J. Kerman, E. A. Dauler, J. K. W. Yang, K. M. Rosfjord, V. Anant, K. K. Berggren, G. N. Gol'tsman, and B. M. Voronov, "Constriction-limited Detection Efficiency of Superconducting Nanowire Single-photon Detectors," *Appl. Phys. Letters*, vol. 90, no. 10, pp. 101110, 2007.
- L. Kang, B. B. Jin, X. Y. Liu, X. Q. Jia, J. Chen, Z. M. Ji, W. W. Xu, P. H. Wu, S. B. Mi, A. Pimenov, Y. J. Wu, and B. G. Wang, "Suppression of Superconductivity in Epitaxial NbN Ultrathin Films," *Journal of Appl. Phys.*, vol. 109, no. 3, pp. 033908, 2011.

Freeform Robotic Stereolithography

A. G. Stevens*, C. R. Oliver*, M. Kirchmeyer, J. Wu, L. Chin, E. S. Polsen, C. Archer, C. Boyle, J. Garber, A. J. Hart
*authors contributed equally
Sponsorship: NSF, SMART

Additive manufacturing by layerwise photopolymerization, i.e., sterolithography, is attractive due to its high resolution and diversity of materials chemistry; however, traditional stereolithography methods are restricted to planar substrates and single-axis machine configurations. We present a robotic system capable of maskless layerwise photopolymerization on curved surfaces, enabling production of large-area conformal patterns and the construction of freeform objects. The system comprises an industrial six-axis robot and a custom-built maskless projector end-effector. Use of the system involves scanning the freeform substrate, generation of a triangulated toolpath with curved layers that represents the target object to be printed, precision mounting of the substrate in the robot workspace, and robotic photopatterning of the target object by coordinated motion of the robot and substrate. We demonstrate printing of conformal patterns on spheres of various sizes, and construction of miniature three-dimensional objects without requiring support features (Figure 1). Improvement of the motion accuracy and development of freeform tool paths could enable construction of large polymer parts beyond the size and support structure constraints of traditional stereolithography systems

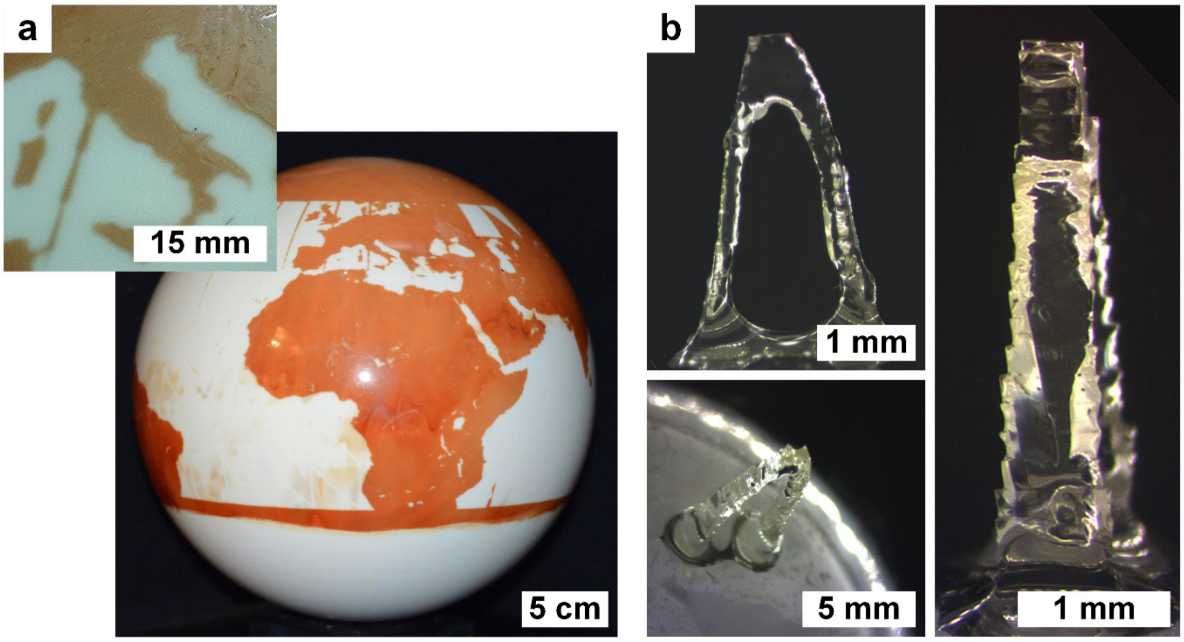

▲ Figure 1: Demonstrations of robotic stereolithography: (a) conformal patterning of photoresist (orange) on a spherical substrate (white); (b) miniature arch printed via robotic stereolithography (200-µm layers) on a spherical substrate.

FURTHER READING

- A. G. Stevens, C. R. Oliver, M. Kirchmeyer, J. Wu, L. Chin, E. Polsen, C. Archer, C. Boyle, J. Garber, and A. J. Hart, "Freeform Robotic Stereolithography," submitted for publication.

Measuring Phonon Mean Free Path Distributions in Materials via Quasiballistic Thermal Transport by Using Grating Nanostructures

L. Zeng, R. He, D. Wang, S. Huberman, V. Chiloyan, Z. Ren, G. Chen
Sponsorship: S3TEC, DOE

Thermal transport in non-metals generally consists of contributions from phonons spanning a wide range of mean free paths (MFPs). Knowledge of phonon MFP distributions is important for both fundamental understanding of microscopic energy transport in materials and many technological applications, including thermal management in microelectronics and thermal conductivity engineering in thermoelectric energy conversion. The thermal conductivity accumulation function is a key metric that describes the distribution of phonon MFPs that contribute to heat transport. To gain insight into materials' MFP distributions, the Nanoengineering Laboratory in the Department of Mechanical Engineering at MIT has been developing thermal conductivity spectroscopy techniques by utilizing a femtosecond ultrafast pump-probe setup.

The key idea of reconstructing material's MFP distribution is based upon combining experimental observation of quasiballistic thermal transport and solution of the phonon Boltzmann transport equation. Accessing the quasiballistic transport regime requires creating characteristic heater sizes comparable with the phonon MFPs. Since phonon MFPs in many materials of interest span from nanometers to micrometers, we lithographically patterned 2D metallic nanodots on top of the sample to function as both heat absorbers and temperature transducers during measurement. To avoid direct photo-excitation in opaque samples, we used a bilayer hybrid nanostructure to effectively localize the heating with nanometer scale resolution while preventing laser transmission into the substrate. Using this hybrid nanostructure approach, we studied length-dependent thermal transport in many materials, including Si, GaAs, GaN, and SiGe, and developed techniques to map out their intrinsic phonon MFP distributions. We then simplified the hybrid approach by utilizing 1D metallic wire grid polarizers to minimize carrier excitation in the substrate. At present, we are applying the simplified technique to measure MFP distributions in a range of materials, including some select thermoelectric materials. The measurement results will shed light on how to further tailor the thermal conductivity for energy applications.

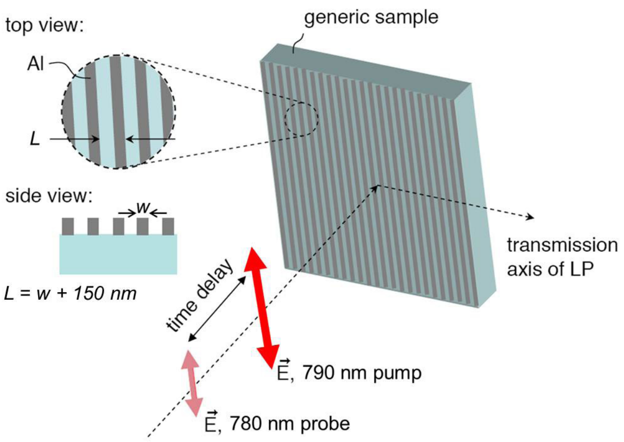

▲ Figure 1: Schematic of our sample structures and experimental technique. The samples are composed of metal grating on top of substrates of interests and are measured by an ultrafast optical time-domain thermoreflectance technique in the RK lab at MIT.

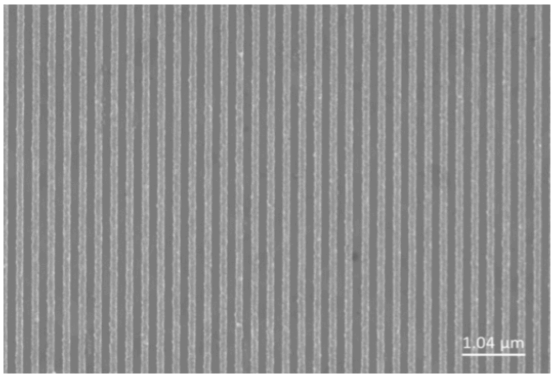

▲ Figure 2: Fabricated ~100 nm wide (period = 260nm) one-dimensional aluminum metal grating on top of a $Nb_{0.95}Ti_{0.05}FeSb$ substrate using the ebeam machine Elionix in Microsystems Technology Laboratories at MIT.

FURTHER READING

- L. Zeng and G. Chen, "Disparate Quasiballistic Heat Conduction Regimes from Periodic Heat Sources on a Substrate," *Journal of Applied Physics*, vol. 116, pp. 064307, 2014.
- Y. Hu, L. Zeng, A. J. Minnich, M. S. Dresselhaus, and G. Chen, "Spectral Mapping of Thermal Conductivity through Nanoscale Ballistic Transport," *Nature Nanotechnology*, vol. 10, pp. 701, 2015.
- L. Zeng, K. C. Collins, Y. Hu, M. N. Luckyanova, A. A. Maznev, S. Huberman, V. Chiloyan, J. Zhou, X. Huang, K. A. Nelson, and G. Chen, "Measuring Phonon Mean Free Path Distributions by Probing Quasiballistic Phonon Transport in Grating Nanostructures," *Scientific Reports*, vol. 5, pp. 17131, 2015.

Quantitative Analysis and Modeling of Templated Solid-State Dewetting of Thin Single-Crystal Ni Films

Y. A. Shin, K. Keane, G. H. Kim, W. C. Carter, C. V. Thompson
Sponsorship: NSF

It has been shown that templated solid-state dewetting of single crystal films (120 nm thick) can be used to make periodic complex structures with dimensions smaller than the templating patterns, making it a potential self-assembly method (Figure 1). A quantitative understanding of dewetting mechanisms is critical for design of self-assembled structures made through dewetting. In the past, we have studied corner, pinch-off, and Rayleigh instabilities. We are currently studying the fingering instability using single-crystal Ni films that have been patterned with edges lying along different in-plane crystallographic orientations. These edges were also patterned with periodic perturbations having various wavelengths. We found that some edges with specific in-plane crystallographic alignments were resistant to development of fingering instabilities, even with templating, and became straight as they retracted during dewetting. In the case of edges with other crystallographic alignments, we have shown that templating with patterned edge perturbations can be used to control the period of the fingering instability that develops the edges retract during dewetting (Figure 2). We are developing a kinetic Monte Carlo model to better understand mechanisms of the fingering instability.

In parallel with studies of templated fingering instabilities, we aim to generate smaller-scale dewetting structures using templated solid-state dewetting. Finer dewetting structures require thinner films. However, natural hole formation becomes easier as the film thickness is decreased, and uncontrolled formation of natural holes limits our ability to decrease the length-scale of dewetting structures, as naturally forming holes interrupt processes controlled through templating. We are developing methods to identify the cause of natural hole formation and to control it. After achieving control of natural hole formation, we will study dewetting phenomenologies in ultra-thin single crystal films and test the potential of templated solid-state dewetting as a self-assembly method for fabrication of nanostructures.

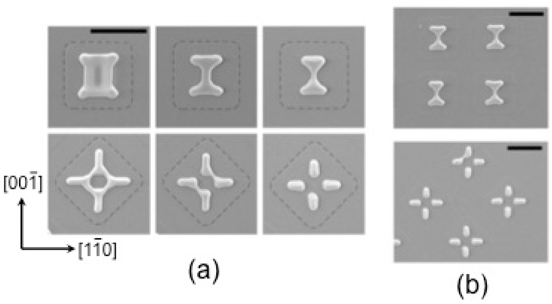

▲Figure 1: (a) Partially dewetted patches patterned from a (100) Ni film into squares with different in-plane orientations; annealing time increases from left to right (b) Highly reproducible templated dewetting patterns. Scale bar: 10 μm.

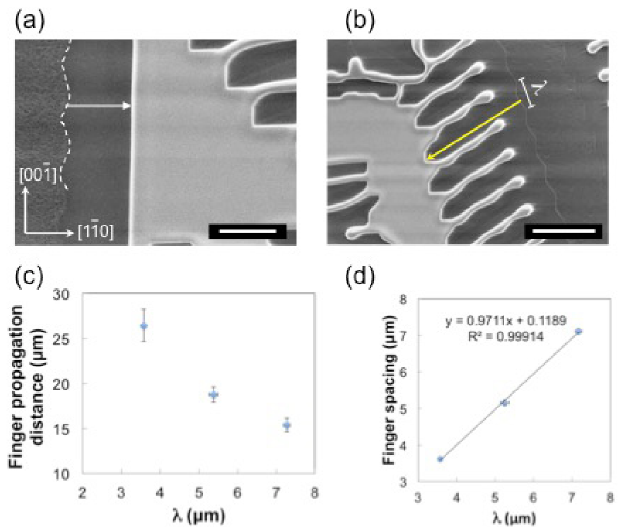

▲Figure 2: (a) Edge retraction at patterned edge aligned along a kinetically stable orientation in Ni (110) film. (b) Development of fingering instability in a kinetically non-stable orientation. (c) Relationship between finger spacing as a function of intended perturbation, λ. Scale bar: (a) 5 μm and (b) 10 μm. λ: 5.364 μm.

FURTHER READING

- C. V. Thompson, "Solid-state Dewetting of Thin Films," *Annual Review of Materials Research,* vol. 42, pp. 399-434, 2012.
- R. V. Zucker, G. H. Kim, J. Ye, W. C. Carter, and C. V. Thompson, "The Mechanism of Corner Instabilities in Single-crystal Thin Films During Dewetting," *Journal of Appl. Phys.*, vol. 119, pp. 125306, 2016.
- G. H. Kim and C. V. Thompson, "Effect of Surface Energy Anisotropy on Rayleigh-like Solid-state Dewetting and Nanowire Stability," *Acta Materialia,* vol. 84, pp. 190, 2015.

Optimization of Vertically-Aligned CNT Carpets' Macro- and Nano-properties for Supercapacitor and Capacitive Deionization

M. Hashempour, H. Mutha, E. N. Wang, C. V. Thompson
Sponsorship: MITEI, Progetto Roberto Rocca

The science and technology of water desalination is receiving increasingly intensive attention due to human population growth and subsequent growing demands in domestic, industrial and agricultural sectors. Currently, desalination technology relies mainly on energy intensive techniques such as multi-stage flash (MSF), multi-effect distillation (MED), and reverse osmosis (RO). Capacitive deionization (CDI) is an emerging high-efficiency charge-based desalination technique with the ability to remove a wide range of ionic contaminants with high recovery rates. In CDI, an electrical potential difference is maintained between high-surface-area electrodes as a salt water stream passes through them, resulting in adsorption of anions and cations at the surface of positively and negatively polarized electrodes, respectively. Since CDI removes salt ions from water rather than treating the bulk water molecules, it requires much less energy than competing techniques. One of the main research directions in the field of CDI is development of electrode materials with high electrical conductivity, electrochemical stability, and morphologies allowing for a maximized surface area along with a minimized distance for ionic migration. In this project, we investigated the optimization of vertically aligned carbon nanotube (CNT) carpets for this application. CNTs were synthesized via chemical vapor deposition (CVD) and over a wide range of growth variables. We realized that the flow rate or partial pressure of the carbon precursor gas (C_2H_4 in our work) has the most fundamental effect on a carpet's macro-properties such as areal and volumetric density due to the modification of the number of CNT walls as well as their number density (Figure 1 a-d). Electrochemical studies of these CNTs in a supercapacitor set-up (Figure 2 a-b) confirm the highest gravimetric capacities (up to 25% compared to other CNTs) are found for CNTs grown at the lowest C_2H_4 flow rates, which provided the highest specific surface area and lowest number of CNT walls. The highest volumetric capacitance (by a factor of 2 compared to other CNTs) was, in contrast, found for CNTs grown at higher C_2H_4 flow rates, which provided the highest number density and lowest inter-CNT spacing. Preliminary CDI experiments were carried out, and successful capacitive desalination via these electrodes was demonstrated (Figure 2 c). More detailed parametric studies of the CDI performance along with development of an ion transport model are underway.

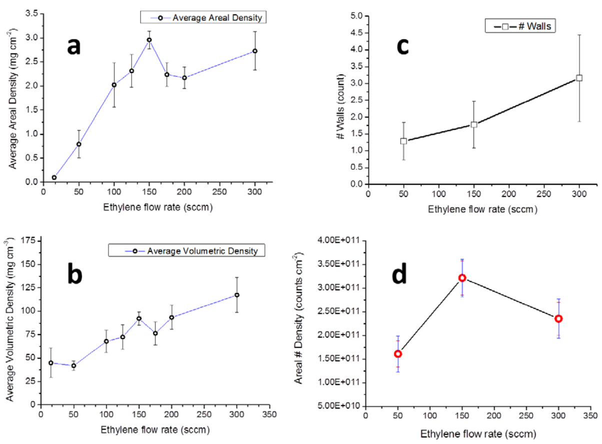

▲Figure 1: (a) areal density and (b) volumetric density of CNT carpets, (c) average number of walls and (d) number density of CNTs.

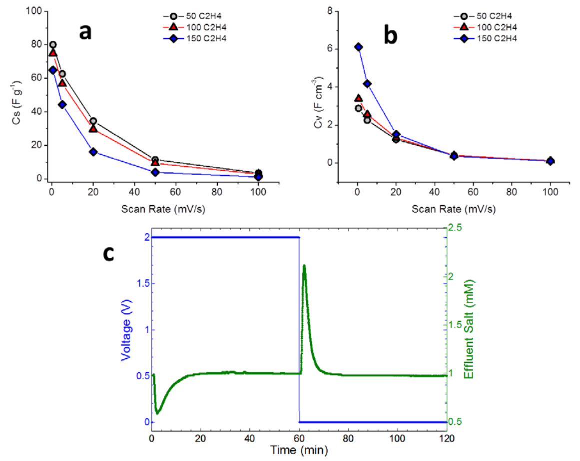

▲Figure 2: (a) gravimetric and (b) volumetric capacitance of CNTs in 50 mM NaCl solution, and (c) demonstration of salt concentration decrease in the brine flow upon the application of potential (adsorption) and its increase upon removal of the potential (desorption).

FURTHER READING

- M. A. Shannon, P. W. Bohn, M. Elimelech, J. G. Georgiadis, B. J. Mariñas, and A. M. Mayes, "Science and Technology for Water Purification in the Coming Decades," *Nature*, vol. 452, pp. 301–310, 2008.
- M. E. Suss, S. Porada, X. Sun, P. M. Biesheuvel, J. Yoon, and V. Presser, "Water Desalination via Capacitive Deionization: What Is It and What Can We Expect from It?" *Energy Env. Sci*. vol. 8, pp. 2296–2319, 2015.

Liquid Spreading in Ceramic-Coated Carbon Nanotube Films and Patterned Microstructures

H. Zhao, A. J. Hart
Sponsorship: NIH

We study the capillary-driven liquid spreading behavior on films and patterned microstructures of ceramic-coated vertically aligned carbon nanotubes (CNTs) (see Figure 1). The nanoscale porosity and micro-scale dimensions of the CNT structures, which can be precisely varied by the fabrication process, enable quantitative measurements that can be related to analytical models of the spreading behavior. Moreover, the alumina coating deposited conformally on the CNTs by atomic layer deposition (ALD) prevents capillary-induced deformation of the CNTs upon wetting and recession of the meniscus, which has complicated previous studies of this topic. CNT samples are fabricated on quartz substrates, enabling optical imaging of the contact line from the bottom of the substrate. A power-law liquid spreading behavior is observed on non-patterned CNT substrates and is explained using a scaling model based on the balance of capillary driving force and the viscous drag force (see Figure 2). Using these insights, we design micropatterned surfaces with controllable spreading rates and study the pinning-depinning behavior of the contact line. The nanoscale porosity, controllable surface chemistry, and mechanical stability of coated CNTs provide significantly enhanced liquid-solid interfacial area compared to solid microstructures. As a result, these surface designs may be useful for applications such as phase-change heat transfer, biomolecule capture, and electrochemical energy storage.

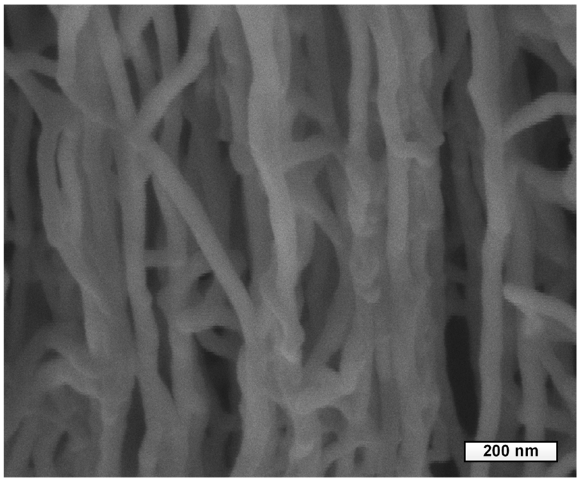

▲ Figure 1: Scanning electron microscope image showing side view of a vertically aligned CNT forest conformally coated with 15-nm-thick Al_2O_3 by ALD.

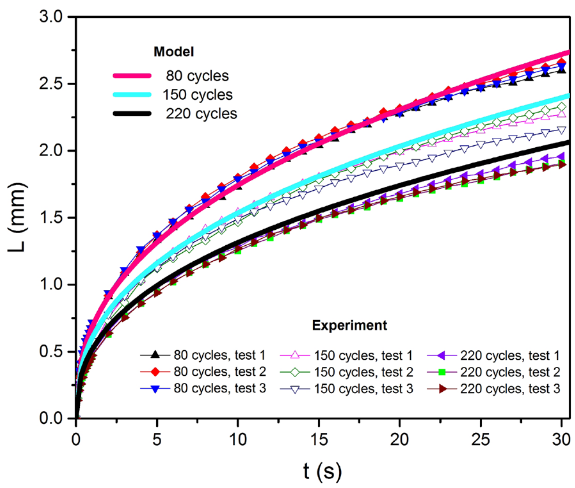

▲ Figure 2: Modeling and experimental measurement of liquid spreading on CNT forest with different Al_2O_3 coating thicknesses, showing a power-law scaling behavior.

FURTHER READING

- A. Brieland-Shoultz, S. Tawfick, S. J. Park, M. Bedewy, M. R. Maschmann, J. W. Baur, and A. J. Hart, “Scaling the Stiffness, Strength, and Toughness of Ceramic-Coated Nanotube Foams into the Structural Regime,” *Advanced Functional Materials*, vol. 24, pp. 5728–5735, 2014.

Influence of Density Gradients on the Thermal Conductivity and Mechanical Compliance of Carbon Nanotube Forests

C. JacoS. Schiffres, S. Huberman, J. Li, G. Chen, A. J. Hart

Vertically aligned carbon nanotubes (VACNTs), often called CNT "forests," show promise to enable high performance thermal interface materials based on the thermal properties of individual CNTs and their collective mechanical compliance. Measurements of the thermal conductivity of individual, suspended CNTs have given values as high as 3000 $Wm^{-1}K^{-1}$; however, the thermal conductivities of CNT forests have varied widely, from 0.5 to 267 $Wm^{-1}K^{-1}$. Previous studies have shown the influence of boundary resistances, phonon scattering at CNT-CNT contacts, and intrinsic CNT defects on individual and collective CNT thermal properties. However, understanding of the collective growth of CNT forests, particularly of height-dependent morphology and density variations, has not been related to direct measurements of thermal conductivity. Such knowledge is important to improve the CNT growth process to give improved forest thermal conductivity and to engineer the mechanical and thermal properties of CNT-based thermal interfaces for specific applications.

Using frequency-domain thermoreflectance (FDTR), we characterize the thermal conductivity of CVD-grown VACNTs. FDTR is a non-contact method that uses continuous wave (CW) lasers to induce local heating in a thin film while measuring temperature response due to temperature-dependent reflectance changes in the sample. Owing to the height of the VACNT forests grown, from 10's μm to 100's μm, we treat them as thin films for the purpose of FDTR measurements. From our group's previous studies on the stages of CNT forest growth, we understand that density gradients occur along the height of the forest. As such we model these gradients as discrete layers within the forest for the purpose of thermal analysis. The resulting data were compared to known height and density gradients with the VACNTs to show correlation between macroscopic forest properties and the impact on thermal performance. Additionally, we perform compressive modulus testing to correlate thermal and mechanical performance of the forests.

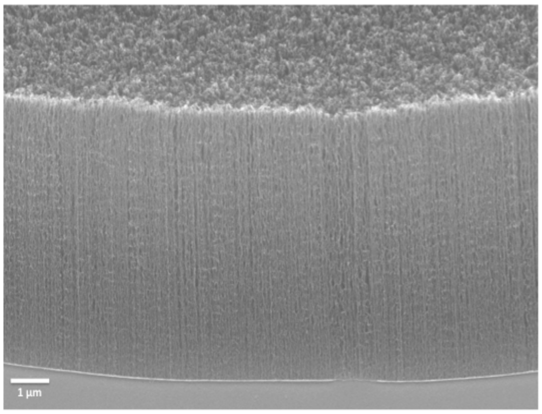

▲ Figure 1. Typical view of CNT forest edge. Known density variations occur along height of the forest.

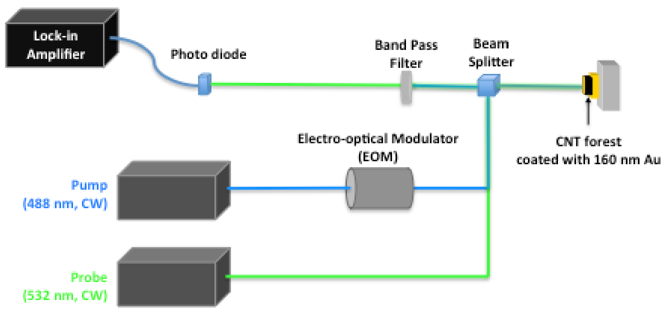

▲ Figure 2. Schematic of FDTR setup for thermal characterization of CNT forest. 160 nm of Au sputtered on top of forest acts as thermal transducer. The reflectance of this layer changes with temperature, which is recorded by the photodiode.

FURTHER READING

- M. Bedewy, E. R. Meshot, M. J. Reinker, and A. J. Hart, "Population Growth Dynamics of Carbon Nanotubes," *ACS Nano,* vol. 5, no. 11, pp. 8974–89, 2011.
- P. Kim, L. Shi, A. Majumdar, and P. McEuen, "Thermal Transport Measurements of Individual Multiwalled Nanotubes," *Physical Review Letters,* vol. 87, no. 21, p. 215502, 2001.
- Y. Gao, A. M. Marconnet, R. Xiang, S. Maruyama, and K. E. Goodson, "Heat Capacity, Thermal Conductivity, and Interface Resistance Extraction for Single-walled Carbon Nanotube Films using Frequency-domain Thermoreflectance," *IEEE Transactions on Components, Packaging and Manufacturing Technology,* vol. 3, no. 9, pp. 1524–1532, 2013.

Predictive Synthesis of Freeform Carbon Nanotube Microarchitectures by Strain-Engineered Chemical Vapor Deposition

S. J. Park, H. Zhao, S. Kim, M. De Volder, A. J. Hart
Sponsorship: AFOSR, NSF, NIH

High throughput fabrication of microstructured surfaces with multi-directional, re-entrant, or otherwise curved features is becoming increasingly important for applications such as phase change heat transfer, adhesive gripping, and control of electromagnetic waves. Toward this goal, curved microstructures of aligned carbon nanotubes (CNTs) can be fabricated by engineered variation of the CNT growth rate within each microstructure, such as by patterning of the CNT growth catalyst partially upon a layer that retards the CNT growth rate. Here, we develop a finite-element simulation framework for predictive synthesis of complex CNT microarchitectures by this strain-engineered growth process. The simulation is informed by parametric measurements of the CNT growth kinetics and the anisotropic mechanical properties of the CNTs, and it predicts the shape of CNT microstructures with impressive fidelity. Moreover, the simulation allows us to visualize the internal stress distribution that results from extreme deformation of the CNT structures during growth and shows that delamination of the interface between the differentially growing segments occurs at a critical shear stress. Guided by these insights, we perform experiments to study the time- and geometry-dependent stress development and show that corrugating the interface between the segments of each microstructure mitigates the interface failure. Last, we present a methodology for 3D microstructure design based on "pixels" that prescribe directionality to the resulting microstructure and show that this framework enables the predictive synthesis of more complex architectures including twisted and truss-like forms.

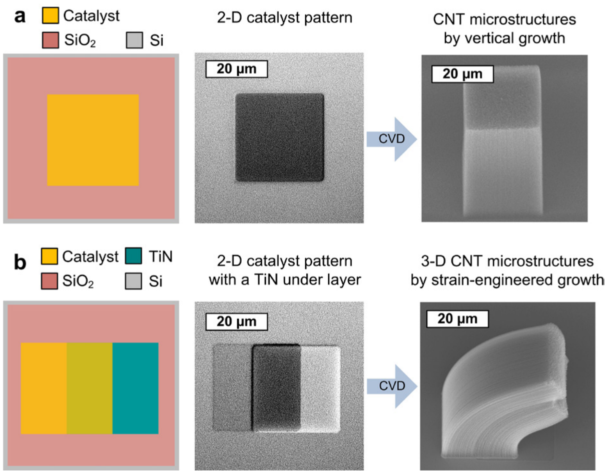

▲Figure 1: Catalyst pattern design and exemplary results for (a) vertical and (b) curved (strain-engineered) CNT microstructure growth.

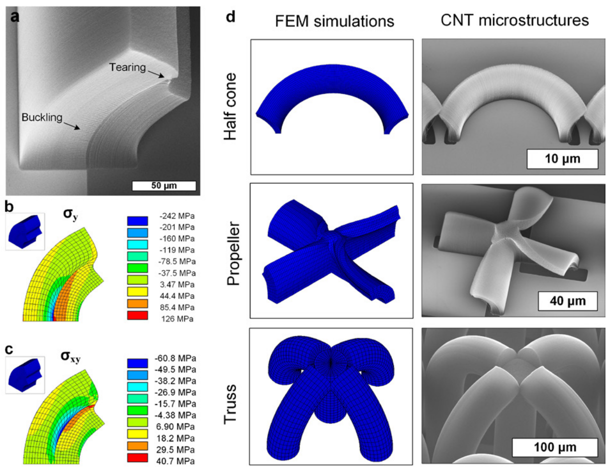

▲Figure 2: (a) SEM image of curved CNT microstructure showing tearing at the top of the interface and local CNT buckling lower along the interface. (b)-(c) Finite element method (FEM) simulations of axial and shear stress distributions. (d) Comparison of FEM simulations to SEM images for the "half cone," "propeller," and "microtruss" CNT microstructures.

FURTHER READING

- M. De Volder, S. J. Park, S. Tawfick, and A. J. Hart, "Strain-Engineered Manufacturing of Freeform Carbon Nanotube Microstructures," *Nature Communications*, vol. 5, pp. 4512, 2014.
- J. Meaud, T. Sain, B. Yeom, S. J. Park, A. Brieland-Shoultz, G. Hulbert, N. A. Kotov, A. J. Hart, E.M. Arruda, and A.M. Waas, "Simultaneously High Stiffness and Damping in Nanoengineered Microtruss Composites," *ACS Nano*, vol. 8, pp. 3468-3475, 2014.

Verified Nanoscale Engineering of Diamond Nitrogen-Vacancy Centers

M. E. Trusheim, D. Scarabelli, O. Gaathon, S. J. Wind, D. Englund
Sponsorship: AFOSR, DTRA

The nitrogen-vacancy (NV) center in diamond has been intensely investigated as a spin qubit in quantum information processing applications. Central to the implementation of these schemes is engineering NV centers on the scale of coherent dipole-dipole coupling. Here, we present and characterize a fabrication technique for creating arrays of NV centers on the 10-nm scale through implantation masking.

We begin with an Au/Cr stack on ultra-pure diamond and pattern apertures in a spin-coated PMMA layer using electron beam lithography (Figure 1a). After development, we perform angular evaporation of Ti, which serves as a hard mask for pattern transfer into the Au layer though Ar milling. The resulting nano-apertures have a diameter of ~10 nm and a 40- nm pitch (Figure 1b). We then implant ^{15}N with a predicted depth of 10 nm and masking isolation of $5*10^4$. Finally, we remove the masking layers and form NVs through wet chemical processes and thermal annealing.

Following fabrication, we image the resulting NV centers below the optical diffraction limit through wide-field super resolution microscopy. This technique, illustrated in Figure 1c-e, isolates photoluminescence (PL) from individual NV centers through selective magnetic resonance addressing (Figure 1d), allowing the reconstruction of their positions (Figure 1e). We then collect statistics on NV positions for different implantation aperture configurations, verifying that the produced NVs match the predicted distribution (Figure 1f).

We characterize the spin coherence properties of the NVs created through our process with Hahn echo and CPMG-N sequences. The array-average coherence time $T_{2,echo}$ = 10 μs was increased to $T_{2,CPMG\text{-}128}$ = 67 μs, with a relation $T_{2,CPMG\text{-}N} = T_{2\_1} * N^{\lambda}$ and scaling parameter λ= 0.69±0.05 describing the NV performance (Figure 1h). The NV coherence times achieved allow entanglement of NV pairs over a distance of 10 nm, comparable to the measured positioning accuracy.

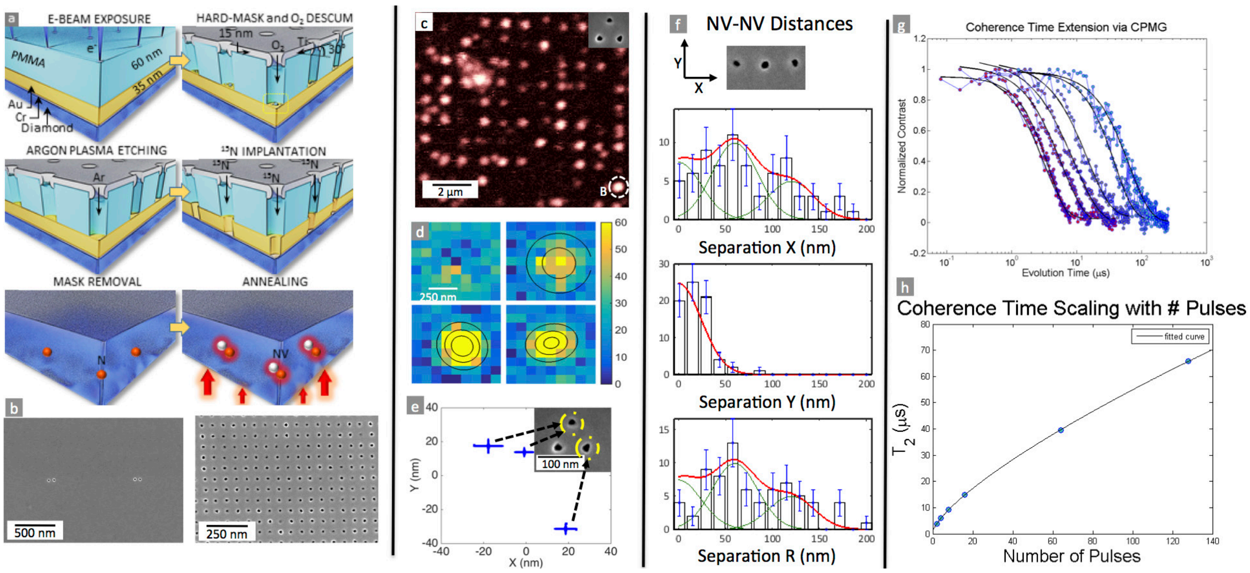

▲Figure 1: Engineered NV arrays. a) Fabrication process. b) Resulting mask apertures. c) PL image of an array of triangular aperture configurations. d) Spin contrast images of the indicated site in c). e) Reconstructed NV positions. f) Statistics on pairwise NV-NV spacings for implantation through a linear triple aperture configuration h) Scaling of T_2 with number of pulses.

FURTHER READING

- I. Bayn, *et al*, "Generation of Ensembles of Individually Resolvable Nitrogen Vacancies Using Nanometer-scale Apertures in Ultrahigh-aspect Ratio Planar Implantation Masks," *Nano Letters*, vol. 15, pp. 1751-1758, 2015.
- E. H. Chen, O. Gaathon, M. E. Trusheim, and D. R. Englund, "Wide-field Multispectral Super-resolution Imaging Using Spin-dependent Fluorescence in Nanodiamonds," *Nano Letters*, vol. 13, pp. 2073-2077, 2013.

Research on CMOS-Compatible High-K Dielectrics for Magnetic Memory

S. Kim, H. L. Tuller in collaboration with A. J. Tan, G. S. Beach
Sponsorship: CMSE/IRG, NSF

High-k dielectrics play a key role in modern microelectronic circuitry, given their ability to provide reduced leakage currents while providing adequate capacitance in ever smaller nano-dimensioned metal-oxide semiconductor field-effect transistor (MOSFET) devices. Recently, the Beach group at MIT demonstrated the ability to modulate the magnetic properties of transition metal thin films by electrical bias across thin films of Gd_2O_3. The reversible switching was demonstrated to be assisted by the electro-migration of oxygen ions to and away from the transition metal/Gd_2O_3 interface. This novel process, now called "magneto-ionic control" creates new opportunities for nonvolatile information storage. In this study, we have begun a more detailed examination of the properties of Gd_2O_3 and related oxides, to establish how their defects and nanostructures impact oxygen ion transport and, in turn, magneto-ionic device properties.

FURTHER READING

- U. Bauer, L. Yao, A. J. Tan, P. Agrawal, S. Emori, H.L. Tuller, S. van Dijken, and G. Beach, "Magneto-ionic Control of Interfacial Magnetism," *Nature Materials*, 14, 174-181, 2015.

Folding of Graphene Hinge Structures Dispersed in Solution

M. Hempel, T. Palacios, J. Kong
Sponsorship: AFOSR

Two-dimensional materials such as graphene, hexagonal boron nitride, and molybdenum disulfide have opened up a new chapter in electronics. They can be used to fabricate a variety of electronic devices from CMOS logic to photodetectors or sensors. Currently, however, devices made from 2D materials have been used only on flat surfaces, which do not exploit their full potential. Given the extreme thinness and flexibility of these materials, more sophisticated three-dimensional device structures can be imagined by using techniques such as folding and cutting, analogous to origami techniques.

In order to realize this vision, we are investigating the folding of strips of graphene in a controlled manner. The fabrication process of these hinges, as shown in Figure 1a-d, starts with an oxidized silicon piece with a sacrificial 40-nm- thick aluminum layer that is patterned by photolithography. Next, a monolayer of graphene is transferred and patterned into strips by a short oxygen plasma etching. Subsequently, a 50-nm-thick gold layer is deposited by electron beam evaporation and patterned by a lift-off process. The gold is used to anchor the graphene to the substrate on one side of the hinge as well as to stiffen the graphene film in between the joints. In the final step, the device is etched in a diluted (10%) hydrochloric acid solution, which dissolves the sacrificial aluminum layer and decouples the graphene from the surface.

After the fabrication process is completed, the silicon piece with graphene hinges is submerged in deionized water mixed with cholate hydroxide, which acts as a surfactant that keeps the graphene from sticking to itself.

So far, we have been able to pattern the graphene into strips and release them partially in solution. Figure 1e shows patterned and partially suspended graphene strips that were released from the substrate. The wrinkles and folds confirm that the strips are detached from the surface. In the future, our goal is to control this folding and buckling and to investigate the targeted folding of more advanced structures such as transistors, which would allow us to reduce the device footprint at equal performance.

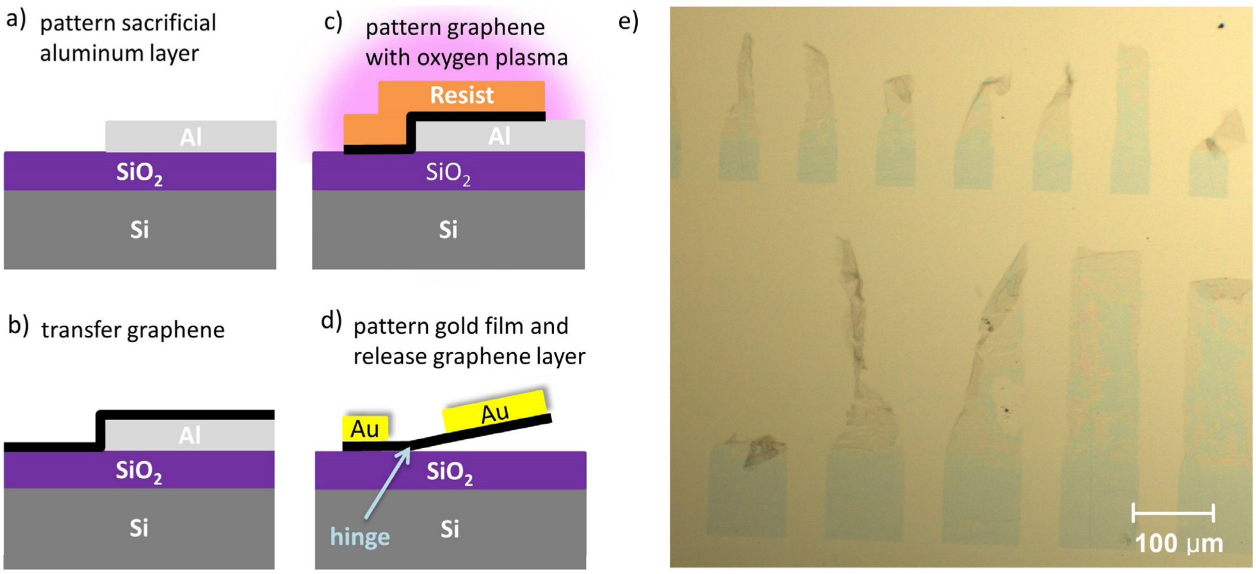

▲ Figure 1: a-d) Steps of fabricating a graphene hinge on an oxidized silicon substrate with gold film reinforcement, e) optical micrograph of partially floating graphene strips in solution. The wrinkles and folds confirm that the strips are detached from the surface.

FURTHER READING

- M. K. Blees, A. W. Barnard, P. A. Rose, S. P. Roberts, K. L. McGill, P. Y. Huang, A. R. Ruyack, J. W. Kevek, B. Kobrin, D. A Muller, and P. L. McEuen, "Graphene Kirigami," *Nature*, vol. 524, no. 7564, pp. 204-207, August 2015.
- J. Choi, H. J. Kim, M. C. Wang, J. Leem, W. P. King, and S. Nam, "Three-Dimensional Integration of Graphene via Swelling, Shrinking, and Adaptation," *Nano Letters*, vol. 15, pp. 4525–4531, June 2015.

Electrospray-Printed Graphene Oxide Nanostructured Humidity Sensor

A. P. Taylor, L. F. Velásquez-García
Sponsorship: Edwards Vacuum

Conductometric gas sensors based on the chemoresistive response of semiconducting metal oxide films are widely used due to their simplicity, flexibility in production, and broad applicability to many fields. Typically, the adsorption of a gas molecule on the surface of a metal oxide alters surface electronic properties, causing a change in electrical conductivity. Although many metal oxides could be used for gas sensing, only a few show the appropriate combination of adsorption ability, catalytic activity, sensitivity, and thermodynamic stability. These select metal oxides (e.g., SnO_2, TiO_2, and ZnO), however, are the least active from the catalytic point of view. To alleviate this problem, doping with redox-active noble metal nanoparticles, such as Pt, Au, and Pd, is done to enhance conductivity response. Unfortunately, noble metals are expensive, thereby precluding their use in low-cost applications. An appealing alternative material for reactive gas sensing is graphene oxide (GO) because of its high sensitivity to adsorbed surface species and compatibility with harsh environments.

We developed low-cost conductometric gas sensors t hat use an ultrathin film made of a matrix of GO nanoflakes as a transducing element. The devices were fabricated by lift-off metallization and near-room temperature, atmospheric pressure electrospray printing using a shadow mask. The sensors detect humidity at room temperature without requiring any post-heat treatment, harsh chemical reduction, or doping with metal nanoparticles. The printed GO devices (Figure 1) show a linear relationship between the resistance of the GO sensors and relative humidity in the 10-60% range (Figure 2); considering that they were fabricated with different electrospray printing recipes, the similarity between the linear response of the two devices suggests a common underlying physical sensing mechanism dependent on the intrinsic properties of the material. The power consumption of the printed sensors was estimated at 6 µW or less in the 10-60% relative humidity range.

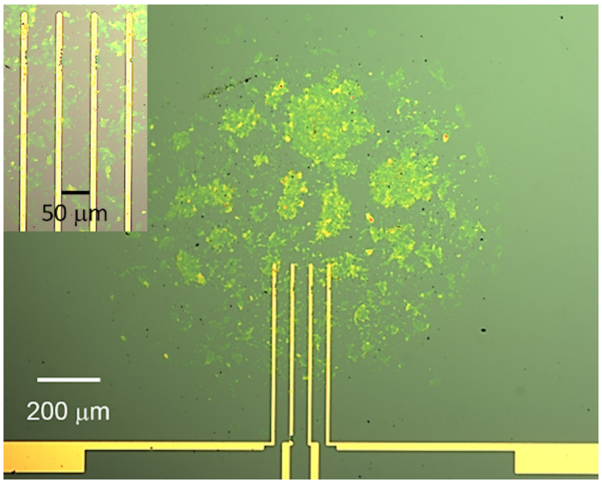

▲ Figure 1: Optical micrograph of a conductometric GO humidity sensor with a four-point probe electrode configuration and an inset showing a close-up view of the active area (top left corner). From A. P. Taylor and L. F. Velásquez-García, *Nanotechnology*, 2015.

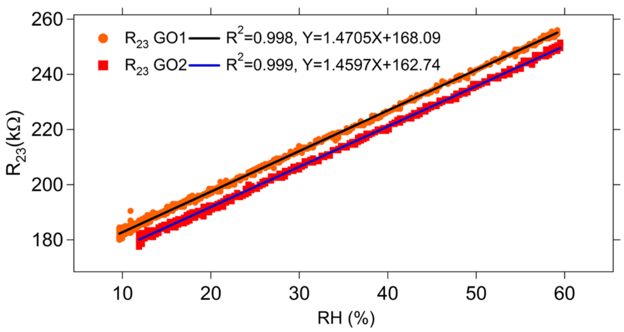

▲ Figure 2: Resistance versus relative humidity for two electrospray-printed GO sensors. From A. P. Taylor and L. F. Velásquez-García, *Nanotechnology*, 2015.

FURTHER READING

- F. A. Hill, E. V. Heubel, P. Ponce de Leon, and L. F. Velásquez-García, "High-Throughput Ionic Liquid Ion Sources Using Arrays of Microfabricated Electrospray Emitters with Integrated Extractor Grid and Carbon Nanotube Flow Control Structures," *Journal of Microelectromechanical Systems*, vol. 23, no. 5, pp. 1237-1248, 2014.
- A. P. Taylor and L. F. Velásquez-García, "Electrospray-Printed Graphene Oxide Nanostructured Gas Sensors," *Nanotechnology*, vol. 26, pp. 505301-505309, 2015.
- A. P. Taylor and L. F. Velásquez-García, "Microwatt-Powered, Low-Cost, Printed Graphene Oxide Humidity Sensors for Distributed Network Applications," *PowerMEMS 2015, Journal of Physics: Conference Series*, vol. 660, pp. 12134-12139, 2015.

3D Printing of Electronic 2D Materials

E. McVay, T. Palacios
Sponsorship: NASA

In this project we are meshing 3D printing and inkjet technology to apply two-dimensional materials on a large scale to create "smart objects" that can sense and process their environment. We are modifying a 3D printer to give it inkjet and extrusion printing capabilities, as well as developing 2D material inks and designing the device and circuit applications that this system will be applied to make. The printer can extrude standard polylactic acid plastic, conductive filaments, and flexible substrate materials; it is also fitted with a STMicroelectronics inkjet head that is well suited for printing the 2D material inks (see Figure 1). Thus far we have focused on printing graphene oxide, molybdenum disulfide (MoS_2), and tungsten diselenide (WSe_2) flakes. The graphene oxide prints can be reduced to graphene via laser sintering to achieve a sheet resistance of 680 ohms/square; these traces can also function as strain sensors. We are developing MoS_2 dispersions with the goal of using this material to print the channel layer of a transistor, as MoS_2 transistors have shown even higher sensitivity than graphene in light and gas-sensing applications. Furthermore, we have developed WSe_2 dispersions which, when printed and contacted with platinum, show a photo-responsive current (see Figure 2). With WSe_2 and printed metals, we can begin to fabricate solar cells that can provide energy to the proposed sensing system. The end goal of this project is to demonstrate the use of 2D materials in sensor, energy harvesting, and energy storage circuit blocks to create "smart skins" that can be used in applications from monitoring the structural integrity of machinery to keeping track of a person's health through smart textiles.

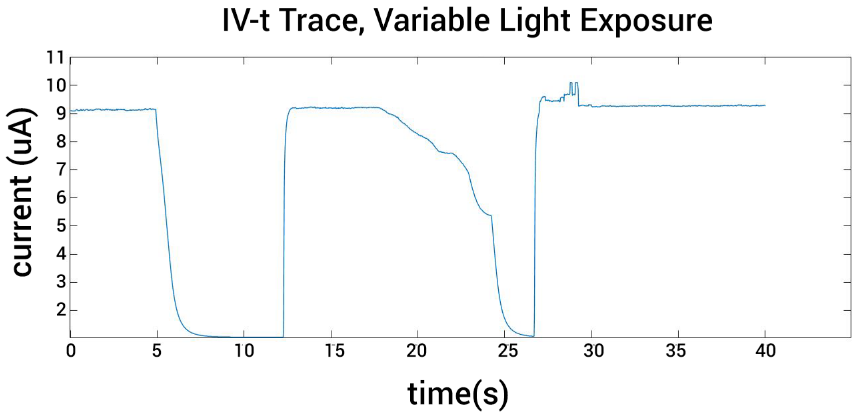

◀ Figure 1: Graphene-WSe2-platinum light sensor (area = 0.25 cm^{-2}) current output with response to pulsed light (200 W/cm^2), over time. Figure 1: The 3D printer with dual extruders and inkjet printhead (attached behind the dual extruders, shown in the upper right-hand corner).

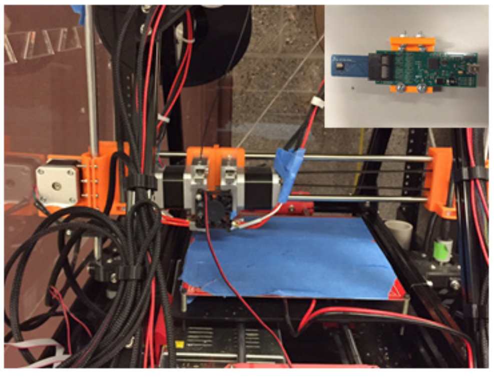

◀ Figure 2: The 3D printer with dual extruders and inkjet printhead (attached behind the dual extruders, shown in the upper right-hand corner).

FURTHER READING

- M. F. El-Kady, V. Strong, S. Dubin, and R. B. Kaner, "Laser Scribing of High-Performance and Flexible Graphene-Based Electrochemical Capacitors," *Science*, vol. 335, no. 6074, pp. 1326-1330, 2012.
- S. Wang, P. K. Ang, Z. Wang, A. L. L. Tang, J. T. L. Thong, and K. P. Loh, "High Mobility, Printable, and Solution-Processed Graphene Electronics," *Nano Letters*, vol. 10, pp. 92-98, 2010.
- D. Sarkar, W. Liu, X. Xie, A. Anselmo, S. Mitragotri, and K. Banerjee, "MoS2 Field-Effect Transistor for Next-Generation Label-Free Biosensors," *ACSNano*, vol. 8, no. 4, pp. 3992-4003, 2014.

A Rational Strategy for Transferring Graphene onto Rough Substrates

J.-Y. Hong, J. Kong
Sponsorship: NSF Center for Integrated Quantum Materials

Degradation in the intrinsic properties of chemical vapor deposition (CVD)-grown graphene, as a result of the imperfect transfer process, is a crucial issue that must be solved for successful applications of graphene. Here, we develop a very simple, yet effective, approach, based on distinctive features (i.e., physical, mechanical, and chemical properties) of ethylene vinyl acetate (EVA) as a support/carrier material, for transferring CVD-grown graphene from a growth substrate onto rough substrates. This novel and facile method not only results in satisfactory transfer on substrates with terraces or grooves, but also gives rise to a successful result for uneven growth substrates (textured and also crumpled).

Under our experimental condition, the elastic modulus (E) values of the polymer/graphene films were estimated as 995.0 ± 5.0 and 46.5 ± 1.5 MPa for the poly(methyl methacrylate) (PMMA)/graphene and EVA/graphene films, respectively (Figures 1a and b). It should be noted that the approximately one-twentieth-lower E value of the EVA/graphene film implies a tremendously lower stiffness in comparison with the PMMA/graphene film, and it is also anticipated that the EVA/graphene film would follow the surface of the underlying substrate much better and have a tighter attachment to the surface (Figure 1c and d).

Figure 2 shows the optical microscopy (OM) and atomic force microscopy (AFM) images of graphene on SiO_2/Si substrates obtained by the conventional PMMA-supported transfer process and the EVA transfer process. White arrows in Figure 2a and c indicate the PMMA residues on graphene as are typically observed while for the EVA case such residues can hardly be found. Furthermore, wrinkles can be clearly seen in the PMMA-transferred graphene (black arrow in Figure 2a and c) but are much less frequently seen in the hot-water bath EVA-transferred graphene. Consequently, the graphene transferred with EVA support/carrier material exhibits superior electrical performance compared with most presently used transfer methods.

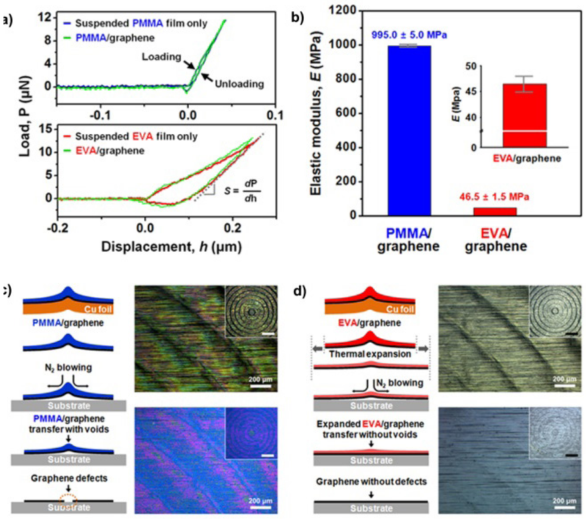

▲Figure 1: Representative (a) load–displacement curves and (b) E values for polymer/graphene films. Comparison of thermal expansion effects between (c) PMMA/graphene and (d) EVA/ graphene during the transfer process.

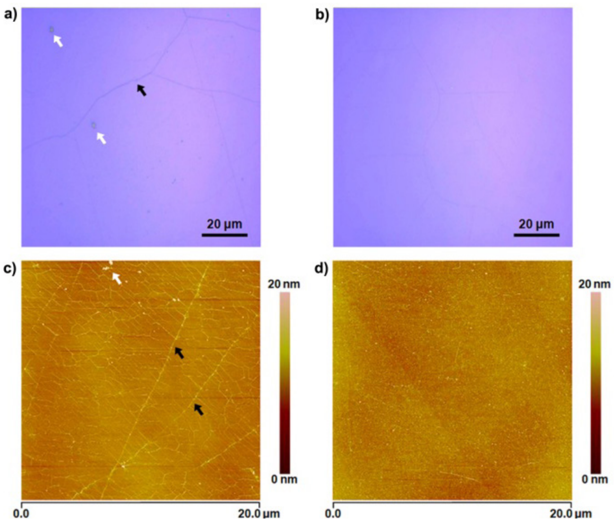

▲Figure 2: The OM and AFM images of monolayer graphene transferred to 300-nm SiO_2/Si substrate by using the (a, c) PMMA-supported and (d) EVA-supported transfer methods.

FURTHER READING

- J.-Y. Hong, Y. C. Shin, A. Zubair, Y. Mao, T. Palacios, M. S. Dresselhaus, S. H. Kim, and J. Kong, "A Rational Strategy for Graphene Transfer on Substrates with Rough Features," *Advanced Materials*, vol. 28, pp. 2382-2392, 2016.

Large-Area Synthesis of High-Quality Uniform Few-Layer $MoTe_2$

L. Zhou, K. Xu, A. Zubair, J. Kong, M. S. Dresselhaus
Sponsorship: NSF, ONR

Two-dimensional transition metal dichalcogenides (TMDs) have been attracting increasing interest owing to their unique structures and remarkable properties, which make them promising materials for a wide range of applications related, for example, to electronics, optoelectronics, valleytronics, spintronics, and catalysis. Because of the smaller bandgap compared with other group VI TMDs, single- and few-layer $MoTe_2$ holds promise for use in easily controllable ambipolar field-effect transistors and extends the operating range of TMD optoelectronic devices from the visible to the near-infrared range. In particular, the bandgap, which is quite close to that of Si (~ 1.1 eV); the strong absorption throughout the solar spectrum; and the strong spin-orbit coupling suggest that $MoTe_2$ is a highly attractive material for use in electronic devices, photovoltaic devices, spintronic, and valley-optoelectronic devices. A crucial step toward the practical application of $MoTe_2$ in electronics and optoelectronics is the controlled production of high-quality, large-area, and atomically thin $MoTe_2$ films. Thus far, single- and few-layer $MoTe_2$ have been achieved only using "top-down" exfoliation methods. Thus a technology for the mass-production of high-quality, large-area, and atomically thin $MoTe_2$ films is highly desirable. Our group has developed a chemical vapor deposition (CVD) synthesis to produce large-area, uniform, and highly crystalline few-layer 2H and 1T´ $MoTe_2$ films. We found that these two different phases of $MoTe_2$ can be grown based on the choice of Mo precursor. The resulting $MoTe_2$ phase and the efficiency of the tellurization are both strongly dependent on the oxidation state of the Mo precursor. Mo film was deposited onto a SiO_2/Si substrate by electron beam evaporation. Then, the Mo film was fully oxidized in air and changed to MoO_3. The resulting MoO_3 film was placed in a ceramic crucible containing Te powder in CVD system and was tellurized into a $MoTe_2$ film after annealing in tellurium vapor at 700 ˚C. The film is uniform and continuous across the whole area, as can be seen from the homogeneous color contrast in the image (Figure 1). When using Mo (instead of MoO_3) as a precursor, a 1T′ $MoTe_2$ film (Figure 2) can also be grown under the same growth conditions mentioned above. Due to the high crystalline structure, the as-grown few-layer 2H $MoTe_2$ films display electronic properties that are comparable with those of mechanically exfoliated MoTe2 flakes. Since our high-quality, atomically thin $MoTe_2$ films are highly homogenous, and the size of the films is limited only by the size of the substrate, our growth method paves the way for large-scale application of $MoTe_2$ in high-performance nanoelectronics and optoelectronics.

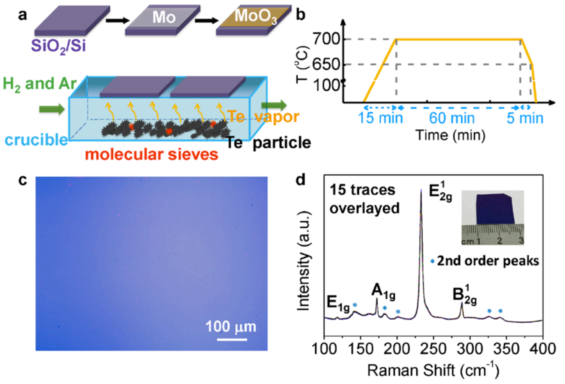

▲ Figure 1: Synthesis of 2H $MoTe_2$. (a) Illustration of $MoTe_2$ CVD process. (b)Temperature-controlled sequence used for a typical growth of $MoTe_2$. (c)Typical optical image of an as-synthesized $MoTe_2$ film on a 300nm SiO_2/Si substrate. (d)Raman spectra of a $MoTe_2$ film at 15 different locations on the sample. Inset: Photograph of a $MoTe_2$ film on a 1.6×1.8 cm^2 SiO_2/Si substrate.

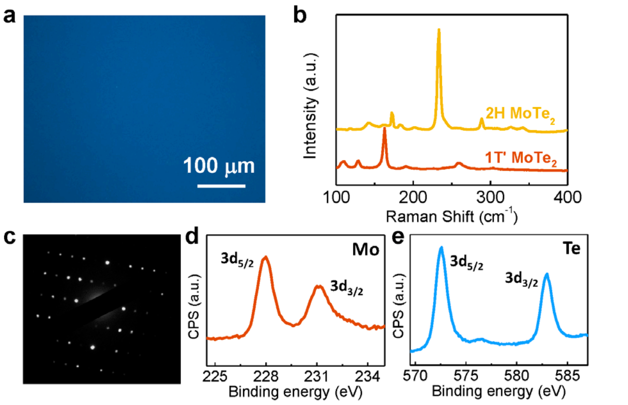

▲ Figure 2: Characterizations of the resulting 1T′ $MoTe_2$ film. (a) Typical optical image of an as-synthesized 1T' $MoTe_2$ film on 300nm SiO_2/Si. (b) Raman spectra of 1T′ (red) compared to 2H (orange) $MoTe_2$ films. (c) SAED pattern for the 1T′ $MoTe_2$. (d & e) High-resolution XPS spectra for Mo 3d (d) and Te 3d (e) spectra of a 1T′ $MoTe_2$ film.

FURTHER READING

- Y.-F. Lin, Y. Xu, S.-T. Wang, S.-L. Li, M. Yamamoto, A. Aparecido-Ferreira, W. Li, H. Sun, S. Nakaharai, W.-B. Jian, K. Ueno, K. Tsukagoshi, "Ambipolar $MoTe_2$ Transistors and Their Applications in Logic Circuits," *Adv. Mater.*, vol. 26, issue 20, pp. 3263, 2014.
- C. Ruppert, O. B. Aslan, and T. F. Heinz, "Optical Properties and Band Gap of Single- and Few-Layer $MoTe_2$ Crystals," *Nano Letters*, vol. 14, no 11, pp. 6231, 2014.
- D. H. Keum, S. Cho, J. H. Kim, D.-H. Choe, H.-J. Sung, M. Kan, H. Kang, J.-Y. Hwang, S. W. Kim, H. Yang, K. J. Chang, Y. H. Lee, "Bandgap Opening in Few-Layered Monoclinic $MoTe_2$," *Nat. Phys.*, vol. 11, pp. 482, 2015.

Photonics and Optoelectronics

Stochastic Simulation and Robust Design Optimization of Integrated Photonic Filters

T. W. Weng, D. Melati, A. Melloni, L. Daniel
Sponsorship: NSF

Photonics is rapidly emerging as a mature and promising technology, and it is evolving from a pure research topic to a market-ready player, aiming at achieving large production volumes and small fabrication costs. Pushed by these motivations, process design kits, circuit simulators, generic foundry approaches, and multi-project-wafer runs are quickly changing the way that photonic circuits are conceived and designed. On the other hand, stochastic uncertainties such as fabrication variations are unavoidable in production processes. It is well known that such uncertainties can have a dramatic impact on the functionality of fabricated circuits. In order to obtain a high quality design of a photonic circuit, it is important to include such uncertainties during the early design stages. Hence, uncertainty quantification techniques become fundamental instruments to efficiently obtain the statistical information and to achieve a high-quality design.

Monte Carlo simulation is commonly exploited to evaluate the impact of fabrication uncertainties on the functionality of the designed circuits. Although effective, it suffers from a slow convergence rate and requires long computation time. Meanwhile, stochastic spectral methods have recently been regarded as a promising alternative for statistical analysis due to their fast convergence. The key idea is to approximate the output quantity of interest (e.g., the bandwidth of a filter) with a set of orthonormal polynomial basis functions, known as generalized polynomial chaos expansion. Our goal in this work is to develop an efficient, robust design-optimization technique based on the state-of-the-art sampled-based stochastic spectral methods, which are mainly used for statistical analysis in the field of uncertainty quantification. Figure 1 shows a fifth-order directly coupled ring resonator used to demonstrate our technique. Due to fabrication process variations, the gap g and effective phase index neff of each ring resonator are uncertain, so the 3dB bandwidth varies greatly. In this example, we would like to design the nominal gap g for each ring that minimizes the mean-square-error of 3dB bandwidth. Figure 2 plots simulation results of the un-optimized nominal design and optimized nominal design. We show that the optimized circuits are more robust to fabrication process variations and achieve a reduction of 11 % to 35 % in the mean-square-errors of the 3dB bandwidth compared to un-optimized nominal designs.

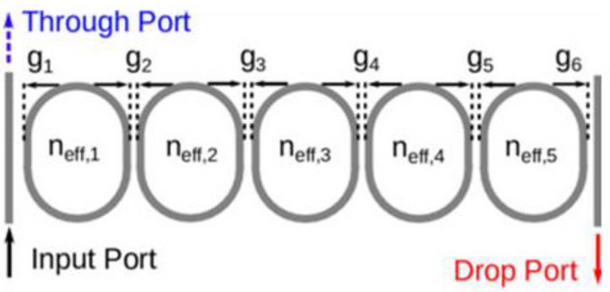

▲ Figure 1: A 5-ring coupled resonator.

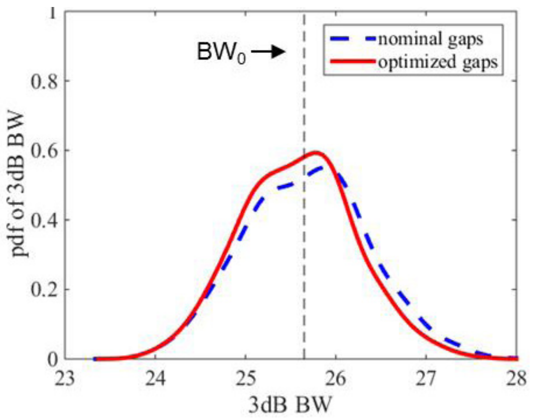

▲ Figure 2: Probability density functions of 3dB. Bandwidth if the un-optimized nominal design (blue dash line) and optimized nominal design (red line).

FURTHER READING

- D. Melati, A. Alippi, and A. Melloni, "Waveguide-based Technique for Wafer-level Measurement of Phase and Group Effective Refractive Indices," *Journal of Lightwave Technology*, pp. 99:1-1, 2015.
- D. Xiu and G. E. Karniadakis, "Modeling Uncertainty in Flow Simulations via Generalized Polynomial Chaos," *Journal of Computational Physics*, vol. 187, pp. 137-167, 2003.

Germanium Photodetectors on Amorphous Substrates for Electronic-Photonic Integration

B. S. Pearson, L. C. Kimerling, J. Michel
Sponsorship: ARPA-E

Silicon photonics has emerged as a leading technology to overcome the bandwidth and energy efficiency bottlenecks of standard metal interconnects. Integration of photonics in the back-end-of-line (BEOL) of a standard CMOS process enables the advantages of optical interconnects while benefiting from the low-cost of monolithic integration. However, processing in the BEOL requires device fabrication on amorphous substrates and constrains processing to ≤450˚C. A germanium photodetector was fabricated while adhering to these processing constraints in order to demonstrate a proof of concept for BEOL integration.

Crystalline Ge was grown on SiO_2 by selective deposition in geometrically confined channels. The emerging Ge grains were coalesced to fill a lithographically defined trench, forming the active area of a photodetector. The Ge was measured to have a tensile strain of 0.5%, which was caused by thermal expansion mismatch with the substrate, and concentrated by small voids from imperfect coalescence. The resolved shear stress was determined to be below the critical resolved shear stress, verifying that dislocation generation does not occur in this material. The strain was shown to increase the absorption of Ge at long wavelengths, allowing for implementation along the entire telecom window.

A Schottky barrier to *p*-type Ge was developed by the addition of a 1-nm tunneling Al_2O_3 layer between an Al/Ge metal contact. This de-pinned the Fermi level, creating a barrier height of 0.46eV. The Schottky contacts enabled the fabrication of metal-semiconductor-metal (MSM) photodetectors on epitaxial Ge with dark current densities of 2.1 x 10^{-2} Acm^{-2}. Gain was observed in these photodetectors, with internal quantum efficiencies (IQE) of 405%. MSM detectors were also made using Ge on SiO_2, exhibiting an IQE of 370%. This is the first demonstration of IQE > 100% in a Ge MSM or *pin* photodetector and proves the feasibility of making high-performance active photonic devices while adhering to BEOL processing constraints.

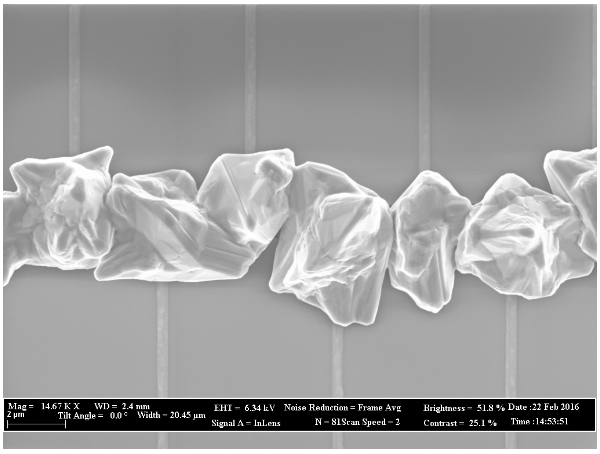

▲Figure 1: Plane-view SEM image of coalesced Ge grains that are grown on SiO_2 at 450 °C. After planarization, this serves as the active material for BEOL-compatible MSM photodetectors.

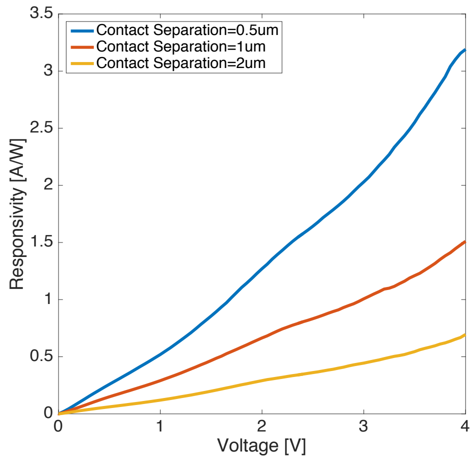

▲Figure 2: Responsivity of crystalline Ge MSM photodetectors with different contact separations under 980-nm illumination. An IQE of 405% is measured at a bias of 4 V and contact separation of 0.5 µm.

Superconducting Nanowire Single-photon Detector on Aluminum Nitride

D. Zhu, H. Choi, T.-J. Lu, Q. Zhao, A. Dane, F. Najafi, D. R. Englund, K. K. Berggren
Sponsorship: DARPA, AFOSR, NSF

Superconducting nanowire single-photon detectors (SNSPDs) offer high detection efficiency, low timing jitter, low dark counts, short reset time, and broad spectral response. This unique combination of properties has made SNSPDs an attractive choice for quantum information processing applications. Recent advances in photonic integrated single-photon sources and quantum memories have created increasing demand for on-chip integration of high performance SNSPDs, toward realizing a complete on-chip photonic quantum processor. Among various waveguide materials, aluminum nitride (AlN) stands out as a promising candidate. It has a broad spectral window of transparency, intrinsic electro-optic and piezoelectric properties, and a low fluorescence rate. To date, direct fabrication of high efficiency SNSPDs on AlN has not been demonstrated.

We have now successfully fabricated high-efficiency niobium nitride (NbN) SNSPDs on AlN-on-sapphire substrates. The NbN thin films were deposited using reactive DC magnetron sputtering at 840^{O}C. The films had a thickness of ~5 nm, critical temperature of 10.6–11.4K, and sheet resistance of 500–550 Ω/square. We adopted a 2-element superconducting nanowire avalanche photodetector (2-SNAP) design with 60-nm wire width to achieve high quantum efficiency and signal-to-noise ratio. Figure 1 shows scanning electron micrographs (SEM) of fabricated devices. The devices were tested at 2.45K under 1550-nm illumination and showed saturated detection efficiency (an indication of high internal quantum efficiency), sub-60-ps jitter, and ~6 ns reset time (see Figure 2). The devices were designed for integration on AlN single mode waveguides operating at 637-nm wavelength, corresponding to the zero-photon line of nitrogen vacancy centers in diamond. Since the quantum efficiency of SNSPDs increases with photon energy, we expect more prominent saturation behavior at 637 nm. We are now working towards fabricating AlN waveguides on the detector chips and integrating single-photon sources and quantum memories to realize a full single-photon quantum circuit.

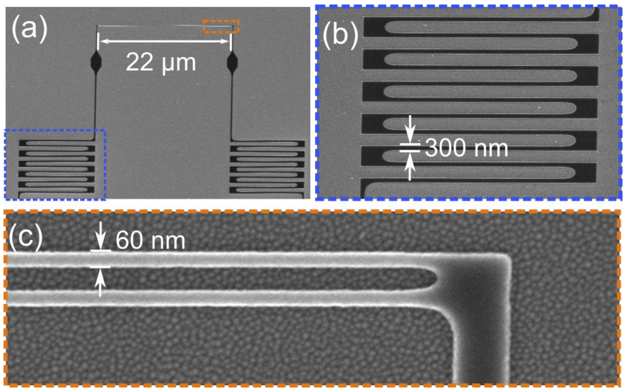

▲ Figure 1: (a) SEM of the fabricated device. (b) The serial inductor region, made of 300-nm-wide meander nanowires. (c) The active region of the detector, which consists of two parallel nanowires with 60-nm width, 80-nm gap, and 22-μm length.

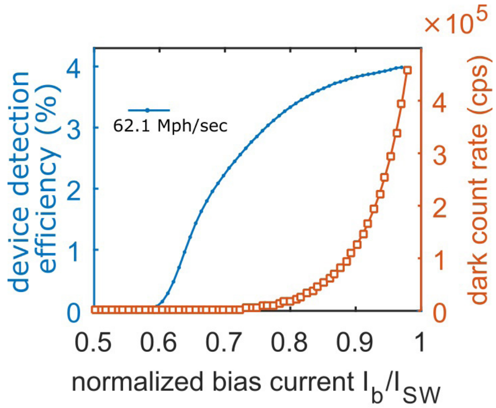

▲ Figure 2: Detection efficiency and background count rate vs. bias current. The detection efficiency enters the saturation region when bias current approaches the switching current. The absolute value in DE was limited by the unpolished back surface of the chip.

FURTHER READING

- G. N. Gol'tsman, O. Okunev, G. Chulkova, A. Lipatov, A. Semenov, K. Smirnov, B. Voronov, A. Dzardanov, C. Williams, and R. Sobolewski, "Picosecond Superconducting Single-photon Optical Detector," *Appl. Phys. Letters*, vol. 79, pp. 705, 2001.
- C. Xiong, W. H. P. Pernice, X. Sun, C. Schuck, K. Y. Fong, and H. X. Tang, "Aluminum Nitride as a New Material for Chip-scale Optomechanics and Nonlinear Optics," *New Journal of Physics*, vol. 14, no. 9, pp. 095014, 2012.
- F. Marsili, F. Bellei, F. Najafi, A. E. Dane, E. A. Dauler, R. J. Molnar, and K. K. Berggren, "Efficient Single Photon Detection from 500 nm to 5 μm Wavelength," *Nano Letters*, vol. 12, pp. 4799–4804, 2012.

Temporally and Spatially Resolved Photon-sensing in a Slow-wave Nanowire

Q. Zhao, D. Zhu, N. Calandri, F. Bellei, A. N. McCaughan, A. E. Dane, H. Wang, D. F. Santavicca, K. K. Berggren
Sponsorship: NSF, AFOSR

We have demonstrated spatially- and time-resolved photon counting in a single superconducting nanowire, which was designed as a slow-wave transmission line. We were able to discriminate where and when photons landed along a continuous nanowire of 20-mm-long and 300 nm wide. Instead of using an array of discrete photodetectors to acquire an optical image, the slow-wave nanowire (SWN) is meandered into a 286 µm × 193 µm square and has an equivalent pixel number of over 300. In addition to this spatial resolution, the arrival time of each photon was simultaneously resolved with a timing jitter of 100 ps for photons with a wavelength of 1.5 µm.

The spatial and temporal photodetection information was read out by measuring the difference and sum of the pulse arrival times on the nanowire's two outputs, respectively. This method was possible because we designed our superconducting nanowire such that it behaved not only as a single-photon detector, but also as a slow-wave transmission line. When a photon is absorbed, creating a hotspot, two electrical pulses are generated and propagate towards the two ends of the nanowire. By measuring the arrival times of the two electrical pulses, we determined the location of photon absorption from the difference and the photon arrival time from the sum. Signals propagate along the nanowire at a velocity of several percent of the speed of light, tens of times slower than an identical transmission line made from normal metals because the nanowire has high kinetic inductance. Combining the slow-wave transmission line with our 3 ps electrical timing uncertainty allows us to determine the position at which the photon was observed to a precision of 30 µm.

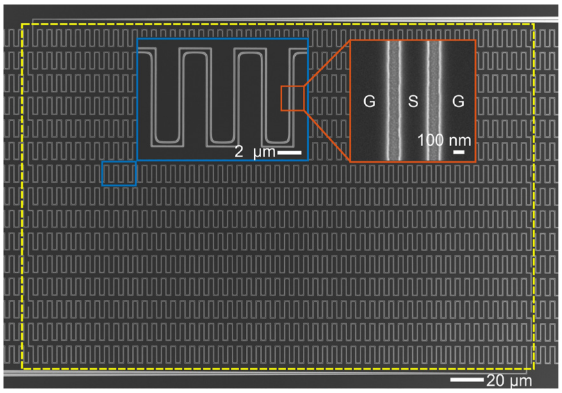

▲ Figure 1: SEM image of the slow-wave nanowire. We designed the nanowire into a coplanar waveguide. The signal line, a 300-nm-wide nanowire with a 100-nm-wide gap to the ground plan, is made from the same NbN film. The total length of the slow-wave nanowire (SWN) is 20 mm.

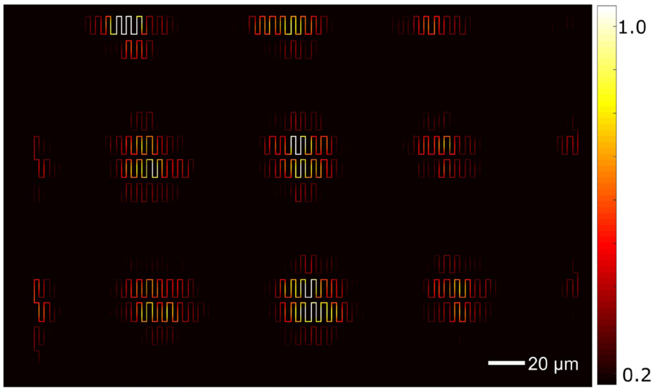

▲ Figure 2: An optical image taken by the slow-wave nanowire. The wavelength of the light used is 780 nm. A metal mesh with a period of 75 µm was put on top of the imager to create this pattern.

FURTHER READING

- Q. Zhao, A. McCaughan, F. Bellei, F. Najafi, D. De Fazio, A. Dane, Y. Ivry, and K. K. Berggren, "Superconducting-nanowire Single-photon-detector Linear Array," *Appl. Phys. Letters*, vol. 103, no. 14, pp. 142602, 2013.
- H. T. Su, Y. Wang, F. Huang, and M. J. Lancaster, "Superconducting Delay Lines," *Journal of Supercond. Nov. Magn.*, vol. 21, pp. 7–16, 2008.

Development of Compact and Scalable Packaging for a Fiber-Coupled Single-Photon Detector Array

F. Bellei, D. Zhu, H. Choi, L. Archer, J. Mower, D. Englund, K. K. Berggren
Sponsorship: ONR, DARPA, AFOSR

Superconducting nanowire single-photon detectors (SNSPDs) combine high speed, low timing jitter, and high detection efficiency, making them suitable for quantum-secured communications. We are developing a package to couple an array of single-mode 1550-nm-wavelength optical fibers to an array of SNSPDs. Unlike previous coupling methods, our design uses the high density of single-mode fiber arrays to integrate eight detectors, coupled one-to-one, to optical fibers within an area $<1\,\mathrm{cm} \times 1\,\mathrm{cm}$. Figure 1(a) shows the CAD design of the package. The fiber array was glued to the SNSPD chip and attached to a copper mount with a clamp. The chip was wire-bonded to an eight-channel PCB for read-out. The copper mount was designed to mount in a closed-cycle cryostat. Figure 1(b) shows a schematic of the alignment method. The detectors were spaced on the chip to match the pitch of the fiber array.

The SNSPD chip and the fiber array were aligned using an IR imaging system. After gluing we dipped the chip and array in liquid helium and verified that the glue resisted the thermal cycling. We fabricated a 32-element series-2-superconducting nanowire avalanche photodetector) array with 250-µm pitch matching the 32-element fiber array spacing. The fiber array was controlled on two rotational axes and one translational axis. The chip was controlled on the two orthogonal translational axes for a total control on five axes. We are currently integrating the detector chip in a cryostat with base temperature of 2.9 K, which will become the eight-channel single-photon receiver. We will use this system in flood-light quantum key distribution experiment.

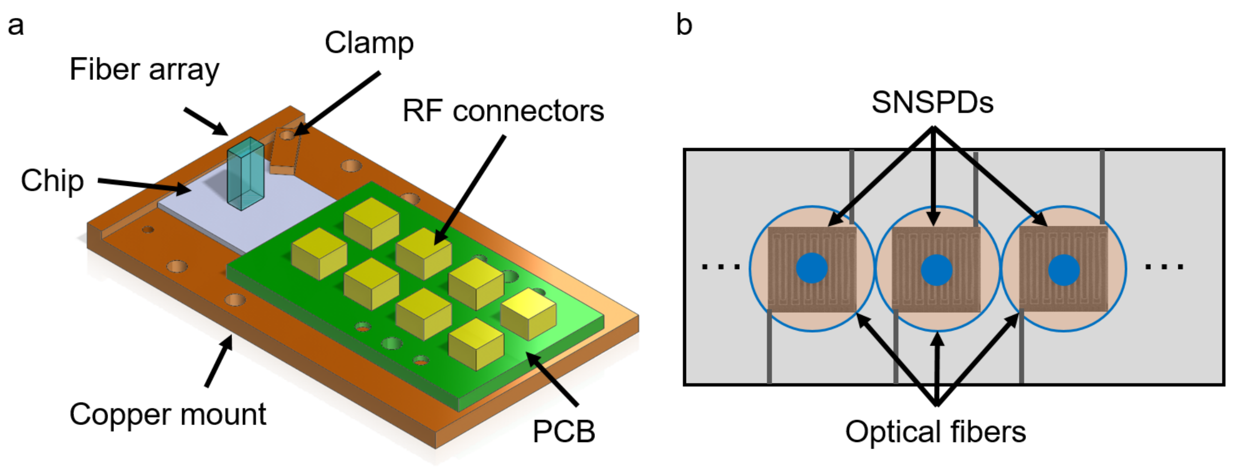

▲ Figure 1. (a) CAD design of the package holding the SNSPD chip and fiber array. (b) Schematic of three detectors of the SNSPD array aligned to three elements of the fiber array. We use the high precision of micro-fabrication techniques to match the detectors' spacing to the fibers' pitch.

FURTHER READING

- G. N. Gol'tsman, O. Okunev, G. Chulkova, A. Lipatov, A. Semenov, K. Smirnov, B. Voronov, A. Dzardanov, C. Williams, and R. Sobolewski, "Picosecond Superconducting Single-photon Optical Detector," *Appl. Phys. Letters*, vol. 79, no. 6, pp. 705, 2001.
- F. Bellei, A. P. Cartwright, A. N. McCaughan, A. E. Dane, F. Najafi, Q. Zhao, and K. K. Berggren, "Free-space-coupled Superconducting Nanowire Single-photon Detectors for Infrared Optical Communications," *Opt. Express*, vol. 24, no. 4, pp. 3248, February 2016.

Light Modulators for Holographic Video Displays

V. M. Bove, Jr., S. Jolly, N. Savidis, B. Datta
Sponsorship: MIT Media Lab Research Consortium, Center for Terrestrial Sensing, AFRL

In this research (a collaboration with Dr. Daniel Smalley of Brigham Young University), we design and fabricate acousto-optic, guided-wave modulators in proton-exchanged lithium niobate for use in holographic and other high-bandwidth displays. Guided-wave techniques make possible the fabrication of modulators that are higher in bandwidth and lower in cost than analogous bulk-wave acousto-optic devices or other spatial light modulators used for diffractive displays; these techniques enable simultaneous modulation of red, green, and blue light. In particular, we are investigating multichannel variants of these devices with an emphasis on maximizing the number of modulating channels to achieve large total bandwidths. To date, we have demonstrated multichannel full-color modulators capable of displaying holographic light fields at standard-definition television resolution and at video frame rates. Figures 1 and 2 show a schematic diagram of our device and an image displayed using it, respectively. Our current work explores a variant of this technology that is suitable for wearable holographic displays, fabricated using femtosecond laser micromachining.

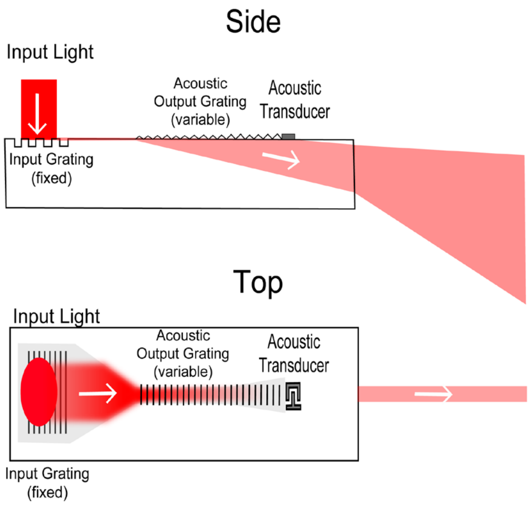

▲ Figure 1: Diagram of our modulator (one channel).

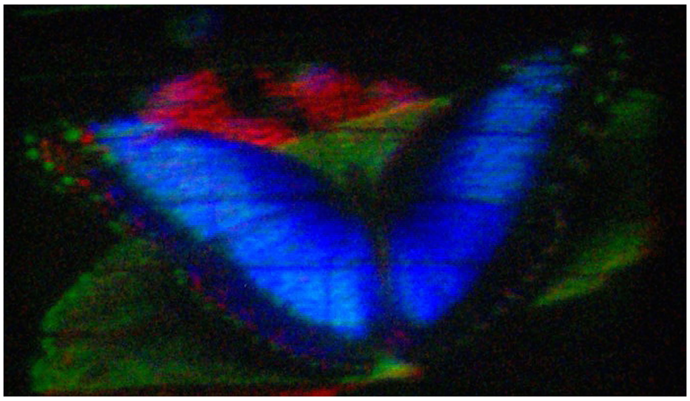

▲ Figure 2: Color holographic image displayed using our modulator.

FURTHER READING

- D. E. Smalley, Q. Y. J. Smithwick, V. M. Bove, Jr., J. Barabas, and S. Jolly, "Anisotropic Leaky-mode Modulator for Holographic Video Displays," *Nature*, vol. 498, pp. 313-317, 2013.
- N. Savidis, S. Jolly, B. Datta, T. Karydis, and V. M. Bove, Jr., "Fabrication of Waveguide Spatial Light Modulators via Femtosecond Laser Micromachining," *SPIE Advanced Fabrication Technologies for Micro/Nano Optics and Photonics IX*, pp. 9759, 2016.
- S. Jolly, N. Savidis, B. Datta, V. M. Bove, Jr., and D. Smalley, "Progress in Off-plane Computer-generated Waveguide Holography for Near-to-eye 3D Display," *SPIE Practical Holography XXX: Materials and Applications*, pp. 9771, 2016.

Lab-on-Chip Dark-Field Imaging Device with Tunable Emission Profile

C. Chazot, Y. Kim, I. Coropceanu, M. Bawendi, M. Kolle
Sponsorship: MTL, MISTI

Dark-field microscopy is a well-known imaging technique used to enhance the contrast in unstained samples by suppressing low spatial frequency contributions (areas of uniform intensity), thereby emphasizing high spatial frequency components (for instance edges) in the image. The sample is illuminated with light incident on the sample at a high angle that is not collected by the objective lens, unless it is scattered by the imaged object. Even though it is a simple method that provides high-quality images, it usually requires a classic bulky optical microscope, with dedicated objectives and filtering cubes. Here, we present research aimed at creating a lab-on-chip dark-field imaging device, which can provide dark-field imaging capabilities without the need for sophisticated equipment. We produce a micro-patterned fluorescent surface with a spatially tunable light emission profile, consisting of quantum dots in a polymer matrix sandwiched between a Bragg reflector on the top and semi-spherical micro-concavities at the bottom. While the quantum dots emit light in all directions, the confinement between the Bragg mirror and the semi-spherical cavities allow light to exit from the surface only in a limited angle range. The color of the emitted light is determined by the quantum dots' emission spectrum, while directionality is imposed by the stop band of the Bragg reflector. Tuning of the Bragg reflector band-gap, or the combination of Bragg reflectors with different band-gaps, allows for the creation of a rich variety of light emission profiles. To maximize light emission in the desired limited angle range, an array of bioinspired, hexagonally arranged semi-spherical gold micro-reflectors is used. Each patterned surface measures 1" x 1", and more than 10 Bragg reflectors can be assembled on it, providing the same number of dark-field imaging ring profiles. A sample placed on top of the surface will be illuminated with light of the desired angular distribution only, which for dark-field imaging would be at angles larger than the numerical aperture of the imaging objective. This surface with tailorable light emission profiles constitutes a highly compact, simple, tunable solution for dark-field imaging, and it could for instance find application in miniaturized imaging devices for microbiology.

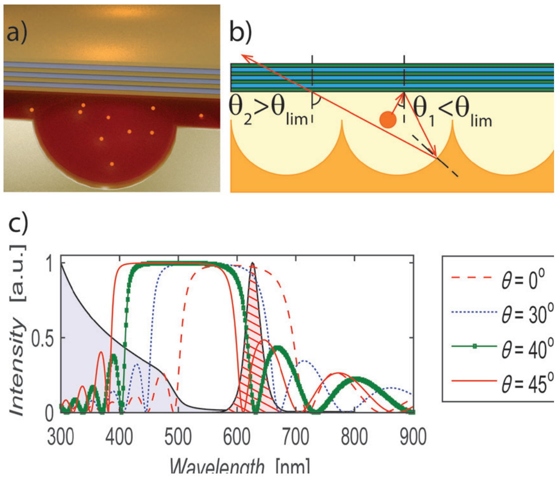

▲ Figure 1: a) Schematic of the design. From bottom to top: semispherical gold reflector, quantum dots in PMMA, and Bragg reflector. b) Scheme of principle for the amplification of the ring of light with the patterned surface. c) Angle dependence of the reflectivity of a Bragg reflector centered at 585 nm in oil (n=1.5). The blue and the red-hatched regions represent the absorption and emission, respectively, of the quantum dots.

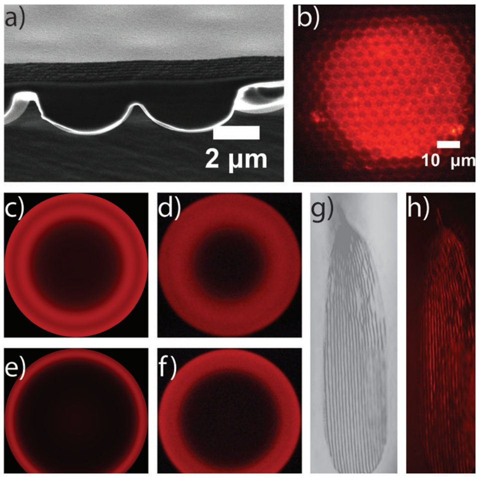

▲ Figure 2: a) SEM cross-sectional view of the device. b) Top view of the device. c), d) Comparison of the c) Modelled ring profile with the d) experimental one for a Bragg reflector centered at 585 nm in oil. e), f) Comparison of the e) modelled ring profile with the f) experimental one for a Bragg reflector centered at 643 nm in oil. g), h) Imaging of a scale of the *Papilio Blumei* butterfly with g) bright field imaging and h) surface-enabled dark-field imaging.

FURTHER READING

- M. Kolle, P. M. Salgard-Cunha, M. R. J. Scherer, F. Huang, P. Vukusic, S. Mahajan, J. J. Baumberg, and U. Steiner, "Mimicking the Colourful Wing Scale Structure of the *Papilio* Butterfly," *Nature Nanotechnology,* vol. 5, no. 7, pp. 511-515, 2010.

Low-Loss Planar Chalcogenide Glass Photonics

Q. Du, Y. Huang, J. Li, D. Kita, J. Michon, H. Lin, L. Li, C. Smith, K. Richardson, W. Zhang, J. Hu
Sponsorship: NSF, DOE

Chalcogenide glasses (ChGs) are widely recognized as the material of choice for sensing, flexible substrate integration and all-optical signal processing due to their broad transparency window in the infrared region, low processing temperature, and high Kerr nonlinearity. In addition, their high refractive indices enable small optical mode volume without suffering from excessive radiative loss. Nevertheless, unlike standard integrated photonic materials with well-established processing protocols such as silicon and silica, planar processing of ChGs remains much less mature despite their exceptional optical properties.

The ChG devices were fabricated on 6" silicon wafers with 3-µm thermally grown oxide coating. A piranha clean was performed prior to film deposition to ensure pristine wafer surface quality. Subsequently, $Ge_{23}Sb_7S_{70}$ (GSS) bulk glass was thermally evaporated onto the wafer to form a 450-nm-thick ChG film. A 400-nm-thick ZEP resist was then spun onto the glass film and exposed on an Elionix ELS-F125 e-beam system. The resist was then developed by rinsing in ZED-N50 to reveal the patterns. Reactive-ion etching was then carried out on a PlasmaTherm RIE etcher with fluorine chemistry. Channel waveguides were fabricated by etching through the entire GSS layer. After etching, remaining resists were stripped by soaking the sample in N-Methyl-2-pyrrolidone. The fluorine-etched samples underwent an additional oxygen plasma treatment step to remove the fluorocarbon polymer deposited on the waveguide sidewalls formed during the plasma process. SEM images of the waveguide are shown in Figures a and and the transmission of the waveguide resonator is provided in Figure c. We successfully demonstrated a record high Q on chip ChG resonator of 1.2×10^6.

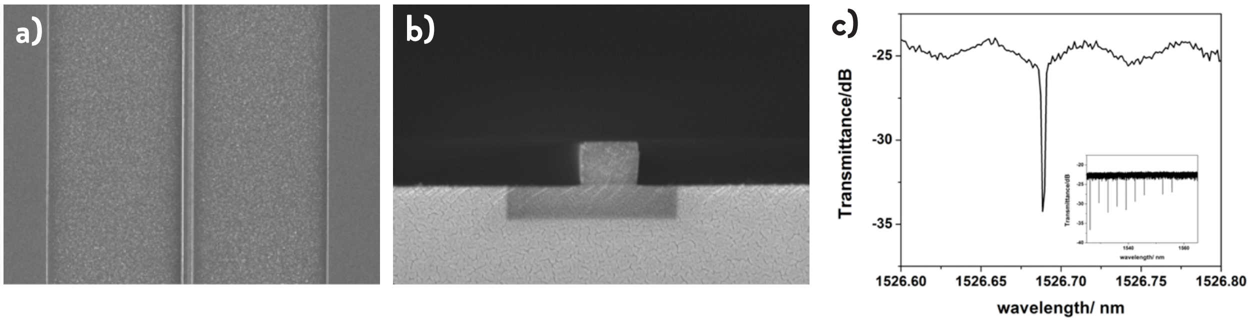

▲ Figure 1: a) SEM top view of GSS waveguide. b) cross- sectional view, and c) transmission spectrum of the waveguide resonator.

FURTHER READING

- L. Li, H. Lin, S. Qiao, Y. Zou, S. Danto, K. Richardson, J. D. Musgraves, N. Lu, and J. Hu, "Integrated Flexible Chalcogenide Glass Photonic Devices," *Nat. Photonics,* vol. 8, pp. 643-649, 2014.
- J. Hu, L. Li, H. Lin, Y. Zou, Q. Du, C. Smith, S. Novak, K. Richardson, and J. D. Musgraves, "Chalcogenide Glass Microphotonics: Stepping into the Spotlight," *Am. Ceram. Soc. Bull.* vol. 94, pp. 24-29, 2015.
- Y. Chen, H. Lin, J. Hu, and M. Li, "Heterogeneously Integrated Silicon Photonics for the Mid-infrared and Spectroscopic Sensing," *ACS Nano,* vol. 8, pp. 6955-6961, 2014.

On-chip Mid-infrared Gas Detection Using Chalcogenide Glass Waveguide

Z. Han, P. Lin, V. Singh, L. C. Kimerling, J. Hu, K. Richardson, A. Agarwal, D. T. H. Tan
Sponsorship: Ministry of Defense, Singapore

We demonstrate an on-chip sensor for room-temperature detection of methane gas using a broadband spiral chalcogenide glass waveguide coupled with an off-chip laser and detector. The waveguide is fabricated using UV lithography patterning and lift-off after thermal evaporation. We measure the intensity change due to the presence and concentration of methane gas in the mid-infrared (MIR) range.

The GeSbS waveguide is fabricated by thermal evaporation and patterned by contact mask and UV lithography in MTL's Exploratory Materials Laboratory (EML). A polydimethylsiloxane (PDMS) chamber is placed on top of the waveguide that holds the gas. We use a spiral-structure design to increase the interaction length, and we use tapered waveguide structures to avoid high absorption loss at the intersection of the polymer chamber sidewall with the chalcogenide glass waveguide. The methane absorption peak at 3310 nm is used to quantify methane concentration in nitrogen down to 2.5 vol. %. At 3310 nm the calculated absorbance per centimeter of methane calculated from the experimental data is 1.9, which matches the value from the NIST spectral database. This work provides an approach for broadband planar MIR gas sensing.

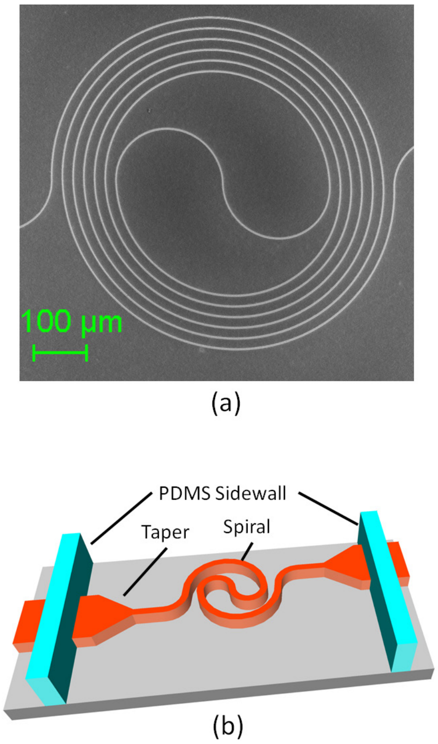

◀ Figure 1: (a) Top view SEM image of a 2-µm-wide single-mode spiral waveguide. (b) A schematic representation of the waveguide design. At the juncture where light crosses the PDMS gas chamber sidewall, the waveguide is 15 µm wide to better confine the light within the waveguide and decrease the absorption loss from PDMS. Within the chamber, the waveguide is tapered down to a single-mode width of 2 µm to enhance evanescence, which leads to enhanced gas-photon interaction.

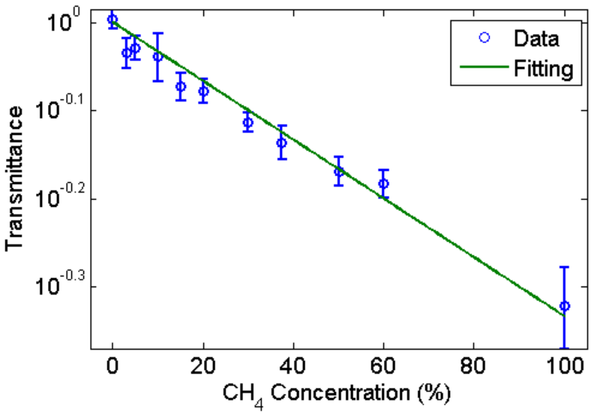

▲ Figure 2: Transmittance with different methane concentrations. Y-axis is shown in log scale. At 3310 nm, optical transmission for different methane concentrations is measured, showing a responsivity of 0.77.

FURTHER READING

- Z. Han, P. Lin, V. Singh, L. C. Kimerling, J. Hu, K. Richardson, A. Agarwal, and D. T. H. Tan, "On-chip Mid-infrared Gas Detection Using Chalcogenide Glass Waveguide," *Applied Physics Letters*, Cambridge: Cambridge University Press, vol. 108, pp. 141106, 2016.
- P. T. Lin, V. Singh, J. Wang, H. Lin, J. Hu, K. Richardson, J. D. Musgraves, I. Luzinov, J. Hensley and L. C. Kimerling, "Si-CMOS Compatible Materials and Devices for Mid-IR Microphotonics," *Optical Materials Express*, vol. 3, no. 9, pp. 1474-1487, 2013.
- Y. Chen, H. Lin, J. Hu, and M. Li, "Heterogeneously Integrated Silicon Photonics for the Mid-infrared and Spectroscopic Sensing," *ACS Nano*, vol. 8, no. 7, pp. 6955-6961, 2014.

Electronic and Optoelectronic Transport of Transitional Metal Dichalcogenides

Y. Yang, Q. Ma, J. I. J. Wang, Y.-A. Cheng, K. Watanabe, T. Taniguchi, H. O. H. Churchill, P. Jarillo-Herrero
Sponsorship: ONR, AFOSR, DOE

We are investigating electronic and optoelectronic devices based on atomically thin two-dimensional semiconductors such as the transistion metal dichalcogenides MoS_2 and WSe_2. These materials are interesting because they may display new basic physical phenomena not presenting in other materials. Only three atoms thick, they are inherently flexible and transparent materials. We characterize their electronic transport properties and potential for optoelectronic applications. To measure the transport properties of dichalcogenide devices as a function of temperature, we must make low-resistance electrical contacts to the material. To achieve this, we encapsulate few-layer $WSe2_2$ in hexagonal boron nitride that has been patterned to allow ionic liquid doping of the contact region (Figure 1). This technique simultaneously protects the WSe_2 surface above and below, resulting in the highest mobility few-layer WSe_2 devices reported to date.

In addition, due to the ultrathin nature of the devices, interlayer transport across different two-dimensional materials becomes very efficient and reveals unique properties. For instance, the vertical MoS_2-BN-graphene van der Waals heterostructure exclusively allows hole transport (after optical excitation) across the BN barrier based on the band alignment, which could lead to novel functionalities (Figure 2).

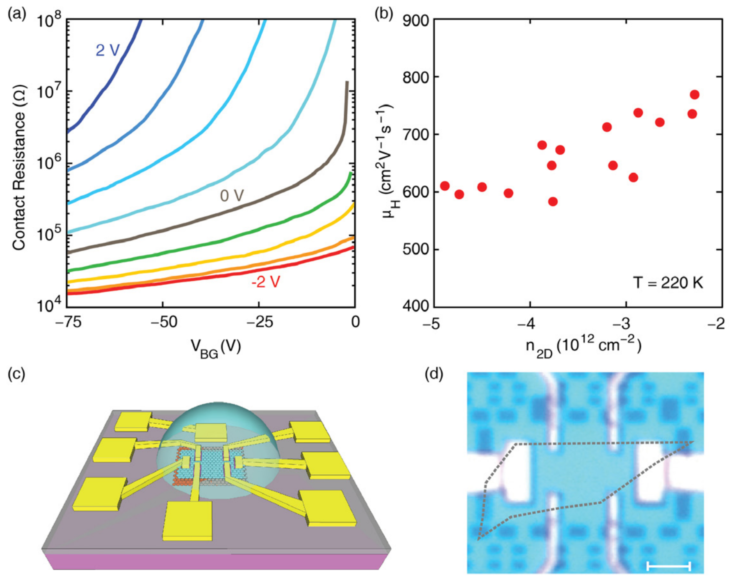

▲ Figure 1: WSe_2 electronic transport. (a) Contact resistance and (b) Hall mobility at 220 K. (c) Schematic and (d) Optical image of the device.

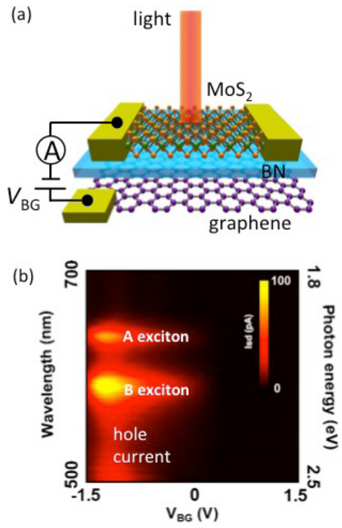

▲ Figure 2: MoS_2-BN-graphene vertical photocurrent. (a) Schematic of the measurement. (b) Vertical photocurrent as a function of the interlayer voltage and excitation photon energy.

FURTHER READING

- J. I. Wang, Y. Yang, Y. Chen, K. Watanabe, T. Taniguchi, H. O. H. Churchill, and P. Jarillo-Herrero, "Electronic Transport of Encapsulated Graphene and WSe2 Devices Fabricated by Pick-up of Pre-patterned hBN," *Nano Letters*, vol. 15, no. 3, pp 1898–1903, 2015.

High-Responsivity Graphene-Boron Nitride Photodetector in a Silicon Photonic Integrated Circuit

R.-J. Shiue, Y. Gao, C. Peng, J. Goldstein, D. K. Efetov, D. R. Englund
Sponsorship: EFRC Center for Excitonics

The remarkable electrical and optical properties of graphene are promising for efficient optoelectronic devices. However, a long-lasting issue in graphene-based devices is a relatively low absorption coefficient, which is 2.3% due to its ultra-thin thickness. To enhance the light-matter interaction in this single atomic layer material, graphene has been integrated into optical waveguides and cavities. By coupling graphene to the guided mode in a silicon waveguide, previously demonstrated graphene photodetectors can exhibit a maximum absorption of 60% of the input light with a maximum of responsivity of 0.1 A/W.

In this work, we demonstrate a graphene-hexagonal boron nitride (hBN) photodetector integrated with a silicon waveguide. In addition to the enhanced absorption of graphene on top of a waveguide, an extra gate terminal serves to manipulate the Fermi energy (E_F) in graphene to assist the separation of photo-excited carriers. The maximum responsivity of the device is 0.36 A/W, corresponding to an internal quantum efficiency of 15% at zero source-drain bias voltage (V_{DS}). At high frequencies, the device exhibits a 3dB cut-off frequency at 42 GHz.

Figure 1 shows the schematic of the graphene-hBN photodetector. Encapsulated single-layer graphene was transferred onto a silicon waveguide using a van der Waals (vdW) assembly technique. Two metal contacts (source and drain) were deposited on graphene to extract photocurrent. An extra gate metal electrode was deposited 50 μm away from the graphene channel. We then coated a layer of polymer electrolyte (Poly(ethylene oxide) plus $LiClO_4$) on the entire sample to control the carrier densities in graphene via the gate electrode. Tuning V_{GS} and V_{DS} can adjust the potential profile of the metal-graphene junction to achieve different internal quantum efficiencies of the photodetector. We measured a maximum responsivity of 0.36 A/W at V_{GS} = 2 V and V_{DS} = 1.2 V, as shown in Figure 2. The six-fold pattern of the photocurrent mapping indicates a strong photothermoelectric (PTE) effect for the photocurrent generation.

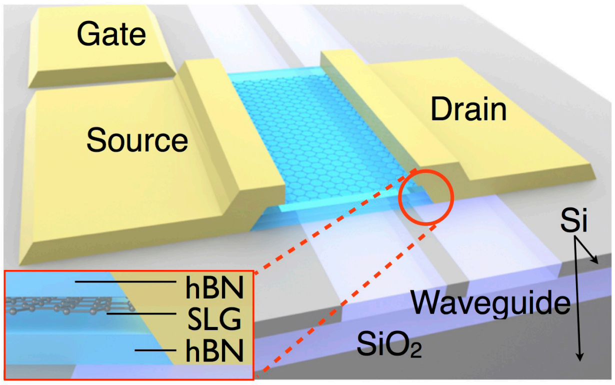

▲ Figure 1: Schematic of a waveguide-integrated graphene-boron nitride photodetector. Single layer graphene (SLG) is encapsulated by top and bottom hexagonal boron nitride (hBN) layers.

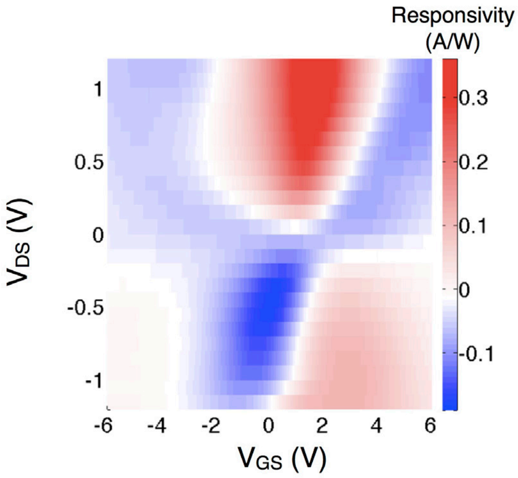

▲ Figure 2: Photocurrent mapping of the waveguide-integrated graphene photodetector as a function of gate-souce (V_{GS}) and drain-source (V_{DS}) voltages.

FURTHER READING

- R.-J. Shiue, Y. Gao, Y. Wang, C. Peng, A. Robertson, D. K. Efetov, S. Assefa, F. Koppens, J. Hone, and D. Englund, "High-Responsivity Graphene-Boron Nitride Photodetector and Autocorrelator in a Silicon Photonic Integrated Circuit," *Nano Letters*, vol. 15, pp. 7288-7293, 2015.
- Y. Gao, R.-J. Shiue, X. Gan, L. Li, C. Peng, I. Meric, L. Wang, A. Szep, D. Walker Jr., J. Hone, and D. Englund, "High-Speed Electro-Optic Modulator Integrated with Graphene Boron-Nitride Heterostructure and Photonic Crystal Nanocavity," *Nano Letters*, vol. 15, pp. 2001-2005, 2015.
- X. Gan, R.-J. Shiue, Y. Gao, I. Meric, T. F. Heinz, K. Shepard, J. Hone, S. Assefa, and D. Englund, "Chip-Integrated Ultrafast Graphene Photodetector with High Responsivity," *Nature Photonics*, vol. 7, pp. 883-887, 2013.

High-yield Creation of Diamond Defect Centers in Photonic Crystal Cavities

T. Schröder, L. Li, M. Walsh, M. E. Trusheim, I. Bayn, J. Zheng, S. Mouradian, H. Bakhru*, D. R. Englund
*SUNY Polytechnic Institute
Sponsorship: AFOSR PECASE, AFOSR Quantum Memories MURI, ARL CDQI, Sandia National Lab., Brookhaven National Lab

The negatively charged nitrogen vacancy defect center (NV) in diamond is a promising solid-state spin system for the implementation of quantum information processes. It has excellent electron spin coherence times of up to 600 ms in bulk and has been applied as a spin qubit in a two-node quantum network for quantum entanglement and teleportation. These first proof-of-principle experiments indicate the potential for networks with large scale entanglement and cluster state generation. However, entanglement success rates are presently several orders of magnitude smaller than the NV spin coherence times, limiting entanglement to two nodes. Optical cavities, on the other hand, could increase these rates by Purcell-enhancing the NV zero phonon line (ZPL) spontaneous emission rate.

Here, we report on the scalable creation of NV-cavity and -photonic systems where the NV is located within 30 nm from the device mode maximum. For an exemplary sample, we determine 1.1(+/- 0.2) NVs per cavity and exactly one single NV in every third cavity. In addition, we show 20-fold Purcell enhancement of multiple single NV-cavity systems. This targeted generation of coupled NV-cavity systems represents a crucial step towards the fabrication of scalable solid-state quantum networks. Furthermore, we show that our method can be applied to a variety of nanostructured diamond and solid-state samples such as μ-waveguides and grating structures for enhanced photon collection where the exact positioning of an NV is crucial for the performance of the photonic device.

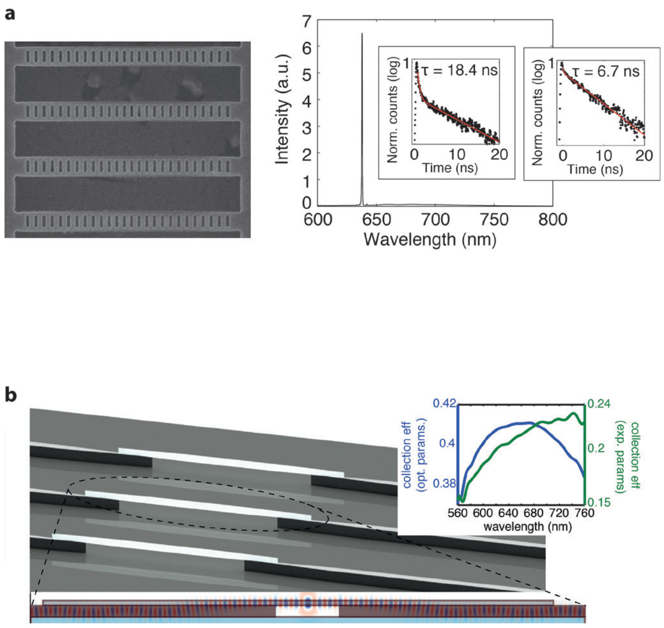

▲ Figure 1: a, Scanning electron micrograph of 1d photonic crystal cavities in diamond; Enhanced ZPL of single NV at 18 K with lifetime reduction and rate enhancement <50. Illustration of PIC with μ-waveguides containing single NVs; collection properties.

FURTHER READING

- L. Li, T. Schröder, E. H. Chen, M. Walsh, I. Bayn, J. Goldstein, O. Gaathon, M. E. Trusheim, M. Lu, J. Mower, M. Cotlet, M. L. Markham, D. J. Twitchen, and D. Englund, "Coherent Spin Control of a Nanocavity-enhanced Qubit in Diamond," *Nature Communications*, vol. 6, pp. 6173, 2015.
- S. L. Mouradian, T. Schröder, C. B. Poitras, L. Li, J. Goldstein, E. H. Chen, J. Cardenas, M. L. Markham, D. J. Twitchen, M. Lipson, and D. Englund, "The Scalable Integration of Long-lived Quantum Memories into a Photonic Circuit," *Phys. Rev. X*, vol. 5, pp. 031009, 2015.
- T. Schröder, E. Chen, L. Li, M. Walsh, M. E. Trusheim, I. Bayn, and D. Englund, "Targeted Creation and Purcell Enhancement of NV Centers within Photonic Crystal Cavities in Single-crystal Diamond," *CLEO: 2014. FW1B.6 (Optical Society of America)*, 2016.

Circular Gratings for Efficient Collection from Implanted Silicon Vacancy Centers in Diamond

J. Zheng, M. E. Trusheim, T. Schröder, M. Walsh, C. Stavrakas, B. Pingault, M. Gündoğan, C. Hepp, J. L. Pacheco, E. Bielejec, M. Atatüre, D. R. Englund

The fluorescence of silicon vacancy centers (SiV), in contrast to the most extensively studied nitrogen vacancy centers, exhibits a sharp and spectrally almost lifetime-limited emission with approximately 80% emitting into its zero photon line at 737 nm. This trait greatly benefits their use as qubits for quantum information systems and as probes for precision measurement. For both applications, the efficient detection of the fluorescence from SiV is of essential importance. Here, we report the efficient fluorescence collection from implanted SiV in bulk diamond located in a nanofabricated chirped circular grating structure, as Figure 1b shows (perspective view).

The proposed and demonstrated circular grating structure consists of a series of concentric air slits in diamond with the emitter located at the concentric center. The grating structure has a red dot indicating the SiV. The chirped circular grating structure is obtained through a numerical optimization process with the collection efficiency for a low numerical aperture (NA) of only 0.4 as the figure of merit. Figure 1d indicates that the electromagnetic field is confined in the lateral direction and the dipole emits mainly downwards. The predicted collection efficiency with an NA of 0.4 is 41.4% for collection from the bottom (Figure 1c) and 1.4% for collection from the top (Figure 1a), resulting in a directionality of 30: we expect to collect about 30x more photons from the bottom. Sample fabrication is performed using transferred mask lithography followed by focused Si ion implantation to create SiV. The fabricated sample is shown in Figure 1f. Our recent optical measurements show that the emission from the SiV preferentially goes to the bottom in the presence of the circular grating. The total collected number of photons from the bottom is about 4.9 times greater than that from the top of the sample (Figure 1e). We expect to further improve the collection efficiency by adding additional reflective layers and performing the measurement on tens of micrometer-thick diamond samples where higher NA optics are accessible and less aberration is induced.

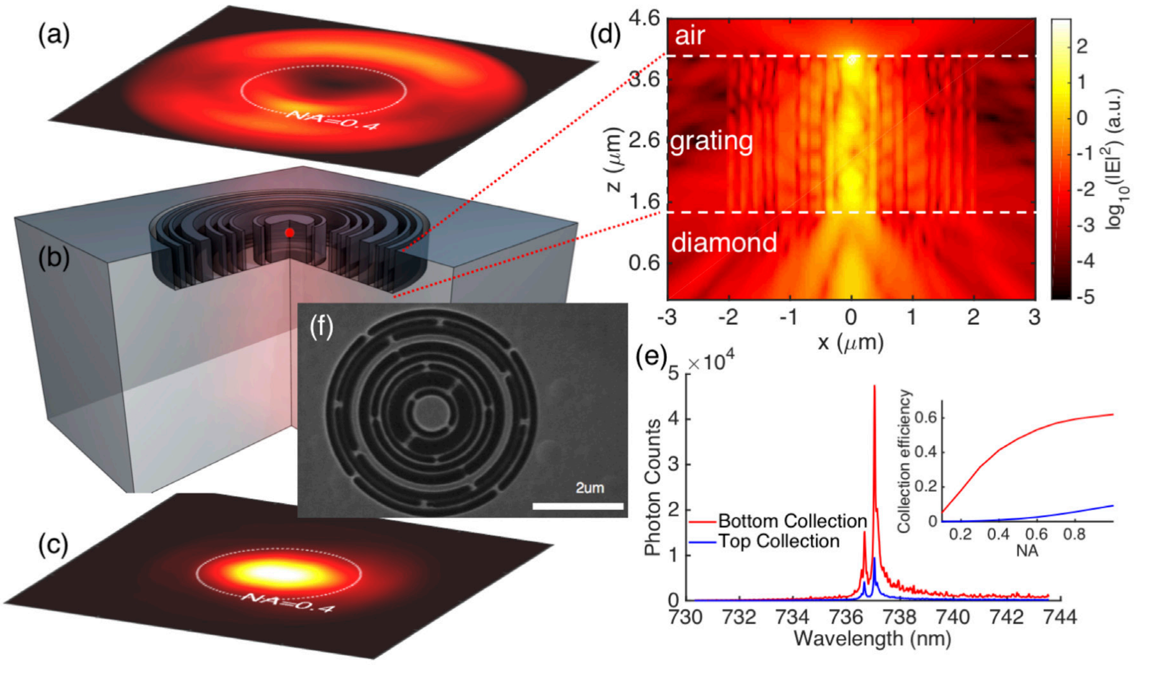

▲ Figure 1: Simulated far field profile for (a) top and (c) bottom side collection. (b) Illustration of the grating structure. (d) Simulated intensity distribution in the cross-sectional view. (e) The measured spectrally-resolved fluorescence intensity. The inset shows the simulated collection efficiency for top and bottom collection. (f) Scanning electron micrograph of the fabricated device.

FURTHER READING

• L. Li, E. H. Chen, J. Zheng, S. L. Mouradian, F. Dolde, T. Schröder, S. Karaveli, M. L. Markham, D. J. Twitchen, and D. Englund, "Efficient Photon Collection From a Nitrogen Vacancy Center in a Circular Bullseye Grating," *Nano Letters*, vol. 15, no. 3, pp. 1493-1497, 2015.

Ultrafast Fluorescent Decay Induced by Metal-mediated Dipole-dipole Interaction in Two-dimensional Molecular Aggregates

Q. Hu, D. Jin, S. H. Nam, J. Xiao, Y. Liu, X. Zhang, N. X. Fang
Sponsorship: NSF, AFOSR

A two-dimensional molecular aggregate (2DMA), a thin sheet of strongly interacting dipole molecules self-assembled at a close distance on an ordered lattice, is a fascinating fluorescent material. It is distinctively different from the single or colloidal dye molecules or quantum dots in most previous research.

In the paper, we verify that when a 2DMA is placed at a nanometric distance from a metallic substrate, the strong and coherent interaction between the dipoles inside the 2DMA dominates its fluorescent decay at picosecond timescale. We fabricate the 2DMA samples with different distances from the Ag substrate and measure the lifetime and photoluminescence intensity using a streak camera (Figure 1). Our interacting lattice-dipole calculation reveals that the metal-mediated dipole-dipole interaction shortens the fluorescent lifetime to about one half (Figure 2(A)) and increases the energy dissipation rate by ten times more than expected from the non-interacting single-dipole picture (Figure 2(B)). Our finding can enrich our understanding of nanoscale energy transfer in molecular excitonic systems and may designate a new direction for developing fast and efficient optoelectronic devices.

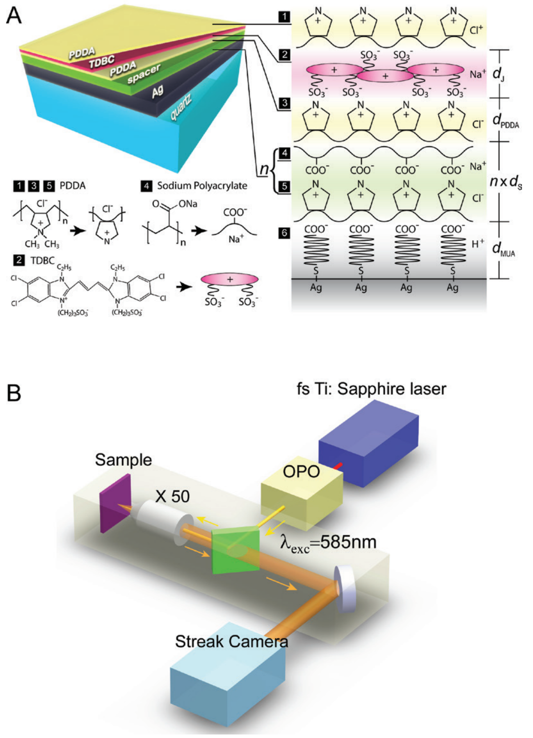

▲ Figure 1: (a) Schematic of the fabricated molecular multilayer structure. The layers are formed one by one via the adsorption between positively and negatively charged molecules. (b) Schematic of the measurement setup. From bottom to top, it consists of 100-nm Ag, MUA bonding layer, $(PDDA/PolyArc)_n$ spacer layer, and (PDDA/TDBC/PDDA) cyanine layer encapsulated in PDDA.

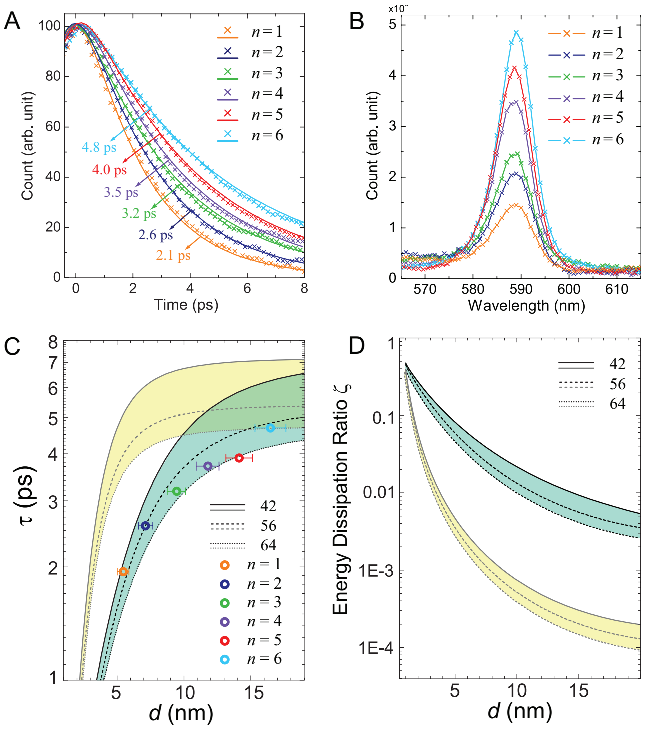

▲ Figure 2: (a) Time-resolved photon counts (marks) and exponential fitting curves (solid lines). (B) Photoluminescence intensity of the sample with different numbers of spacer layers *n*. (C) Calculated lifetime based on the single-dipole model (yellow) and lattice-dipole model (green) as a function of distance ***d*** from the substrate. The measured lifetime from Fig. 2(A) is plotted with circles. (D) Calculated energy dissipation ratio based on the single-dipole model (yellow) and lattice-dipole model (green) as a function of distance ***d***.

FURTHER READING

- T. Kobayashi, "Chapters 2 and 3," *J-Aggregates*, World Scientific Publishing Co. Pte. Ltd. Singapore, 1996.
- P. Anger, P. Bharadwaj, and L. Novotny, "Enhancement and Quenching of Single-molecule Fluorescence," *Phys Rev Letters*, vol. 96, pp. 113002, 2006.
- M. R. Philpott and P. G. Sherman, "Excitons and Polaritons in Monomolecular Layers," *Phys Rev* vol. 12, pp. 5381-5394, 1975.

Foldable and Cytocompatible Sol-gel TiO_2 Photonics

L. Li, P. Zhang, H. Lin, S. Geiger, A. Zerdoum, O. Ogbuu, Q. Du, X. Jia, J. Hu

Flexible integrated photonics, a new technology that has started to burgeon only in the past few years, enables a wide cross-section of emerging applications ranging from flexible optical interconnects to conformal sensors on biological tissues. TiO_2, a typically biocompatible material, works as a good candidate for the fabrication of biocompatible and flexible integrated photonics. Using a sol-gel method, we deposited amorphous TiO_2 films at a low temperature (< 250 °C), and they exhibited a low optical loss of 3 dB/cm. Structural and optical properties of the films were characterized by FT-IR, Uv-vis, Refractometry, etc. Further, we fabricated and tested TiO_2 optical waveguides and resonators monolithically integrated on flexible polymer substrates and resonator quality factors as high as 20,000 were measured. Despite the inherent mechanical rigidity of the TiO_2 material, we experimentally demonstrated repeated folding of the devices down to < 0.3 mm radius without degrading their optical performance by using the developed multi-neutral-axis mechanical design. Finally, we showed through in-vitro tests that the TiO_2 devices are non-cytotoxic. These results indicate that sol-gel TiO_2 can serve as a promising material platform for novel biophotonic devices.

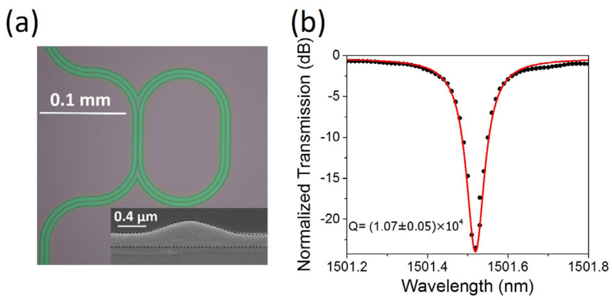

▲ Figure 1: Sol-gel TiO_2 thin film and photonic devices characterization. (a) Optical microscope top-view image of a TiO_2 rib racetrack resonator. The inset shows the cross-sectional SEM image of the bus waveguide; (b) Normalized optical transmission spectra of a TiO_2 rib racetrack resonator with a loaded Q-factor of (1.07 ± 0.05) × 10^4.

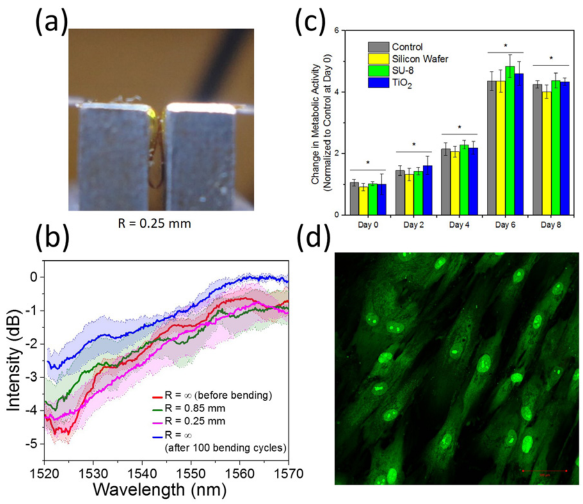

▲ Figure 2: Mechanical and biocompatible test. (a) Photos of the fiber butt coupling testing set-up for in-situ measurement of optical transmission characteristics at a bending radius of 0.25 mm; (b) Normalized optical transmission spectra of a flexible TiO_2 waveguide after bending at different radii; (c) Proliferation of hMSCs in indirect contact with sensor materials; (d) Confocal images of live/dead stained day 10 hMSCs cultured in direct contact with TiO_2.

FURTHER READING

- L. Li, P. Zhang, W. Wang, H. Lin, A. Zerdoum, S. Geiger, Y. Liu, N. Xiao, Y. Zou, O. Ogbuu, Q. Du, X. Jia, J. Li, and J. Hu, "Foldable and Cytocompatible Sol-gel TiO_2 Photonics," *Sci. Rep.*, vol. 5, p. 13832, 2015.
- L. Li, H. Lin, S. Qiao, Y. Zou, S. Danto, K. Richardson, J. D. Musgraves, N. Lu, and J. Hu, "Integrated Flexible Chalcogenide Glass Photonic Devices," *Nat. Photonics*, vol. 8, pp. 643-649, 2014.

Towards Lasing in Colloidal Quantum Dots Using Nanobeam Photonic Crystal Cavities

T. S. Mahony, P. B. Deotare, V. Bulović
Sponsorship: NSF, EFRC Center for Excitonics

Techniques in biology and medicine such as imaging, sensing, and other lab-on-chip applications require the use of visible lasers. Currently, there exist no tunable, compact, visible lasers that are well suited to this purpose. We propose the use of CdSe/CdZnS core-shell colloidal quantum dots, which are solution-processed nanocrystals with high brightness that are size-tunable and therefore spectrally tunable sources, to be used as gain for such lasers. We have identified nanobeam photonic crystal cavities as resonators that have high quality factors and low mode volumes and are well suited for integrated applications due to their waveguide geometry. By coupling the light emission from colloidal quantum dots into a single mode nanobeam photonic crystal cavity, we will demonstrate low-threshold, compact, tunable lasers.

To create our nanobeam cavities, we mix colloidal quantum dots into poly methyl methacrylate (PMMA) in solution. We spin coat the resulting solution, forming a composite film of colloidal quantum dots embedded into a PMMA polymer matrix. Since PMMA is used as an ebeam resist, we are able to nanopattern the films and undercut them, suspended the structures in air, as in Figure 1. Under optical excitation, these structures demonstrate enhanced luminescence through the cavity mode, as Figure 2 shows. By fitting the mode to a Lorentzian lineshape, we can extract a cavity quality factor of around 3000.

We are now studying ways to increase the optical gain in our structures to make them lase. By studying the effect of concentration of colloidal quantum dots in PMMA films on the film quality, we have determined that we can increase the density of dots by a factor of 5. We also are optimizing our lithography to increase the quality factor of our nanobeam photonic crystal cavities. Similar polymeric cavities with Q's of 36,000 have been reported in the literature, so we estimate a potential improvement of about an order of magnitude can be achieved in our cavities as well. We are also performing spectroscopy of our colloidal quantum dots, to ensure they are of good optical quality for lasing applications. We will measure their optical gain using a transient absorption setup and a variable stripe length setup.

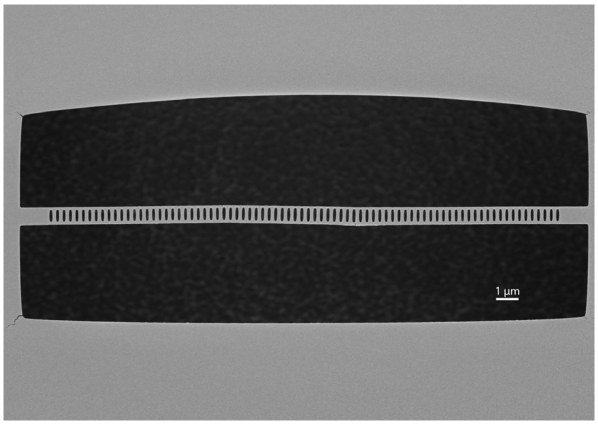

▲ Figure 1: SEM images showing a suspended nanobeam photonic crystal cavity. Film cracks and warping are caused by the process of imaging devices since the polymer film is nonconductive and heats up under high-energy electron flux.

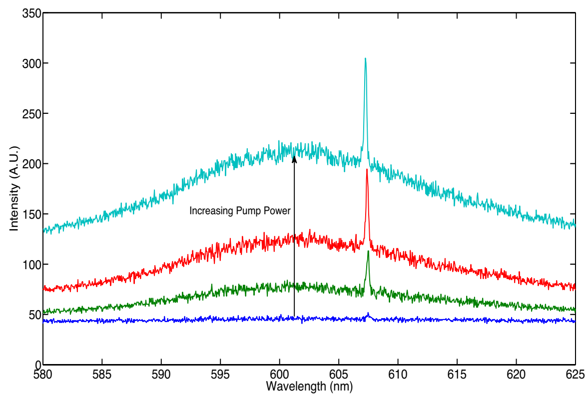

▲ Figure 2: Photoluminescence spectra taken of a nanobeam photonic crystal cavity showing enhanced luminescence through the cavity mode as a function of increasing pump power. Optical excitation is with a 400-nm laser.

FURTHER READING

- C. Dang, J. Lee, C. Breen, J. S. Steckel, S. Coe-Sullivan, and A. Nurmikko, "Red, Green and Blue Lasing Enabled by Single-exciton Gain in Colloidal Quantum Dot Films," *Nat Nano*, vol. 7, no. 5, pp. 335–339, May 2012.
- K. Roh, C. H. Dang, J. Lee, S. Ahn, H. Jeon, C. Breen, J. S. Steckel, S. Coe-Sullivan, and A. Nurmikko, "High Performance, Spatially Coherent, Multicolor Distributed Feedback Lasers in Optically Pumped Colloidal Quantum Dots," *CLEO: 2013*, pp. CTh4G.7, 2013.
- Q. Quan and M. Loncar, "Deterministic Design of Wavelength Scale, Ultra-high Q Photonic Crystal Nanobeam Cavities," *Opt. Express*, vol. 19, no. 19, pp. 18529–18542, September 2011.

Research Centers

Center for Integrated Circuits and Systems

Professor Hae-Seung Lee, Director

The Center for Integrated Circuits and Systems (CICS) at MIT, established in early 1998, is an industrial consortium created to promote new research initiatives in circuits and systems design, as well as to promote a tighter technical relationship between MIT's research and relevant industry. Seven faculty members participate in the CICS: Director Hae-Seung Lee, Duane S. Boning, Anantha Chandrakasan, David Perreault, Charles Sodini, and Vivienne Sze. In September 2014, we welcomed our newest CICS faculty member, Ruonan Han. Prof. Han's research focuses on high frequency circuits and their applications reaching up to the THz ranges. Terahertz wave is opening up tremendous opportunities in non-ionizing medical imaging, biochemical molecule spectroscopy, ultra-high-speed communication, etc. His research group focuses on bridging the THz Gap that is difficult to reach via traditional electronic and optic methods, spanning from electronic device engineering, analog/microwave circuit design, to innovations of system architecture.

CICS investigates a wide range of circuits and systems, including wireless and wireline communication, high-speed and RF circuits, microsensor/actuator systems, imagers, digital and analog signal processing circuits, biomedical circuits, and power conversion circuits, among others.

We strongly believe in the synergistic relationship between industry and academia, especially in practical research areas of integrated circuits and systems. CICS is designed to be the conduit for such synergy. At present, participating companies include Analog Devices, Inc., IBM, Linear Technology, Maxim Integrated, Marvell Technology Group, MediaTek, and Texas Instruments.

CICS's research portfolio includes all research projects that the seven participating faculty members conduct, regardless of source(s) of funding, with a few exceptions.

Technical interaction between industry and MIT researchers occurs on both a broad and individual level. Since its inception, CICS recognized the importance of holding technical meetings to facilitate communication among MIT faculty, students, and industry. We hold two informal technical meetings per year open to CICS faculty, students, and representatives from participating companies. Throughout each full-day meeting, faculty and students present their research, often presenting early concepts, designs, and results that have not been published yet. The participants then offer valuable technical feedback, as well as suggestions for future research. More intimate interaction between MIT researchers and industry takes place during work on projects of particular interest to participating companies. Companies may invite students to give on-site presentations, or they may offer students summer employment. Additionally, companies may send visiting scholars to MIT or enter into a separate research contract for more focused research for their particular interest. The result is truly synergistic, and it will have a lasting impact on the field of integrated circuits and systems.

MIT/MTL Center for Graphene Devices and 2D Systems

Professor Tomás Palacios, Director

The MIT/MTL Center for Graphene Devices and 2D Systems (MIT-CG) brings together MIT researchers and industrial partners to advance the science and engineering of graphene and other two-dimensional materials.

Graphene and other two-dimensional (2D) materials are revolutionizing electronics, mechanical and chemical engineering, physics and many other disciplines thanks to their extreme properties. These materials are the lightest, thinnest, strongest materials we know of, at the same time that they have very rich electronic and chemical properties. For more than 40 years, MIT has led the work on the science and engineering of 2D materials. More recently, since 2011, the MIT/MTL Center for Graphene Devices and 2D Systems (MIT-CG) has played a key role in coordinating most of the work going on at MIT on these new materials, and in bringing together MIT faculty and students, with leading companies and government agencies interested in taking these materials from a science wonder to an engineering reality.

Specifically, the Center explores advanced technologies and strategies that enable 2D materials, devices and systems to provide discriminating or break-through capabilities for a variety of system applications ranging from energy generation/storage and smart fabrics and materials to optoelectronics, RF communications and sensing. In all these applications, the MIT-CG supports the development of the science, technology, tools and analysis for the creation of a vision for the future of new systems enabled by 2D materials.

Some of the multiple benefits of the Center's membership include complimentary attendance to meetings, industry focus days, and live webcasting of seminars related to the main research directions of the Center. The members of the Center also gain access to a resume book that connects students with potential employers, as well as access to timely white papers on key issues regarding the challenges and opportunities of these new technologies. There are also numerous opportunities to collaborate with leading researchers on projects that address some of today's challenges for these materials, devices and systems.

MIT/MTL Gallium Nitride (GaN) Energy Initiative

Professor Tomás Palacios, Director

The MIT/MTL Gallium Nitride (GaN) Energy Initiative (MIT GaN) is an interdepartmental program that brings together 10 MIT faculty and more than 40 other researchers and industrial partners to advance the science and engineering of GaN-based materials and devices for energy applications.

The GaN Energy Initiative provides a holistic approach to GaN research for energy applications and it coordinates work on the growth, technology, novel devices, circuits and systems to take full advantage of the unique properties of GaN. The GaN Energy Initiative is especially interested in developing new beyond-state-of-the-art solutions to system-level applications in RF power amplification, mixed signal electronics, energy processing and power management, as well as advanced optoelectronics. Most of the work is done on GaN materials and devices that are compatible with Si fabrication technologies, in close collaboration with industrial partners to accelerate the insertion of these devices into systems.

The MIT/MTL Gallium Nitride (GaN) Energy Initiative organizes numerous activities to advance the understanding of GaN materials, technology and devices. Some of these activities include webcast of seminars and annual meetings, as well as joint collaborations with industry partners. The Initiative also elaborates a resume book of graduating students and provides timely access to white papers and pre-prints through its website.

The MIT Medical Electronic Device Realization Center

Professor Charles Sodini, Director

The vision of the MIT Medical Electronic Device Realization Center (MEDRC) is to revolutionize medical diagnostics and treatments by bringing health care directly to the individual and to create enabling technology for the future information-driven healthcare system. This vision will, in turn, transform the medical electronic device industry. Specific areas that show promise are wearable or minimally invasive monitoring devices, medical imaging, portable laboratory instrumentation, and the data communication from these devices and instruments to healthcare providers and caregivers.

Rapid innovation in miniaturization, mobility, and connectivity will revolutionize medical diagnostics and treatments, bringing health care directly to the individual. Continuous monitoring of physiological markers will place capability for the early detection and prevention of disease in the hands of the consumer, shifting to a paradigm of maintaining wellness rather than treating sickness. Just as the personal computer revolution has brought computation to the individual, this revolution in personal medicine will bring the hospital lab and the physician to the home, to emerging countries, and to emergency situations. From at-home cholesterol monitors that can adjust treatment plans, to cell phone-enabled blood labs, these system solutions containing state-of-the-art sensors, electronics, and computation will radically change our approach to health care. This new generation of medical systems holds the promise of delivering better quality health care while reducing medical costs.

The revolution in personal medicine is rooted in fundamental research in microelectronics from materials to sensors, to circuit and system design. This knowledge has already fueled the semiconductor industry to transform society over the last four decades. It provided the key technologies to continuously increase performance while constantly lowering cost for computation, communication and consumer electronics. The processing power of current smart phones, for example, allows for sophisticated signal processing to extract information from this sensor data. Data analytics can combine this information with other patient data and medical records to produce actionable information customized to the patient's needs. The aging population, soaring healthcare costs, and the need for improved healthcare in developing nations are the driving force for the next semiconductor industry's societal transformation, Medical Electronic Devices.

The successful realization of such a vision also demands innovations in the usability and productivity of medical devices, and new technologies and approaches to manufacture devices. Information technology is a critical component of the intelligence that will enhance the usability of devices; real-time image and signal processing combined with intelligent computer systems will enhance the practitioners' diagnostic intuition. Our research is at the intersection of Design, Healthcare, and Information Technology innovation. We perform fundamental and applied research in the design, manufacture, and use of medical electronic devices and create enabling technology for the future information-driven healthcare system.

The MEDRC has established a partnership between microelectronics companies, medical device companies, medical professionals, and MIT to collaboratively achieve needed radical changes in medical device architectures, enabling continuous monitoring of physiological parameters such as cardiac vital signs, intracranial pressure and cerebral blood flow velocity. Since its founding in 2011, MEDRC has grown from two to five sponsoring companies with several other companies in serious discussions. There are currently fifteen MEDRC funded research projects that are defined by ten MIT faculty, ten clinicians and our sponsoring companies supporting approximately twenty students. A visiting scientist from a project's sponsoring company is present at MIT. Ultimately this individual is the champion that helps translate the technology back to the company for commercialization and provide the industrial viewpoint in the realization of the technology. MEDRC projects have the advantage of insight from the technology arena, the medical arena, and the business arena, thus significantly increasing the chances that the devices will fulfill a real and broad healthcare need as well as be profitable for companies supplying the solutions. With a new trend toward increased healthcare quality, disease prevention, and cost-effectiveness, such a comprehensive perspective is crucial.

In addition to the strong relationship with MTL, MEDRC is associated with MIT's Institute for Medical Engineering and Science (IMES) that has been charged to serve as a focal point for researchers with medical interest across MIT. MEDRC has been able to create strong connections with the medical device and microelectronics industry, venture-funded startups, and the Boston medical community. With the support of MTL and IMES, MEDRC will serve as the catalyst for the deployment of medical devices that will reduce the cost of healthcare in both the developed and developing world.

Faculty Profiles

Anuradha M. Agarwal

Principal Research Scientist
Materials Processing Center

Planar, integrated, Si-CMOS-compatible microphotonics platform for on-chip MIR hyperspectral imaging and chem-bio sensing applications; radiation effects on silicon microphotonics.

Rm. 13-4126 | 617-253-5302 | anu @ mit . edu

GRADUATE STUDENTS

Zhaohong Han, DMSE
Danhao Ma. DMSE
Corentin Monmeyran, DMSE
Peter Su, DMSE

SUPPORT STAFF

Lisa Sinclair, Administrative Assistant II

SELECTED PUBLICATIONS

S. Grillanda, V. Singh, V. Raghunathan, F. Morichetti, A. Melloni, L. Kimerling, and A. M. Agarwal, "Gamma Radiation Effects on Silicon Photonic Waveguides," *Optics Letters,* 41 (13), 3053-3056, 2016.

S. Novak, C. Li, N. Borodinov, Z. Han, C. Monmeyran, N. Patel, Q. Du, C. Lumdee, P. Kik, W. Deng, A. M. Agarwal, J. Hu, I. Luzinov, K. Richardson, "Electrospray Deposition of Uniform Thickness Ge23Sb7S70 and As40S60 Chalcogenide Glass Films," *Journal of Virtual Experiments* 54379R3, 2016.

N. Borodinov, J. Giammarco, N. Patel, A. M. Agarwal, K. R O'Donnell, C. J. Kucera, L. G. Jacobsohn, I. Luzinov, "Stability of Grafted Polymer Nanoscale Films toward Gamma Irradiation," *ACS Applied Materials & Interfaces,* 7 (34), 19455-19465, 2015.

N. S Patel, C. Monmeyran, A. M. Agarwal, L. C. Kimerling, "Point defect states in Sb-doped germanium," *Journal of Applied Physics,* 118 (15), 155702, 2015.

S. Grillanda, V. Singh, V. Raghunathan, S. Shutthanandan, F. Morichetti, A. Melloni, L. C. Kimerling, and A. M. Agarwal, "Effects of High-Energy Irradiation on Silicon Oxynitride and Silicon Photonic Waveguides," *Integrated Photonics Research (IPR)*, July 18-20, 2016.

S.Novak, V. Singh, C. Monmeyran, A. Ingram, Z.Han, H.Lin, N. Borodinov, N. Patel, Q. Du, J. Hu, I. Luzinov, R. Golovchak, A. M. Agarwal, and K. Richardson, "Effect of Gamma Exposure on Chalcogenide Glass Films for Microphotonic Devices," *IEEE Nuclear and Space Radiation Effects Conference (NSREC),* July 11-15, 2016.

Q. Du, Y. Huang, O. Ogbuu, V. Singh, C. Monmeyran, N. Patel, A. M. Agarwal and J. Hu, "Gamma Radiation Induced Effects in Silicon Nitride and Amorphous Silicon Films and Photonic Devices," *IEEE Nuclear and Space Radiation Effects Conference (NSREC),* July 11-15, 2016.

Y. Guo, J. Wang, Z. Han, L. C. Kimerling, A. M. Agarwal, J. Michel, Z. Zheng, G. Li, L.Zhang, "Mid-IR Kerr Frequency Comb Generation from 4000 to 10000 nm in a CMOS-compatible Germanium Microcavity," *Conference on Lasers and Electro-Optics (CLEO),* June 5-10, 2016.

Z. Han, D. Tan, P. T. Lin, and A. M. Agarwal, "Mid-Infrared Methane Sensing by Chalcogenide Glass Waveguides," *Glass and Optical Materials Division (GOMD),* May 22-26, 2016.

C. Monmeyran, Y. Cai, R. M. Gwilliam, I. F. Crowe, E. Napolitani, J. Michel, A. M. Agarwal, L. C. Kimerling, "Fluorine Retention in Co-implanted Germanium," *Spring Materials Research Society (MRS),* March 28-April 1, 2016.

C. Monmeyran, N. Patel, A. M. Agarwal, K. Wada, L. C. Kimerling, "Deep States and Their Annealing Kinetics in Gamma Irradiated Bulk Germanium Studied by DLTS," *28th International Conference on Defects in Semiconductors, (ICDS),* July 27-31, 2015.

Polina Anikeeva

Class of 1942 Career Development Associate Professor
Department of Materials Science and Engineering

Neuroprosthetic materials and devices: chemistry, device physics, fabrication and testing in biological systems. Minimally invasive neural stimulation.

Rm. 8-425 | 617-253-3301 | anikeeva @ mit . edu

POSTDOCTORAL ASSOCIATES

Elizabeth Canovic, RLE
Danijela Gregurec, RLE
Mehmet Kanik, RLE, Simons Fellow
Siyuan Rao, RLE, Chinese Government Fellow
Dekel Rosenfeld, RLE, MIT-Technion Fellow

GRADUATE STUDENTS

Andres Canales, DMSE
Ritchie Chen, DMSE
Michael Christiansen, DMSE, NDSEG Fellow
Chi Lu, DMSE
Junsang Moon, DMSE, Samsung Fellow
Seongjun Park, EECS, Samsung Fellow
Alexander Senko, DMSE, NDSEG Fellow

UNDERGRADUATE STUDENTS

Alexander Derry, DMSE
Jeewoo Kang, School of Science
Jueun Lee, EECS
Eric Taylor, DMSE
Jun Yung Yoon, MechE
Ha Yung Yoon, MechE

VISITORS

Ligia Stocce Barbosa, Federal University of São Carlos
Sarah Hescham, U. Maastricht

SUPPORT STAFF

Ayn Inserto, Administrative Assistant II

SELECTED PUBLICATIONS

R. Chen, M. G. Christiansen, A. Sourakov, A. Mohr, Y. Matsumoto, S. Okada, A. Jasanoff, P. Anikeeva, "High-performance Ferrite Nanoparticles Through Nonaqueous Redox Phase Tuning," *Nano Letters*, 16, pp. 1345, 2016.

R. A. Koppes, S. Park, T. Hood, X. Jia, N. A. Poorheravi, A. K. H. Achyuta, Y. Fink, P. Anikeeva, "Thermally Drawn Fibers as Nerve Guidance Scaffolds," *Biomaterials*, 81, pp. 27, 2016.

P. Anikeeva, "Optogenetics Unleashed," *Nat. Biotechnol*, 34, pp. 43, 2016.

Y. Matsumoto, R. Chen, P. Anikeeva, A. Jasanoff, "Engineering Intracellular Biomineralization and Biosensing by a Magnetic Protein," *Nat. Comms*, 6, pp. 8721, 2015.

C. N. Loynachan, G. Romero, M. G. Christiansen, R. Chen, R. Ellison, T. T. O'Malley, U. P. Froriep, D. M. Walsh, P. Anikeeva, "Targeted Magnetic Nanoparticles for Remote Magnetothermal Disruption of Amyloid-β Aggregates," *Adv. Health. Mater*, 4, pp. 2100, 2015.

P. Anikeeva, R. A. Koppes, "Restoring the Sense of Touch," *Science*, 350, pp. 274, 2015.

S. Park, R. A. Koppes, U. P. Froriep, X. Jia, A. K. H. Achyuta, B. L. McLaughlin, P. Anikeeva, "Optogenetic Xontrol of Nerve Growth," *Sci. Rep.* 5, pp. 9669, 2015.

R. Chen, G. Romero, M. G. Christiansen, A. Mohr, P. Anikeeva, "Wireless Magnetothermal Deep Brain Stimulation," *Science*, 347, pp. 1477-1480, 2015.

A. Canales, X. Jia, U. P. Froriep, R. A. Koppes, C. M. Tringides, J. Selvidge, C. Lu, L. Wei, C. Hou, Y. Fink, P. Anikeeva, "Multifunctional Fibers for Optical, Electrical and Chemical Interrogation of Neural Circuits in Vivo," *Nat. Biotechnol.* 33, p. 277-284, 2015.

C. Lu, U.P. Froriep, A. Canales, R. A. Koppes, V. Caggiano, J. Selvidge, E. Bizzi, P. Anikeeva, "Polymer Fiber Probes Enable Optical Control of Spinal Cord and Muscle Function in Vivo," *Adv. Funct. Mater.* 42, pp. 6732-6737, 2014.

M. G. Christiansen, A. W. Senko, R. Chen, G. Romero Uribe, P. Anikeeva, "Magnetically Multiplexed Heating of Single Domain Nanoparticles," *Appl. Phys. Letters*, 104, 213103, 2014.

L. A. Guynaydin, L. Grosenick, J. C. Finkelstein, I. V. Kauvar, L. E. Fenno, A. Adhikari, S. Lammel, J. J. Mirzabekov, R. D. Airan, K. M. Tye, P. Anikeeva, R. C. Malenka, K. Deisseroth, "Natural Neural Projection Dynamics Underlying Social Behavior Modulation," *Cell 157*, 1525, 2014.

H. Liske, X. Qian, P. Anikeeva, K. Deisseroth, S. Delp, "Optical Control of Neuronal Excitation and Inhibition Using a Single Opsin Protein, ChR2," *Scientific Reports*, 3:3110, 2013.

R. Chen, M. G. Christiansen, P. Anikeeva, "Maximizing Hysteretic Losses in Magnetic Ferrite Nanoparticles via Model-driven Synthesis and Materials Optimization," *ACS Nano*, 7, 8990, 2013.

Dimitri A. Antoniadis

Ray and Maria Stata Professor of Electrical Engineering
Department of Electrical Engineering & Computer Science

Research is in the field of nanoscale solid-state electronic devices and the application of new materials systems and new structures to transistors for deeply scaled electronics.

Rm. 39-427a | 617-253-4693 | daa @ mtl . mit . edu

GRADUATE STUDENTS

Winston Chern, EECS
Ujwal Radhakrishna, EECS
Tao Yu, EECS

SUPPORT STAFF

Steven O'Hearn, Administrative Assistant II

SELECTED PUBLICATIONS

P. Choi, S. Goswami, U. Radhakrishna, D. Khanna, C-C. Boon, H-S Lee, D. A. Antoniadis, L-S. Peh, "A 5.9-GHz Fully Integrated GaN Frontend Design With Physics-Based RF Compact Model," *Microwave Theory and Techniques*, IEEE Transactions on 62 (4), pp. 1163-1173, 2015.

J. Lin, D. A. Antoniadis, J. A. del Alamo, "Physics and Mitigation of Excess OFF-State Current in InGaAs Quantum-Well MOSFETs," *IEEE Trans. Electr. Dev.* 62 (5), pp. 1448 - 1455, 2015.

S. Rakheja, M. S. Lundstrom, and D. A. Antoniadis, "An Improved Virtual-Source-Based Transport Model for Quasi-Ballistic Transistors—Part I: Capturing Effects of Carrier Degeneracy, Drain-Bias Dependence of Gate Capacitance, and Nonlinear Channel-Access Resistance," *IEEE Trans. Electr. Dev.* 62 (9), pp 2786 - 2793, 2015.

S. Rakheja, M. S. Lundstrom, and D. A. Antoniadis, "An Improved Virtual-Source-Based Transport Model for Quasi-Ballistic Transistors—Part II: Experimental Verification," *IEEE Trans. Electr. Dev. 62* (9), pp. 2794 - 2801, 2015.

J. Lin, D. A. Antoniadis, J. A. del Alamo, "Impact of Intrinsic Channel Scaling on InGaAs Quantum-Well MOSFETs," *IEEE Transactions on Electronic Devices*, 62 (11), pp. 3470 - 3476, 2015.

U. Radhakrishna, P. Choi, L-S. Peh, D. A. Antoniadis, "MIT Virtual Source RF Model as a Tool for GaN-Based LNA and Oscillator Design," *Compound Semiconductor Integrated Circuit Symposium (CSICS)*, (IEEE) pp. 1-4, 2015.

U. Radhakrishna, S. Lim, P. Choi, T. Palacios, D. A. Antoniadis, "GaNFET Compact Model for Linking Device Physics, High Voltage Circuit Design and Technology Optimization," *International Electron Devices Meeting (IEDM)*, 2015.

T. Yu, U. Radhakrishna, J. L. Hoyt, D. A. Antoniadis, "Understanding the Limit of Gate Efficiency (GE) on the Ultimate Steepness of InGaAs/GaAsSb Quantum-well Tunnel-FET: Experiments, Modeling and Design Guidelines for Steep Switching," *International Electron Devices Meeting (IEDM)*, 2015.

J. A. del Alamo, D. A. Antoniadis, J. Lin, W. Lu, A. Vardi, X. Zhao, "III-V MOSFETs for Future CMOS" *Compound Semiconductor Integrated Circuit Symposium (CSICS)*, pp. 1-4, 2015.

L. Yu, D. El-Damak, S. Ha, S. Rakheja, L. Xi Ling, J. Kong, D. A. Antoniadis, A. Chandrakasan, T. Palacios, "MoS_2 FET Fabrication and Modeling for Large-Scale Flexible Electronics," *Symposium on VLSI Technology*, pp. T144 - T145, 2015.

L. Yu, S. Saxena, C. Hess, I.A.M. Elfadel, D. A. Antoniadis, D. S. Boning, "Statistical Library Characterization Using Belief Propagation Across Multiple Technology Nodes," *Design, Automation & Test in Europe Conference & Exhibition*, pp. 1383 - 1388, 2015.

S. Rakheja, and D. A. Antoniadis, "Physics-based Compact Modeling of Charge Transport in Nanoscale Electronic Devices," *International Electron Devices Meeting (IEDM)*, 2015.

J. Lin, D. A. Antoniadis, and J. A. del Alamo, "A CMOS-compatible Fabrication Process for Scaled Self-Aligned InGaAs MOSFETs," *30th International Conference on Compound Semiconductor Manufacturing Technology* (CS MANTECH), pp. 12.2, Scottsdale, USA, May 18-21, 2015.

Karl K. Berggren

Professor

Department of Electrical Engineering & Computer Science

Current research focuses on methods of nanofabrication, especially applied to superconductive quantum circuits, photodetectors, high-speed superconductive electronics, and energy systems.

Rm. 36-219 | 617-324-0272 | berggren @ mit . edu

POSTDOCTORAL ASSOCIATES

Mostafa Bedewy, RLE
Richard Hobbs, RLE
Yachin Ivry, RLE
Chung-Soo Kim, RLE
Amir Tavakkoli K. G., RLE
Qingyuan Zhao, RLE

GRADUATE STUDENTS

Navid Abedzadeh, EECS
Akshay Agarwal, EECS
Lucy Archer, Physics
Francesco Bellei, EECS
Andrew Dane, EECS
Hyung Wan Do, EECS
Sarah Goodman, DMSE
Vitor Manfrinato, EECS
Adam McCaughan, EECS
Vitor Manfrinato, EECS
Faraz Najafi, EECS
Sam Nicaise, EECS
Kameron Oser, EECS
Yujia Yang, EECS
Di Zhu, EECS

UNDERGRADUATE STUDENTS

Nathnael Abebe, EECS
Corey Cleveland, EECS

VISITORS

Wenping Li, Beihang University
Marco Turchetti, Politecnico di Torino

SUPPORT STAFF

James Daley, Research Specialist
Kathryn Fischer, Fiscal Assistant
Dorothy Fleischer, Administrative Assistant
Mark Mondol, Assistant Director

SELECTED PUBLICATIONS

P. Kruit, R. G. Hobbs, C-S. Kim, Y. Yang, V. R. Manfrinato, J. Hammer, S. Thomas, P. Weber, B. Klopfer, C. Kohstall, T. Juffmann, M. A. Kasevich, P. Hommelhoff, K. K. Berggren, "Designs for a Quantum Electron Microscope," *Ultramicroscopy* 164, 31-45, 2016.

F. Najafi, F. Marsili, V. B. Verma, Q. Zhao, M. D. Shaw, K. K. Berggren, and S. W. Nam, "Superconducting Nanowire Architectures for Single Photon Detection," *Superconducting Devices in Quantum Optics*, R. H. Hadfield and G. Johansson, Eds. Springer International, 2016.

Q. Zhao, D. Zhu, N, Calandri, A. E. Dane, A. N. McCaughan, F. Bellei, H-Z. Wang, D. F. Santavicca, K. K. Berggren, "A Scalable Single-photon Imager Using a Single Superconducting Nanowire," *arXiv*:1605.08693, 2016.

F. Bellei, A. P. Cartwright, A. N. McCaughan, A. E. Dane, F. Najafi, Q. Zhao, K. K. Berggren, "Free Space-coupled Superconducting Nanowire Single Photon Detectors For Infrared Optical Communications," *Optics Express* 24(4), 3248-3257, 2016.

J.-B. Chang, Y. H. Kim, E. Thompson, Y. H. No, N. H. Kim, J. Arrieta, V. R. Manfrinato, A. E. Keating, K. K. Berggren, "The Orientations of Large Aspect-Ratio Coiled-Coil Proteins Attached to Gold Nanostructures," *Small* 12(11), 1498-1505, 2016.

A. Tavakkoli K. G., S. M. Nicaise, K. R. Gadelrab, A. Alexander-Katz, C.A. Ross, K. K. Berggren, "Multilayer Block Copolymer Meshes by Orthogonal Self-assembly," *Nature Communications* 7, 10518 2016.

J. J. Cheng, S. M. Nicaise, K. K. Berggren, S. Gradečak, "Dimensional Tailoring of Hydrothermally Grown Zinc Oxide Nanowire Arrays," *Nano Letters*, 16(1), 2016.

A. N. McCaughan, Q. Zhao, K. K. Berggren, "NanoSQUID Operation Using Kinetic Rather Than Magnetic Induction," *Scientific Reports* 6, 28095, 2016.

R. G. Hobbs, V. R. Manfrinato, Y. Yang, S. A. Goodman, L. Zhang, E. A. Stach, K. K. Berggren, "High-energy Surface and Volume Plasmons in Nanopatterned sub-10-nm Aluminum Nanostructures," *Nano Letters*, 16(7), 4149-4157, 2016.

F. Najafi, F. A. Dane, F. Bellei, Q. Zhao, K. Sunter, A. McCaughan, K. K. Berggren, "Fabrication process yielding saturated nanowire single-photon detectors with 24-ps jitter," *IEEE Journal of Selected Topics in Quantum Electronics* 21(2), article #3800507, 2015.

K. A. Sunter, A. E. Dane, C. I. Lang, K. K. Berggren, "Infrared Transmissometer to Measure the Thickness of NbN Thin Films," *Applied Optics* 54 (18), 5743-5749, 2015.

Duane S. Boning

Clarence J. LeBel Professor of Electrical Engineering
Professor of Electrical Engineering & Computer Science
Department of Electrical Engineering & Computer Science

Design for manufacturability of processes, devices, and circuits. Understanding variation in semiconductor, photonics and MEMS manufacturing, emphasizing statistical, machine learning, and physical modeling of spatial and operating variation in circuits, devices, and CMP, electroplating, spin coating, etch, and embossing processes.

Rm. 39-415a | 617-253-0931 | boning @ mtl . mit . edu

POSTDOCTORAL ASSOCIATES

Yahya Hosseini, MTL

GRADUATE STUDENTS

Naomi Arnold, ESD and Sloan
Hongge Chen, EECS
Ana Maria Ortiz Garcia, ESD and Sloan
Chris Lang, EECS
John Lee, EECS

VISITORS

Masahiro Sakuta, Hitachi HiTech

SUPPORT STAFF

Jami Hinds, Administrative Assistant II
Nick Moscato, Administrative Assistant II
Leslie Quinn, Administrative Assistant II

SELECTED PUBLICATIONS

H. Boo, D. S. Boning, and H. S. Lee, "A 12b 250MS/s Pipelined ADC with Virtual Ground Reference Buffers," *IEEE Journal on Solid-State Circuits*, vol. 50, no. 12, pp. 2912-2921, December 2015.

D. S. Boning, W. Fan, Y. Zhuang, Y. Sampurno, and A. Philipossian, "Planarization with Suspended Polyurethane Beads and a Stiff Counterface: Pad-in-a-Bottle Experiments and Simulation," *International Conference on Planarization Technology (ICPT),* pp. 54-57, Phoenix, AZ, October 2015.

J. H. Lee, J. Jimenez, X. Zhang, D. S. Boning, and B. W. Anthony, "Ultrasound Image-based Absolute Concentration Measurement Technique for Materials with Low Scatterer Concentration," *2015 IEEE International Ultrasonics Symposium (IUS)*, Taipei, Taiwan, October 2015.

J. H. Lee, J. Jimenez, I. R. Butterworth, C. Castro-Gonzalez, S. K. Shukla, B. Marti-Fuster, L. Elvira, D. S. Boning, and B. W. Anthony, "Measurement of Very Low Concentration of Microparticles in Fluid by Single Particle Detection using Acoustic Radiation Force Induced Particle Motion," *2015 IEEE International Ultrasonics Symposium (IUS),* Taipei, Taiwan, October 2015.

W. H. Teh, D. S. Boning, and R. E. Welsch, "Multi-Strata Stealth Dicing Before Grinding for Singulation-Defects Elimination and Die Strength Enhancement: Experiment and Simulation," *IEEE Trans. on Semiconductor Manufacturing,* vol. 28, no. 3, pp. 408-423, August 2015.

W. H. Teh, D. S. Boning, and R. Welsch, "Multistrata Subsurface Laser-Modified Microstructure With Backgrind-Assisted Controlled Fracture for Defect-Free Ultrathin Die Fabrication," *IEEE Trans. on Components, Packaging and Manufacturing Technology*, vol. 5, no. 7, pp. 1006-1018, July 2015.

W. H. Teh, D. S. Boning, and R. Welsch, "Multi-strata Subsurface Laser Die Singulation to Enable Defect-free Ultra-thin Stacked Memory Dies," *AIP Advances*, vol. 5, no. 5, 057128:1-7, May 2015.

V. Michael Bove, Jr.

Principal Research Scientist
Media Arts and Sciences/Media Lab

Sensing, communication, user interface, and display (particularly 3D and holographic) for consumer electronics. Materials and fabrication methods for diffractive light modulators.

Rm. E15-448 | 617-253-0334 | vmb @ media . mit . edu

POSTDOCTORAL ASSOCIATES

Nickolaos Savidis, MAS

GRADUATE STUDENTS

Bianca Datta, MAS
Sundeep Jolly, MAS
Everett Lawson, MAS
Andrew MacInnes, MAS
Philippa Mothersill, MAS
Daniel Novy, MAS
Laura Perovich, MAS
Edwina Portocarrero, MAS
Ali Shtarbanov, MAS

SUPPORT STAFF

Kristin Hall, Administrative Assistant II

SELECTED PUBLICATIONS

K. Nakamura, H. Takagi, T. Goto, P. B. Lim, H. Horimai, H. Yoshikawa, V. M. Bove Jr., and M. Inoue, "Improvement of Diffraction Efficiency of Three-dimensional Magneto-optic Spatial Light Modulator with Magnetophotonic Crystal," *Appl. Phys. Letters,* 108, 022404, 2016.

N. Savidis, S. Jolly, B. Datta, T. Karydis, and V. M. Bove, Jr., "Fabrication of Waveguide Spatial Light Modulators via Femtosecond Laser Micromachining," *Proc. SPIE Advanced Fabrication Technologies for Micro/Nano Optics and Photonics* IX, 9759, 2016.

S. Jolly, N. Savidis, B. Datta, V. M. Bove, Jr., and D. Smalley, "Progress in Off-plane Computer-generated Waveguide Holography for Near-to-eye 3D Display," *Proc. SPIE Practical Holography XXX: Materials and Applications*, 9771, 2016.

D. E. Smalley, S. McLaughlin, C. Leach, J. Kimball V. M. Bove, Jr., and S. Jolly, "Progress on Characterization and Optimization of Leaky-mode Modulators for Holographic Video," *Journal Micro/Nanolith. MEMS MOEMS* 14(4), 041308, doi:10.1117/1.JMM.14.4.041308, August 27, 2015.

S. Jolly, E. Dreshaj, and V. M. Bove, Jr., "Computation of Fresnel Holograms and Diffraction-specific Coherent Panoramagrams for Full-color Holographic Displays Based on Anisotropic Leaky-mode Modulators," *Proc. SPIE Practical Holography XXIX*, 9386, 2015.

Vladimir Bulović
Associate Dean for Innovation
Fariborz Maseeh Professor of Emerging Technology
Department of Electrical Engineering & Computer Science

Physical properties of organic and organic/inorganic nanocrystal composite thin films and structures, and development of nanostructured electronic and optoelectronic devices. Applications of nanostructured materials in large-scale technologies.

Rm. 13-3138 | 617-253-7012 | bulovic @ mit . edu

RESEARCH SCIENTISTS

Anna Osherov, RLE
Annie Wang, RLE

POSTDOCTORAL ASSOCIATES

Giovanni Azzellino, RLE
Parag Deotare, RLE
Harold Hwang, RLE
Anna Osherov, RLE
Samuel Stranks, RLE, Oxford University, Marie Curie Fellow
Annie Wang, RLE

GRADUATE STUDENTS

Patrick Brown, Physics, Fannie and John Hertz Foundation Graduate Fellowship and the National Science Foundation Graduate Research Fellowship
Wendi Chang, EECS
Joel Jean, EECS, National Science Foundation Graduate Research Fellowship
Thomas Mahony, EECS, National Science Foundation Graduate Research Fellowship
Apoorva Murarka, EECS
Farnaz Niroui, EECS, NSERC Postgraduate Scholarship-Doctoral
Melany Sponseller, EECS
Geoffrey Supran, DMSE
Richard Swartout, EECS, Tata Fellowship
Mengfei Wu, EECS
Sihan Xie, DMSE
Haz Zhu, Physics

UNDERGRADUATE STUDENTS

Roberto Brenes, EECS

VISITORS

Hafez Abdelaziz, American University of Cairo
Nageh Allam, American University of Cairo
Ahmad Amer, American University of Cairo
Roberto Brenes, EECS
Mayuran Saravanapavanantham, University of Waterloo
Petar Todorovich, University of Waterloo

SUPPORT STAFF

Samantha Farrell, Administrative Assistant II

SELECTED PUBLICATIONS

J. Jean, A. Wang, and V. Bulović, "In Situ Vapor-deposited Parylene Substrates for Ultra-thin, Lightweight Organic Solar Cells," *Organic Electronics,* vol. 31, pp. 120-126, 2016.

A. Murarka, J. H. Lang, and V. Bulović, "Printed Membrane Electrostatic MEMS Microspeakers," In *2016 IEEE 29th International Conference on Micro Electro Mechanical Systems (MEMS)*, Jan 24-28, pp. 1118-1121, 2016.

M. Wu, D. N. Congreve, M. W. B. Wilson, J. Jean, N. Geva, M. Welborn, T. Van Voorhis, V. Bulović, M. G. Bawendi, and M. A. Baldo, "Solid-state Infrared-to-Visible Upconversion Sensitized by Colloidal Nanocrystals," *Nature Photonics* vol. 10, pp. 31-34, 2016.

G. J. Supran, K. W. Song, G. W. Hwang, R. E. Correa, J. Scherer, E. A. Dauler, Y. Shirasaki, M. G.Bawendi, and V. Bulović, "High-Performance Shortwave-Infrared Light-Emitting Devices Using Core–Shell (PbS–CdS) Colloidal Quantum Dots," *Advanced Materials,* vol. 27, pp. 1437-1442, 2015.

P. B. Deotare, W. Chang, E. Hontz, D. N. Congreve, L. Shi, P. D. Reusswig, B. Modtland *et al*, "Nanoscale transport of charge-transfer states in organic donor-acceptor blends," *Nature Materials*, vol. 14, pp. 1130-1134, 2015.

C. H. M Chuang, A. Maurano, R. E. Brandt, G. W. Hwang, J. Jean, T. Buonassisi, V. Bulović, and M. G. Bawendi, "Open-circuit voltage deficit, radiative sub-bandgap states, and prospects in quantum dot solar cells," *Nano Letters* vol. 15, pp. 3286-3294, 2015.

J. Jean, P. R. Brown, R. L. Jaffe, T. Buonassisi, and V. Bulović, "Pathways for Solar Photovoltaics," *Energy & Environmental Science,* vol. 8, pp. 1200-1219, 2015.

E. Hontz, W. Chang, D. N. Congreve, V. Bulović, M. A. Baldo, and T. Van Voorhis, "The Role of Electron–Hole Separation in Thermally Activated Delayed Fluorescence in Donor–Acceptor Blends," *The Journal of Physical Chemistry C,* vol. 119, pp. 25591-25597, 2015.

W. Chang, G. M. Akselrod, and V.Bulović, "Solid-State Solvation and Enhanced Exciton Diffusion in Doped Organic Thin Films under Mechanical Pressure," *ACS Nano,* vol. 9, pp. 4412-4418, 2015.

F. Niroui, A. I. Wang, E. M. Sletten, Y. Song, J. Kong, E. Yablonovitch, T.M. Swager, J. H. Lang, and V. Bulović, "Tunneling Nanoelectromechanical Switches Based on Compressible Molecular Thin Films," *ACS Nano,* vol. 9, pp. 7886-7894, 2015.

Tonio Buonassisi

Associate Professor
Department of Mechanical Engineering

Solar energy conversion; photovoltaics; power system design and optimization; novel manufacturing technologies

Rm. 35-213 | 617-253-5130 | buonassisi @ mit . edu

RESEARCH SCIENTISTS

Mariela Castillo, MechE
Marius Peters, MechE
Jim Serdy, MechE

POSTDOCTORAL ASSOCIATES

Robert Hoye, MechE
Vera Steinmann, MechE

GRADUATE STUDENTS

Riley Brandt, MechE, NSF Fellow
Rupak Chakraborty, MechE, TOTAL Fellow
Mallory Jensen, MechE, NSF Fellow
Rachel Kurchin, DMSE
Erin Looney, MechE, NSF Fellow
Jonathan Mailoa, EECS, Martin Family Fellow
Ashley Morishige, MechE, NDSEG Fellow
David Berney Needleman, MechE, NDSEG Fellow
Felipe Oviedo, MechE
Jeremy Poindexter, DMSE
Alex Polizzotti, MechE, NSF Fellow
Sarah Sofia, MechE
Sterling Watson, MechE, Tata Fellow
Patricia Yen, MechE, NSF Fellow
Amanda Youssef, MechE

UNDERGRADUATE STUDENTS

Juan M. Angulo, MechE
Luisa Barrera, DMSE
Dayna E. Erdmann, MechE
Kathleen V. Guerra, MechE
Frances Lenahan, DMSE

VISITORS

Hannu Laine, Aalto University, Finland
Liu Zhe, Solar Energy Research Institute of Singapore

SUPPORT STAFF

Janice McCarthy, Administrative Assistant II

SELECTED PUBLICATIONS

D.M. Powell, V.P. Markevich, J. Hofstetter, M. Ann Jensen, A.E. Morishige, S. Castellanos, B. Lai, A.R. Peaker, and T. Buonassisi, “Exceptional Gettering Response of Epitaxially Grown Kerfless Silicon,” *Journal of Applied Physics* 119, 065101, 2016.

J. Hofstetter, C. del Cañizo, H. Wagner, S. Castellanos, and T. Buonassisi, “Material Requirements for the Adoption of Unconventional Silicon Crystal and Wafer Growth Techniques for High-efficiency Solar Cells,” *Progress in Photovoltaics* 24, 122–132, 2016.

S.C. Siah, R.E. Brandt, K. Lim, L.T. Schelhas, R. Jaramillo, M.D. Heinemann, D. Chua, J. Wright, J.D. Perkins, C.U. Segre, R.G. Gordon, M.F. Toney, and T. Buonassisi, “Dopant Activation in Sn-doped Ga_2O_3 Investigated by X-ray Absorption Spectroscopy,” *Applied Physics Letters* 107, 252103, 2015.

V. Steinmann, R.E. Brandt, T. Buonassisi, “Non-cubic Solar Cell Materials,” *Nature Photonics* 9, 355, 2015.

J. P. Mailoa, C. D. Bailie, E. C. Johlin, E. T. Hoke, A. J. Akey, W. H. Nguyen, M. D. McGehee, T. Buonassisi, “A 2-Terminal Perovskite/Silicon Multijunction Solar Cell Enabled by a Silicon Tunnel Junction,” *Applied Physics Letters* 106, 121105, 2015.

R.E. Brandt, V. Stevanovic, D.S. Ginley, and T. Buonassisi, “Identifying Defect-tolerant Semiconductors with High Minority-carrier Lifetimes: Beyond Hybrid Lead Halide Perovskites,” *MRS Comm.* 5, 265, 2015.

H. Liu, Z. Ren, Z. Liu, A.G. Aberle, T. Buonassisi, and I.M. Peters, “The Realistic Energy Yield Potential of GaAs-on-Si Tandem Solar Cells: A Theoretical Case Study,” *Optics Express* 23, A382– A390, 2015.

Z. Ren, J.P. Mailoa, Z. Liu, H. Liu, S.C. Siah, T. Buonassisi, and I.M. Peters, “Numerical Analysis of Radiative Recombination and Reabsorption in GaAs/Si Tandem,” *IEEE Journal of Photovoltaics* 5, 1079–1086, 2015.

M. Ann Jensen, J. Hofstetter, A.E. Morishige, G. CoLettersi, B. Lai, D.P. Fenning, and T. Buonassisi, “Synchrotron-based Analysis of Chromium Distributions in Multicrystalline Silicon for Solar Cells,” *Applied Physics Letters* 106, 202104, 2015.

A.E. Morishige, H.S. Laine, J. Schön, A. Haarahiltunen, J. Hofstetter, C. del Cañizo, M.C. Schubert, and T. Buonassisi, “Building Intuition of Iron Evolution During Solar Cell Processing Through Analysis of Different Process Models,” *Applied Physics A* 120, 1357, 2015.

Anantha Chandrakasan
Department Head, Vannevar Bush Professor of Electrical Engineering & Computer Science
Department of Electrical Engineering & Computer Science

Design of digital integrated circuits and systems. Energy efficient implementation of signal processing, communication and medical systems. Circuit design with emerging technologies.

Rm. 38-107 | 617-258-7619 | anantha @ mtl . mit . edu

POSTDOCTORAL ASSOCIATES
Dina El-Damak, EECS
Arun Paidimarri, MTL
Rabia Tugce Yazicigil, MTL

GRADUATE STUDENTS
Omid Abarii, EECS
Georgios Angelopoulos, EECS
Mohamed Radwan Abdelhamid, EECS
Ishwarya Ananthabhotla, EECS
Utsav Banerjee, EECS
Avishek Biswas, EECS
Nachiket Desai, EECS
Chuhong Duan, EECS
Preetinder Garcha, EECS
Jason Gao, EECS
Taehoon Jeong, EECS
Chiraag Juvekar, EECS
Harneet Khurana, EECS
Bonnie Lam, EECS
Phillip Nadeau, EECS
Sirma Orguc, EECS
Michael Price, EECS
Priyanka Raina, EECS
Mehul Tikekar, EECS
Gilad Yahalom, EECS
Frank Yaul, EECS

SUPERUROP AND UROP
Cimran Virdi
Lisa Ho
Skanda Koppula
Sheena Nie

VISITORS
Dennis Buss, Texas Instruments
Marisa Lopez-Vallejo, Universidad Politécnica de Madrid
Bo Wang

SUPPORT STAFF
Margaret Flaherty, Senior Administrative Assistant
Lindsay Shanahan, Administrative Assistant II

PUBLICATIONS

A. Paidimarri, N. Ickes, A. P. Chandrakasan, "A +10 dBm BLE Transmitter With Sub-400 pW Leakage for Ultra-Low Duty Cycles," *IEEE Journal of Solid-State Circuits,* vol. 51, no. 6, pp.1331-1346, June 2016.

P. Nadeau, A. Paidimarri, A. P. Chandrakasan, "Ultra Low-Energy Relaxation Oscillator With 230 fJ/cycle Efficiency," *IEEE Journal of Solid-State Circuits,* vol. 51, no. 4, pp. 789-799, April 2016.

D. Jeon, N. Ickes, P. Raina, H. C. Wang, A. P. Chandrakasan, "A 0.6V 8mW 3D Vision Processor for a Navigation Device for the Visually Impaired," *IEEE International Solid-State Circuits Conference (ISSCC),* February 2016.

C. S. Juvekar, H. M. Lee, J. Kwong, A. P. Chandrakasan, "A Keccak-based Wireless Authentication Tag with Per-query Key Update and Power-glitch Attack Countermeasures," *IEEE International Solid-State Circuits Conference (ISSCC),* February 2016.

F. Yaul, A. P. Chandrakasan, "A sub-µW 36nV/√Hz Chopper Amplifier for Sensors Using a Noise-efficient Inverter-based 0.2V-supply Input Stage," *IEEE International Solid-State Circuits Conference (ISSCC),* February 2016.

O. Abari, D. Vasisht, D. Katabi, A. P. Chandrakasan, "Caraoke: An E-Toll Transponder Network for Smart Cities," *ACM Special Interest Group on Data Communication (SIGCOMM),* August 2015.

G. Angelopoulos, M. Médard, A. P. Chandrakasan, "Adapt-Cast: An Integrated Source to Transmission Scheme for Wireless Sensor Networks," *IEEE International Conference on Communications (ICC),* pp. 2894-2899, June 2015.

P. Nadeau, A. Paidimarri, A. P. Chandrakasan, "4.2 pW Timer for Heavily Duty-Cycled Systems," *IEEE Symposium on VLSI Circuits (VLSIC),* pp. 240-241, June 2015.

D. El-Damak, A. P. Chandrakasan, "Solar Energy Harvesting System with Integrated Battery Management and Startup Using Single Inductor and 3.2nW Quiescent Power," *IEEE Symposium on VLSI Circuits (VLSIC),* pp. 280-281, June 2015.

L. Yu, D. El-Damak, S. Ha, S. Rakheja, X. Ling, D. Antoniadis, J. Kong, A. P. Chandrakasan, T. Palacios, "MoS_2 FET Fabrication and Modeling for Large-Scale Flexible Electronics," *IEEE Symposium on VLSI Technology (VLSIT),* June 2015.

G. Yahalom, A. Wang, U. Ko, A. P. Chandrakasan, "A Vertical Solenoid Inductor for Noise Coupling Minimization in 3D-IC," *IEEE Radio Frequency Integrated Circuits (RFIC) Symposium,* pp. 55-58, May 2015.

Luca Daniel

Professor
Department of Electrical Engineering & Computer Science

Development of numerical techniques: uncertainty quantification & stochastic integral equation solvers for high dimension parameter spaces; Parameterized model reduction. Applications: cmos MEMS resonators, silicon photonic devices, analog RF circuits & passives; human cardiovascular circulatory system; Magnetic Resonance Imaging systems.

Rm. 36-849 | 617-253-2631 | luca @ mit . edu

POSTDOCTORAL ASSOCIATES

Ian Butterworth, RLE
Zheng Zhang, EECS

GRADUATE STUDENTS

Bichoy Bahr, EECS
José E. C. Serrallés, EECS
Tsui-Wei (Lily) Weng, EECS

UNDERGRADUATE STUDENTS

Andrew Rouditchenko, EECS
Driss Hafdi, EECS
Xavier A. Soriano, EECS
Khaled Moharam, EECS

VISITORS.

Raffaele Ardito, Politecnico di Milano
Kim Batselier, University of Hong Kong
Luca D'Alessandro, Politecnico di Milano
Georgy Guryev, SkolTech Moscow
Paolo Maffezzoni, Politecnico di Milano
Daniele Melati, Politecnico di Milano
Andrea Melloni, Politecnico di Milano
Arezoo Saberi, Politecnico di Milano
Bruno Scaglioni, Politecnico di Milano
Ngai Wong, University of Hong Kong
Wenjian Yu, Tsinghua University
Zdravko Zubac, Ghent University

SUPPORT STAFF

Chadwick Collins, Administrative Assistant

SELECTED PUBLICATIONS

L. D'Alessandro, B. Bahr, L. Daniel, D. Weinstein, R. Ardito, "BESO Approach to Topology Optimization of GaN Phononic Crystals," *ECCOMAS*, Crete, June 2016.

J. E. C. Serrallés, L. Daniel, J.K. White, D.K. Sodickson, R. Lattanzi, and A.G. Polimeridis, "Global Maxwell Tomography: A Novel Technique for Electrical Properties Mapping Based on MR Measurements and Volume Integral Equation Formulations," *Int. Symp AP-S–URSI*, Fajardo, Puerto Rico, June 2016.

Z. Zhang, T.-W. Weng, L. Daniel, "A Big-Data Approach to Handle Process Variations: Uncertainty Quantification by Tensor Recovery," *IEEE Workshop on Signal and Power Integrity*, 4 pages, Turin, Italy, May 2016.

B. Bahr, L. Daniel, D. Weinstein, "Optimization of Unreleased CMOS-MEMS RBTs," *Int. Frequency Control Symp IFCS 2016*, New Orleans, LA, May 2016.

T-W. Weng, D. Melati, A. Melloni, L. Daniel, "Statistical Analysis and Robust Design Optimization of Integrated Photonic Filters," *Nanophotonics*, April 2016 (Invited).

W. Yu, B. Zhang, C. Zhang, H. Wang, L. Daniel, "Utilizing Macromodels in Floating Random Walk Based Capacitance Extraction," IEEE/ACM Design Automation Conf in Europe, Dresden, March 2016.

P. Maffezzoni, B. Bahr, Z. Zhang, L. Daniel, "Reducing Phase Noise in Multi-Phase Oscillators," *IEEE Trans. on Circuits and Systems* 63-I(3): 379-388, March 2016.

Y.C. Hsiao, L. Daniel. "CAPLET: A Highly Parallelized Field Solver for Capacitance Extraction Using Instantiable Basis Functions," *IEEE Trans on Computer-Aided Design of Integr. Circuits & Systems*, vol. 35, no. 3, March 2016.

J.F. Villena, A. Polimeridis, Y.Eryaman, E. Adalsteinsson, L. Wald, J. White, L. Daniel, "Fast Electromagnetic Analysis of Transmit RF Coils Based on Accelerated Integral Equation Methods," *Trans Biomed. Eng.*, January 2016.

H. Liu, X. Y.Z. Xiong, K. Batselier, L. Jiang, L. Daniel, Ngai Wong, "STAVES: Speedy Tensor-Aided Volterra-Based Electronic Simulator," *International Conference on Computer Aided Design*, Austin, TX, 583-588, November 2015.P. Maffezzoni, L. Daniel, N. Shukla, S. Datta, A. Raychowdhury, "Modeling and Simulation of Vanadium Dioxide Relaxation Oscillators," *IEEE Trans. on Circuits & Systems* 62(9):2207-2215, September 2015.

I. Butterworth, J. Seralles, C.S. Mendoza, L. Giancardo, L. Daniel, "A Wearable Physiological Hydration Monitoring Wristband Through Multi-path Non-contact Dielectric Spectroscopy in the Microwave Range," *IEEE MTT-S 2015 (IMWS-BIO)*, Taipei, pp. 60-61, September 2015.

Z. Mahmood, P. McDaniel, B. Guerin, B. Keil, M. Vester, E. Adalsteinsson, L.L. Wald, L. Daniel, "General Design Approach and Practical Realization of Decoupling Matrices for Parallel Transmission Coils," *Magnetic Resonance in Medicine*, July 2015.

Jesús A. del Alamo
MTL Director, Donner Professor
Professor of Electrical Engineering
Department of Electrical Engineering & Computer Science

Nanometer-scale III-V compound semiconductor transistors for future digital, RF, microwave and millimeter wave applications. Reliability of compound semiconductor transistors. Diamond transistors.

Rm. 38-246 | 617-253-4764 | alamo @ mit . edu

RESEARCH SCIENTISTS
Alon Vardi, MTL
Zongyou Yin, MTL

GRADUATE STUDENTS
Xiaowei Cai, EECS
Dongsung Choi, EECS, ILJU Foundation Fellow
Alex Guo, EECS, NDSEG Fellow
Jianqiang Lin, EECS
Wenjie Lu, EECS
Shireen Warnock, EECS, Texas Instruments Fellow
Yufei Wu, EECS
Xin Zhao, DMSE

UNDERGRADUATE STUDENTS
Lisa Kong, DMSE
Allison Lemus, EECS
John Niroula, Physics

SUPPORT STAFF
Elizabeth Kubicki, Administrative Assistant II
Mary O'Neil, Senior Administrative Assistant

SELECTED PUBLICATIONS
F. Hemmi, C. Thomas, Y.-C. Lai, A. Higo, A. Guo, S. Warnock, J. A del Alamo, S. Samukawa, T. Otsuji, and T. Suemitsu, "The Effect of Neutral Beam Etching on Device Isolation in AlGaN/GaN HEMTs," *Compound Semiconductor Week (CSW)*, Toyama, Japan, June 26-30, 2016.

J. A. del Alamo, "Nanometer-Scale III-V CMOS," Invited Plenary Talk at *Compound Semiconductor Week (CSW)*, Toyama, Japan, June 26-30, 2016.

A. Vardi, J. Lin, W. Lu, X. Zhao, and J. A. del Alamo, "High Aspect Ratio InGaAs FinFETs with Sub-20 nm Fin Width," *VLSI Technology Symposium*, Honolulu, HI, June 13-17, 2016.

J. M. López-Villegas, N. Vidal, and J. A. del Alamo, "Toroidal versus Spiral Inductors in Multilayered Technologies," *IEEE Radio Frequency Integrated Circuits Symposium (RFIC)*, San Francisco, CA, May 22-24, 2016.

J. A. del Alamo, "Nanoscale III-V CMOS," Invited Tutorial at *SEMI Advanced Semiconductor Manufacturing Conference (ASMC)*, Saratoga Spring, NY, May 16-19, 2016.

S. Warnock and J. A. del Alamo, "Progressive Breakdown in High-Voltage GaN MIS-HEMTs," *IEEE International Reliability Physics Symposium (IRPS)*, Pasadena, CA, April 17-21, 2016.

A. Guo and J. A. del Alamo, "Negative-Bias Temperature Instability of GaN MOSFETs," *IEEE International Reliability Physics Symposium (IRPS)*, Pasadena, CA, April 17-21, 2016.

J. Lin, Y. Wu, J. A. del Alamo, and D. A. Antoniadis, "Analysis of Resistance and Mobility in InGaAs Quantum-Well MOSFETs from Ballistic to Diffusive Regimes," *IEEE Transactions on Electron Devices*, vol. 63, no. 4, pp. 1464-1470, April 2016.

J. Lin, X. Cai, Y. Wu, D. A. Antoniadis, and J. A. del Alamo, "Record Maximum Transconductance of 3.45 mS/μm for III-V FETs," *IEEE Electron Device Letters*, vol. 37, no. 4, pp. 381-384, April 2016.

J. Lin, D. A. Antoniadis, and J. A. del Alamo, "InGaAs Quantum-Well MOSFET Arrays for Nanometer-Scale Ohmic Contact Characterization," *IEEE Transactions on Electron Devices*, vol. 63, no. 3, pp. 1020-1026, March 2016.

S. Warnock, and J. A. del Alamo, "Characterization of Dielectric Breakdown in High-Voltage GaN MIS-HEMTs," *Microelectronics Reliability & Qualification Working Meeting*, El Segundo, CA, February 9-10, 2016.

W. Lu, J. K. Kim, J. F. Klem, S. D. Hawkins, and J. A. del Alamo, "An InGaSb p-Channel FinFET," *IEEE International Electron Devices Meeting*, Washington, D.C., pp. 819-822, December 6-9, 2015.

A. Vardi, X. Zhao, and J. A. del Alamo, "Quantum-Size Effects in Sub-10 nm Fin Width InGaAs FinFETs," *IEEE International Electron Devices Meeting*, Washington, D.C., pp. 807-810, December 6-9, 2015.

J. Lin, D. A. Antoniadis, and J. A. del Alamo, "Impact of Intrinsic Channel Scaling on InGaAs Quantum-Well MOSFETs," *IEEE Transactions on Electron Devices*, vol. 62, no. 11, pp. 3470-3476, November 2015.

J. A. del Alamo, D. A. Antoniadis, J. Lin, W. Lu, A. Vardi, and X. Zhao, "III-V MOSFETs for Future CMOS," *IEEE Compound Semiconductor IC Symposium*, New Orleans, LA, October 11-14, 2015.

Mildred S. Dresselhaus

Institute Professor
Department of Physics
Department of Electrical Engineering & Computer Science

Carbon nanostructures including nanotubes and graphene
Rm. 13-3005 | 617-253-6864 | millie @ mgm . mit . edu

POSTDOCTORAL ASSOCIATE

Lin Zhou, RLE

GRADUATE STUDENTS

Shengxi Huang, EECS
Yuxuan Lin, EECS
Ricardo Pablo Pedro, Chemistry
Kai Xu, EECS
Xu Zhang, EECS
Ahmad Zubair, EECS

SUPPORT STAFF

Read Schusky, Administrative Assistant II

SELECTED PUBLICATIONS

S. X. Huang, L. B. Liang, X. Ling, A. A. Puretzky, D. B. Geohegan, B. B. Sumpter, J. Kong, V. Meunier, M. S. Dresselhaus, "Low-frequency Interlayer Raman Modes to Probe Interface of Twisted Bilayer MoS_2," *Nano Letters,* 16(2):1435, 2016.

X. Ling, S. X. Huang, E. H. Hasdeo, L. B. Liang, W. M. Parkin, Y. Tatsumi, A. R. T. Nugraha, A. A. Puretzky, P. M. Das, B. G. Sumpter, D. B. Geohegan, J. Kong, R. Saito, M. Drndic, V. Meunier, M. S. Dresselhaus, "Anisotropic Electron-photon and Electron-phonon Interactions in Black Phosphorus," *Nano Letters,* Article ASAP, 2016.

X. Ling, Y. X. Lin, Q. Ma, Z. Q. Wang, Y. Song, L. Yu, S. X. Huang, W. J. Fang, X. Zhang, A. L. Hsu, Y. Q. Bie, Y.H. Lee, Y. M. Zhu, L. J. Wu, J. Li, P. Jarillo-Herrero, M. Dresselhaus, T. Palacios, J. Kong, "Parallel Stitching of 2D materials," *Adv. Mat.* 28(12):2322, 2016.

L. Zhou, K. Xu, A. Zubair, A. D. Liao, W. J. Fang, F. P. Ouyang, Y.H. Lee, K. Ueno, R. Saito, T. Palacios, J. Kong, M. S. Dresselhaus, "Large-area Synthesis of High-quality Uniform Few-layer $MoTe_2$," *JACS* 137(37):11892, 2015.

X. Ling, L. B. Liang, S. X. Huang, A. A. Puretzky, D. B. Geohegan, B. G. Sumpter, J. Kong, V. Meunier, M. S. Dresselhaus, "Low-frequency Interlayer Breathing Modes in Few-layer Black Phosphorus," *Nano Letters,* 15(6):4080, 2015.

W. J. Fang, A. Hsu, Y. C. Shin, A. Liao, S. X. Huang, Y. Song, X. Ling, M. S. Dresselhaus, T. Palacios, J. Kong, "Application of Tungsten as a Carbon Sink for Synthesis of Large-domain Uniform Monolayer Graphene Free of Bilayers/ Multilayers," *Nanoscale* 7(11):4929, 2015.

X. Ling, W. J. Fang, Y. H. Lee, P. T. Araujo, X. Zhang, J. F. Rodriguez-Nieva, Y. X. Lin, J. Zhang, J. Kong, M. S. Dresselhaus, "Raman Enhancement Effect on Two-dimensional Layered Materials: Graphene, h-BN and MoS_2," *Nano Letters,* 14(6):3033, 2014.

W. J. Fang, A. L. Hsu, Y. Song, A. G. Birdwell, M. Amani, M. Dubey, M. S. Dresselhaus, T. Palacios, J. Kong, "Asymmetric Growth of Bilayer Graphene on Copper Enclosures Using Low-pressure Chemical Vapor Deposition," *ACS Nano* 8(6):6491, 2014.

X. Zhang, A. Hsu, H. Wang, Y. Song, J. Kong, M. S. Dresselhaus, T. Palacios, "Impact of Chlorine Functionalization on High-mobility Chemical Vapor Deposition Grown Graphene," *ACS Nano* 7(8):7262, 2013.

Y. H. Lee, L. L. Yu, H. Wang, W. J. Fang, X. Ling, Y. M. Shi, C. T. Lin, J. K. Huang, M. T. Chang, C. S. Chang, M. Dresselhaus, T. Palacios, L. J. Li, J. Kong, "Synthesis and Transfer of Single-layer Transition Metal Disulfides on Diverse Surfaces," *Nano Letters,* 13(4):1852, 2013.

D. L. Mafra, J. Kong, K. Sato, R. Saito, M. S. Dresselhaus, P. T. Araujo, "Using Gate-modulated Raman Scattering and Electron-phonon Interactions to Probe Single-layer Graphene: A Different Approach to Assign Phonon Combination Modes," *PRB* 86(19):195434, 2012.

A. Reina, X. Jia, J. Ho, D. Nezich, H. Son, V. Bulović, M. S. Dresselhaus, J. Kong, "Large Area, Few-layer Graphene Films on Arbitrary Substrates by Chemical Vapor Deposition," *Nano Letters,* 9(1):30, 2009.

K. Nakada, M. Fujita, G. Dresselhaus, M. S. Dresselhaus, "Edge State in Graphene Ribbons: Nanometer Size Effect and Edge Shape Dependence," *PRB* 54(24):17954, 1996.

R. Saito, M. Fujita, G. Dresselhaus, M. S. Dresselhaus, "Electronic-structure of Chiral Graphene Tubules," *Appl. Phys. Letters,* 60(18):2204, 1992.

Dirk R. Englund

Jamieson Career Development Professor
Department of Electrical Engineering & Computer Science

Development of semiconductor quantum information processing devices and systems, quantum enhanced sensors, and nanophotonic and electro-optic devices.

Rm. 36-591 | 617-324-7014 | englund @ mit . edu

POSTDOCTORAL ASSOCIATES

Dmitri Efetov, RLE
Gabriele Grosso, RLE
Mikkel Heuck, RLE
Sinan Karaveli, RLE
Tim Schröder, RLE

GRADUATE STUDENTS

Eric Bersin, NASA GSRP Fellow
Darius Bunandar, Physics
Edward Chen, EECS, NASA GSRP Fellow
Hyeongrak Choi, EECS
Hannah Clevenson, EECS, NASA GSRP Fellow
Christopher Foy, EECS, NSF Fellow
Jordan Goldstein, EECS
Donggyu Kim, MSE
Catherine Lee, EECS
Tsung-Ju Lu, EECS, NSF NDSEG Fellow
Hyowon Moon, EECS
Sara Mouradian, EECS
Mihir Pant, EECS
Cheng Peng, EECS
Reyu Sakakibara, EECS, NSF Fellow
Ren-Jye Shiue, EECS
Anubhav Sinha, EECS
Gregory Steinbrecher, EECS, NDSEG Fellow
Carson Teale, EECS, MIT Lincoln Laboratory Fellow
Matthew Trusheim, EECS, NSF IGERT Fellow
Michael Walsh, EECS
Noel Wan, EECS
Jiabao Zheng, Columbia EE

UNDERGRADUATE STUDENTS

Uttara Chakraborty, EECS & Physics
Tamara Dordevic, Physics
Amir Karamlou, EECS
Margaret Pavlovich, Physics
Mihika Prabhu, EECS & Physics
Marisa Sotolongo, Physics
Liang Zhou, EECS

SUPPORT STAFF

Janice Balzer, Administrative Assistant

SELECTED PUBLICATIONS

L. Li, Tim Schröder, Ed. H. Chen, M. Walsh, I. Bayn, J. Goldstein, O. Gaathon, M. E. Trusheim, M. Lu, J. Mower, M. Cotlet, M. L. Markham, D. J. Twitchen, D. Englund, "Coherent Spin Control of a Nanocavity-enhanced Qubit in Diamond," *Nature Communications* 6, 6173, 2015.

H. Clevenson, M. E. Trusheim, T. Schröder, C. Teale, D. Braje, and D. Englund, "Broadband Magnetometry and Temperature Sensing with a Light Trapping Diamond Waveguide," *Nature Physics AOP*, 2015.

D. Bunandar, Z. Zhang, H. H. Shapiro, and D. Englund, "Practical High-dimensional Quantum Key Distribution with Decoy States," *Phys. Rev.* A 91, 022336, 2015.

F. Najafi, J. Mower, N. C. Harris, F. Bellei, A. Dane, C. Lee, X. Hu, P. Kharel, F. Marsili, S. Assefa, K. K. Berggren, and D. Englund, "On-chip Detection of Non-classical Light by Scalable Integration of Single-photon Detectors," *Nature Communications* 6, 5873, 2015.

L. Li, E. H. Chen, J. Zheng, S. L. Mouradian, F. Dolde, T. Schröder, S. Karaveli, M. L. Markham, D. J. Twitchen, D. Englund, "Efficient Photon Collection from a Nitrogen Vacancy Center in a Circular Bullseye Grating," *Nano Letters* 15, 2015.

Y. Gao, R.-J. Shiue, X. Gan, L. Li, C. Peng, I. Meric, L. Wang, A. Szep, D. Walker Jr., J. Hone, and D. Englund, "High-Speed Electro-Optic Modulator Integrated with Graphene-Boron Nitride Heterostructure and Photonic Crystal Nanocavity," *Nano Letters* 15 (3), pp 2001–2005, 2015.

I. Bayn, E. H. Chen, M. E. Trusheim, L. Li, T. Schröder, O. Gaathon, M. Lu, A. Stein, M. Liu, K. Kisslinger, H. Clevenson, and D. Englund, "Generation of Ensembles of Individually Resolvable Nitrogen Vacancies Using Nanometer-Scale Apertures in Ultrahigh-Aspect Ratio Planar Implantation Masks," *Nano Letters* 15, 2015.

C. Lee, Z. Zhang, G. Steinbrecher, H. Zhou, J. Mower, T. Zhong, L. Wang, X. Hu, R. D. Horansky, V. B. Verma, A. E. Lita, R. P. Mirin, F. Marsili, M. D. Shaw, S. W. Nam, G. W. Wornell, F. N. C. Wong, J. H. Shapiro, and D. Englund, "Entanglement-based Quantum Communication Secured by Nonlocal Dispersion Cancellation," *Phys. Rev.* A 90, 062331, 2014.

J. S. Hodges, N. Y. Yao, D. Maclaurin, C. Rastogi, M. D. Lukin, and D. Englund, "Timekeeping with Electron Spin States in Diamond," *Physical Review* A 87, 032118, 2013.

X. Gan, R.-J. Shiue, Y. Gao, I. Meric, T. F. Heinz, K. Shepard, J. Hone, S. Assefa, & D. Englund, "Chip-integrated Ultrafast Graphene Photodetector with High Responsivity," *Nature Photonics* 7, 883, 2013.

Nicholas X. Fang

Associate Professor
Department of Mechanical Engineering

Nanophotonic and acoustic materials and devices; physics, nanofabrication, instrumentation

Rm. 3-435b | 617-253-2247| nicfang @ mit . edu

GRADUATE STUDENTS

Zheng Jie Tan, DMSE
Yoon Kyung Eunnie Lee, MechE

SUPPORT STAFF

Chevalley Duhart, Administrative Assistant II

SELECTED PUBLICATIONS

A. Kumar, A. Nemilentsau, K. H. Fung, G. Hanson, N. X. Fang, T. Low, "Chiral Plasmon in Gapped Dirac Systems," *Phys. Rev. B*, 93, 041413(R), 2016.

X. Li, N. X. Fang, P. M. Ferreira, W. Chern, I. S. Chun, K. Hsu, "Method of Forming an Array of High Aspect Ratio Semiconductor Nanostructures," U. S. Patent 8,980,656, March 17, 2015.

D. Jin, Q. Hu, D. Neuhauser, F. von Cube, Y. Yang, R. Sachan, T. S. Luk, D. C. Bell, and N. X. Fang, "Quantum-Spillover Enhanced Surface-Plasmonic Absorption at the Interface of Silver and High-Index Dielectrics," *Phys. Rev. Letters*, 115, article no. 193901, 2015.

A. Kumar, T. Low, K. H. Fung, P. Avouris, and N. X. Fang, "Tunable Light-matter Interaction and the Role of Hyperbolicity in Graphene-hBN System," *Nano Letters*, 15 (5), 3172–3180, 2015.

C. Shen, J. Xu, N. X. Fang, and Y. Jing, "Anisotropic Complementary Acoustic Metamaterial for Canceling out Aberrating Layers," *Phys. Rev. X*, 4, 041033, 2014.

X. Zheng, H. Lee, T. H. Weisgraber, M. Shusteff, J. DeOtte, E. B. Duoss, J. D. Kuntz, M. M. Biener, Q.Ge, J. A. Jackson, S. O. Kucheyev, N. X. Fang, and C. M. Spadaccini, "Ultra-Light, Ultrastiff Mechanical Metamaterials," *Science*, 344 (6190), 1373-1377, 2014.

A. Kumar, K. H. Fung, M. T. H. Reid, and N. X. Fang, "Photon Emission Rate Engineering Using Graphene Nanodisc cavities," *Opt. Express*, 22, 6400, 2014.

Q. Hu, D. Xu, Y. Zhou, R. Peng, R.Fan, N. X. Fang, Q.Wang, X. Huang & M. Wang, "Position-sensitive Spectral Splitting with a Plasmonic Nanowire on Silicon Chip," *Scientific Report*, 3, 3095, 2013.

N. Boechler, J. K. Eliason, A. Kumar, A. A. Maznev, K. A. Nelson, and N. Fang, " Interaction of a Contact Resonance of Microspheres with Surface Acoustic Waves," *Phys. Rev. Letters*, 111, 036103, 2013.

H. Lee, J. Zhang, H. Jiang, and N. X. Fang, "Prescribed Pattern Transformation in Swelling Gel Tubes by Elastic Instability," *Phys. Rev. Letters*, 108, article no. 214304, 2012.

Y. Cui, K. H. Fung, J. Xu, H. Ma, J. Yi, S. He, and N. X. Fang, "Ultra-broadband Light Absorption by a Sawtooth Anisotropic Metamaterial Slab," *Nano Letters*, 12, pp1443-1447, 2012.

A. Kumar, K. H. Hsu, K. E. Jacobs, P. M. Ferreira, and N. X. Fang, "Direct Metal Nano-imprinting Using an Embossed Solid Electrolyte Stamp," *Nanotechnology*, 22(2), article no. 155302, 2011.

S. Zhang, C. G. Xia, and N. X. Fang, "Broadband Acoustic Cloak for Ultrasound Waves," *Physical Review Letters*, 106, article no. 024301, 2011.

W. Chern, K. Hsu, I.-S. Chun, B. P. de Azeredo, N. Ahmed, K.-H. Kim, J. Zuo, N. Fang, P. Ferreira, and X. Li, "Nonlithographic Patterning and Metal-Assisted Chemical Etching for Manufacturing of Tunable Light-Emitting Silicon Nanowire Arrays," *Nano Letters*, 10:5, pp 1582-1588, 2010.

S. Zhang, L. Yin, and N. X. Fang, "Focusing Ultrasound with an Acoustic Metamaterial Network," *Phys. Rev. Letters*, vol. 102, article no. 194301, 2009.

K. H. Hsu, P. L. Schultz, P. M. Ferreira, and N. X. Fang, "Electrochemical Nanoimprinting with Solid-State Superionic Stamps," *Nano Letters*, 7:2, 446-451, 2007.

N. X. Fang, H. Lee, C, Sun, and X. Zhang, "Sub–Diffraction-Limited Optical Imaging with a Silver Superlens," *Science*, vol. 308(5721), pp. 534-537, 2005.

Karen K. Gleason

Associate Provost and Alexander and I. Michael Kasser Professor
Department of Chemical Engineering

Functional polymers, conducting polymers, dielectric polymers, hydrogels, and composite organic/inorganic structures deposited using initiated chemical vapor deposition (iCVD) and/or oxidative chemical vapor deposition (oCVD)

Rm. 3-240 | 617-253-5066 | kkg @ mit . edu

POSTDOCTORAL ASSOCIATES

Do Han Kim, ChemE
Hossein Sojoudi, MechE
Minghui Wang, ChemE

GRADUATE STUDENTS

Si Won Choi, ChemE
Won Jun Jo, ChemE, Samsung Fellow
Andong Liu, ChemE
Priya Moni, MatE
Amelia Servi, MechE
Xiaoxue Wang, ChemE

UNDERGRADUATE STUDENTS

Natalie Delumpa-Alexander, ChemE
Brook Eyob, ChemE
Alan Mohr, ChemE
Kaitlyn Mullin, DMSE
Nolan Peard, Mathematics
Matthew Wilson, ChemE

VISITORS

Hilal Goktas, Çanakkale Onsekiz Mart Üniversitesi, Turkey

SUPPORT STAFF

Anthee Travers, Senior Administrative Assistant
Alina Haverty, Administrative Assistant II

SELECTED PUBLICATIONS

R. Yang, H. Jang, R. Stocker, and K. K. Gleason, "Synergistic Prevention of Biofouling in Seawater Desalination by Zwitterionic Surfaces and Low-level Chlorination," *Advanced Materials*, vol. 26, pp. 1711–1718, doi: 10.1002/adma.201304386, 2014.

R. Yang, E. Goktekin, M.H. Wang, and K.K. Gleason, "Molecular Fouling Resistance of Zwitterionic and Amphiphilic Initiated Chemically Vapor-deposited (iCVD) Thin Films," *Journal Biomaterials Science–Polymer Edition*, vol. 25, pp. 1687–1702. doi: 10.1080/09205063.2014.95124, 2014.

A. T. Paxson, J. L. Yagüe, K. K. Gleason, and K. K. Varanasi, "Stable Dropwise Condensation for Enhancing Heat Transfer via the Initiated Chemical Vapor Deposition (iCVD) of Grafted Polymer Films," *Advanced Materials*, vol. 26, pp. 418–423. doi: 10.1002/adma.201303065 (frontispiece), 2014.

R. Yang, T. Buonassisi, K. K. Gleason, "Organic Vapor Passivation of Silicon at Room Temperature," *Advanced Materials,* vol. 25, pp. 2078-2083, doi: 10.1002/adma.201204382 (frontispiece), 2013.

A. M. Coclite, R. M. Howden, D. C. Borrelli, C. D. Petruczok, R. Yang, J. L. Yague, A. Ugar, N. Chen, S. Lee, W. J. Jo, A. Liu, X. Wang, and, K. K. Gleason, "CVD Polymers: A New Paradigm for Surface Modification and Device Fabrication," *Advanced Materials*, vol. 25, pp. 5392-5423, doi:10.1002/adma.201301878, 2013.

J. Yin, J. L. Yague, D. Eggenspieler, K. K. Gleason, and M. C. Boyce, "Deterministic Order in Surface Micro-topologies Through Sequential Wrinkling," *Advanced Materials*, vol. 24, pp. 5441-5446, doi: 10.1002/adma.201201937 (frontispiece), 2012.

A. Asatekin and K. K. Gleason, "Polymeric Nanopore Membranes for Hydrophobicity-Based Separations by Conformal Initiated Chemical Vapor Deposition," *Nano Letters,* vol. 11, no. 2, pp. 677-686, doi: 10.1021/nl103799d, 2011.

M. C. Barr, J. A. Rowehl, R. R. Lunt, J. Xu, A. Wang, C. M. Boyce, S. G. Im, V. Bulović, and K. K. Gleason, "Direct Monolithic Integration of Organic Photovoltaic Circuits on Unmodified Paper," *Advanced Materials*, vol. 23, pp. 3500-3505, doi:10.1002/adma.201101263 (frontispiece), 2011.

S. H. Baxamusa, and K. K. Gleason, "Random Copolymer Films with Molecular-scale Compositional Heterogeneities that Interfere with Protein Adsorption," *Advanced Functional Materials,* vol. 19, no. 21, pp. 3489–3496, doi: 10.1002/adfm.200900943, 2009.

Jongyoon Han

Professor
Department of Electrical Engineering & Computer Science
Department of Biological Engineering

Nanofluidic / Microfluidic technologies for advanced biomolecule analysis and sample preparation: cell and molecular sorting, novel nanofluidic phenomena, biomolecule separation and pre-concentration, seawater desalination and water purification, neurotechnology.

Rm. 36-841 | 617-253-2290 | jyhan @ mit . edu

POSTDOCTORAL ASSOCIATES

Bee Luan Khoo, SMART Center
Bumjoo Kim, RLE
Minseok Kim, RLE
Sung Hee Ko, RLE
Yin Lu, SMART Center
Hyunryul Ryu, RLE
Smitha Thamarath Surendran, SMART Center

GRADUATE STUDENTS

Kyungyong Choi, EECS
Siwon Choi, ChemE
Matthew Flavin, EECS
Teng Yang Jing, SMART Center, NUS
Taehong Kwon, EECS
Wei Ouyang, EECS
Rou Jun Toh, SMART Center, NTU
Aoli Xiong, SMART Center, NTU
Chia-Chen 'Debbie' Yu, EECS

VISITORS

Dr. Jose Israel Martinez Lopez, Monterry Tec, Mexico
Dr. Aniruddh Sarkar, Ragon Institute
Dr. Lidan Wu, Broad Institute

SUPPORT STAFF

Susan Davco, Administrative Assistant II

SELECTED PUBLICATIONS

L. Liu, S. Huang, X. Xu, J. Han, "Study of Individual Erythrocyte Deformability Susceptibility to INFeD and Ethanol Using a Microfluidic Chip," *Scientific Reports* 6, 22929, 2016.

A. Sarkar, H. W. Hou, A. E. Mahan, J. Han, and G. Alter, "Multiplexed Affinity-Based Separation of Proteins and Cells Using Inertial Microfluidics," *Scientific Reports* 6, 23589, 2016.

S. V. Pham, H. Kwon, B. Kim, J. K. White, G. Lim, J. Han, "Helical Vortex Formation in Three-dimensional Electrochemical Systems with Ion Selective Membranes," *Physical Review E* 93, 033114, 2016.

H. W. Hou, L. Wu, D. P. Amador-Munoz, M. Pinilla Vera, A. Coronata, J. A. Englert, B. D. Levy, R. M. Baron, and J. Han, "Broad Spectrum Immunomodulation Using Biomimetic Blood Cell Margination for Sepsis Therapy," *Lab on a Chip* 16, 688- 699, 2016.

L.Wu, A. M. Claas, A. Sarkar, D. A. Lauffenburger, J. Han, "High-throughput Protease Activity Cytometry Reveals Dose-dependent Heterogeneity in PMA-mediated ADAM17 Activation," *Integrative Biology* 7, 513 – 524, 2015.

M. E. Warkiani, L. Wu, A. K. P. Tay, and J. Han "Large Volume Microfluidic Cell Sorting," *Annual Review of Biomedical Engineering* 17(1), 1-34, 2015.

H. W. Hou, R. P. Bhattacharyya, D. T. Hung, J. Han "Direct Detection and Drug-resistance Profiling of Bacteremias Using Inertial Microfluidics," *Lab on a Chip* 15, 2297-2307, 2015.

T. F. Kong, W. Ye, W. K. Peng, H. W. Hou, Marcos, P. R. Preiser, N. Nguyen, J. Han, "Enhancing Malaria Diagnosis Through Microfluidic Cell Enrichment and Magnetic Resonance Relaxometry Detection," *Scientific Reports* 5, 11425, 2015.

C. M. Birch, H. W. Hou, J. Han, and J. C. Niles, "Identification of Malaria Parasite-infected Red Blood Cell Surface Aptamers by Inertial Microfluidic SELEX (I-SELEX)," *Scientific Reports* 5, 11347, 2015.

M. E. Warkiani, A. K. P. Tay, G. Guan, and J. Han, "Membrane-less Microfiltration Using Inertial Microfluidics," *Scientific Reports* 5, 11018, 2015.

X. Huang, S. Huang, L. C. Ong, J. C.-S. Lim, R. J. M. Hurst, A. T. Mushunje, P. T. Matsudaira, J. Han, P. R. Preiser, "Differential Spleen Remodeling Associated with Different Levels of Parasite Virulence Controls Disease Outcome in Malaria Parasite Infections," *mSphere*,1(1) 00018-15, 2015.

Ruonan Han

Emanuel E. Landsman (1958) Career Development Assistant Professor
Department of Electrical Engineering & Computer Science

Integrated circuits and systems operating from RF to THz frequencies for communication and sensing applications. On-chip high-frequency electromagnetic passive structures for energy-efficient signal generation, radiation, and coupling.

Rm. 39-527a | 617-324-5281 | ruonan @ mit . edu

GRADUATE STUDENTS

Jack Holloway, EECS, MIT Lincoln Lab Fellowship
Zhi Hu, EECS
Cheng Wang, EECS
David Elliot Williams, EECS
Michael A. Wu, EECS
Guo Zhang, EECS

UNDERGRADUATE STUDENTS

Yuecheng Yang, EECS

VISITORS

Rui Ma, Mistubishi Electric Research Labs
Tingting Shi, Fudan University
Luis Valenzuela, California PolyTech. State University

SUPPORT STAFF

Joanna Maclver, Administrative Assistant II

SELECTED PUBLICATIONS

C. Jiang, A. Mostajeran, R. Han, H. Sherry, A. Cathelin, and E. Afshari, "A 320GHz Subharmonic Mixing Coherent Imager in 130nm SiGe BiCMOS," *IEEE Int. Solid-State Circuit Conf. (ISSCC)* Digest of Technical Papers, pp. 432-433, 2016.

D Y. Kim, S. Park, R. Han, and K. K. O, "Design and Demonstration of 820-GHz Array Using Diode-Connected NMOS Transistors in 130-nm CMOS for Active Imaging," *IEEE Trans. Terahertz Science and Technology*, vol. 6, no. 2, pp. 306-317, March 2016.

R. Han, C. Jiang, A. Mostajeran, M. Emadi, H. Aghasi, H. Sherry, A. Cathelin, and E. Afshari, "A SiGe Terahertz Heterodyne Imaging Transmitter with 3.3mW Radiated Power and Fully-Integrated Phase-Locked Loop," *IEEE Journal of Solid-State Circuits (JSSC)*, vol. 50, no. 12, pp. 2935-2947, December 2015.

Z. Ahmad, D. Kim, R. Han, W. Choi and K. K. O, "THz Imaging Circuits in CMOS," *IEEE Asia-Pacific Microwave Coherence (APMC)*, December 2015.

R. Han and E. Afshari, "Filling the Terahertz Gap with Sand: High-Power Terahertz Radiators in Silicon," *IEEE Bipolar/BiCMOS Circuits and Technology Meeting (BCTM)*, Boston, MA, October 2015.

R. Han, C. Jiang, A. Mostajeran, M. Emadi, H. Aghasi, H. Sherry, A. Cathelin, and E. Afshari, "A 320GHz Phase-Locked Transmitter with 3.3mW Radiated Power and 22.5dBm EIRP for Heterodyne THz Imaging Systems," *IEEE Int. Solid-State Circuit Conf. (ISSCC)* Digest of Technical Papers, pp. 15-17, 2015.

A. John Hart
Associate Professor, Mitsui Career Development Chair
Department of Mechanical Engineering

Nanostructured materials; additive manufacturing; machine design and automation; self-assembly; composite materials; energy storage; surface engineering; mechanochemistry; research methods.

Rm. 35-212 | 617-324-7022 | ajhart @ mit . edu

POSTDOCTORAL ASSOCIATES
Michael Bono, MechE
Kehang Cui, MechE
Piran Kidambi, MechE
Sanha Kim, MechE
Ryan Oliver, MechE
Alvin Orbaek White, MechE
Sebastian Pattinson, MechE, NSF SEES Fellow

GRADUATE STUDENTS
Stuart Baker, EECS
Justin Beroz, MechE, NDSEG Fellow
Nicholas Dee, MechE, NSF Fellow
Jamison Go, MechE
Yue Guan, MechE
Emily Hanhauser, MechE
Christine Jacob, MechE, Lockheed Fellow
Bethany Lettersiere, MechE
John Lewandowski, MechE, NDSEG Fellow
Dhanushkodi Mariappan, MechE
Nigamaa Nayakanti, MechE
Crystal Owens, MechE, NSF Fellow
Ryan Penny, MechE
Abhinav Rao, MechE
Ron Rosenberg, MechE, Tata Fellow
Adam Stevens, MechE, NDSEG Fellow
Alvin Tan, DMSE
Hangbo Zhao, MechE

UNDERGRADUATE STUDENTS
Lillian Chin, EECS
David Dellal, MechE
Max Malinowski, MechE
Jacob Rothman, MechE
Adrian Samsel, MechE

SUPPORT STAFF
Haden Quinlan, Administrative Assistant II

SELECTED PUBLICATIONS
Ya'akobovitz, M. Bedewy, A. Rao, A. J. Hart. "Strain Relaxation and Resonance of Carbon Nanotube Forests Under Electrostatic Loading," *Carbon*, vol. 96, pp. 250-258, 2016.

C. R. Oliver, E. Gourgou, D. Bazopoulou, N. Chronis, A. J. Hart. "On-demand Isolation and Manipulation of C. Elegans by *in vitro* Maskless Photopatterning," *PLoS ONE*, vol. 11, 2016.

S. Ryu, P. Lee, J. B. Chou, R. Xu, R. Zhao, A. J. Hart, and S. Kim. "Extremely Elastic Wearable Carbon Nanotube Fiber Strain Sensor for Monitoring of Human Motion," *ACS Nano*, vol. 9, 5929–5936, 2015.

B. Rajabifar, S. Kim, K. Slinker, G. J. Ehlert, A. J. Hart, and M. R. Maschmann, "Three-dimensional Machining of Carbon Nanotube Forests Using Water-assisted Scanning Electron Microscope Processing," *Applied Physics Letters*, vol. 107, 2015.

L. Si, H. Wei, L. Min, T. Mingguang, S. Tawfick, A. J. Hart, Z. Qi, X. Hao. "Anisotropic Microwave Conductivity Dispersion of Horizontally Aligned Multi-walled Carbon-nanotube Thin Film on Flexible Substrate," *IEEE Transactions on Microwave Theory and Techniques*, vol. 63, pp. 3588–3594, 2015.

A. K. Yetisen, A. F. Coskun, G. England, S. Cho, H. Butt, J. Hurwitz, M. Kolle, A. Khademhosseini, A. J. Hart, A. Folch, S. H. Yun. "Art on the Nanoscale and Beyond," *Advanced Materials*, 2015.

J. Go, A. J. Hart. "A Framework for Teaching the Fundamentals of Additive Manufacturing and Enabling Rapid Innovation," *Additive Manufacturing*, to be published.

H. Zhao, J. J. Wie, D. Copic, C. R. Oliver, A .O. White, S. Kim, A. J. Hart. "High-fidelity Replica Molding of Glassy Liquid Crystalline Polymer Microstructures," *ACS Applied Materials and Interfaces*, to be published.

Y. C. Chen, H. W. Baac, K. T. Lee, K. Teichert, A. J. Hart, L. J. Guo, E. Yoon. "Selective Single Cell Detachment and Retrieval for Downstream Analyses Using Nanosecond Laser Pulses in CNT-Coated Microwell Arrays," *The 19th International Conference on Miniaturize Systems for Chemistry and Life Sciences*, Gyeongju, Republic of Korea, 2015.

A. G. Stevens, C. R. Oliver, L. Chin, A. J. Hart. "Photopatterning of Freeform Surfaces Using a Modular Robotic System," *26th Annual International Solid Freeform Fabrication Symposium*, Austin, TX, 2015.

C. R. Oliver, N. Spielberg, A. J. Hart. "Dynamic Printing of Cells and Microbeads for Custom Microfluidic Assays," *26th Annual International Solid Freeform Fabrication Symposium*, Austin, TX, 2015.

Juejun (JJ) Hu

Merton C. Flemings Assistant Professor
Department of Materials Science & Engineering

Integrated photonics, optical thin films, glass and amorphous materials, silicon photonics, light management in photovoltaics, magneto-optical isolation, integration on unconventional substrates (polymers, optical crystals, 2-D materials, etc.), infrared imaging, spectroscopy.

Rm. 13-4054 | 302-766-3083 | hujuejun @ mit . edu

RESEARCH SCIENTISTS

Tian Gu, DSME

POSTDOCTORAL ASSOCIATES

Lan Li, DSME
Hongtao Lin, DSME

GRADUATE STUDENTS

Derek Kita, DMSE
Qingyang Du, DMSE
Jerome Michon, DMSE
Duanhui Li, DMSE
Gufan Yin, DMSE
Tian Xie, DMSE
Sarah Geiger, DMSE
Okechukwu Ogbuu, DMSE

UNDERGRADUATE STUDENTS

Rebecca Eisenach, DMSE

VISITORS

June Li, Visiting Student
Yizhong Huang, Visiting Student

SUPPORT STAFF

Lisa Sinclair, Administrative Assistant II

SELECTED PUBLICATIONS

L. Zhu, F. Liu, H. Lin, J. Hu, Z. Yu, X. Wang, and S. Fan, "Angle-selective Perfect Absorption with Two-dimensional Materials," *Light Sci. Appl.*, vol. 5, e16052, 2016.

L. Li, P. Zhang, W. Wang, H. Lin, A. Zerdoum, S. Geiger, Y. Liu, N. Xiao, Y. Zou, O. Ogbuu, Q. Du, X. Jia, J. Li, and J. Hu, "Foldable and Cytocompatible Sol-gel TiO_2 Photonics," *Sci. Rep.*, vol. 5, 13832, 2015.

X. Sun, Q. Du, T. Goto, M. Onbasli, D. H. Kim, N. Aimon, J. Hu, and C. A. Ross, "Single-step Deposition of Cerium Substituted Yttrium Iron Garnet for Monolithic on-chip Optical Isolation," *ACS Photonics*, vol. 2, pp. 856-863, 2015.

J. Hu, L. Li, H. Lin, Y. Zou, Q. Du, C. Smith, S. Novak, K. Richardson, and J. D. Musgraves, "Chalcogenide Glass Microphotonics: Stepping into the Spotlight," *Am. Ceram. Soc. Bull.*, vol. 94, pp. 24-29, 2015.

L. Li, H. Lin, S. Qiao, Y. Zou, S. Danto, K. Richardson, J. D. Musgraves, N. Lu, and J. Hu, "Integrated Flexible Chalcogenide Glass Photonic Devices," *Nat. Photonics*, vol. 8, pp. 643-649, 2014.

Y. Chen, H. Lin, J. Hu, and M. Li, "Heterogeneously Integrated Silicon Photonics for the Mid-infrared and Spectroscopic Sensing," *ACS Nano* 8, 6955-6961, 2014.

Y. Zou, D. Zhang, H. Lin, L. Li, L. Moreel, J. Zhou, Q. Du, O. Ogbuu, S. Danto, J. D. Musgraves, K. Richardson, K. Dobson, R. Birkmire, and J. Hu, "High-Performance, High-Index-Contrast Chalcogenide Glass Photonics on Silicon and Unconventional Nonplanar Substrates," *Adv. Opt. Mater.* vol. 2, pp. 478-486, 2014.

Y. Zou, L. Moreel, L. Savelli, H. Lin, J. Zhou, L. Li, S. Danto, J. D. Musgraves, K. Richardson, K. Dobson, R. Birkmire, and J. Hu, "Solution Processing and Resist-free Nanoimprint Fabrication of Thin Film Chalcogenide Glass Devices: Inorganic-organic Hybrid Photonic Integration," *Adv. Opt. Mater.*, vol. 2, pp. 759-764, 2014.

J. Hu, L. Li, H. Lin, P. Zhang, W. Zhou, and Z. Ma, "Flexible Integrated Photonics: Where Materials, Mechanics and Optics Meet," *Opt. Mater. Express*, vol. 3, pp. 1313-1331, 2013.

H. Lin, L. Li, Y. Zou, S. Danto, J. D. Musgraves, K. Richardson, S. Kozacik, M. Murakowski, D. Prather, P. Lin, V. Singh, A. M. Agarwal, L. C. Kimerling, and J. Hu, "Demonstration of High-Q Mid-infrared Chalcogenide Glass-on-silicon Resonators," *Opt. Letters*, vol. 38, pp. 1470-1472, 2013.

L. Bi, J. Hu, P. Jiang, D. Kim, G. Dionne, L. C. Kimerling, and C. A. Ross, "On-chip Optical Isolation in Monolithically Integrated Nonreciprocal Optical Resonators," *Nat. Photonics*, vol. 5, pp. 758-762, 2011.

Pablo Jarillo-Herrero
Associate Professor
Department of Physics

Quantum electronic transport and optoelectronics with low dimensional materials, such as graphene, transition metal dichalcogenides, and topological insulators. Nanofabrication of van der Waals heterostructures. Mesoscopic physics and superconductivity.

Rm. 13-2017 | 617-253-3653 | pjarillo @ mit . edu

POSTDOCTORAL ASSOCIATES
Yaqing Bie, Physics
Landry Bretheau, Physics
Efren Navarro-Moratalla, Physics
Joel I-Jan Wang, Physics

GRADUATE STUDENTS
Yuan Cao, EECS
Valla Fatemi, Physics
Dahlia Klein, Physics, NSF Fellow
Jason Luo, Physics, Singapore Fellow
Qiong Ma, Physics
Luiz Gustavo Pimenta Martins, Physics, Brazil Fellow
Melis Tekant, Physics, NDSEG Fellow
Yafang Yang, Physics

UNDERGRADUATE STUDENTS
Andres Mier, Physics
Saranesh Prebambu, Physics
Christina Wang, Physics

SUPPORT STAFF
Monica Wolf, Administrative Assistant II

SELECTED PUBLICATIONS
Q. Ma, T. I. Andersen, N. L. Nair, N. M. Gabor, M. Massicotte, C. H. Lui, A. F. Young, W. Fang, K. Watanabe, T. Taniguchi, J. Kong, N. Gedik, F. H. L. Koppens, P. Jarillo-Herrero, "Tuning Ultrafast Electron Thermalization Pathways In a Van Der Waals Heterostructure," *Nature Physics*, vol. 12, 128, 2016.

M. T. Allen, O. Shtanko, I. Cosma Fulga, A. Akhmerov, K. Watanabi, T. Taniguchi, P. Jarillo-Herrero, L. S. Levitov, A. Yacoby, "Spatially Resolved Edge Currents And Guided-Wave Electronic States In Graphene," *Nature Physics*, vol. 12, 128, 2016.

K.J. Tielrooij, L. Orona, A. Ferrier, M. Badioli, G. Navickaite, S. Coop, S. Nanot, B. Kalinic, T. Cesca, L. Gaudreau, Q. Ma, A. Centeno, A. Pesquera, A. Zurutuza, H. de Riedmatten, P. Goldner, F.J. García de Abajo, P. Jarillo-Herrero, F.H.L. Koppens, "Electrical Control of Optical Emitter Relaxation Pathways enabled by Graphene," *Nature Physics,* vol. 11, 281, 2015.

V. Fatemi, B. Hunt, H. Steinberg, S.L. Eltinge, F. Mahmood, N. P. Butch, K. Watanabe, T. Taniguchi, N. Gedik, R. Ashoori, P. Jarillo-Herrero, "Electrostatic Coupling Between Two Surfaces of a Topological Insulator Nanodevice," *Phys. Rev. Letters*, 113, 206801, 2014.

Q. Ma, N.M. Gabor, T.I. Andersen, N.L. Nair, K. Watanabe, T. Taniguchi, P. Jarillo-Herrero, "Competing Channels for Hot Electron Cooling in Graphene," *Phys. Rev. Letters*, 112, 247401, 2014.

S. Dai, Z. Fei, Q. Ma, A. S. Rodin, M. Wagner, A. S. McLeod, M. K. Liu, W. Gannett, W. Regan, K. Watanabe, T. Taniguchi, M. Thiemens, G. Dominguez, A. H. Castro Neto, A. Zettl, F. Keilmann, P. Jarillo-Herrero, M. M. Fogler, D. N. Basov, "Tunable Phonon Polaritons in Atomically Thin Van Der Waals Crystals of Boron Nitride," *Science* 343, 1125, 2014.

B.W. Baugher, H.O.H. Churchill, Y. Yang, P. Jarillo-Herrero, "Optoelectronic Devices Based On Electrically Tunable P-N Diodes In A Monolayer Dichalcogenide," *Nature Nanotechnology*, vol. 9, 262, 2014.

P.K. Herring, A.L. Hsu, N.M. Gabor, Y.C. Shin, J. Kong, T. Palacios, and P. Jarillo-Herrero, "Photoresponse of an Electrically Tunable Ambipolar Graphene Infrared Thermocouple," *Nano Letters*, vol. 14, 901, 2014.

A. F. Young, J. D. Sanchez-Yamagishi, B. Hunt, S. H. Choi, K. Watanabe, T. Taniguchi, R. C. Ashoori, P. Jarillo-Herrero, "Tunable Symmetry Breaking and Helical Edge Transport in a Graphene Quantum Spin Hall State," *Nature*, vol. 505, 528, 2014.

Y. H. Wang, H. Steinberg, P. Jarillo-Herrero, N. Gedik, "Observation of Floquet-Bloch States on the Surface of a Topological Insulator," *Science*, vol. 342, 453, 2013.

B.W. Baugher, H.O.H. Churchill, Y. Fang, P. Jarillo-Herrero, "Intrinsic Electronic Transport Properties of High Quality Monolayer and Bilayer MoS2," *Nano Letters*, vol. 13, 4212, 2013.

B. Hunt, J. D. Sanchez-Yamagishi, A. F. Young, K. Watanabe, T. Taniguchi, P. Moon, M. Koshino, P. Jarillo-Herrero, R. C. Ashoori, "Massive Dirac Fermions And Hofstadter Butterfly in a Van Der Waals Heterostructure," *Science*, vol. 340, 1427, 2013.

Ali Khademhosseini

Professor of Medicine, Harvard Medical School
HST Affiliated Faculty, Health Sciences and Technology (HST) Program

Micro- and nanoscale biomaterials, microfabrication and 3D-bioprinting, organ on a chip systems, vascularized tissues with appropriate microarchitectures, regulating stem cell differentiation, with microengineered systems.

Rm. 76-661 | 617-768-8395 | alik @ mit . edu

POSTDOCTORAL ASSOCIATES

Byambaa Batzaya, HST
Mohamadmahdi Samandari, HST
Parisa Pour Shahid Saeed Abadi, HST
Grissel Trujillo-de Santiago, Tecnológico de Monterrey
Kan Yue, HST

GRADUATE STUDENTS

Gouri Chandrabhatla, SRM University
Wanjun Liu, Donghua University
Amir Nasajpour, Harvard
Gyan Prakash, IIT Guwahati
João Ribas, University of Coimbra
Antea Risso, EPFL

UNDERGRADUATE STUDENTS

Claudia Del Toro Runzer, Tecnológico de Monterrey
Ricardo Hernández Medina, Tecnológico de Monterrey
Serena Mandla, University of Toronto
Pamela Rellstab, Tecnológico de Monterrey

VISITORS

Nasim Annabi
Mario Moisés Álvarez, Tecnológico de Monterrey
Mehmet Remzi Dokmeci
Su-Ryon Shin
Ali Tamayol
Yu Shrike Zhang

SUPPORT STAFF

Brett Losen

SELECTED PUBLICATIONS

D. Loessner, C. Meinert, E. Kaemmerer, L. C. Martine, K. Yue, P. A. Levett, T. J. Klein, F.P.W. Melchels, A. Khademhosseini, D. W. Hutmacher, "Functionalization, Preparation and Use of Cell-Laden Gelatin Methacryloyl-Based Hydrogels as Modular Tissue Culture Platforms," *Nature Protocols,* vol. 11, pp. 727-746. 2016.

S. R. Shin, R. Farzad, A. Tamayol, V. Manoharan, P. Mostafalu, Y. S. Zhang, M. Akbari, S. M. Jung, D. Kim, M. Comotto, N Annabi, F.E. Al-Hazmi, M. R. Dokmeci, A. Khademhosseini, "A Bioactive Carbon Nanotube-Based Ink for Printing 2D and 3D Flexible Electronics," *Advanced Materials,* 2016.

A. Tamayol, M. Akbari, Y. Zilberman, M. Comotto, E. Lesha, L. Serex, S. Bagherifard, Y. Chen, G. Fu, S. K. Ameri, W. Ruan, E. L. Miller, M. R. Dokmeci, S. Sonkusale, A. Khademhosseini, "pH-Sensing Hydrogel Fibers: Flexible pH-Sensing Hydrogel Fibers for Epidermal Applications," *Advanced Healthcare Materials,* vol. 5, pp. 624-624, June 2016.

S. Ahadian, S. Yamada, J. Ramón-Azcón, M. Estili, X. Liang, K. Nakajima, H. Shiku, A. Khademhosseini, T. Matsue,"Hybrid Hydrogel-Aligned Carbon Nanotube Scaffolds to Enhance Cardiac Differentiation of Embryoid Bodies," *Acta biomaterialia,* vol. 31, pp. 134-143, 2016.

M. M. Alvarez, J. C. Liu, G. Trujillo-de Santiago, B.-H. Cha, A. Vishwakarma, A. Ghaemmaghami, A. Khademhosseini, "Delivery strategies to control inflammatory response: Modulating M1-M2 polarization in tissue engineering applications," *Journal of Controlled Release,* in press, 2016.

Y. S. Zhang, J-B. Chang, M. M. Alvarez, G.Trujillo-de Santiago, J. Alemán, B. Batzaya, V. Krishnadoss, A. A. Ramanujam, M. Kazemzadeh-Narbat, F. Chen, P. W. Tillberg, M. R. Dokmeci, E. S. Boyden, A. Khademhosseini, "Hybrid Microscopy: Enabling Inexpensive High-Performance Imaging through Combined Physical and Optical Magnifications," *Scientific Reports,* March 6, 2016.

P. Hassanzadeh, M. Kazemzadeh-Narbat, R. Rosenzweig, X. Zhang, A. Khademhosseini, N. Annabi, M. Rolandi, "Ultrastrong and Flexible Hybrid Hydrogels Based on Solution Self-Assembly Of Chitin Nanofibers in Gelatin Methacryloyl (GelMA)," *Journal of Materials Chemistry B,* vol. 4, pp. 2539-2543, 2016.

Y. S. Zhang, F. Busignani, J. Ribas, J. Alemán, T. N. Rodrigues, S. A. M. Shaegh, S. Massa, C. B. Rossi, I. Taurino, S-R. Shin, G. Calzone, G. M. Amaratunga, D. L. Chambers, S. Jabari, Y. Niu, V. Manoharan, M. R. Dokmeci, S. Carrara, D. Demarchi, A. Khademhosseini, "Google Glass-Directed Monitoring and Control of Microfluidic Biosensors and Actuators," *Scientific Reports,* 6, 2016.

K. Yue, G. Trujillo-de Santiago, M. M. Alvarez, A. Tamayol, N. Annabi, A. Khademhosseini, "Synthesis, Properties, And Biomedical Applications Of Gelatin Methacryloyl (GelMA) Hydrogels," *Biomaterials,* vol. 73, pp. 254-271, 2015.

Sang-Gook Kim

Professor
Department of Mechanical Engineering

Micro energy harvesting, solar water splitting, piezoelectric MEMS, complex systems design.

Rm. 1-306 | **617-452-2472** | **sangkim @ mit . edu**

POSTDOCTORAL ASSOCIATES

Jeffrey Chou, MIT-Battelle Fellow
Asmaa El-Faer, IBN-Khaldoun Fellow
Seongwoo Ryu, MIT-SUTD Fellow

GRADUATE STUDENTS

Mohammed Bhouri, DME
Xinhao Li, DME
Katherine Smyth, DME
Yu Wang, DMSE
Ruize Xu, DME

UNDERGRADUATE STUDENTS

Kelsey Seto, DME

VISITORS

Wei-Lek Kwan, SUTD

SUPPORT STAFF

Lorraine Rabb, Senior Administrative Assistant

SELECTED PUBLICATIONS

K. Smyth and S.-G. Kim, "Experiment and Simulation Validated Analytical Equivalent Circuit Model for Piezoelectric Micro-Machined Ultrasonic Transducer," *IEEE Transactions on Ultrasonics Ferroelectrics and Frequency Control,* vol. 62, no. 4, 2015.

S. Ryu, J.B. Chou, K. Lee, D. Lee, S.H. Hong, R. Zhao, H. Lee, and S.-G Kim (2015), "Direct Insulation-to-Conduction Transformation of Adhesive Catecholamine for Simultaneous Increases of Electrical Conductivity and Mechanical Strength of CNT Fibers," *Advanced Materials,* v. 27, issue 21, pp. 3221, doi: 10.1002/adma.201500914, 2015.

S. Ryu, P. Lee; J. Chou, R. Xu, R. Zhao, J. Hart, and S.-G. Kim, "Fabrication of Extremely Elastic Wearable Strain Sensor Using Aligned Carbon Nanotube Fibers For Monitoring Human Motion," *ACS Nano,* 9 (6), pp. 5929-5936, doi: 10.1021/acsnano.5b00599, 2015.

G. De Pasquale, S.-G. Kim, and D. De Pasquale, "GoldFinger: Wireless Human-Machine Interface with Dedicated Software and Biomechanical Energy Harvesting System," *IEEE/ASME Transactions on Mechatronics* [10834435], 1-1, 2015.

R. Xu and S.-G. Kim, "MEMS Energy Harvesting From Low Frequency and Low-G Vibrations," *MRS Spring Meeting,* San Francisco, 2015.

J. B. Chou, D. P. Fenning, Y. Wang, M. A.M. Polanco, J. Hwang, A. El Faer, F. Sammoura, J. Viegas, M. Rasras, A. Kolpak, Y. Shao-Horn, S.-G. Kim "Broadband Photoelectric Hot Carrier Collection with Wafer-Scale Metallic-Semiconductor Photonic Crystals," *42nd IEEE Photovoltaic Specialist Conference,* New Orleans, 2015.

R. Xu and S.-G. Kim, "Bi-stable Buckled Beam Structures for Low-frequency, Low-g Energy Harvesting," *10th Energy Harvesting Workshop,* Blacksburg, Virginia, 2015.

H. Fu, R. Xu, K. Seto, E. Yeatman, and S.-G. Kim, "Energy Harvesting from Human Motion using Footstep Induced Airflow," *Power MEMS 2015, Boston, USA, Journal of Physics: Conference Series,* vol. 660, 012031, 2015.

R. Xu and S.-G. Kim, "Low-Frequency Low–g MEMS Piezoelectric Energy Harvesting," *Power MEMS 2015, Boston, USA, Journal of Physics: Conference Series* 660,012013, 2015.

G. De Pasquale, S.-G. Kim, and D. De Pasquale, "Optical HMI with biomechanical energy harvesters integrated in textile supports," *Power MEMS 2015, Boston, USA, Journal of Physics: Conference Series,* vol. 660, 012031, 2015.

Y. Wang, J.B. Chou, A. Elfaer, and S.-G. Kim, "Simulation Study of Metallic Photonic Crystal for Enhanced Hot Electron Transfer in Electrochemical Cells," *MRS Fall Meeting,* Boston, 2015.

A. Elfaer, Y. Wang, J.B. Chou, and S.-G. Kim, "Gold Nanorods Coated Metallic Photonic Crystal for Enhanced Hot Electron Transfer in Electrochemical Cells," *MRS Fall Meeting, MRS Advances*, Boston, 2015.

P. Dahal, J. Chou, Y. Wang, S.-G. Kim, and J. Viegas. "Comparative Study of Multilayered Nanostructures for Enhanced Solar Optical Absorption," *MRS Advances,* 2015.

N. S. Rajput, S.-G. Kim, J. B. Chou, J. Abed, J. Viegas, and M. Jouiad, "Electron Beam Induced Rapid Crystallization of Water Splitting Nanostructures," *MRS Advances,* 2015.

Mathias Kolle

Assistant Professor
Department of Mechanical Engineering

Dynamic optical materials formed from elastomers and fluids; biological & bio-inspired photonic materials; mechano-responsive tunable photonic fibers; morphogenesis of biological photonic architectures; marine optics; nanofabrication techniques for soft, tunable micro-optical components; bio-sensing using responsive photonic materials; Bio-manufacture of photonic components.

Rm. 3-162 | 617-324-7639 | mkolle @ mit . edu

GRADUATE STUDENTS

Anthony McDougal, MechE
Ben Miller, MechE
Sara Nagelberg, MechE
Joseph Sandt, MechE

UNDERGRADUATE STUDENTS

Chris Argenti, MechE
Alonzo Lopez, MechE
Carolyn Lu, EECS
Natalie, Nicolas, MechE
Marcus Urann, MechE

VISITORS

Andreas Leber, University of Erlangen

SUPPORT STAFF

Sean Buhrmester, Administrative Assistant II

SELECTED PUBLICATIONS

L. Li, M. J. Connors, M. Kolle, G. T. England, D. Speiser, X. Xiang, J. Aizenberg, and C. Ortiz, "Multifunctionality of Chiton Biomineralized Armor with an Integrated Visual System," *Science* 350, pp. 952-956, 2015.

L. Li, S. Kolle, J. C. Weaver, C. Ortiz, J. Aizenberg, and M. Kolle, "A Highly Conspicuous Mineralized Composite Photonic Architecture in the Translucent Shell of the Blue-Rayed Limpet," *Nature Communications* 6, 6322, 2015.

G. England, M. Kolle, P. Kim, M. Khan, P. Munoz, E. Mazur, and J. Aizenberg, "Bioinspired Micrograting Arrays Mimicking The Reverse Color Diffraction Elements Evolved by the Butterfly *Pierella Luna*," *Proc. Nat. Acad. Sci. USA* 111, 15630-15634, 2014.

K.R. Phillips, N. Vogel, Y. Hu, M. Kolle, C.C. Perry, and J. Aizenberg, "Tunable Anisotropy in Inverse Opals and Emerging Optical Properties" *Chemistry of Materials* 26, 1622-1628, 2014.

Y. Vasquez, M. Kolle, L. Mishchenko, B. D. Hatton, and J. Aizenberg, "Three-Phase Co-Assembly: In-situ Incorporation of Nanoparticles into Tunable, Highly-Ordered, Porous Silica Films," *ACS Photonics* 1, 53-60, 2014.

M. Francke, M. Kreysing, A. Mack, J. Engelmann, A. Karl, F. Makarov, J. Guck, M. Kolle, H. Wolburg, R. Pusch, G. von der Emde, S. Schuster, H.-J. Wagner, and A. Reichenbach, "Grouped Retinae and Tapetal Cups in Some Teleostian Fish: Occurrence, Structure, and Function," *Prog. Retin. Eye. Res.* 38, 43-69, 2013.

M. Kolle, A. Lethbridge, M. Kreysing, J. J. Baumberg, J. Aizenberg, and P. Vukusic, "Bio-Inspired Band-Gap Tunable Elastic Optical Multilayer Fibres," *Advanced Materials* 25, 2239-2245, 2013.

A. M. Kats, J. S. Byrnes, R. Blanchard, M. Kolle, P. Genevet, J. Aizenberg, and F. Capasso, "Enhancement Of Absorption and Color Contrast in Ultra-Thin Highly Absorbing Optical Coatings," *Appl. Phys. Letters,* 103, 101104, 2013.

B. D. Hatton, I. Wheeldon, M. J. Hancock, M. Kolle, J. Aizenberg, and D. E. Ingber, "An Artificial Vasculature for Adaptive Thermal Control of Windows," *Solar Energy Materials and Solar Cells,* 117, 429-436, 2013.

P. Kim, Y. Hu, J. Alvarenga, M. Kolle, Z. Suo, and J. Aizenberg, "Rational Design of Mechano-Responsive Optical Materials by Fine Tuning the Evolution of Strain-Dependent Wrinkling Patterns," *Advanced Optical Materials* 1, 381-388, 2013.

Jing Kong

Professor

Department of Electrical Engineering & Computer Science

Synthesis, processing and characterization of nanomaterials and various application development. One particular area is on chemical vapor deposition synthesis of two dimensional materials including graphene, hexagonal Boron Nitride and transition metal dichalcogenides.

Rm. 13-3065 | 617-324-4068 | jingkong @ mit . edu

RESEARCH SCIENTISTS

Sungmi Jung, RLE

POSTDOCTORAL ASSOCIATES

Yan Chen, RLE
Boris Desiatov, RLE, MIT-Technion Fellow
Wenjing Fang, RLE
Jin-Yong Hong, RLE
Xiang Ji, RLE

GRADUATE STUDENTS

Marek Hempel, EECS
SeongSoon Jo, DMSE
Yi Song, EECS
Cong Su, NSE
Haozhe Wang, MechE

VISITORS

Fei Hui, Soo Chow University
Fangping Ouyang, Central South University
Bo Wang, Hong Kong U. Science & Technology
Jihao Yin, Beihang University

SUPPORT STAFF

Teresa Availa, Administrative Assistant II

SELECTED PUBLICATIONS

S. M. Jung, D. J. Preston, H. Y. Jung, Z. Deng, E. N. Wang, and J. Kong, "Porous Cu Nanowire Aerosponges from One-Step Assembly and their Applications in Heat Dissipation," *Advanced Materials*, vol. 28, pp. 1413-1419, 2016.

W. Fang, A. Hsu, Yi Song, and J. Kong, "A Review of Large-Area Bilayer Graphene Synthesis by Chemical Vapor Deposition," *Nanoscale*, vol. 7, pp. 20335-20351, 2015.

Y. Song, W. Fang, R. Brenes, and J. Kong, "Challenges and Opportunities for Graphene as Transparent Conductors in Optoelectronics," *Nano Today*, vol. 10, pp. 681-700, 2015.

S. Kim, A. Hsu, M. Park, S. H. Chae, S. J. Yun, J. Lee, D. H. Cho, W. Fang, C. Lee, T. Palacios, M. S. Dresselhaus, K. Kim, Y. Lee, and J. Kong, "Synthesis of Large-Area Multilayer Hexagonal Boron Nitride for High Material Performance" *Nature Communications*, vol. 6, 2015.

D. L. Mafra, T. Ming, and J. Kong, "Facile Graphene Transfer Directly to Target Substrates with a Reusable Metal Catalyst," *Nanoscale*, vol. 7, pp. 14807-14812, 2015.

L. Zhou, K. Xu, A. Zubair, A. D. Liao, W. Fang, F. Ouyang, Y.-H. Lee, K. Ueno, R. Saito, T. Palacios, J. Kong, and M. S. Dresselhaus, "Large-Area Synthesis of High-Quality Uniform Few-Layer $MoTe_2$," *Journal of the American Chemical Society*, vol. 137, pp. 1892-11895, 2015.

D. J. Preston, D. L. Mafra, N. Miljkovic, J. Kong, and E. N. Wang, "Scalable Graphene Coatings for Enhanced Condensation Heat Transfer," *Nano Letters*, vol. 15, pp. 2902-2909, 2015.

G. M. Akselrod, T. Ming, C. Argyropoulos, T. B. Hoang, Y. X. Lin, X. Ling, D. R. Smith, J. Kong, and M. H. Mikkelsen, "Leveraging Nanocavity Harmonics for Control of Optical Processes in 2D Semiconductors," *Nano Letters*, doi: 10.1021/acs.nanoLetters.5b01062, 2015.

X. Ling, W. Fang, Y.-H. Lee, P. T. Araujo, X. Zhang, J. F. Rodriguez-Nieva, Y. Lin, J. Zhang, J. Kong, and M. S. Dresselhaus, "Raman Enhancement Effect on Two-Dimensional Layered Materials: Graphene, h-BN and MoS_2," *Nano Letters*, vol. 14, no. 6, pp. 3033-3040, June 11, 2014.

S. M. Jung, H. Y. Jung, W. Fang, M. S. Dresselhaus, and J. Kong, "A Facile Methodology for the Production of in Situ Inorganic Nanowire Hydrogels/Aerogels," *Nano Letters*, vol. 14, no. 4, pp. 1810-1817, April 9, 2014.

Jeffrey H. Lang

Vitesse Professor

Department of Electrical Engineering & Computer Science

Analysis, design and control of electro-mechanical systems with application to: traditional rotating machinery and variable-speed drives; micro/nano-scale (MEMS/NEMS) sensors and actuators; flexible structures; and the dual use of actuators as force and motion sensors.

Rm. 10-176 | 617-253-4687 | lang @ mit . edu

POSTDOCTORAL ASSOCIATES

Matthew. Angle, RLE
Ujwal Radhakrishna, RLE (June 2016)

GRADUATE STUDENTS

Stephanie Chen, EECS
Matthew D'Asaro, EECS
Kayla Esquivel, EECS
Felipe Garza, EECS
Rakesh Kumar, EECS
Apoorva Murarka, EECS
Nathan Monroe, EECS
Farnaz Niroui, EECS
Abraham Shin, EECS

UNDERGRADUATE STUDENTS

Daniel Sheen, EECS

SUPPORT STAFF

Donna Gale, Administrative Assistant II

SELECTED PUBLICATIONS

M. E. D'Asaro, D. Sheen, and J. H. Lang, "Thin Flexible and Stretchable Tactile Sensor Based on a Deformable Microwave Transmission Line," *Proceedings: Hilton Head Sensors, Actuators and Microsystems Workshop*, Hilton Head, SC, June 5-9, 2016.

M. Chen, M. Araghchini, K. K. Afridi, J. H. Lang, C. R. Sullivan, and D.J. Perreault, "A Systematic Approach to Modeling Impedances and Current Distribution in Planar Magnetics," *IEEE Transactions on Power Electronics*, 31, pp. 560-580, January 2016.

S. Zhao, A. Paidimarri, N. Ickes, M. Araghchini, J. H. Lang, J. Ma, Y. Ramadass, and D. Buss, "Extending the Bandwidth of Piezoelectric Energy Harvesting Through the Use of Bias Flip," *Proceedings: IEEE S3S Conference*, doi: 10.1109/S3S.2015.7333534, Sonoma, CA, October 5-8, 2015.

S. Zhao, A. Paidimarri, N. Ickes, M. Araghchini, J. H. Lang, J. Ma, Y. Ramadass, and D. Buss, "Extending The Bandwidth of Piezoelectric Energy Harvesting Through the Use of Bias Flip," *Proceedings: IEEE S3S Conference*, doi: 10.1109/S3S.2015.7333534, Sonoma, CA, October 5-8, 2015.

F. Niroui, E. M. Sletten, Y. Song, Jing Kong, Timothy M. Swager, J. H. Lang, and V. Bulović, "Tunneling Nano-Electromechanical Switches," *Proceedings: 4th Berkeley Symposium on Energy Efficient Electronic Systems*, doi: 10.1109/E3S.2015.7336790, Berkeley, CA, October 1-2, 2015.

W. J. Ong, E. M. Sletten, F. Niroui, J. H. Lang, V. Bulović, and T. M. Swager, "Electromechanically Actuating Molecules," *Proceedings: 4th Berkeley Symposium on Energy Efficient Electronic Systems*, Online publication doi: 10.1109/E3S.2015.7336809, Berkeley, CA, October 1-2, 2015.

C. U. Hail, P. C. Knodel, J. H. Lang, and J. G. Brisson, "A Linearly-Actuating Variable-Reluctance Generator for Thermoacoustic Engines," *Journal of Energy Conversion and Management*, 100, pp. 168-176, August 2015.

F. Niroui, A. I. Wang, E. M. Sletten, Y. Song, J. Kong, E. Yablonovitch, T. M. Swager, J. H. Lang, and V. Bulović, "Tunneling Nanoelectromechanical Switches Based on Compressible Molecular Thin Films," *ACS Nano*, 10.1021/acsnano.5b02476, August 5, 2015.

M. Ilic, S. Cvijic, J. H. Lang, and J. Tong, "Optimal Voltage Management for Enhancing Electricity Market Efficiency," *Proceedings: IEEE PES General Meeting*, doi: 10.1109/PESGM.2015.7286009, Denver, CO, July 26-30, 2015.

M. Ilic, S. Cvijic, J. H. Lang, J. Tong, and D. Obadina, "Operating Beyond Today's PV Curves: Challenges and Potential Benefits," *Proceedings: IEEE PES General Meeting*, doi: 10.1109/PESGM.2015.7286495, Denver, CO, July 26-30, 2015.

S. S. Seok, A. Wang, M. Y. Chuah, D. J. Hyun, J. Lee, D. M. Otten, J. H. Lang, and S. Kim, "Design Principles for Energy Efficient Legged Locomotion And Implementation on the MIT Cheetah Robot," *IEEE/ASME Transactions on Mechatronics*, 20, 1117-1129, June 2015.

W. Chang, A. Murarka, A. Wang, J. H. Lang, and V. Bulović, "Electrically Tunable Organic Vertical-Cavity Surface-Emitting Laser," *Proceedings: CLEO 2015*, San Jose, CA, May 10-15, 2015.

F. Niroui, E. M. Sletten, P. B. Deotare, A. I. Wang, T. M. Swager, J. H. Lang, and V. Bulović, "Controlled Fabrication of Nanoscale Gaps Using Stiction," *Proceedings: IEEE MEMS Workshop*, 85-88, Estoril, Portugal, January 18-22, 2015.

Hae-Seung Lee

ATSC Professor of EECS
Director of Center for Integrated Circuits and Systems
Department of Electrical Engineering & Computer Science

Analog and mixed-signal integrated circuits, with a particular emphasis in data conversion circuits in scaled CMOS.

Rm. 39-521 | **617-253-5174** | **hslee @ mtl . mit . edu**

POSTDOCTORAL ASSOCIATES

Sungwon Chung, EECS

GRADUATE STUDENTS

Hyun Ho Boo, EECS
Taehoon Jeong, EECS
Harneet Singh Khurana, EECS
Changwook Min, HST
Sabino Pietrangelo, EECS
Joohyun Seo, EECS
Xi Yang, EECS
Do Yeon Yoon, EECS

SUPPORT STAFF

Carolyn Collins, Administrative Assistant II
Elizabeth Kubicki, Administrative Assistant II

SELECTED PUBLICATIONS

K. Chen, H.-S. Lee, and C. G. Sodini, "A Column-Row-Parallel ASIC Architecture for 3D Portable Medical Ultrasonic Imaging," *IEEE Journal of Solid-State Circuits*, vol. 51, no. 3, pp. 738-751, March 2016.

H. H. Boo, D. S. Boning, H.-S. Lee, "A 12b 250MS/s Pipelined ADC with Virtual Ground Reference Buffers," *IEEE Journal of Solid-State Circuits*, vol. 50, no. 12, pp. 2912-2921, December 2015.

D.-Y. Yoon, S. Ho, and H.-S. Lee, "An 85dB DR, 74.6dB SNDR, 50MHz BW CT MASH ΔΣ Modulator in 28nm CMOS," *IEEE Journal of Solid-State Circuits,* vol. 50, no. 12, pp. 2880-2890, December 2015.

H.-S. Lee "Switched Capacitor Circuits Having Level-Shifting Buffer Amplifiers, and associated Methods," *US patent no. 9214912*, December 15, 2015.

H.-S. Lee "Buffer Amplifier Circuit" *US patent no. 9154089*, October 6, 2015.

J. Seo, S. J. Pietrangelo, H.-S. Lee, and C. G. Sodini, "Carotid Arterial Blood Pressure Waveform Monitoring Using a Portable Ultrasound System," *Proceedings of the Annual Conference of the Engineering in Medicine and Biology Society*, Milan, Italy, September 2015.

C. G. Sodini, J. Seo, S. J. Pietrangelo, T. Heldt, E. S. Winokur, D. He, and H.-S. Lee, "Mean Arterial Blood Pressure and Pulse Pressure Wave Measurement with Low Cost Technologies," *Proceedings of the Annual Conference of the Engineering Medicine and Biology Society*, Milan, Italy, September 2015.

S. Chung and H.-S. Lee, "200 MS/s 98-dB SNRTrack-and-Holdin 0.25-um GaN HEMT," *Proceedings of the IEEE Custom Integrated Circuits Conference*, September 2015.

J. Seo, S. Pietrangelo, H.-S. Lee, and C. G. Sodini, "Noninvasive Arterial Blood Pressure Waveform Monitoring Using Two-Element Ultrasound System," *IEEE Trans. Ultrasonics, Ferroelectrics, and Frequency Control*, vol. 62, no. 4, pp. 776-784, March 2015.

H. H. Boo, D. S. Boning, H.-S. Lee, "A 12b 250MS/s Pipelined ADC with Virtual Ground Reference Buffers," *IEEE ISSCC Digest of Technical Papers*, pp. 282-283, February 2015.

D.-Y. Yoon, S. Ho, and H.-S. Lee, "A 85dB DR, 74.6dB SNDR, 50MHz BW CT MASH ΔΣ Modulator in 28nm CMOS" *IEEE ISSCC Digest of Technical Papers*, pp. 272-273, February 2015.

K. Chen, B.C. Lee, K. Thomenius, B. Khuri-Yakub, H.-S. Lee, and C. G. Sodini, "Over 20 dB Reduction of Tx 2nd-Order Harmonic using Interleaved Checker Board I&Q Excitation," *IEEE Transactions on Ultrasonics, Ferroelectrics, and Frequency Control*, September 2014.

Luqiao Liu

Robert Shillman (1974) Career Development Assistant Professor
Department of Electrical Engineering & Computer Science

Spintronics; spin based logic and memory device; nanoscale magnetic material for information storage and microwave application; fabrication technique of magnetic nanodevices; spin related phenomena in semiconductor, topological insulator, superconductors and low dimensional material; magnetic dynamics.

Rm. 39-553a | 617-253-0019 | luqiao @ mit . edu

GRADUATE STUDENTS

Joseph Finley, EECS

SUPPORT STAFF

Steven O'Hearn, Administrative Assistant II

SELECTED PUBLICATIONS

L. Q. Liu, "Supercurrent Induced Spin Accumulation in Superconductors with Spin Orbit Interaction," *Intermag and Magnetic Material and Magnetism Joint Conference*, January 2016.

L. Q. Liu, A. Richardella, I. Garate, Y. Zhu, N. Samarth, C. T. Chen, "Spin-Polarized Tunneling Study of Spin-Momentum Locking in Topological Insulators," *Physical Review B*, vol. 91, 235437, 2015.

L. Q. Liu, "Spin Polarized Tunneling Study on Spin Hall Metals And Topological Insulators," Invited talk at *IEEE International Magnetics Conference*, May 2015.

Scott Manalis
Viterbi Professor
Departments of Biological and Mechanical Engineering

Development of quantitative and real-time techniques for biomolecular detection and single cell analysis. We use conventional silicon processing techniques to fabricate fluidic devices, and exploit the unique physical properties associated with micro- and nanoscale dimensions for developing precision measurement methods.

Rm. 76-261 | 617-253-5039 | srm @ mit . edu

RESEARCH SPECIALISTS
Nick Calistri, KI
Christopher Chin, KI
Kris Payer, MTL

POSTDOCTORAL ASSOCIATES
Josephine Bagnall, KI
Arif Cetin, KI
Scott Knudsen, BE
Selim Olcum, KI

GRADUATE STUDENTS
Nate Cermak, CSB
Nigel Chou, BE
Bashar Hamza, EECS
Vivian Hecht, BE
Joon Ho Kang, Physics
Robert Kimmerling, BE
Clara Park, MechE
Max Stockslager, MechE

UNDERGRADUATE STUDENTS
Jennifer Li, BE
Lucy Yang, BE

SUPPORT STAFF
Mariann Murray, Administrative Assistant II

SELECTED PUBLICATIONS

S. Olcum, N. Cermak, S. C. Wasserman, S. R. Manalis, "High-speed Multiple-Mode Mass-Sensing Resolves Dynamic Nanoscale Mass Distributions," *Nature Communications*, vol. 6, 7070, 2015.

S. Byun, V. C. Hecht, S. R. Manalis, "Characterizing Cellular Biophysical Responses to Stress by Relating Density, Deformability, and Size," *Biophysical Journal*, vol. 109, no. 8, pp. 1565-73, 2015.

S. Olcum, N. Cermak, S. C. Wasserman, K. S. Christine, H. Atsumi, K. R. Payer, W. J. Shen, J. C. Lee, A. M. Belcher, S. N. Bhatia, S. R. Manalis, "Weighing Nanoparticles in Solution at the Attogram Scale," *PNAS*, vol. 111, no. 4, pp. 1310-1315, 2014.

S. Byun, S. Son, D. Amodei, N. Cermak, J. Shaw, J. H. Kang, V. C. Hecht, M. M. Winslow, T. Jacks, P. Mallick, S. R. Manalis, "Characterizing Deformability and Surface Friction of Cancer Cells," *PNAS*, vol. 110, no. 19, pp. 7580-7585, 2013.

S. Son, A. Tzur, Y. Weng, P. Jorgensen, J. Kim, M. W. Kirschner, S. R. Manalis, "Direct Observation of Mammalian Cell Growth and Size Regulation," *Nature Methods*, vol. 9, pp. 910-912, 2012.

W. H. Grover, A. K. Bryan, M. Diez-Silva, S. Suresh, J. M. Higgins, S. R. Manalis, "Measuring Single-Cell Density," *PNAS*, vol.108, pp. 10992-10996, 2011.

J. Lee, R. Chunara, W. Shen, K. Payer, K. Babcock, T. Burg, S. R. Manalis, "Suspended Microchannel Resonators with Piezoresistive Sensors," *Lab on a Chip*, vol. 11, pp. 645-651, 2011.

J. Lee, W. Shen, K. Payer, T. Burg, S. R. Manalis, "Toward Attogram Mass Measurements in Solution with Suspended Nanochannel Resonators," *Nano Letters*, vol. 10, pp. 2537-2542, 2010.

M. Godin, F. F. Delgado, S. Son, W. H. Grover, A. K. Bryan, A. Tzur, P. Jorgensen, K. Payer, A. D. Grossman, M. W. Kirschner S. R. Manalis, "Using Buoyant Mass to Measure the Growth of Single Cells," *Nature Methods*, vol. 7, pp. 387-391, 2010.

J.E. Sader, T. P. Burg, S. R. Manalis, "Energy Dissipation in Microfluidic Beam Resonators," *Journal of Fluid Mechanics*, vol. 650, pp. 215-250, 2010.

A. K. Bryan, A. Goranov, A. Amon, S. R. Manalis, "Measurement of Mass, Density, and Volume of Yeast Through the Cell Cycle," *PNAS*, vol. 107, no. 3, pp. 999-1004, 2010.

T.P. Burg, J.E. Sader, S. R. Manalis, "Non-Monotonic Energy Dissipation in Microfluidic Resonators," *Physical Review Letters*, vol. 102, no. 22, 228103, 2009.

T. P. Burg, M. Godin, W. Shen, G. Carlson, J. S. Foster, K. Babcock, S. R. Manalis, "Weighing of Biomolecules, Single Cells, and Single Nanoparticles in Fluid," *Nature*, vol. 446, pp. 1066-1069, 2007.

Jürgen Michel

Senior Research Scientist
Materials Processing Center

Silicon photonics for optical interconnects. Ge epitaxy for detectors, modulator, and lasers. Novel optical designs for concentrator solar cells. High performance, Si based, parallel junction photovoltaic cells with thermal management. Octave spanning optical frequency comb generation.

Rm. 13-4110 | 617-253-7091 | jmichel @ mit . edu

POSTDOCTORAL ASSOCIATES

Lin Zhang
TaeWan Kim
Bing Wang, SMART Center

GRADUATE STUDENTS

Brian Albert, DMSE
Brian Pearson, MechE
Zhaohong Han, DMSE
Cong Wang, SMA Graduate Fellowship
Yiding Lin, SMA Graduate Fellowship

SUPPORT STAFF

Lisa Sinclair, Administrative Assistant II

SELECTED PUBLICATIONS

L. Z. Broderick, B. R. Albert, B. S. Pearson, L. C. Kimerling, J. Michel "Design for Energy: Modeling of Spectrum, Temperature and Device Structure Dependences of Solar Cell Energy," *Solar Energy Materials and Solar Cells* 136, pp. 48-63, 2015.

C. Bao, Y. Yan, L. Zhang, Y. Yue, N. Ahmed, A. M. Agarwal, L. C. Kimerling, J. Michel, and A. E. Willner, "Increased Bandwidth with Flattened and Low Dispersion in a Horizontal Double-Slot Silicon Waveguide," *Journal of Optical Society of America. B* 32, pp. 26-30, 2015.

C. Bao, L. Zhang, L. C. Kimerling, J. Michel, and C. Yang, "Soliton Breathing Induced by Stimulated Raman Scattering and Self-Steepening in Octave-Spanning Kerr Frequency Comb Generation," *Opt Express* 23, pp. 18665-18670, 2015.

Z. Zhou, B. Yin, and J. Michel, "On-chip light sources for silicon photonics," *Light: Science & Applications,* vol. 4, e358, 2015.

R. Chen, X. Li, Q. Deng, J. Michel, and Z. Zhou, "Thermally Tunable Resonator Using Directly Integrated Metallic Heater," *2015 International Conference On Optical Instruments and Technology: Micro/Nano Photonics And Fabrication, Proceedings of SPIE* 9624, article no. 96240D, 2015.

C. Bao, L. Zhang, L. C. Kimerling, J. Michel, and C. Yang, "Raman Scattering and Kerr Shock Induced Breather Soliton in Kerr Frequency Comb Generation," *CLEO: Science and Innovations,* Paper# JTu5A.40, 2015.

C. Wang, B. Wang, K. E. K. Lee, S. F. Yoon, and J. Michel, "A Yellow InGaP Light Emitting Diode Epitaxially Grown on Si Substrate," *Asia Communications and Photonics Conference,* 2015.

C. Lu, J. Luo, Y. Ji, K. Kitayama, H. Tam, K. Xu, P. Ghiggino, and N. Wada, eds., *OSA Technical Digest* [Online]. Optical Society of America, 2015, paper AS3A.3, November 2015.

Tomás Palacios
Associate Professor
Department of Electrical Engineering & Computer Science

Design, fabrication and characterization of novel electronic devices in wide bandgap semiconductors and two dimensional materials; polarization and bandgap engineering; transistors for sub-mm wave power and digital applications; new ideas for power conversion & generation; interaction of biological systems with semiconductor materials and devices; large area & ubiquitous electronics based on two dimensional materials.

Rm. 39-567a| 617-324-2395 | tpalacios @ mit . edu

POSTDOCTORAL ASSOCIATES
Amirhasan Nourbakhsh, EECS
Noelia Vico Trivino, EECS

GRADUATE STUDENTS
Nadim Chowdhury, EECS
Marek Hempel, EECS
Sameer Joglekar, DMSE
Yuxuan Lin, EECS
Charles Mackin, EECS
Elaine McVay, EECS
Daniel Piedra, EECS
Robert Radway, EECS
Min Sun, EECS
Lili Yu, EECS
Xu Zhang, EECS
Yuhao Zhang, EECS
Ahmad Zubair, EECS

UNDERGRADUATE STUDENTS
Eric Koch, EECS
Ayrton Munoz, EECS

SUPPORT STAFF
Joseph Baylon, Administrative Assistant II

SELECTED PUBLICATIONS
X. Ling, Y. Lin, Q. Ma, Z. Wang, Y. Song, L. Yu, S. Huang, W. Fang, X. Zhang, A.L. Hsu,Y. Bie, Y.-H. Lee, Y. Zhu, L. Wu, J. Li, P. Jarillo-Herrero, M. Dresselhaus, T. Palacios, J. Kong, "Parallel Stitching of 2D Materials," *Adv. Mater.*, vol. 28, pp. 2322–2329, January 2016.

L. Yu, D. El-Damak, S. Ha, X. Ling, Y. Lin, A. Zubair, Y. Zhang, Y.-H. Lee, J. Kong, A. Chandrakasan, T. Palacios, "Enhancement-Mode Single-layer CVD MoS_2 FET Technology for Digital Electronics," *2015 IEEE International Electron Devices Meeting (IEDM)*, pp. 32.3.1 - 32.3.4, December 2015.

D. Piedra, B. Lu, M. Sun, Y. Zhang, E. Matioli, F. Gao, JW. Chung, O. Saadat, L. Xia, M. Azize, T. Palacios, "Advanced Power Electronic Devices Based on Gallium Nitride (GaN)," *International Electron Devices Meeting (IEDM) IEEE*, pp. 16-6, December 2015.

Y. Zhang, H.-Y. Wong, M. Sun, S. Joglekar, L. Yu, N. A. Braga, R. V. Mickevicius, T. Palacios, "Design Space and Origin of Off-State Leakage in Gan Vertical Power Diodes," *2015 IEEE International Electron Devices Meeting (IEDM)*, pp. 35.1. 1-35.1. 4, December 2015.

T. Suemitsu, K. Kobayashi, S. Hatakeyama, N. Yasukawa, T. Yoshida, T. Otsuji, D. Piedra, T. Palacios, "A New Process Approach for Slant Field Plates in Gan-Based High-Electron-Mobility Transistors," *Japanese Journal of Applied Physics*, vol. 55(1S), pp.01AD02, November 2015.

S. M. Kim, A. Hsu, M. H. Park, S. H. Chae, S. J. Yun, J. S. Lee, D. H. Cho, W. Fang, C. Lee, T. Palacios, M, Dresselhaus, "Synthesis of Large-Area Multilayer Hexagonal Boron Nitride for High Material Performance," *Nature Communications,* vol. 6, pp. 8662, October 2015.

A. L. Hsu, P. K. Herring, N. M. Gabor, S. Ha, Y. C. Shin, Y. Song, M. Chin, M. Dubey, A. P. Chandrakasan, J. Kong, P. Jarillo-Herrero, T. Palacios, "Graphene-Based Thermopile for Thermal Imaging Applications," *Nano Letters* 15, vol. 11, pp. 7211-7216, October 2015.

X. Zhang, T. Schiros, D. Nordlund, Y. C. Shin, J. Kong, M. Dresselhaus, T. Palacios, "X-Ray Spectroscopic Investigation of Chlorinated Graphene: Surface Structure and Electronic Effects," *Advanced Functional Materials*, vol. 25(26), pp.4163-4169, July 2015.

Y. Zhang, M. Sun, H. Y. Wong, Y. Lin, P. Srivastava, C. Hatem, M. Azize, D. Piedra, L. Yu, T. Sumitomo, N. A. de Braga, T. Palacios, "Origin and Control of OFF-State Leakage Current in GaN-on-Si Vertical Diodes," *Electron Devices, IEEE Transactions*, vol. 62(7), pp. 2155-61, July 2015.

L. Yu, A. Zubair, E. J. G. Santos, X. Zhang, Y. Lin, Y. Zhang, T. Palacios, "High-Performance WSe2 Complementary Metal Oxide Semiconductor Technology and Integrated Circuits," *Nano Letters*, vol. 15, no. (8), pp. 4928-4934, July 2015.

David Perreault

Professor and Associate Department Head
Department of Electrical Engineering & Computer Science

Power electronics and energy conversion systems, high-efficiency radio-frequency power amplifiers and rf applications, Renewable energy systems, applications of power electronics in industrial, commercial, scientific, transportation, and biomedical systems

Rms. 10-039 and 38-435 | 617-258-6038 | djperrea @ mit . edu

RESEARCH SCIENTISTS

David M. Otten, RLE

POSTDOCTORAL ASSOCIATES

Minjie Chen, RLE

GRADUATE STUDENTS

Rose Abramson, EECS
Anas Al Bastami, EECS
Alex Hanson, EECS
Yiou He, EECS
Wardah Inam, EECS, Tata Fellow
Alex Jurkov, EECS
Seungbum Lim, RLE, Samsung Fellow
Konstantin Martynov, EECS
Juan Santiago-Gonzalez, EECS, NSF Fellow

UNDERGRADUATE STUDENTS

Julia Belk, EECS
Natalie Mionis, EECS
Rachel Yang, EECS
Ben (Thipok) Rak-amnouykit, EECS
Weston Braun, EECS

SUPPORT STAFF

Donna Gale, Administrative Assistant II
Myung-Hee Vabulas, Administrative Assistant II

SELECTED PUBLICATIONS

S. Lim, D. M. Otten, and D. J. Perreault, "AC-DC Power Factor Correction Architecture Suitable for High Frequency Operation," *IEEE Transactions on Power Electronics*, vol. 31, no. 4, pp. 2937-2949, April 2016.

M. Chen, M. Araghchini, K. K. Afridi, J. H. Lang, and D. J. Perreault, "A Systematic Approach to Modeling Impedances and Current Distribution in Planar Magnetics," *IEEE Transactions on Power Electronics*, vol. 31, no. 1, pp. 560-580, January 2016.

T. W. Barton and D. J. Perreault, "Theory and Implementation of RF-Input Outphasing Power Amplification," *IEEE Transactions on Microwave Theory and Techniques*, vol. 63, no. 12, pp. 4273-4283, December 2015.

D. M. Giuliano, M. E. D'Asaro, J. Zwart, and D.J. Perreault, "Miniaturized Low-Voltage Power Converters with Fast Transient Response," *IEEE Journal of Emerging and Selected Topics in Power Electronics*, vol. 2, no. 3, pp. 395-405, September 2014.

B. J. Pierquet and D. J. Perreault, "A Single-Phase Photovoltaic Inverter Topology with a Series-Connected Power Buffer," *IEEE Transactions on Power Electronics*, vol. 28, no. 10, pp. 4603-4611, October 2013.

A. D. Sagneri, D. I. Anderson, and D. J. Perreault, "Optimization of Transistors for Very High Frequency dc-dc Converters," *IEEE Transactions on Power Electronics*, vol. 28, no. 7, pp. 3614-3626, July 2013.

R. C. N. Pilawa-Podgurski and D. J. Perreault, "Sub-Module Integrated Distributed Maximum Power Point Tracking for Solar Photovoltaic Applications," *IEEE Transactions on Power Electronics*, vol. 28, no. 6, pp. 2957-2967, June 2013.

P.A. Godoy, S. Chung, T.W. Barton, D.J. Perreault, and J.L. Dawson "A 2.4-GHz, 27-dBm Asymmetric Multilevel Outphasing Power Amplifier in 65-nm CMOS," *IEEE Journal of Solid-State Circuits*, vol. 47, no. 10, pp. 2372-2384, October 2012.

R. C. N. Pilawa-Podgurski and D. J. Perreault, "Merged Two-Stage Power Converter with Soft-Charging Switched-Capacitor Stage in 180 nm CMOS," *IEEE Journal of Solid-State Circuits*, vol. 47, no. 7, pp. 1557-1567, July 2012.

Y. Han, A. Li, G. Cheung, C. R. Sullivan, and D. J. Perreault, "Evaluation of Magnetic Materials for Very High Frequency Power Applications," *IEEE Transactions on Power Electronics*, vol. 27, no. 1, pp. 425-435, January 2012.

J. Hu, A. D. Sagneri, J. M. Rivas, Y. Han, S. M. Davis, and D. J. Perreault, "High-Frequency Resonant SEPIC Converter with Wide Input and Output Voltage Ranges," *IEEE Transactions on Power Electronics*, vol. 27, no. 1, pp. 189-200, January 2012

Martin A. Schmidt

Provost
Professor
Department of Electrical Engineering & Computer Science

Micro and nanofabrication of sensors, actuators and electronic devices, micro-electromechanical systems (MEMS), design of micromechanical sensors and actuators, and micro/nanofabrication technology.

Rm. 3-208 | 617-253-7817 | maschmid @ mit . edu

RESEARCH SCIENTIST

Hanqing Li

GRADUATE STUDENTS

Parker Gould, EECS
Mitchell Hsing, EECS

SUPPORT STAFF

Chase Bronstein, Administrative Assistant I
Mary Niskala, Senior Administrative Assistant

SELECTED PUBLICATIONS

P. A. Gould, M. D. Hsing, H. Q. Li, K. K. Gleason, and M. A. Schmidt, "An Ultra-Low Cost Deep Reactive Ion Etching (DRIE) Tool For Flexible, Small Volume Manufacturing," *Transducers 2015: The 18th International Conference on Solid-State Sensors, Actuators, and Microsystems*, June 2015.

H. Zhou, H. Q. Li, V. Sharma, and M. A. Schmidt, "A Single-stage Micromachined Vacuum Pump Achieving 164 Torr Absolute Pressure," *2011 IEEE 24th Invitational Conference on Micro Electrical Management Systems (MEMS)*, pp. 1095-1098, January 2011.

C. E. Packard, A. Muraka, E. W. Lam, M. A. Schmidt, and V. Bulović, "Contact-Printed Microelectromechanical Systems," *Advanced Materials*, vol. 22, Issue 16, pp. 1840-1844, April 2010.

K. Deshpande, J. H. Meldon, M. A. Schmidt, and K. F. Jensen, "SOI-Supported Microdevice for Hydrogen Purification Using Palladium-Silver Membranes," *Journal of Microelectromechanical Systems*, vol. 19, Issue 2, pp. 402-409, April 2010.

H. Li and M. A. Schmidt, "Microengine Fabrication," *Multi-Wafer Rotating MEMS Machines*, published by Springer US, pp. 57-156, January 2010.

E. W. Lam, H. Li, and M. A. Schmidt, "Silver nanoparticle structures realized by digital surface micromachining," *Transducers 2009: The 15th International Conference on Solid-State Sensors, Actuators and Microsystems*, pp. 1698-1701, June 2009.

Charles G. Sodini
LeBel Professor
Department of Electrical Engineering & Computer Science

Electronics and integrated circuit design and technology. Specifically, technology intensive integrated circuit and systems design with application toward medical electronic devices for personal monitoring of clinically relevant physiological signals.

Rm. 39-527b | 617-253-4938 | sodini @ mtl . mit . edu

GRADUATE STUDENTS
Grant Anderson, EECS
Margaret Delano, EECS
Sabino Petriangelo, EECS
Sidney R. Primas, EECS
Joohyun Seo, EECS

SUPPORT STAFF
Joanna MacIver, Administrative Assistant II

SELECTED PUBLICATIONS
K. Chen, H. S. Lee, and C. G. Sodini, "A Column-Row-Parallel ASIC Architecture for 3-D Portable Medical Ultrasonic Imaging," *IEEE Journal of Solid State Circuits*, pp. 738-751, March 2016.

D. He, E. S. Winokur, and C. G. Sodini, "An Ear-worn Vital Signs Monitor," *IEEE Transactions on Biomedical Engineering*, pp. 2547-2552, November 2015.

J. Seo, S. Pietrangelo, H.-S. Lee, and C. G. Sodini, "Noninvasive Arterial Blood Pressure Waveform Monitoring Using Two-Element Ultrasound System," *Ultrasonics*, IEEE Transactions on Ferroelectrics, and Frequency Control, pp. 776-784, September 2015.

E. S. Winokur, T. O'Dwyer, and C. G. Sodini, "A Low-Power, Dual-Wavelength Photoplethysmogram (PPG) SoC With Static and Time-Varying Interferer Removal," *IEEE Transactions on Biomedical Circuits and Systems*, pp.581-589, August 2015.

D. He and C. G. Sodini, "A 58nW ECG ASIC with Motion-tolerant Heartbeat Timing Extraction for Wearable Cardiovascular Monitoring," *IEEE Transactions on Biomedical Circuits and Systems*, August 2014.

Vivienne Sze

Emanuel E. Landsman (1958) Career Development Assistant Professor
Department of Electrical Engineering & Computer Science

Joint design of signal processing algorithms, architectures, VLSI and systems for energy-efficient implementations. Applications include video coding, image processing and computer vision.

Rm. 38-260 | 617-324-7352 | sze @ mit . edu

GRADUATE STUDENTS

Yu-Hsin Chen, EECS, NVidia Fellowship
Ariana Eisenstein, EECS
James Noraky, EECS
Amr Suleiman, EECS, ODGE Fellowship
Mehul Tikekar, EECS
Tien-Ju Yang, EECS
Zhengdong Zhang, EECS

UNDERGRADUATE STUDENTS

Michael Holacheck, EECS
Akshay Padmanabha, EECS
Diana Wofk, EECS

SUPPORT STAFF

Janice Balzer, Administrative Assistant II

SELECTED PUBLICATIONS

A. Suleiman, Z. Zhang, V. Sze, "A 58.6mW Real-Time Programmable Object Detector with Multi-Scale Multi-Object Support Using Deformable Parts Model on 1920x1080 Video at 30fps," *Symposium on VLSI*, June 2016.

Y.-H. Chen, J. Emer, V. Sze, "Eyeriss: A Spatial Architecture for Energy-Efficient Dataflow for Convolutional Neural Networks," *International Symposium on Computer Architecture (ISCA)*, June 2016.

Y.-H. Chen, T. Krishna, J. Emer, V. Sze, "Eyeriss: An Energy-Efficient Reconfigurable Accelerator for Deep Convolutional Neural Networks," *IEEE International Conference on Solid-State Circuits (ISSCC)*, pp. 262-264, February 2016.

A. Suleiman, V. Sze, "An Energy-efficient Hardware Implementation of HOG-based Object Detection at 1080HD 60 fps with Multi-scale Support," *Journal of Signal Processing Systems, SiPS Special Issue*, December 2015.

Z. Zhang, V. Sze, "Rotate Intra Block Copy for Still Image Coding," *IEEE International Conference on Image Processing (ICIP)*, September 2015.

Y.-H. Chen, V. Sze, "A Deeply Pipelined CABAC Decoder for HEVC Supporting Level 6.2 High-Tier Applications," *IEEE Transactions on Circuits and Systems for Video Technology (TCSVT)*, vol. 25, no. 5, pp. 856-868, May 2015.

Carl V. Thompson

Stavros Salapatas Professor of Materials Science and Engineering
Department of Materials Science & Engineering

Processing and property optimization of thin films and nanostructures for applications in electronic, microelectromechanical, and electromechanical devices and systems. Interconnect and device reliability.

Rm. 13-5069 | 617-253-7652 | cthomp @ mit . edu

POSTDOCTORAL ASSOCIATES

Riko I. Made
Mazdak Hashempour Igderi
Daniele Perego
Wardhana Sasangka
Makdak Hemp

GRADUATE STUDENTS

Ahmed Al-Obeidi, DMSE
Thomas Batcho, DMSE
Chee Ying Khoo, SMA Fellow, NTU
Jinghui, Miao DMSE
Yoon Ah Shin, DMSE
Lin Xu, DMSE
Govindo Syaranamual, SMA Fellow, NTU
L. T. Ye, SMA Fellow, NUS
Gao Yu, SMA Fellow, NTU
Wen Zheng, MIT
Rachel Zucker, DMSE

SUPPORT STAFF

Kathleen Fitzgerald, Administrative Assistant II

SELECTED PUBLICATIONS

D. G. Kwabi, M. Tulodziecki, N. Pour, D. M. Itkis, C. V. Thompson, and Y. Shao-Horn, "Controlling Solution-mediated Reaction Mechanisms of Oxygen Reduction Using Potential and Solvent for Aprotic Lithium-oxygen Batteries," *Journal of Phys. Chem. Letters,* 2016.

R.V. Zucker, G. H. Kim, J. Ye, W. C. Carter, and C.V. Thompson, "The Mechanism of Corner Instabilities in Single-Crystal Thin Films During Dewetting," *Journal of Appl. Phys.*, vol. 119, pp. 125306:1-10, 2016.

R. V. Zucker, W. C. Carter, C. V. Thompson, "Power-Law Scaling Regimes for Solid-State Dewetting of Thin Films," *Scripta Materialia*, vol. 116, pp. 143, 2016.

D. G. Kwabi, V. S. Bryantsev, T. P. Batcho, D. M. Itkis, C. V. Thompson, and Y. Shao-Horn, "Experimental and Computational Analysis of the Solvent-Dependent O_2/Li+-O_2-Redox Couple: Standard Potentials, Coupling Strength, and Implications for Lithium–Oxygen Batteries," *Angewandte Chemie*, vol. 128, pp. 3181, 2016.

A. Al-Obeidi, D. Kramer, R. Moenig, and C.V. Thompson, "Mechanical Stresses and Crystallization of Lithium Phosphorous Oxynitride-Coated Germanium Electrodes During Lithiation and Delithiation," *Journal of Power Sources*, vol. 306, pp. 817, 2016.

C. Y. Khoo, H. Liu, W. A. Sasangka, R. I. Made, N. Tamura, M. Kunz, A. S. Budiman, C. L. Gan, and C. V. Thompson, "Impact of Deposition Conditions on the Crystallization Kinetics of Amorphous GeTe Films," *Journal of Mat. Sci.*, vol. 51, no. 4, pp. 1864, 2016.

S. A. Jang, H. J. Lee, C. V. Thompson, C. A. Ross, and Y. J. Oh, "Crystallographic Analysis of the Solid-State Dewetting of Polycrystalline Gold Film Using Automated Indexing in a Transmission, Electron Microscope," *APL Mater.*, vol. 3, pp. 126103, 2015.

H. Z. Yu and C. V. Thompson, "Stress Engineering Using Low Oxygen Background Pressures During Volmer-Weber Growth of Polycrystalline Nickel Films," *Journal of Vac. Sci. and Tech.* A33, pp. 021504, 2015.

G. H. Kim and C. V. Thompson, "Effect of surface energy anisotropy on Rayleigh-like solid-state dewetting and nanowire stability," *Acta Materialia*, 84, pp. 190, 2015.

W. A. Sasangka, C. L. Gan, D. Lai, C. S. Tan, and C. V. Thompson, "Characterization of the Young's Modulus, Residual Stress and Fracture Strength of Cu-Sn-In Thin Films using Combinatorial Deposition and Micro-Cantilevers," *Journal of Micromechanics and Microengineering*, vol. 25, 035023, 2015.

C.Q. Lai, W. Zheng, W. K. Choi, and C. V. Thompson, "Metal Assisted Anodic Etching of Silicon," *Nanoscale*, vol. 7, pp. 11123, 2015.

N. Ortiz-Vitoriano, T. P. Batcho, D. G. Kwabi, B. Han, N. Pour, K. P. C. Yao, C. V. Thompson and Y. Shao-Horn, "Rate-Dependent Nucleation and Growth of NaO_2 in Na-O_2 batteries," *Journal of Phys. Chem. Letters,* vol. 6, pp. 2636, 2015.

A. Al-Obeidi, D. Kramer, C. V. Thompson, and R. Mönig, "Mechanical stresses and morphology evolution in germanium thin film electrodes during lithiation and delithiation," *Journal of Power Sources*, vol. 297, pp. 472-480, 2015.

Kripa K. Varanasi
Associate Professor of Mechanical Engineering
Department of Mechanical Engineering

Intersection of interfacial engineering, thermal-fluids, and materials & manufacturing. Central theme is the design and manufacturing of nanoengineered surfaces and their applications to energy, water, oil & gas, agriculture, transportation, electronics cooling systems for significant efficiency enhancements.

Rm. 35-209 | 617-324-5608 | varanasi @ mit . edu

RESEARCH SCIENTISTS
Seyed Mahmoudi, DMSE

POSTDOCTORAL ASSOCIATES
Sushant Anand, MechE, Branco Weiss Fellow
Nada Bjelobrk, MechE
Paris Cox, MechE
Arindam Das, MechE
Susmita Dash, MechE
Navdeep Dhillon, MechE
Nasim Hyder, ChemE
Gibum Kwon, MechE
Jolet de Ruiter, MechE, NWO Rubicon Fellow
Dan Soto, MechE

GRADUATE STUDENTS
Maher Damak, MechE, TATA Fellow
Taylor Farnham, MechE
Henri Girard, MechE
Ingrid Fuller Guha, EECS
Karim Khalil, MechE
Sami Khan, TPP/MechE
Samantha McBride, MechE, NSF Fellow
Divya Panchanathan, MechE
Leonid Rapoport, MechE
Sudarshan Sarathy, MechE
Brian Solomon, MechE
Srinivas Bengaluru Subramanyam, DMSE

SUPPORT STAFF
Lauren Wolinsky, Administrative Assistant II

SELECTED PUBLICATIONS

A.O. Ahmed, M. Khaled, B. S. Yilbas, N. Abu-Dheir, K. K. Varanasi, Y. K. Toumi, "Surface and Wetting Characteristics of Textured Bisphenol-A based Polycarbonate Surfaces: Acetone-Induced Crystallization Texturing Methods," *Journal of Applied Polymer Science*, vol. 133, pp. 43074, 2016.

B. S. Yilbas, H. Ali, M. Khaled, N. Al-Aqeeli, N. Abu-Dheir, K.K. Varanasi, "Influence of Dust and Mud on the Optical, Chemical, and Mechanical Properties of a PV Protective Glass," *Scientific Reports*, vol. 5, pp. 15833, 2015.

R. Narhe, S. Anand, K. Rykaczewski, M-G Medici, G.Wenceslao, K.K. Varanasi, D. Beysens, "Inverted Leidenfrost-like Effect During Condensation," *Langmuir*, vol. 31, pp. 5353-5363, 2015.

B. S. Yilbas, M. Khaled, N. Al-Aqeeli, N. Abu-Dheir, K.K. Varanasi, "Characteristics of Laser Textured Silicon Surface and Effect of Mud Adhesion on Hydrophobicity," *Applied Surface Science*, vol. 351, pp. 880-888, 2015.

K. A. Stoerzinger, T. W. Hong, G. Azimi, E.J. Crumlin, M. D. Biegalski, H. Bluhm, K. K. Varanasi, Y. Shao-Horn, "Reactivity of Perovskites with Water: Role of Hydroxylation in Wetting and Implications for Oxygen Electrocatalysis," *The Journal of Physical Chemistry C*, vol. 119, pp. 18504-18512, 2015.

A. Ugur, F. Katmis, M. Li, L. Wu, Y. Zhu, K. K. Varanasi, K. K. Gleason, "Low-Dimensional Conduction Mechanisms in Highly-Conductive and Transparent Conjugated Polymers," *Advanced Materials*, vol. 27, pp. 4604-4610, 2015.

P. R. Jones, X. Hao, E. R. Cruz-Chu, K. Rykaczewski, K. Nandy, T. M. Schutzius, K. K. Varanasi, C. Megaridis, J. H. Walther, P. Koumoutsakos, H. D. Espinosa, N. Patankar, "Sustaining Dry Surfaces Under Water," *Scientific Reports*, vol. 5, pp. 12311, 2015.

N. Dhillon, J. Buongiorno, K. K. Varanasi, "Critical Heat Flux Maxima During Boiling Crisis on Textured Surfaces," *Nature Communications*, vol. 6, pp. 8247, 2015.

Luis Fernando Velásquez-García

Principal Scientist
Microsystems Technology Laboratories

Micro- and nano-enabled multiplexed scaled-down systems for space, energy, healthcare, manufacturing, and analytical applications. 3-D printed MEMS/NEMS, carbon nanotubes; electrospray, electrospinning, field emission, field ionization, plasmas, X-rays; electrical and chemical nanosatellite propulsion, plasma sensors, portable mass spectrometry, high-voltage, 3D MEMS packaging, x-ray sources, tactile displays and sensors, ultracapacitors.

Rm. 39-657 | 617-253-0730 | lfvelasq @ mit . edu

POSTDOCTORAL ASSOCIATES

Anirban Basu, MTL
Daniel Olvera Trejo, MTL
Ran Wang, MTL

VISITORS

Frank Boehm, Critical Flow Technologies
Anthony Taylor, Edwards Vacuum

SUPPORT STAFF

Carolyn Collins, Administrative Assistant II
Valerie DiNardo, Administrative Assistant II

SELECTED PUBLICATIONS

D. Olvera Trejo and L. F. Velásquez-García, "SLA 3-D Printed MEMS Coaxial Electrospray Sources For Uniform Generation of Core-Shell Microparticles," *Technical Digest 17th Solid-State Sensor, Actuator and Microsystems Workshop,* Hilton Head Island SC, USA, pp. 176 -179, June 5-9, 2016.

P. J. Ponce de Leon and L. F. Velásquez-García, "Optimization of Capillary Flow Through Open-Microchannel and Open-Micropillar Arrays," *Journal of Physics D-Applied Physics*, vol. 49, no. 5, pp. 1-13, 055501 February 2016.

A. P. Taylor and L. F. Velásquez-García, "Electrospray-Printed Nanostructured Graphene Oxide Gas Sensors," *Nanotechnology*, vol. 26, no. 50, pp. 505301:1-8, December 2015.

L. F. Velásquez-García, "SLA 3D-Printed Arrays of Miniaturized, Internally-Fed, Polymer Electrospray Emitters," *Journal of Microelectromechanical Systems*, vol. 24, no. 6, pp. 2117–2127, December 2015.

F. A. Hill and L. F. Velásquez-García, "Advances In Vertical Solid-State Current Limiters For Regulation Of High-Current Field Emitter Arrays," *15th International Conference on Micro and Nanotechnology for Power Generation and Energy Conversion Applications (PowerMEMS 2015)*, Boston, Massachusetts, USA, December 1–4, 2015; *Journal of Physics Conference Series*, vol. 660, pp. 012037:1-5, 2015.

A. Taylor and L. F. Velásquez-García, "Microwatt-Powered, Low-Cost, Printed Graphene Oxide Humidity Sensor for Distributed Sensor Networks," *15th International Conference on Micro and Nanotechnology for Power Generation and Energy Conversion Applications (PowerMEMS 2015),* Boston, MA, USA, December 1–4, 2015; *Journal of Physics Conference Series,* vol. 660, pp. 012134:1-5, 2015.

A. Basu, M. A. Perez, and L. F. Velásquez-García, "Miniaturized, Electrostatic, High-Vacuum Ion Pump Using A Nanostructured Field Emission Electron Source," *15th International Conference on Micro and Nanotechnology for Power Generation and Energy Conversion Applications (PowerMEMS 2015),* Boston, MA, USA, December 1–4, 2015; *Journal of Physics Conference Series,* vol. 660, pp. 012027:1-5, 2015.

E. V. Heubel and L. F. Velásquez-García, "Microfabricated Retarding Potential Analyzers With Enforced Aperture Alignment for Improved Ion Energy Measurements in Plasmas," *Journal of Microelectromechanical Systems*, vol. 24, no. 5, pp. 1355–1369, October 2015.

P. J. Ponce de Leon, F. A. Hill, E. V. Heubel, and L. F. Velásquez-García, "Parallel Nanomanufacturing via Electrohydrodynamic Jetting from Microfabricated Externally-Fed Emitter Arrays," *Nanotechnology*, vol. 26, no. 22, pp. 225301:1-10, June 2015.

C. Dong, M. E. Swanwick, D. Keithley, F. X. Kärtner, and L. F. Velásquez-García, "Multiplexing and Scaling-Down of Nanostructured, Photon-Triggered Silicon Field Emitter Arrays for Maximum Total Electron Yield," *Nanotechnology*, vol. 26, no. 26, pp. 265202:1-11, June 2015.

A. Basu, M. E. Swanwick, A. A. Fomani, and L. F. Velásquez-García, "A Portable X-ray Source With a Nanostructured Pt-coated Silicon Field Emission Cathode for Absorption Imaging of low-Z Materials," *Journal of Physics D-Applied Physics*, vol. 48, no. 22, pp. 225501:1-11, May 2015.

Joel Voldman

Professor
Department of Electrical Engineering & Computer Science

Microtechnology for basic cell biology, applied cell biology, neuroscience, and human health.

Rm. 36-824 | 617-253-2094 | voldman @ mit . edu

POSTDOCTORAL ASSOCIATES

Marc Castellarnau
Anna Fendyur
Thibault Honegger
Javier Prieto

GRADUATE STUDENTS

Aalap Dighe, MechE
Burak Dura, EECS
Jaemyon Lee, EECS
Lisa Liu, EECS
Boying Meng, EECS
Hao-wei Su, EECS
SarveshVarma, EECS
Dan Wu, MechE

UNDERGRADUATE STUDENTS

Giri Anand, EECS
Alex Jaffe, EECS

VISITORS

Rodrigo Balam Muñoz Soto, Tecnológico de Monterrey

SUPPORT STAFF

Chadwick Collins, Administrative Assistant II

SELECTED PUBLICATIONS

S. Varma and J. Voldman, "A Cell-Based Sensor of Fluid Shear Stress for Microfluidics," *Lab on A Chip*, vol. 15, pp. 1563-1573, 2015.

B. Dura and J. Voldman, "Microfluidic Systems for Cell Pairing and Fusion," *Methods Mol. Biol.* vol. 1313, pp. 73-94, 2015.

B. Dura and J. Voldman, "Spatially and Temporally Controlled Immune Cell Interactions Using Microscale Tools," *Current Opinion in Immunology*, vol. 35, pp. 23-29, 2015.

B. Dura, H.-W. Su, and J. Voldman, "Microfluidic Tools for Assaying Immune Cell Function," *Micro Total Analysis Systems*, Gyeongju, Korea, 2015, pp. 60-62, 2015.

B. Dura, S. K. Dougan, M. Barisa, M. M. Hoehl, C. T. Lo, H. L. Ploegh, and J. Voldman, "Profiling Lymphocyte Interactions at the Single-Cell Level by Microfluidic Cell Pairing," *Nature Communications*, vol. 6, pp. 5940, 2015.

M. Castellarnau, G. L. Szeto, H. W. Su, T. Tokatlian, J. C. Love, D. J. Irvine, and J. Voldman, "Stochastic Particle Barcoding for Single-Cell Tracking and Multiparametric Analysis," *Small*, vol. 11, pp. 489-498, 2015.

P. Augustsson and J. Voldman, "Iso-acoustic Focusing for Size-Insensitive Cell Separation Based on Acoustic Properties," in *Micro Total Analysis Systems* 2015 Gyeongju, Korea, pp. 14-16, 2015.

T. Sun, J. R. Kovac, and J. Voldman, "Image-Based Single-Cell Sorting via Dual-Photopolymerized Microwell Arrays," *Analytical Chemistry*, vol. 86, no. 15, pp. 977-981, August 2014.

H.-W. Su, J. L. Prieto, L. Wu, H.-W. Hou, M. P. Vera, D. Amador-Munoz, J. L. Englert, B. D. Levy, R. M. Baron, J. Han, and J. Voldman, "Monitoring Sepsis Using Electrical Cell Profiling in a Mouse Model," in *Micro Total Analysis Systems,* 2014 San Antonio, TX, pp. 327-329, 2014.

T. Honegger, M. Thielen, and J. Voldman, "Three-Dimensional Topological Neural Networks Based on AC Electrokinetic Confinement Of Neurites," *Micro Total Analysis Systems,* San Antonio, Texas, USA, pp. 348-350, 2014.

A. Fendyur, S. Varma, C. T. Lo, and J. Voldman, "Cell-Based Biosensor to Report Dna Damage in Micro- and Nanosystems," *Analytical Chemistry*, vol. 86, no. 15, pp. 7598-7605, August 2014.

B. Dura, Y. Liu, and J. Voldman, "Cell Squeezing-Based Sequential Capture, Pairing and Fusion of Cells," in *Micro Total Analysis Systems,* San Antonio, Texas, USA, pp. 1488-1490, 2014.

B. Dura, Y. Liu, and J. Voldman, "Deformability-based Microfluidic Cell Pairing and Fusion," *Lab on a Chip*, vol. 14, pp. 2783-2790, 2014.

A. Dighe, U. P. Froriep, M. Sunshine, A. Ievins, P. Anikeeva, C. Moritz, and J. Voldman, "Development and *In Vivo* Testing of Reconfigurable Neural Probes for Chronic Electrical Recording," *Hilton Head Workshop 2014: A Solid-State Sensors, Actuators and Microsystems Workshop,* 2014.

Evelyn N. Wang

Associate Professor, Gail E. Kendall Professor
Department of Mechanical Engineering

Heat and mass transport at the micro- and nano-scales, nanoengineered surfaces, and thermal microdevices for applications in thermal management, solar thermal energy conversion, and water desalination.

Rm. 3-461b | 617-324-3311 | enwang @ mit . edu

POSTDOCTORAL ASSOCIATES

Dion Antao, MechE
Banafsheh Barabadi, MechE
Xiansen Li, MechE
Shankar Narayanan
Sameer Rao, MechE
Sungwoo Yang, MechE

GRADUATE STUDENTS

Solomon Adera, MechE
Kevin Bagnall, MechE
David Bierman, MechE
Han-Jae (Jeremy) Cho, MechE
Daniel Hanks, MechE
Hyunho Kim, MechE
Arny Leroy, MechE
Zhengmao Lu, MechE
Heena Mutha, MechE
Dan Preston, MechE
Jean Sack, MechE
Jay Sircar, MechE
Ari Umans, MechE
Kyle Wilke, MechE
Lin Zhao, MechE
Yangying Zhu, MechE

UNDERGRADUATE STUDENTS

Joshua Acosta, MechE
DingRan Dai, MechE
Luis Gasca, MechE
Melissa F. Gianello, MechE
Carlos Jimenez, MechE
Henry Merrow, MechE
Emmanuel Simpri, MechE

VISITORS

Ikuya Kinefuchi, University of Tokyo

SUPPORT STAFF

Alexandra Cabral, Administrative Assistant II

SELECTED PUBLICATIONS

L. Zhao, S. Yang, B. Bhatia, E. Strobach, E. N. Wang, "Modeling Silica Aerogel Optical Performance by Determining its Radiative Properties," *AIP Advances*, 6(2), 2016.

D. S. Antao, S. Adera, Y. Zhu, E. Farias, R. Raj, E. N. Wang, "Dynamic Evolution of the Evaporating Liquid-Vapor Interface in Micropillar Arrays," *Langmuir*, 32(2), p. 519-526, 2016.

D. S. Antao, S. Adera, E. Farias, R. Raj, E. N. Wang, "Visualization of the Evaporating Liquid-Vapor Interface in Micropillar Arrays," *Journal of Heat Transfer*, 138(2), pp. 020910, 2016.

H. Kim, H. J. Cho, S. Narayanan, S. Yang, H. Furukawa, S. Schiffres, X. Li, Y. Zhang, J. Jiang, O. M. Yaghi, E. N. Wang, "Characterization of Adsorption Enthalpy of Novel Water-Stable Zeolites and Metal-Organic Frameworks," *Scientific Reports*, 6, 2016.

Y. Zhu, D. S. Antao, Z. Lu, S. Somasundaram, T. Zhang, E. N. Wang, "Prediction and Characterization of Dry-out Heat Flux in Micropillar Wick Structures," *Langmuir*, 32(7), pp. 1920-1927, 2016.

D. J. Preston, D. L. Mafra, N. Miljkovic, J. Kong, E. N. Wang, "Scalable Graphene Coatings for Enhanced Condensation Heat Transfer," *Nano Letters*, 10(1021), 2015.

S. Narayanan, X. Li, S. Yang, H. Kim, A. Umans, I. S. McKay, E. N. Wang, "Thermal Battery for Portable Climate Control," *Applied Energy*, 149, pp. 104-116, 2015.

Z. Lu, S. Narayanan, E. N. Wang, "Modeling of Evaporation from Nanopores with Nonequilibrium and Nonlocal Effects," *Langmuir*, 31(36), pp. 9817-9824, 2015.

S. Yang, H. Kim, S. Narayanan, I. S. McKay, E. N. Wang, "Dimensionality Effects of Carbon-Based Thermal Additives for Microporous Adsorbents," *Materials and Design*, 85(520), 2015.

X. Li, S. Narayanan, V. K. Michaelis, T. Ong, E. G. Keeler, H. Kim, I. S. McKay, R. G. Griffin, E. N. Wang, "Zeolite Y Adsorbents with High Vapor Uptake Capacity and Robust Cycling Stability for Potential Applications in Advanced Adsorption Heat Pumps," *Microporous and Mesoporous Materials*, 201, pp. 151-159, 2015.

H. J. Cho, J. P. Mizerak, E. N. Wang, "Turning Bubbles on and off During Boiling Using Charged Surfactants," *Nature Communications*, 6, 2015.

Ron Weiss

Professor of Biological Engineering
Professor of Electrical Engineering and Computer Science
Director of Synthetic Biology Center

Synthetic biology. Construction and analysis of synthetic gene networks. Use of computer engineering principles of abstraction, composition, and interface specifications to program cells with sensors and actuators precisely controlled by analog and digital logic circuitry. Emphasis on establishing the engineering foundation for synthetic biology and the pursuit of novel applications enabled by the technology.

Rm. NE47-223 | 617-253-8966 | rweiss @ mit . edu

RESEARCH SCIENTISTS

Stephen Firsing, BE
Maria Hottelet Foley, BE
Leonid Gaidukov, BE
Kalpana Jagtap, BE
John Scarpa, BE
Nevin Summers, BE

POSTDOCTORAL ASSOCIATES

Michelle Chang, BE
Jin Huh, BE
Kevin Lebo, BE
Deepak Mishra, BE
Ely Porter, BE
Lin Quek, BE
Brian Teague, BE
Allen Tseng, BE
Elvira Vitu, IMES

GRADUATE STUDENTS

Giulio Alighieri, ChemE
Jacob Becraft, BE
Tod Cramer, BE
Nicholas Delateur, Chemistry
Jeremy Gam, BE
Ross Jones, BE
Francis Lee, BE
Sebastian Palacios, EECS
Breanna Stillo, BE
Tyler Wagner, BE

UNDERGRADUATE STUDENTS

Lyla Atta, BE
Kathryn Brink, BE
Richard Hall, BE
Kyle Lathem, BE
Christian Richardson, BE

VISITORS

Patrick Fortuna, Queensland, Australia

SUPPORT STAFF

Olga V. Parkin, Senior Administrative Assistant
Kristine Marzilli, Senior Administrative Assistant

SELECTED PUBLICATIONS

P. Guye, M. R. Ebrahimkhani, N. Kipniss, J. J. Velazquez, E. Schoenfeld, S. Kiani, L. G. Griffith, R. Weiss, "Genetically Engineering Self-Organization of Human Pluripotent Stem Cells into a Liver Bud-Like Tissue Using Gata6," *Nature Communications*, doi:10.1038/ncomms10243, January 2016.

S. Kiani, A. Chavez, M. Tutle, R. N. Hall, R. Chari, D. Ter-Ovanesyan, J. Qian, B. W. Pruitt, J. Beal, S. Vora, J. Bucchthal, E. J. K. Kowal, M. R. Ebrahimkhani, J. J. Collins, R. Weiss, and, G. Church, "Cas9 gRNA engineering for genome editing, activation and repression," *Nature Methods,* doi:10.1038nmeth.3580, September 2015.

B. P. Teague and R. Weiss, "Synthetic Communities, the Sum of Parts," *Science*, doi:10.1126/science.aad0876, August 2015.

L. Wroblewska, T. Kitada, K. Endo, V. Siciliano, B. Stillo, H. Saito, and R. Weiss, "Mammalian Synthetic Circuits with Rna Binding Proteins for RNA-Only Deliver," *Nature Biotechnology*, doi:10, 1038/nbt.3301, August 2015.

S. Bhatt, M. K. Gupta, M. Khamaisi, R. Martinez, M. A. Gritsenko, B. K. Wagner, P. Guye, V. Busskamp, J. Shirakawa, G. Wu, C. W. Liew, T. R. Clauss, I. Valdez, A. El Ouaamari, E. Dirice, T. Takatani, H. A. Keenan, R. D. Smith, G. Church, R. Weiss, A. J. Wagers, W.-J. Qian, G. L. King, and R. N. Kulkami, "Preserved DNA Damage Checkpoint Pathway Protects Against Complications in Long-Standing Type 1 Diabetes," *Cell Metabolism,* vol. 4, no. 22, pp. 239-252, August 2015.

Theses Awarded

S.B.

- **Beth Cholst** (M. KOLLE)
  Elastic Stretchable Optical Fibers

M.ENG.

- **Ariana Eisenstein** (V. SZE)
  An FPGA Platform for Demonstrating Embedded Vision Systems
- **Taylor Farnham** (K. K. VARANASI)
  Hydrate Mitigation: Controlling Nucleation, Growth and Adhesion of Clathrate Hydrates
- **Luis Fernandez** (A. P. CHANDRAKASAN)
  Parallel Implementation of Sample Adaptive Offset Filtering Block for Low-Power HEVC Chip
- **Matthew Fox** (V. SZE)
  Functional and Timing Models for a Programmable Hardware Accelerator
- **George Kakuru** (C. G. SODINI)
  Design of On-Chip Measurement Circuits
- **Pranav R. Kaundinya** (R. HAN)
  Synthetic Impedance Generation in mm-Wave Oscillators and Amplifiers
- **Anders Wen-Dao Lee** (C. G. SODINI)
  The Design of a High Precision, Wide Common Mode Range Auto-Zero Comparator
- **Sarathy Sudarshan** (K. K. VARANASI)
  Nanoengineered Surfaces for Controlling Wetting and Electromagnetic Interactions
- **Wegene Tadele** (C. WARDE)
  Design of Optoelectronic Activation Functions for COIN Co-processor
- **Michael Wu** (R. HAN)
  A Common Platform for Current Sensor Product Evaluation in Industrial Automation Applications

S.M.

- **Ermal Dreshaj** (V. M. BOVE, JR.)
  Holosuite: An Exploration into Interactive Holographic Telepresence
- **Chuhong Duan** (A. P. CHANDRAKASAN)
  Energy Efficient Reconfigurable SRAM Using Data-Dependency
- **Preetinder Garcha** (A. P. CHANDRAKASAN)
  Fully Integrated Therman Energy Harvesting System to Start up at 20 mV
- **Sami Khan** (K. K. VARANASI)
  Wetting and Interfacial Properties of Rare-Earth Oxide Ceramics
- **Sara Nagelberg** (M. KOLLE)
  Tunable Liquid Microlenses formed from Dynamically Reconfigurable Double Emulsions
- **Sirma Orguc** (A. P. CHANDRAKASAN)
  0.3v Biopotential Sensor Interface for Stress Monitoring
- **Cheng Peng** (D. ENGLUND)
  Towards Infrared Plasmonics and Nonlinear Optics in Graphene
- **Wendi Reib** (C. G. SODINI)
  Increasing Patient Throughput in the MGH Cancer Center Infusion Unit
- **Joseph Sandt** (M. KOLLE)
  Scalable Manufacture and Synchronized Optical/Mechanical Characterization of Tunable Elastic Photonic Fibers
- **Christopher Wing** (M. KOLLE)
  Bragg Reflector Geometries for Colorimetric Orientation and Deformation Sensing
- **Patricia Yen** (T. BUONASSISSI)
  Determining the Structure-Property-Process Relationships for Laser-Fired Contacts for Solar Cells

S.M. & M. ENG.

- **Naomi Arnold** (D. S. BONING)
  Wafer Defect Prediction with Statistical Machine Learning
- **Ana Maria Ortiz Garcio** (D. S. BONING)
  Evaluating Inventory Ordering Policies: A Methodology and Application
- **Kyle Wilke** (E. N. WANG)
  Thin Film Evaporation from Nanopores for Thermal Management

PH.D.

- **Solomon Adera** (E. N. WANG)
  Thin Film Evaporation on Micropillar Arrays
- **Brian Albert** (L. C. KIMERLING AND J. MICHEL)
  Germanium on Silicon Heteroepitaxy for High Efficiency Photovoltaic Devices
- **Georgios Angelopoulos** (A. P. CHANDRAKASAN AND M. MEDARD)
  Improving the Energy Efficiency and Reliability of Wireless Sensor Networks Using Coding Techniques

PH.D. (CONTINUED)

- **Bichoy Bahr** (L. DANIEL)
  Monolithically Integrated MEMS Resonators and Oscillators in Standard IC Technology.
- **Wubin Bai** (C. A. ROSS)
  Block Copolymer Self-Assembly and Templating Strategies
- **David Berney Needleman** (T. BUONASSISSI)
  Performance Limits of Silicon Solar Cells Due to Structural Defects
- **Hyun Ho Boo** (H.-S. LEE)
  Virtual Ground Reference Buffer Technique in Switched-Capacitor Circuits
- **Riley E. Brandt** (T. BUONASSISSI)
  Accelerating the Development of Novel Photovoltaic Materials
- **Patrick Brown** (V. BULOVIĆ)
  Energy Level Engineering in Colloidal Quantum Dot Solar Cells
- **Sergio Castellanos** (T. BUONASSISSI)
  Electrical-Impact Assessment of Dislocations in Silicon Materials for Solar Cells
- **Rupak Chakraborty** (T. BUONASSISSI)
  Structural Defect Engineering of Tin (Ii) Sulfide for Solar Cells
- **Ritchie Chen** (P. ANIKEEVA)
  High-Performance Ferrite Nanoparticles for Magnetothermal Neural Excitation
- **Bhavya Daya** (A. P. CHANDRAKASAN AND L. S. PEH)
  SC^{2}EPTON: High-Performance and Scalable, Low-Power and Intelligent, Ordered Mesh On-Chip Network
- **Aalap Dighe** (J. VOLDMAN)
  Reconfigurable Neural Probes for Chronic Electrical Recording
- **Bruno Do Valle** (C. G. SODINI)
  Subdermal Implantable EEG Monitor for Seizure Detection
- **Burak Dura** (J. VOLDMAN)
  Microfluidic Single-Cell Technologies for Assaying Lymphocyte Interactions
- **Dina El-Damak** (A. P. CHANDRAKASAN)
  Power Management Circuits for Ultra-low Power Systems
- **Sema Ermez** (S. GRADEČAK)
  Self-seeded III-V Semiconductor Nanowire Growth by Metal-organic Chemical Vapor Deposition (MOCVD)
- **Wenjing Fang** (J. KONG)
  Synthesis of Bilayer Graphene and Hexagonal Boron Nitride by Chemical Vapor Deposition
- **Wenjing Fang** (M. DRESSELHAUS)
  Synthesis of Bilayer Graphene and Hexagonal Boron Nitride
- **Stephen Guerrera** (A. I. AKINWANDE)
  Highly Scaled Silicon Field Emitter Arrays with Integrated Silicon Nanowire Current Limiters
- **Sungjae Ha** (A. P. CHANDRAKASAN AND T. PALACIOS)
  Energy-Aware System Design Using Circuit Reconfigurability with a Focus on Low-Power SRAMs
- **Daniel Hanks** (E. N. WANG)
  Evaporation from Nanoporous Membranes for High Heat Flux Thermal Management
- **Wardah Inam** (D. J. PERREAULT)
  System Analysis and Design of High-Efficiency Power Converters for Grid Operation
- **Ryan Iutzi** (E. FITZGERALD)
  Interband Quantum Tunneling at the Band-Edges in III-V Semiconductor Heterojunctions for Low-Power Logic and Detectors
- **Daniel Kumar** (H.-S. LEE)
  Calibration of Sampling Clock Skew in High-Speed Time-Interleaved ADCs
- **John Haeseon Lee** (D. S. BONING AND B. ANTHONY)
  Measuring the Concentration of Microparticles in Suspension Using 2D Ultrasound Images
- **Luozhou Li** (D. ENGLUND)
  Diamond Device Fabrication for Quantum Information Processing and Sensing
- **Zhipeng Li** (V. STOJANOVIĆ)
  Efficient Baseband Design and Implementation for High-Throughput Transmitters
- **Bolin Liao** (M. DRESSELHAUS)
  Nanoscale Electron, Phonon and Spin Transport in Thermoelectric Materials
- **Seungbum Lim** (D. J. PERREAULT)
  High Frequency Power Conversion Architecture for Grid Interface
- **Maria Luckyanova** (M. DRESSELHAUS)
  Observation and Manipulation of the Wave Nature of Phonon Thermal Transport Through Superlattices
- **Qiong Ma** (P. JARILLO-HERRERO)
  Optoelectronics of Graphene-Based van der Waals Heterostructures
- **Jonathan P. Mailoa** (T. BUONASSISSI)
  Beyond the Shockley-Queisser Limit: Intermediate Band and Tandem Solar Cells Leveraging Silicon and CdTe Technology
- **Vitor Manfrinato** (K. K. BERGGREN)
  Electron-beam Lithography Towards the Atomic Scale and Applications to Nano-Optics
- **Tim Milakovich** (E. FITZGERALD)
  Integration of GaAsP Alloys on Si for High-Efficiency III-V/SI PV

PH.D. (CONTINUED)

- **Ashley E. Morishige** (T. BUONASSISSI)
  Predictive Engineering of Metal Impurities in n-type Crystalline Silicon for Cost-Effective, High-Performance Solar Cells
- **Jacob Mower** (D. ENGLUND)
  Photonic Quantum Computers and Communication Systems
- **Faraz Najafi** (K. K. BERGGREN)
  Superconducting Nanowire Single-Photon Detectors: New Detector Architectures and Integration with Photonic Chips
- **Eric Newton** (M. A. SCHMIDT)
  Design of Curved Electrodes to Enable Large Stroke - Low Voltage Micro Actuators
- **Samuel Nicaise** (K. K. BERGGREN)
  Template-Based Control for Bottom-Up Nanostructures-Multilayer
- **Arun Paidimarri** (A. P. CHANDRAKASAN)
  Circuits and Protocols for Low Duty Cycle Wireless Systems
- **Brian Pearson** (L. C. KIMERLING AND J. MICHEL)
  Germanium Photodetectors on Amorphous Substrates for Electronic-Photonic Integration
- **Michael Price** (A. P. CHANDRAKASAN)
  Energy-Scalable Speech Recognition Circuits
- **Ujwal Radhakrishna** (D. A. ANTONIADIS)
  Modeling Gallium Nitride based High Electron Mobility Transistors: Linking Device Physics to High Voltage and High Frequency Circuit Design
- **Joaquin Rodriguez-Nieva** (M. DRESSELHAUS)
  Novel Electronic Behaviors in Graphene Nanostructures
- **Amelia Servi** (K. K. GLEASON)
  Advancing Hydrophobic Desalination Membranes using Initiated Chemical Vapor Deposition (iCVD)
- **Sophia Sklan** (M. DRESSELHAUS)
  Dynamical Tuning of Phonon Transport for Information and Energy Control
- **Brian Solomon** (K. K. VARANASI)
  Enhancing Separation and Drag Reduction
- **Geoffrey Supran** (V. BULOVIĆ)
  Enhancing Quantum Dot Luminescence in Visible and Infrared Light Emitting Devices
- **Lidan Wu** (J. HAN)
  High Throughput Microfluidic Technologies for Cell Separation and Single Cell Analysis
- **Gilad Yahalom** (A. P. CHANDRAKASAN)
  Analog-Digital Co-Existence in 3D-IC
- **Do Yeon Yoon** (H.-S. LEE)
  A Continuous-Time Multi-Stage Noise-Shaping Delta-Sigma Modulator for Next Generation Wireless Applications
- **Tao Yu** (J. L. HOYT AND D. A. ANTONIADIS)
  InGaAs/GaAsSb Quantum-well Tunnel-FET for Ultra-low Power Applications

Glossary

TECHNICAL ACRONYMS

ADC	Analog-to-Digital Converters
AFE	Analog-front-end
ALD	Atomic layer deposition
CMP	Chemical mechanical polishing
CMOS	Complementary metal–oxide–semiconductor
CNT	Carbon Nanotubes
DRIE	Deep-reactive ion etching
FET	Field-effect transistor
MOSFET	Metal–oxide–semiconductor field-effect transistor

MIT ACRONYMS

BE	Department of Biological Engineering
Biology	Department of Biology
ChemE	Department of Chemical Engineering
CICS	Center for Integrated Circuits and Systems
CMSE	Center for Materials Science and Engineering
↳CMSE/IRG	CMSE Interdisciplinary Research Groups
DMSE	Department of Materials Science & Engineering
EECS	Department of Electrical Engineering & Computer Science
IMES	Institute for Medical Engineering and Science
JWAFS	MIT Abdul Latif Jameel World Water and Food Security Lab
KI	David H. Koch Institute for Integrative Cancer Research
LL	Lincoln Laboratory
MAS	Program in Media Arts & Sciences
MechE	Department of Mechanical Engineering
MEDRC	Medical Electronic Device Realization Center
MIT-CG	MIT/MTL Center for Graphene Devices and 2D Systems
MITEI	MIT Energy Initiative
MIT-GaN	MIT/MTL Gallium Nitride (GaN) Energy Initiative
MISTI	MIT International Science and Technology Initiatives
MIT-SUTD	MIT-Singapore University of Technology and Design Collaboration Office
MIT Skoltech	MIT Skoltech Initiative
MTL	Microsystems Technology Laboratories
NSE	Department of Nuclear Science & Engineering

Physics	Department of Physics
S3TEC	Solid State Thermal Energy Conversion Center
Sloan	Sloan School of Management
SMA	Singapore-MIT Alliance
↳**SMART**	Singapore-MIT Alliance for Research and Technology Center
↳**SMART-LEES**	SMART Low Energy Electronic Systems Center
SUTD-MIT	MIT-Singapore University of Technology and Design Collaboration Office
TPP	Technology and Policy Program

U.S. GOVERNMENT ACRONYMS

AFOSR	U.S. Air Force Office of Scientific Research
AFRL	U.S. Air Force Research Laboratory
ARL	U.S. Army Research Laboratory
↳**ARL-CDQI**	U.S. Army Research Laboratory Center for Distributed Quantum Information
ARPA-E	Advanced Research Projects Agency - Energy (DOE)
DARPA	Defense Advanced Research Projects Agency
↳ **YFA**	DARPA Young Faculty Award DoD, U.S. Department of Defense
DOE	Department of Energy
↳**EFRC**	U.S. Department of Energy: Energy Frontier Research Center (Center for Excitonics)
DTRA	U.S. DoD Defense Threat Reduction Agency
IARPA	Intelligence Advanced Research Projects Activity
NASA	National Aeronautics and Space Administration
NDSEG	National Defense Science and Engineering Graduate Fellowship
NIH	National Institutes of Health
↳**NCI**	National Cancer Institute
NSF	National Science Foundation
↳**CIQM**	NSF Center for Integrated Quantum Materials
↳**CSNE**	NSF Center for Sensorimotor Neural Engineering
↳**E3S**	NSF Center for Energy Efficient Electronics Science
↳**GRFP**	NSF Graduate Research Fellowship Program
↳**MRSEC**	NSF Materials Research Science and Engineering Centers
↳**NEEDS**	NSF Nano-Engineered Electronic Device Simulation Node
ONR	Office of Naval Research
↳**DRIFT-MURI**	Design-for-Reliability Initiative for Future Technologies - Multidisciplinary University Research Initiative

OTHER ACRONYMS

ACE4S	ATIC-SRC Center of Excellence for Energy Efficient Electronics Systems
CONACyT	Consejo Nacional de Ciencia y Tecnología (Mexico)
IEEE	Institute of Electrical and Electronics Engineers
IHP Germany	Innovations for High Performance Microelectronics Germany
ISSCC	International Solid-State Circuits Conference (IEEE)
LEAST	SRC STARnet Center for Low Energy Systems Technology
MASDAR	Masdar Institute of Science and Technology
NSRC	Natural Sciences and Engineering Research Council (Canada)
NTU	Nanyang Technological University
NUS	National University of Singapore
NYSCF	The New York Stem Cell Foundation
SRC	Semiconductor Research Corporation
↳**LEAST**	SRC STARnet Center for Low Energy Systems Technology
↳**MARCO**	Microelectronics Advanced Research Corporation
TSMC	Taiwan Semiconductor Manufacturing Company

Index

Symbols

A

B

C

D

U

V

W

Z

IN APPRECIATION OF OUR MICROSYSTEMS INDUSTRIAL GROUP MEMBER COMPANIES:

Analog Devices, Inc.
Applied Materials
Draper
Edwards Vacuum
Foxconn Electronics
HARTING
Hitachi High-Technologies
Intel
IBM
Lam Research Co.
NEC
Qualcomm
Samsung
STMicroelectronics
TSMC
Texas Instruments